Republic of Iraq
Ministry of Higher Education
and Scientific Research
University of Babylon
College of Engineering
Mechanical Engineering Department

Investigation of Thermal-Hydraulic Characteristics of Four Concentric Tube in Al-Mussaib Thermal Power Plant

A Thesis

Submitted to the College of Engineering, University of Babylon in Partial Fulfillment of the Requirements for the Doctor of Philosophy Degree in Engineering\ Mechanical Engineering\ Power.

By

Rana Ali Hussein Alwan

Supervised by

Prof. Dr. Adil Abbas Al-Moosawy

Prof. Dr. Isam Mejbel Abed

2022

بسم الله الرحمن الرحيم

﴿ وَلَوْلَا فَضْلُ اللَّهِ عَلَيْكَ وَرَحْمَتُهُ لَهَمَّتْ طَائِفَةٌ مِنْهُمْ
أَنْ يُضِلُّوكَ وَمَا يُضِلُّونَ إِلَّا أَنْفُسَهُمْ وَمَا يَضُرُّونَكَ مِنْ
شَيْءٍ وَأَنْزَلَ اللَّهُ عَلَيْكَ الْكِتَابَ وَالْحِكْمَةَ وَعَلَّمَكَ مَا
لَمْ تَكُنْ تَعْلَمُ وَكَانَ فَضْلُ اللَّهِ عَلَيْكَ عَظِيمًا ﴾

صدق الله العلي العظيم

سورة النساء أية ﴿١١٣﴾

Certification

We certify that this thesis entitled ***"Modification and analysis for Heat exchanger performance in Al-Mussaib Thermal Power Plant"*** was prepared by ***Rana Ali Hussein*** under our supervision at the University of Babylon in a partial fulfilment of the requirements for the degree of Doctor of Philosophy in Mechanical Engineering/ Power.

We recommend that this thesis be forwarded for examination in accordance with the regulation of the University of Babylon.

Signature:

Name: ***Prof. Dr. Adil Abbas AL-Moosawy***

Title: Supervisor

Date: / /

Signature:

Name: ***Prof. Dr. Isam Mejbel Abed***

Title: Supervisor

Date: / /

Examining Committee Certification

We certify, that we have read this thesis entitled "**Investigation of Thermal-Hydraulic Characteristics of Four Concentric Tube in Al-Mussaib Thermal Power Plant"** and as an examining committee, examined the student "**Rana Ali Hussein ",** in its content and that in our opinion it meets the standard of thesis for the degree of Doctor of Philosophy in Mechanical Engineering/ Power.

Signature:

Name: ***Prof. Dr. Adil Abbas AL-Moosawy***
Title: Supervisor
Date: / /2022

Signature:

Name: ***Prof. Dr. Isam Mejbel Abed***
Title: Supervisor
Date: / /2022

Signature:

Name: ***Prof. Dr. Qasim Saleh Mahdi***
Title: Chairman
Date: / /2022

Signature:

Name: ***Prof. Dr. Saba Y. Ahmed***
Title: Member
Date: / /2022

Signature:

Name: ***Prof. Dr. Ahmed F. Khudheyer***
Title: Member
Date: / /2022

Signature:

Name: ***Assist Prof. Dr. Akeel Abbas Mohammed***
Title: Member
Date: / /2022

Signature:

Name: ***Assist Prof. Dr. Hameed Kadhem Hamzah***
Title: Member
Date: / /2022

Approval of Mechanical Engineering Department
Head of the Mechanical Engineering Department

Signature:

Name: ***Assist Prof. Dr. Samer M.Abdul Haleem***
Date: / /2022

Approval of the College of Engineering
The Acting Dean of the College of Engineering

Signature:

Name: ***Prof. Dr. Hatem Hadi Obeid***
Date: / /2022

Dedication

I would like to express my gratefulness to my biggest supporters, to the reason of where I am and where I will be my father, mother and dear husband who fulfilled me with encouragement, appreciation and love. Also lastly to who make me feel home and safe, my beloved children.

Rana 2022

Acknowledgments

Deepest appreciation for the almighty Allah for the modest assistance in all aspects of my preparation of this work. As well as my sincere thanks and respect to my supervisors ***Prof. Dr. Adil Abbas AL-Moosawy*** and ***Prof. Dr. Isam Mejbel Abed*** who never hesitated in helping to achieve this.

I also thank all staff and members of the College of Engineering /Mechanical Engineering Department at the University of Babylon for being the greatest cooperators. And my thanks to ***Mr. Hussain H. Rashid*** in mechanical engineering laboratories, and to the staff of the Al-Mussaib thermal power plant.

Rana 2022

Abstract

Heat exchangers are commonly utilized as important components in power plant heat extraction and recovery systems. In many applications, a high performance heat transfer function is crucial. A new design of heat exchanger is achieved to solve the problem in Al-Mussaib thermal power plant. This design consists of four copper pipes with diameter 1 inch(25.4mm), 2 inch(50.8 mm),3 inch(76.2 mm) and 4inch(101.6 mm) and the length of the pipes are 2 m. The hot water is cooled in two stages.

The first stage, the heat transfer is occurred between the hot water in first pipe and raw water in second pipe. While in the second stage, the heat transfer is occurred between the hot water in third pipe and raw water in second pipe and fourth pipe. The flow arrangement in first stage is counter flow while the flow arrangement in second stage is parallel.

Solidworks is used in the design of the four concentric pipe heat exchanger. The inlet temperature of hot water is 40.8°C and the mass flow rate of hot water is 40 l/min. The inlet temperature of cold water for the second and fourth pipes is 28 °C and the mass flow rate of raw water in the second and fourth pipes is 60 l/min and 70 l/min respectively. The purpose of the design is to reduce the temperature of the hot water to 35°C, which is the required temperature in Al- Mussaib thermal power plant.

Computational Fluid Dynamics (CFD) technique had been used to predict temperature, velocity and pressure of water heat exchanger. This is accomplished numerically by solving the Navier Stokes equations for mass, momentum and energy. Solidworks commercial package 2016 with k-Ɛ model is used to solve the governing equation.

Experimental work is done to measure the temperature at inlet and outlet for each pipe, and temperature distribution through pipes . The pressure drop and the pressure value at inlet and outlet for each pipe are measured . The experimental tests are done with different values of mass flow rate for raw water. It was found that the temperature of hot water decreases to 34.7°C at mass flow rate for raw water (60 and 70) l/min, at second pipe and fourth pipe respectively. This is the required outlet temperature from the heat exchanger working mechanism.

The comparison between the experimental and numerical results shows acceptable agreement, and the maximum error is (0.38, 2.2, 3.4 and4.3) % for temperature at first pipe, second pipe, third pipe, fourth pipe respectively. The comparisons of the performance work for this heat exchanger with that of shell and tube, and triple tube heat exchangers. It was found that heat exchangers cannot solve the problems in Al-Mussaib power plant.

NOMENCLATURE		
Symbol	**Title**	**Unit**
a	Annular diameter ratio	
A	Area	m^2
B	Baffle spacing	mm
c_p	Specific Heat Capacity	J/kg. °C
C_r	Capacity ratio	
C_t	Tube clearance	mm
d	Diameter of the pipe	mm
d_{hy}	Hydraulic diameter	mm
D_e	Equivalent diameter	mm
D_s	Shell diameter	mm
f_t	Friction factor	
g	Gravity acceleration	m/s^2
h	Heat transfer coefficient	W/m^2. °C
H max	Maximum head of pump	m
k	Thermal Conductivity	W/m.°C
L	Length of pipe	m
$\dot{m}$	Mass flow rate	l/min
N	number of measurements	
Nu	Nusselt number	
N_b	Number of baffles	
N_t	Number of tubes	
P	Pressure	kpa
Pr	Prandtl number	
P_r	Pitch ratio	
P_t	Tube pitch	mm
q_i	Diffusive heat flux	W/m^2

$\dot{Q}$	Heat transfer rates	W
Q_{max}	Maximum flow rate of pump	l/min
Re	Reynolds number	
R_f	Fouling factor	
R_{th}	Total thermal resistance	
St	Source term	
t	Time	sec
T	Temperature	˚C
u, v, w	Velocity component in Cartesian coordinate	m/s
v	Velocity	m/s
U	Overall heat transfers coefficient	W/m^2. °C
x, y, z	Cartesian coordinate	
X_i	values for measurements	

Subscripts	
Symbol	**Title**
1	First pipe
2	Second pipe
3	Third pipe
av	Average
h	Hot water
i	Inlet
max	Maximum
min	Minimum
n	Raw water
o	Outlet
s	Shell
t	Tube
w	Water

GREEK SYMBOLS		
Symbol	**Title**	**Units**
ρ	Density	kg/m^3
μ	Viscosity	$mPa.s$
ε	Effectiveness	%
Γ	Diffusivity	m^2/s
δ_{ij}	Kronecker delta function	
τ_{ij}^{R}	Reynolds stress tensor	
λ_i	Eigen values	

ABBREVIATIONS	
Symbol	**Title**
CAD	Computer-aided design
CFD	Computational fluid dynamics
DSCTHE	Double spirally coiled tube heat exchanger
DTHE	Double tube heat exchanger
3-D	Three dimension
EES	Engineering Equation Solver
FCPHE	Four concentric pipe heat exchanger
FVM	Finite volume method
GA	Genetic algorithm
IMTD	Integral-mean temperature difference
$LMTD$	Log-mean temperature difference
NTU	Number of transfer units
PCM	Phase change material
PEC	Performance evaluation criteria
PTTs	Perforated twisted tapes
QUICK	Quadratic Upwind Interpolation for Convective Kinematics
RSM	Response Surface Methodology
$S.D$	standard deviation
STT	Simple twisted tapes
S.U	standard uncertainty
TCTHE	Triple concentric tube heat exchanger
TSCTHE	Triple spirally coiled tube heat exchanger

Contents

Contents ***Page No.***

Chapter One

Introduction

Introduction

1.1. General

A heat exchanger is a device that transfers thermal energy between two or more fluids, a solid surface and a fluid, or solid particles and a fluid, all of which are at different temperatures and in thermal contact. There are usually no external heat and work interactions in heat exchangers. Heating or cooling a fluid stream of interest, as well as evaporation or condensation of single or multicomponent fluid streams, are common applications. The fluids exchanging heat are in direct contact in a few heat exchangers. Heat transfer between fluids in most heat exchangers occurs transiently through a separating wall or into and out of a wall. A heat transfer surface separates the fluids in many heat exchangers, ensuring that they do not mix or leak. Tube heat exchangers are frequently used in engineering because of their durable structure, operating flexibility, adaptability, and reliable operation, as well as their capacity to tolerate high temperatures and high pressure, that presented by **Hong [1]**. Tubular heat exchangers are usually made of circular tubes, although they can also be made of elliptical, rectangular, round, or flat twisted tubes in some cases. Because the core geometry may be easily changed by changing the tube diameter, length, and arrangement, the design has a lot of versatility. Tubular heat exchangers are generally used for liquid-to-liquid heat transfer. Shell-and-tube, double-pipe, triple-pipe, and spiral tube exchangers are the different types of tubular exchangers. Except for exchangers with fins on the outside and inner tubes, they are all prime surface exchangers.

1.2. Classification of heat exchanger

There are various types of heat exchanger which are categorized with respect to construction, transfer process, flow and phase. A brief classification of heat exchanger is shown in figure (1-1)

1.3. Types of tubular heat exchanger

1.3.1. Shell and tube heat exchanger

This heat exchanger, depicted in figure (1-2) is made up of a bundle of round tubes installed in a cylindrical shell with the tube axis parallel to the shell's. One fluid circulates inside the tubes, while the other circulates across and along them. Tubes (or tube bundles), shell, frontend head, rear-end head, baffles, and tube sheets are the major components of this exchanger. This type is used in Al-Mussaib thermal power plant. This heat exchanger is used to cool the accessories of thermal power plant. In this heat exchanger the hot water flows through the shell while river water flows through the tubes. There are several advantages and disadvantages for shell and tube heat exchanger. The advantages of this heat exchanger are used in systems with higher operating temperatures and pressures, pressure drop across a tube cooler is less, and tube leaks are easily located and plugged since pressure test is comparatively easy. While the disadvantages are the heat transfer efficiency is less compared to plate type cooler, cleaning and maintenance is difficulty since a tube cooler requires enough clearance at one end to remove the tube nest, and requires more space in comparison to plate coolers.

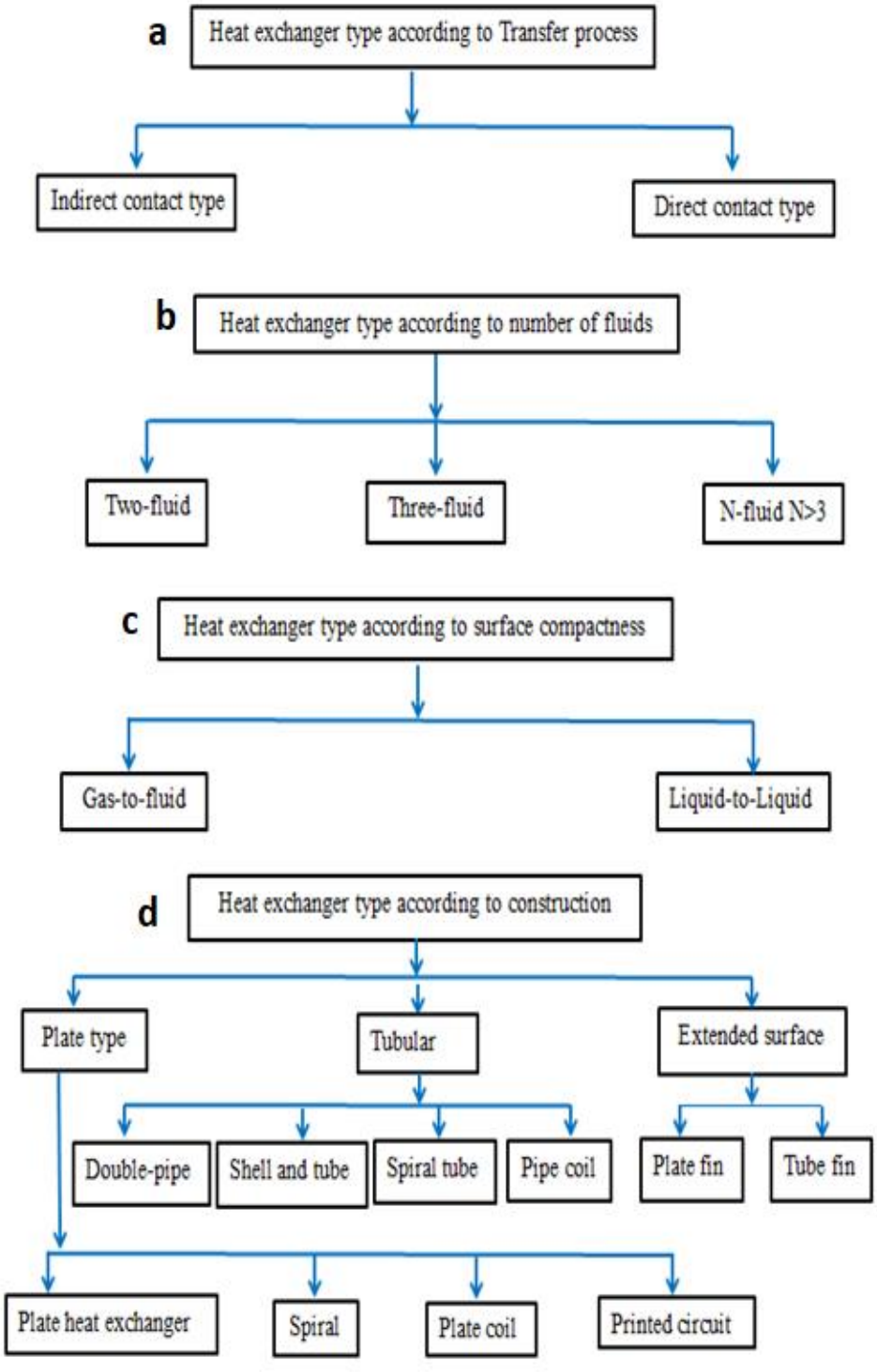

Figure (1-1) classification of heat exchanger.[2]

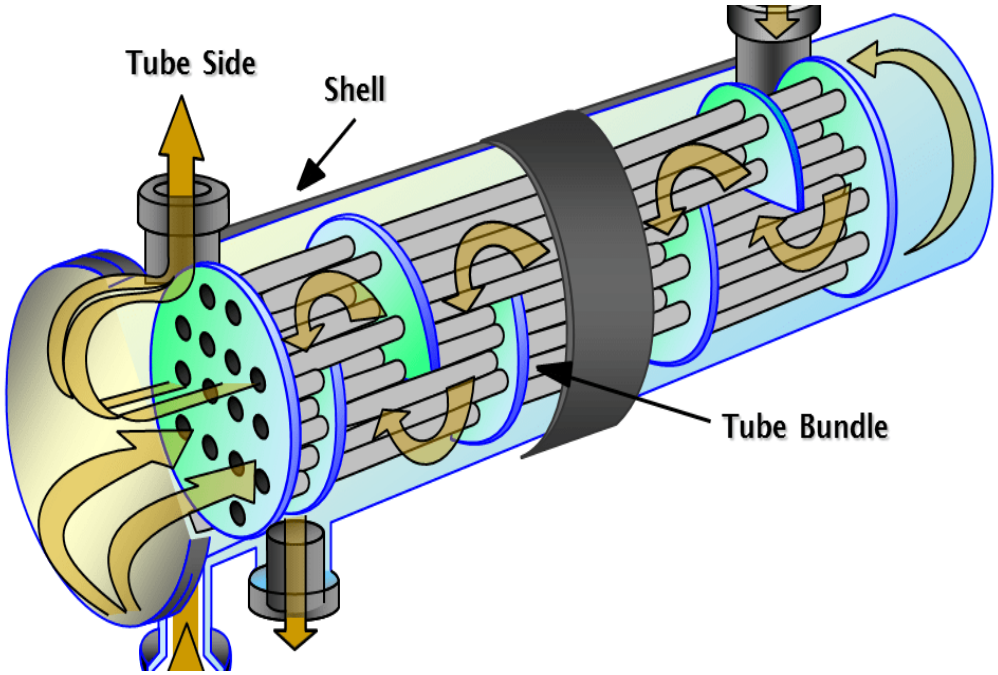

Figure (1-2) shell and tube heat exchanger. Re.[2]

1.3.2. Double pipes heat exchanger

Double pipes heat exchanger normally consists of two concentric pipes, with the inner pipe plain, as seen in figure (1-3). For the best performance for the given surface area, one fluid flows in the inner pipe and the other fluid flows in the annulus between pipes in a counter flow direction. The fluids may flow in a parallel flow direction if the application demands a nearly constant wall temperature. This is the most basic heat exchanger. Flow distribution is not a problem, and disassembly makes cleaning a simple**. Zare et al [3]** presented design of double pipe heat exchanger. The advantages of this type are working excellent capacity for thermal expansion, it is easy to install and clean, and replacement parts are inexpensive and always in supply. While the disadvantages are not cost effective as most shell and tube exchangers, and it requires special gaskets

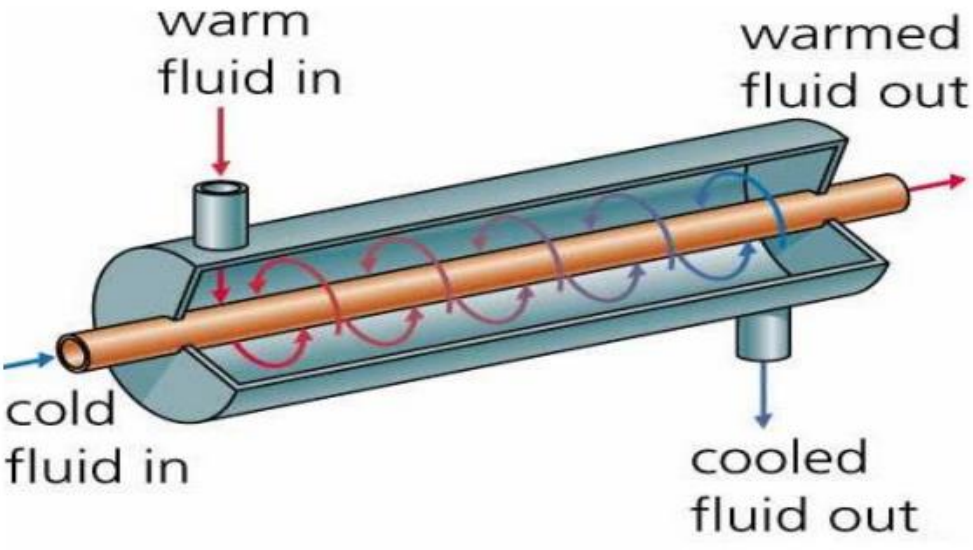

Figure (1-3) double –pipe heat exchanger. Ref. [3].

1.3.3. Triple tube heat exchanger

By adding an intermediary tube, the triple concentric tube heat exchanger (TCTHE) is a modified constructive version of the double concentric tube heat exchanger, as shown in figure (1-4). As a function, a triple concentric heat exchanger is made up of three concentric tubes that can be of various lengths. In comparison to tube in tube heat exchangers, triple concentric heat exchangers provide a larger surface area for heat transfer per unit length and higher overall heat transfer coefficients, this comparison is presented by **Rădulescu et al [4]**. The thermal contact between the fluids was improved by adding the third tube. Furthermore, because these types of heat exchangers can exchange heat between three fluids in one unit, they can provide technical and economic benefits. Heat exchangers with three concentric tubes are employed in a variety of applications, including food processing, cooling, pasteurization, congelation, and concentration. The advantages of triple tube heat exchanger have a large surface area for heat transfer per unit length, and it can be operating to high temperatures and has a good resistance to high pressure.

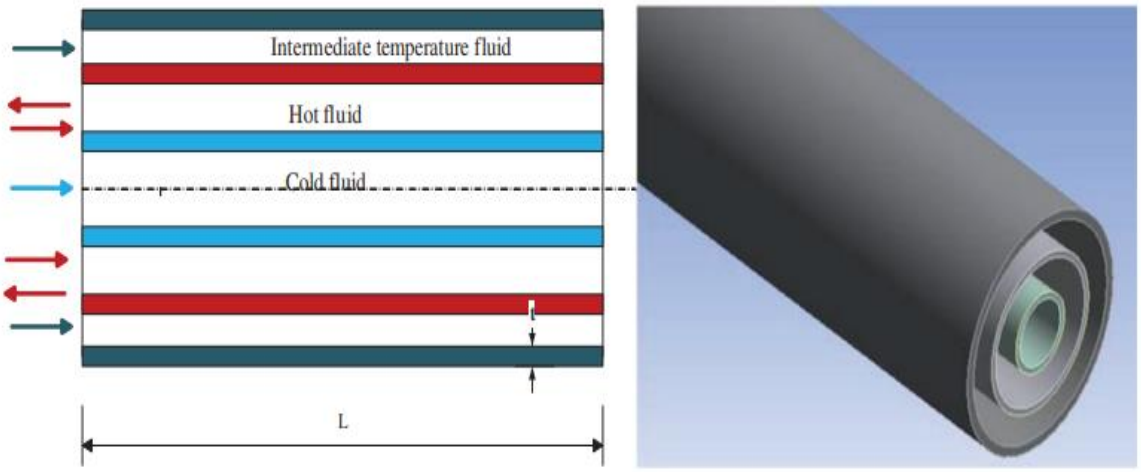

Figure (1-4) triple concentric-tube heat exchanger. Ref.[5].

1.4. Motivation of Present Work

The shell and tube heat exchanger fails to cool the accessories of Al-Mussaib thermal power plant for required cooling temperature. Due to that problem, the objective of this work is conducted to design and build heat exchanger which is used to improve the heat transfer performance for Al-Mussaib accessories of thermal power plan. This is achieved by designing a new heat exchanger which consists of four concentric pipes. The function of working this new heat exchanger is cooling the hot water by two stages with raw water. This new design solves the problems in the Al-Mussaib power plant where the shell and tube heat exchanger failed.

The scope of this study can be summarized in the following works:

Experimental work: The first step includes designing a prototype of four concentric pipe heat exchanger (FCPHE) by using solidworks commercial package 2016 .

Theoretical work: The theoretical work focuses on Computational Fluid Dynamics (CFD) used to predict water flow and temperature fields in heat exchanger. This is accomplished numerically by solving the Navier

Stokes set of partial differential equations for mass, momentum and energy. These equations are applied to finite volumes in the solver to obtain a detailed solution, including velocity and temperature fields. Solidworks commercial package 2016 with k-Ɛ model is used to solve the governing equation.

Chapter Two

Literatures Review

Literature Review

The purpose of the literature review is to summarize the previous work closely related to the present work. Several researchers have investigated the behavior of heat exchangers theoretically and experimentally. It was presented in two sections; the first was the experimental and theoretical studies of heat transfer improvement for double tube heat exchanger .The second section was the experimental and theoretical studies related to triple concentric-tube heat exchanger.

2.1. Experimental and theoretical Investigations for double tube heat exchanger

Hui-fan et al.,[6] presented the Engineering Equation Solver (EES) software, a heat transfer coefficient calculation program about double pipe heat exchanges. Some experimental data were compared to the simulation data for proving that the program can predict the heat transfer coefficient of the double pipe heat exchangers, and then the change of heat transfer coefficient was calculated and analyzed with relevant parameters. The results showed that the heat transfer coefficient of heat exchanger were increasing with the flow of the shell side, the tube side and the logarithmic mean temperature difference, and when the temperature difference equals to 12℃, the total heat transfer coefficient can up to 2400W/m^2. K.

Baadache and Bougriou [7] presented the use of Genetic Algorithm in the sizing of the shell and double concentric tube heat exchanger where the objective function is the total cost which is the sum of the capital cost of the device and the operating cost. The use of the techno economic methods based on the optimization methods of heat exchangers sizing allow to have a device that satisfies the technical specification with the lowest possible levels of operating and investment costs. The logarithmic

mean temperature difference method was used for the calculation of the heat exchange area. This new heat exchanger is more profitable and more economic than the old heat exchanger; the total cost decreased of about 13.16 % . The design modifications and the use of the Genetic Algorithm for the sizing also allow to improve the compactness of the heat exchanger, the study showed that the latter can increase the heat transfer surface area per unit volume until 340 m^2 /m^3.

Zhi Han et al.,[8] integrated a fully developing three-dimensional heat transfer and flow model, a multi-objective optimization aims to fulfill the geometric design for double-tube heat exchangers with inner corrugated tube was investigated in this work with Response Surface Methodology (RSM). Dimensionless corrugation pitch (p/D), dimensionless corrugation height (H/D), dimensionless corrugation radius (r/D) and Reynolds number (Re) are considered as four design parameters. Considering the process parameters, the characteristic numbers involving heat transfer characteristic, resistance characteristic and overall heat transfer performance calculated by CFD, and are served as objective functions to the RSM (Nu_c, f_c, Nu_c/Nu_s, f_c/f_s and h in this paper). The results of optimal designs are a set of multiple optimum solutions, called 'Pareto optimal solutions'. It reveals the identical tendency of Nu_c/Nu_s and f_c/f_s reflecting the conflict between them that means augmenting the heat transfer performance with various design parameters in the optimal situation inevitably sacrificed the increase of flow resistance. According to the Pareto optimal curves, the optimum designing parameters of double pipe heat exchanger with inner corrugated tube under the constrains of $Nu_c/Nu_s \geq 1.2$ are found to be P/D = 0.82, H/D = 0.22, r/D = 0.23, Re = 26,263, corresponding to the maximum value of Ɛ= 1.12.

Rădulescu et al.,[4] presented results of analysis of the heat transfer to cool a petroleum product in two types of concentric tube heat exchangers: double and triple concentric tube heat exchangers. The cooling agent was water. The triple concentric tube heat exchanger was a modified constructive version of double concentric tube heat exchanger by adding an intermediate tube. This intermediate tube improves the heat transfer by increasing the heat area per unit length The results show that for the same length of the heat exchanger, the heat transfer area and the overall heat transfer coefficients for triple concentric tube heat exchanger were higher than for double tube heat exchanger about 57% and 62.8% respectively.

Sheikholeslami et al.,[9] investigated experimentally the heat transfer and pressure loss in an air to water double pipe heat exchanger. Typical circular-ring and perforated circular-ring turbulators were placed in annular pipe. The working fluids were air, flowing in the annular pipe, and water through the inner circular tube. The experiments were conducted for different governing parameters namely; air flow Reynolds number (6000–12,000), pitch ratio (1.83, 2.92 and 5.83) and number of perforated hole (0, 2, 4 and 8). Correlations for friction factor, Nusselt number and thermal performance are presented according to experimental data. Results indicated that using perforated circular-ring leads to obtain lower heat transfer enhancement than the circular-ring because of reduction of intersection angle between the velocity and the temperature field. Thermal performance increases with increase of number of perforated hole but it decreases with increase of Reynolds number and pitch ratio.

Dirker et al.,[10] consisted the experimental facility of a cold-water loop and an annular flow passage test section that was electrically heated. In this experimental study circumferentially averaged local heat transfer coefficients were determined with water for a uniform heat flux boundary

condition on the inner wall in a horizontal concentric annular test section with a length of 1.05 m, a hydraulic diameter of 14.8 mm, and a diameter ratio of 0.648. Local inner wall temperatures were obtained via liquid crystal thermography with the aid of an automated camera position system. Conventional on-center and off-center annular inlet configurations with three inlet sizes were evaluated for Reynolds numbers ranging from 2000 to 7500. It was found that the local heat transfer coefficients were significantly higher at the inlet, and decreased as the boundary layers developed. Local maximum and minimum heat transfer coefficients were identified which may be due to flow impingement caused by the inlet geometry. A new local heat transfer correlation for the turbulent flow in regions close to the inlet of an annular flow passage was developed.

Verma et al.,[11] estimated the heat transfer performance of proposed fabricated heat exchanger using corrugated and non-corrugated pipes. Pitch and depths were varied in case of corrugated pipe. Authors have achieved the maximum heat transfer coefficient and Nussult number with helical shaped ribs of 4 mm pitch and 1.5 mm depth with the variations in Reynolds number from 5000 to 17000, mass flow rates from 0.03 to 0.13 kg/s and 0.04 to 0.14 kg/s for cold and hot fluid respectively. Length and diameter of pipes are 25.4 mm and 2000 mm respectively. Authors have also modeled an artificial neural network (ANN) for predicting heat transfer coefficient, Nussult number and Reynolds number. Value of coefficient of multiple determination are achieved. The R^2 (coefficient of multiple determination) - values is 0.99999, 0.999997 and 0.999993 for Reynolds number, heat transfer and Nusselt number respectively with unknown data set which is very satisfactory.

Sreedhar and Varghese,[12] studied the effect of different longitudinal fin patterns on overall heat transfer coefficient and rate of heat

transfer in concentric double tube heat exchanger using LMTD. More over the temperature distribution inside the tube heat exchanger is found and tabulated using computational fluid dynamics (CFD) by fluent 6 and meshed using GAMBIT. The inner and outer tube diameters were fixed to be 0.03m and 0.06m respectively. The following assumptions were considered for (software) analysis: (i) Fluid flow was laminar. (ii)Hot water passes through the inner tube and cold water in the annular gap for all the 4 cases (Mention no. of cases considered). (iii) Aluminum was used as the tube and fin material, the tube thickness of both the tubes is 0.001m. The inlet of hot water is constant at 3700K and that of the cold water at 3000K. Analysis showed that maximum heat transfer (rate or over all heat transfer coefficient) was observed in the case of having external fins for the inner tube with higher overall heat transfer coefficient of 60.5% increase to that of the base setup.

Mashoofi et al. ,[13] examined the ways to reduce the pressure drop and consequently increase thermal performance enhancement factor of a heat exchanger equipped with twisted tapes. For this purpose, axial perforated twisted tapes (PTTs) with various hole diameters were used instead of simple twisted tapes(STT). Moreover, the variations of the effectiveness with number of transfer units for different heat capacity ratios were presented. The numerical model was well validated with the available experimental results. The results indicated that the use of perforated twisted tape leads to a reduction in pressure drop and heat transfer rate, subsequently; a significant increase in thermal performance enhancement factor was seen compared to simple twisted tapes. In addition, some correlations were formulated to present the numerical results.

Hosseinian and Isfahani [14] investigated the heat transfer enhancement due to the surface vibration for a double pipe heat exchanger,

made of PVDF. In order to create forced vibrations (3–9 m/s^2, 100 Hz) on the outer surface of the heat exchanger electro-dynamic vibrators are used. Experiments were performed at inner Reynolds numbers ranging from 2533 to 9960. The effects of volume flow rate and temperature on heat transfer performance are evaluated. Results demonstrated that heat transfer coefficient increases by increasing vibration level and mass flow rate. The most increase in heat transfer coefficient is 97% which is obtained for the highest vibration level (9 m/s^2) in the experiment range.

Bahmani et al.,[15] investigated the heat transfer and turbulent flow of water/alumina nanofluid in a parallel as well as counter flow double pipe heat exchanger. The governing equations have been solved using FORTRAN code, based on finite volume method. Single-phase and standard k- Ɛ models have been used for nanofluid and turbulent modeling, respectively. The internal fluid has been considered as hot fluid (nanofluid) and the external fluid, cold fluid (base fluid). The effects of nanoparticles volume fraction, flow direction and Reynolds number on base fluid, nanofluid and wall temperatures, thermal efficiency, Nusselt number and convection heat transfer coefficient have been studied. The results indicated that increasing the nanoparticles volume fraction or Reynolds number causes enhancement of Nusselt number and convection heat transfer coefficient. Maximum rate of average Nusselt number and thermal efficiency enhancement are 32.7% and 30%, respectively. Also, by nanoparticles volume fraction increment, the outlet temperature of fluid and wall temperature increase. Study the minimum temperature in the solid wall of heat exchangers, it can be observed that the minimum temperature in counter flow has significantly reduced, compared to parallel flow. However, by increasing Reynolds number, the slope of thermal efficiency enhancement of heat exchanger gradually tends to a constant amount. This

behavior was more obvious in parallel flow heat exchangers. Therefore, using of counter flow heat exchangers was recommended in higher Reynolds numbers.

Hamzah and Nima [16] investigated experimentally the influence of adding fins of copper foam on the characteristics of heat transfer in a double-pipe heat exchanger . The test rig consists of two concentric pipes (copper and Perspex) to form the required double-pipe heat exchanger. The metal foam fins of 40 PPI were made from copper and set at 30° angle with the tube entrance and were distributed in sections inside the annular gap around the inner copper tube to guide the fluid flow and to disturb its structure inside the annular gap. The Reynolds number range for air was from 616 to 2343, with a constant water volume flow rate (2 lpm) in these experiments. The inlet water temperature was controlled at three values (80 °C, 85 °C, and 90 °C). Both parallel and counter flows were examined in this study. The comparison was made between the two cases of with and without insertion of copper foam fins and between parallel and counter flow mode. Results showed that the average heat transfer coefficient and the average Nusselt number were increased as the Reynolds number increased, and their largest values were obtained in case of copper foam fins insertion and for counter flow mode. The important finding was no significant pressure drop was found with the enhancement of heat transfer throughout the annular gap of heat exchanger. Results also showed that the effectiveness values were doubled in case of insertion of the copper foam fins. The counter flow pattern was the most efficient flow pattern than the parallel flow.

Corcoles et al.,[17] studied a 3-D numerical simulations were carried out to analyze the influence of geometrical parameters for eight spirally inner corrugated tubes at turbulent flow (Re =25 × 10^3) in a double pipe

heat exchanger. As a novelty, different combinations of pitch and height in a 3-D inward corrugated tube numerical model were analyzed and validated with an experimental setup. This had not previously been conducted in a double pipe heat exchanger. Furthermore, the numerical model included the entire geometry of the heat exchanger, with dimensions of the computational domain similar to those used in actual commercial applications. Grid independence analysis of the numerical solution was performed based on a 3-D unstructured tetrahedral mesh scheme, considering the Realizable k-Ɛ turbulence model. Case 8, with the highest corrugation height (H/D=0.05) and the lowest helical pitch (P/D=0.682) presented the highest pressure drops in both inner and annular tubes, being 4.15 and 1.27 times higher in the inner tube and in the annulus side than in the smooth tube, respectively. Regarding heat transfer, Case 9, with the smallest helical pitch and an intermediate corrugation height (H/D=0.041) obtained the highest number of transfer units (NTU) value, which, under the experimental conditions of this work, resulted in an increase of 29% compared with the smooth tube. In Cases 7 and 9, the inner tubes showed optimal results when considering the combined influence of the enhanced heat transfer performance and pressure drop using the performance evaluation criteria (PEC)

2.2 Experimental and theoretical Investigations for triple concentric tube heat exchanger

Zuritz [18] explained analytical equations for a triple-tube heat exchanger . They allow for independent computations of bulk (cross-sectional area averaged) fluid temperatures at any axial location along the

heat exchanger and are valid for parallel and counter flow configurations. The equations account for heat losses to the surroundings and were useful for design purposes. Mass flow rates, inlet fluid temperatures and heat transfer coefficients are input parameters required for temperature calculations. Simulations show that the creation of an annular region within the inner pipe increases the overall heat transfer efficiency and reduces the heat exchanger length requirement by almost 25 %. A case study was presented with a complete computational procedure. The results obtained with the different equations were in excellent agreement and proved useful for heat exchanger design and evaluation purposes.

Dirker and Meyer [19] studied the effect of geometric shape of passage's cross-section on its convective heat transfer capabilities. For concentric annuli, the diameter ratio of the annular space plays an important role. Experiments were conducted on water under turbulent flow conditions for a wide range of diameter ratios. The Wilson plot method was used to determine the heat transfer coefficients from which a correlation was developed that could be used to predict the heat transfer coefficients. It was concluded that the correlation deduced from predicted Nusselt numbers accurately within 3% the measured values from diameter ratios between a= 1.7 and a= 5.1 and a Reynolds numbers range of 4000 to 30000.

Valladares [20] detailed one-dimensional steady and transient numerical simulation of the thermal and fluid-dynamic behavior of triple concentrictube heat exchangers had been developed. The governing equations (continuity, momentum and energy) inside the inner tube and the annulus (inner and outer), together with the energy equations in the inner, intermediate and outermost tube wall and insulation, are solved iteratively in a segregated manner. The discretized governing equations in the zones

with fluid flow were coupled using an implicit step by step method. This formulation requires the use of empirical information for the evaluation of convective heat transfer, shear stress and void fraction. An implicit central difference numerical scheme and a line-by-line solver were used in the inner and intermediate tube walls and the outermost tube wall with insulation. All the flow variables (enthalpies, temperatures, pressures, mass fractions, velocities, heat fluxes, etc.) together with the thermophysical properties were evaluated at each point of the grid in which the domain was discretized

Batmaz and Sandeep [21] developed a new procedure to calculate the overall heat transfer coefficients and axial temperature distribution of fluids for a cooling process for different flow rates and inlet temperatures of the fluid streams. The effectiveness of the triple tube heat exchanger(TTHE) was compared to that of a double tube heat exchanger (DTHE) of identical length. Experimentally compared the co-current and countercurrent arrangements in a TTHE. This studied concluded that the overall heat transfer coefficient values were higher in the countercurrent arrangement than in the co-current arrangement. In addition, the effectiveness in the countercurrent arrangement (0.93 to 1.00) was higher than that in the co-current arrangement (0.73 to 0.95).

Zhao and Li [22] explained the derived integral-mean temperature difference (IMTD) formulae, a new modelling technology was presented in detail for the parallel stream three-fluid heat exchanger with two thermal communications, which included the derivation of two IMTD formulae, the design and simulation procedure of IMTD model as well as its validation with previous exact models. The biggest advantage of new model lied in the application of IMTD formulae into the design and simulation of three-fluid heat exchanger. These IMTD formulae were equivalent to the log-

mean temperature difference (LMTD) of two-fluid heat exchanger. The mean temperature difference method perfectly solved the problem of thermal design of two-fluid heat exchanger. Similarly, with the derived IMTD formulae and the proposed convergence-accelerated method in this paper, the developed new model not only realizes fast convergence for the design procedure of three-fluid heat exchanger, but also in simplicity can be comparable to past Sorlie's LMTD approximate model.

Radulescu et al.,[23] proposed that calculation algorithm used in heat transfer studies when triple concentric-tube heat exchangers were involved. The study consists in determining the partial coefficients of heat transfer afferent to three fluids that exchange heat between them based on experimental results. According to experimental mode, the flow in tubes of the heat exchanger was in counter-flow from the hot fluid to two cold ones, while the circulation of the cold fluids was in co-current flow. In the experiment water was used as working fluid, the heat exchange taking place without the phase transformation. The proposed algorithm allowed obtaining useful correlation of partial coefficients of heat transfer calculation for the hot fluid which circulates through the inner annular space, in the transition regime.

Quadir et al.,[24] presented experimental investigation of the performance of a triple concentric pipe heat exchanger. Two combinations of the heat exchanger are used for this purpose and for insulated as well as non-insulated conditions of the heat exchanger. The first one named (N–H–C) which means that the raw water flows through the innermost pipe, hot water flows through the inner annulus and the cold water flows through the outer annulus. The second combination used is named as (C–H–N) where the cold water and raw water interchange between each other while hot water flow remains same as in (N– H–C) configuration. The results showed

that the hot water temperature drops to 30.76 °C from its entry temperature of 52.11° C in (N–H–C) arrangement; while the hot water temperature drops to 33.38 °C from its entry temperature of 50.48 °C in (C–H–N). It was found that the temperature variation along the length of pipe differs substantially for the two arrangements. Temperature of cold water increases rapidly in the non-insulated condition of N–H–C arrangement. Cross over points were found in N–H–C arrangement for higher volume flow rates of the three fluids

Basal and Unal [25] proposed a new type thermal energy storage system consisting of a triple concentric-tube arrangement for the storage performance enhancement. The motivation for the present proposal was that an annulus shaped PCM layer that was in contact with the heat transfer fluid from both inner and outer surfaces provides a larger heat transfer area. For the present purpose, a numerical investigation is conducted by using enthalpy method. Based on the numerical calculations, the effects of system parameters such as mass flow rate and the inlet temperature of the heat transfer fluid and the variation of the tube radii on the system performance were investigated parametrically. The results indicated that, a significant enhancement in the system performance can be achieved by replacing a classical hollow cylinder type storage with the presently proposed triple concentric-tube storage system. Another outcome of the present study was that the most important design parameters for a triple concentric-tube storage system were the radial location and the thickness of the PCM filled annulus.

Quadir et al.,[26] carried out numerical investigation of the performance of a triple concentric pipe heat exchanger .The outside diameters of the three pipes are 0.0508 m, 0.0762 m and 0.1016 m respectively, and their thickness is 1.5 mm only. The overall length of the

heat exchanger is 4 m. The three fluids being considered are hot water, cold water and the normal tap water. They concluded that the predicted temperature variations of the three fluids along the length of the heat exchanger using finite element method follow closely to those obtained from experiments in magnitude and trend provided the overall heat transfer coefficients evaluated from Batmaz and Sandeep relation are used.

Patrascioiu and Radulescu [27] described the experimental setup used for the study of oil–water heat transfer in the triple concentric-tube heat exchanger and mathematical model involves cooling a product in counter-current arrangement in a triple concentric-tube heat exchanger with straight and smooth tubes. For the model elaboration there have been used the equations of heat transfer and of fluid-dynamics, as well as a numerical algorithm to solve systems of non-linear equations. The results showed that the theoretical values of the outlet temperatures have been compared with the experimental temperatures, the average deviation ranging in the domain 3.5- 4.8 %.

Dharmik et al.,[28] showed the CFD analysis of triple concentric tube heat exchanger by using FLUENT Microsoft program. Triple concentric tube heat exchanger performs better than double concentric tube heat exchanger. Water has been used as a working fluid and copper was used as material of tubes. Hot water flows from inner annulus and cold water flows from inner tube and outer annulus. Effect of different inner tube diameters on performance of triple concentric tube heat exchanger was observed for five different inner tube diameters (8 mm, 10 mm, 12 mm, 14 mm and 16 mm). Results indicated that when increase in inner tube diameter heat transfer rates increase for three tubes. While the increase in inner annulus diameter heat transfer rate of hot fluid and inner cold fluid

increased up to 26 mm after that it decreased due to decrease in temperature difference and flow became laminar.

Singh et al.,[29] explained the thermo-hydraulic investigations for triple concentric-tube heat exchanger. The Reynolds number varied from 2800 to 11,000. Experimental investigations have been carried out to measure the variations in temperature of fluid streams along the length of heat exchanger and variations of friction factor and of Nusselt number with Reynolds number. It is concluded that the measured values of friction factors are the lowest for cold water in inner tube and the highest for intermediate temperature water in outer annulus while it varies in between for hot water in inner annulus.The results showed the effectiveness for co-current arrangement, counter-current arrangement, counter-current–co-current arrangement and co-current–counter-current arrangement has been found to be 0.36, 0.51, 0.42 and 0.39, respectively.

Wafelkar and Kamble [30] used different techniques to enhanced the performance of triple concentric heat exchanger. To enhance the effectiveness dimples have been made on the middle tube. Introduction of dimples on the tube surface can increase surface area available for heat transfer. The fluid used was water. Hot water will flow through the middle annular space while cold fluid will flow through the inner tube and outer annular space. The study was carried out to determine the effectiveness of triple tube heat exchanger with dimple tubing. A comparison of effectiveness in triple tube heat exchanger and double tube heat exchanger, it was found that for the same Reynolds number effectiveness of triple tube heat exchanger was 60% more than double tube heat exchanger. After experiments, results indicate that the effectiveness increases with decrease in Reynolds number (hot fluid). Maximum value of effectiveness is 0.4785

obtained at Reynolds number 1944.9454. Low Reynold number ensures maximum period of contact between the flowing fluids (hot & cold fluid).

Gomaa et al.,[31] carried out an experimental and numerical investigations of the triple concentric-tube heat exchanger were presented with particular reference to double tube heat exchanger. The purpose was to present a clear view on the thermo-fluid characteristics of this type of heat exchangers with different key design parameters leading to design optimization. Three fluids being considered which were chilled water in inner tube, hot water in inner annulus, and normal tap water in outer annulus. Numerical CFD model was developed using a finite volume discretization method. The numerical model was validated and then extended to cover more extra design parameters. Four flow patterns were conducted of counter current, co-current, counter current with co-current and co-current with counter current flow. Correlations of Nusselt number, friction factor and heat exchanger effectiveness with the dimensionless design parameters were also presented. The triple tube heat exchanger contributes higher heat exchanger effectiveness and more energy saving compared with double tube heat exchanger per unit length.

Sahoo et al. ,[32] noted an experimental investigation for helical triple concentric tube heat exchanger. The concentric tube heat exchanger was consisting of two annulus and one helical pipe. Different flow arrangements were used in this study that was N-H-C (normal fluid inside - hot at middle - cold in outer annulus) and C-H-N (cold fluid in inner pipe - hot in middle - normal fluid in outer annulus) with parallel and counter flow types. The results showed the N-H-C arrangement of flow was more effective and has more heat transfer rate than the C-H-N arrangement for both parallel and counter flow conditions. The second result showed that

the effectiveness of the heat exchanger is higher up to 20% in N-H-C counter flow as compared to C-H-N counter flow.

Saurabh et al.,[33] presented heat transfer CFD analysis for a concentric triple tube heat exchanger. Theoretical studies were carried out for numerical simulations and evaluation of heat transfer. The performance of Triple Concentric Tube Heat Exchanger was to be evaluated at variable operating conditions. Studies and experimentation have already been carried out for N-H-C and C-H-N configuration in Triple Tube Heat Exchanger. The numerical investigation also had already been carried out for various operating conditions. The results showed that when the flow rate was decreased in the hot tube there was decrease in the temperature rise of the normal and cold fluids.

Boultif and Bougriou [34] simulated a numerical analysis by using the finite difference method to describe the steady and unsteady state thermal behavior of triple concentric- tube heat exchanger with parallel flow and counter flow arrangements. One gives the temperature variations of the three fluids and three walls with time along the triple concentric-tube heat exchanger. The fluids have a time lag and the response of triple concentric-tube heat exchanger in parallel flow configuration was faster than those of a counterflow arrangement, its performances were always lower than those of a counterflow triple concentric-tube heat exchanger. The heat transfer coefficients by convection of the three fluids vary with time in addition to the temperature and the heat exchanger performances were lower in unsteady state than the steady state case.

Wafelkar and Raut,[35] reported an experimental study of heat transfer enhancement in triple tube heat exchanger with copper Oxide (CuO)and Aluminum Oxide (Al_2O_3) nano fluids. Hot water with

temperature range 40˚C to 53˚C will flow through the intermediate annulus area while cold fluid with temperature range of 28 ˚C to 32 ˚C will flow through the inner tube and outer annular space. The nanoparticles were mixed with hot fluid and readings were taken for plain water, 0.033 % volumetric concentration of CuO and 0.033 % volumetric concentration of Al_2O_3. Experimental investigation was carried out for different flow rate of hot fluid. The flow rate of cold fluid was kept constant that was 420 LPH. It was concluded that copper Oxide nanoparticle were expensive and give less effectiveness as compare to Aluminum Oxide. While Aluminum Oxide gives maximum effectiveness at volumetric concentration 0.033%. This gives most economical solution for use of Aluminum oxide - water nano fluid in heat transfer application.

Giovannoni et al.,[36] presented a numerical prediction of thermal performances in a concentric triple tube heat exchanger. A method to increase thermal efficiency and limiting fuel consumption is to recover heat from the combustion products to preheat the cold incoming mixture. Therefore, this study focuses on the interactions between combustion and heat exchanges at small scale. A numerical model of a three concentric tubes combustion chamber was developed and investigated with the aim of evaluating its thermal performances. A 17 species, 73 reactions skeletal mechanism able to describe methane oxidation was utilized for the purpose. A parametric study was carried out varying the mass flow rate and the thermal conductivity of the walls. Also, the effects of utilizing a flame holder in the combustion chamber were investigated. The models defined as double tube and triple tube systems were simulated at different mass flow rates (0.05 g/s, 0.1 g/s and 0.15 g/s), different wall thermal conductivities (0.5 W/m.K and 16 W/m.K) and included a porous medium in the combustion chamber. The conclusion showed that the triple tube

mode better thermal performance than the double tube, as the percentage of heat of combustion transferred to the cold mixture was always higher. Where the percentage reached 43% in the triple tube model and 25% in the double tube model at 0.05 g/s and adiabatic conditions.

Hossain et al.,[37] investigated experimentally the effect of triple concentric tube heat exchanger on the overall heat transfer coefficient. Used three copper tubes of diameter 41.2 mm, 25.35 mm and 12.6 mm and the length of the tubes are 580 mm, 740 mm and 857 mm, respectively. The objective of this study was to reduce the length and material cost as well as increase the heat transfer surface area by adding an intermediate tube to the double concentric tube heat exchanger. The performance of the heat exchanger for different inlet temperatures and mass flow rates are estimated and analyzed. It was found that the overall heat transfer coefficient for triple concentric tube heat exchanger 658.89 W/m^2 K. On the other hand, the overall heat transfer coefficient in equivalent double tube heat exchanger was found of 618.6 W/m ^{2}K. Therefore, for the same heat transfer area, the length of the heat exchanger was 65.17% reduced compared to double tube heat exchanger. It was also observed that heat transfer rate was higher at higher flow rate in inner tube, inner annular space and outer annular space.

Gomaa et al.,[38] carried out experimental and numerical investigation of the triple concentric-tube heat exchanger with inserted ribs. The purpose was to evaluate the performance characteristics of the triple tube heat exchanger with rib inserts. The investigation key design parameters involve water mass flow rate, flow pattern, temperature variation, rib height and rib pitch. Numerical CFD modeling was developed using FLUENT commercial code and validation criteria was done to extend the study parameters with extra ranges. The results revealed that, the

insertion of ribs to the inner annulus fluid flow of the triple tube heat exchanger participate a significant enhancement of the convective heat transfer. Higher performance index was obtained at higher rib pitch and lower rib height. A set of empirical expressions with the dimensionless design parameters have been predicted based on the obtained data.

Zeeshan et al.,[39] presented a numerical and experimental investigation of bi-annulus (two annulus) heat exchanger. The simulations were carried out for different polymer materials along with conventional tube materials mainly metal. The results showed that dimensionless temperature was higher for copper which was used as tube material. For axial length up to 70mm. the temperature rises for polypropylethylene (PEX), by low density polypropylene (LDPE) was 28.3% and 26.4% respectively. However, temperature variation is same for Polypropylene (PP) and Polyvinylidene fluoride (PVDF) for same axial distance. This temperature variation was increased to 72.4%, 67.2%, 58.62% and 56.89% for PEX, LDPE, PP and PVDF respectively as axial distance variation reaches the end of pipe.

Touatit and Bougriou [40] suggested optimal diameters of triple concentric-tube heat exchangers . In this study a techno-economic method to optimize the heat exchanger by determining the optimal diameter corresponding to the minimal total cost of the heat exchanger (functioning and investment). They have only one optimum tube diameter for each heat exchanger which corresponds to the minimum total cost of the heat exchanger (total frictional power expenditure and the fabrication of the heat exchanger) Three types of fluids were used the cold fluid (hydrogen) circulates in the internal tube, the oxygen flows in the outside annular passage and the nitrogen passes in the internal annulus passage. They calculated the effect of the (intermediate tube radius and central tube

radius) of the heat exchanger on the thermal and electric power expenditures and the economic costs. The efficiency of the heat exchanger decreases and then increases beyond intermediate tube radius 35 mm. The efficiency increases with increasing central tube radius, the inner annular passage section decreases the flow velocity and the heat transfer coefficient by convection increases thereby increasing the hot fluid cooling.

Saraireh [41] noted experimentally and numerically of triple pipe heat exchanger. Heat exchanger consists of three tubes made of aluminum with inner tube diameter 10 mm, intermediate tube diameter 20 mm, and outer tube diameter 30 mm. The raw water flows through inner and outer tube countercurrent flow to the hot water. The results indicate that the heat transfer rate between the hot water and raw water in the outer tube was higher than that between hot water and raw water in the inner tube. The larger heat transfer rate was due to the larger surface area between the hot water and the raw water in the outer tube as compared with that of inner tube. It is found that the heat transfer rate increases with increasing volume flow rate. The maximum heat transfer rate is found at higher volume flow rate of hot and raw water. Furthermore, Numerical simulations were carried out to obtain the heat transfer rate from the heat exchanger and compared with experimental data to validate the numerical model. It is found that the numerical model was capable of predicting the heat transfer rate.

Amanuel and Mishra [5] presented that optimization of heat transfer and pressure drop characteristics in a triple concentric tube heat exchanger had been done using the results of numerical simulation. A commercial CFD software ANSYS Fluent ver.17 has been employed for simulating the flow and heat transfer, while optimization has been done by Response surface methodology (RSM) and Genetic algorithm (GA). The effective parameters in the study were Reynolds number ($2500 \leq Re \leq 10000$) and

Length to hydraulic diameter ratio ($100 \leq L/D_h \leq 220$). The optimum values, as well as the functional relationship between the design factors (Re and L/D_h) and response variables (Nu and f), have also been developed. It has been found that both the design factors (Re and L/D_h) have a strong influence on the response variables (Nu and f). With the increase in Re (flow rate), a large growth in Nusselt number and decline in friction factor has been observed. However, with the increase in L/D_h, an enormous decrease in both Nusselt number and friction factor has been found.

Afzal et al.,[42] investigated the performance of triple tube heat exchanger using water and titanium-dioxide (TiO_2) nanofluid as the coolants. The heat exchanger consists of a helical tube (21.2m length) inserted between two straight concentric tubes to enhance the heat transfer. Hot water was flowed through these helical tubes. The air was passed through the central tube. The flow of air inside the centrally placed tube was kept constant at 4.5m/s. Change in effectiveness and overall heat transfer coefficient for flow rates from 20 lpm to 60 lpm was studied. Once the flow rate of hot water was changed and once the flow rate of raw water (flowing through the shell) was changed. The effectiveness reduced with increase in flow rate whereas the overall heat transfer coefficient increased. Overall heat transfer coefficient using water was in the range 50 – 100 $W/m^2 k$ whereas the overall heat transfer coefficient using TiO_2 nanofluid was in the range of 150 -200 W/m^2k. The results showed that the overall heat transfer coefficient increased for TiO_2 nanofluid compared to water was more significant at all flow rates. The improved thermal conductivity of TiO_2 nanofluid causes increase in overall heat transfer coefficient.

Lubis et al.,[43] designed and built triple concentric tube heat exchangers with counterflow which was used to reduce the temperature of the hot fluid. The hot fluid flows in the annulus section on the second

copper tube, then the cold fluid each flows through the first copper tube and annulus portion to the third copper tube. The hot fluid which is water with temperature 60ºC, to heat fluid used water heater with power 1000 watt while cold fluid which is water with temperature 25ºC. These three concentric tube heat exchangers with a total length of the first 2.57 m copper tube with 1½ inch diameter. The second copper tube is 2.22 m in diameter of 1 inch. The copper tube is 1.74 m long with a diameter of 1.75 inch. The fluid in and out fluid temperature gauges on the heat exchanger can be measured thermocouple which are then processed by software instacall and Tracerdag from a computer through the data acquisition module.

Memon et al.,[44] reported modeling and simulation of triple concentric tube heat exchanger by using seven different types of materials that are Copper, Aluminum, Titanium, Stailnless-Steel-430, Stainless-Steel-304, Silver & Copper-Nickle-Alloy. Energy equations were discretized using a finite element based technique and were solved using ANSYS software. This paper exhibits a comprehensive comparison between tube in tube heat exchanger (TTHE) and triple concentric tube heat exchanger (TCTHE) by simulation on ANSYS CFD and demonstrates that TCTHE has a greater heat transfer rate compared to TTHE because of greater heat transfer surface area and higher heat transfer coefficients, hence validating the experimental results. The model contains the three concentrated tubes having inner, intermediate and outer diameters 12mm, 26mm, and 40mm respectively. Cold water flowed though inner and outer tube while hot fluid (petroleum product) flowed in intermediate tube. Numerical results showed that mild steel as best possible tube material among the aforesaid materials.

Tuyen et al.,[45] studied optimization of a Liquid-to-suction triple tube heat exchanger of an R410A refrigerator. The main heat exchangers refrigeration systems include an evaporator, a condenser, and a liquid-to-suction heat exchanger. Where hot liquid refrigerant flows in the inner annulus, and the cold vapor refrigerant is divided between two spaces: the tube side and outer annulus. The study aimed to find the optimum refrigerant flow-rate fraction and diameter of the three tubes in terms of the heat-transfer rate and pressure drop. It is concluded that maximum heat transfers and minimum pressure loss achieved at triple-tube heat exchanger with diameters of 28.58, 34.93, and 41.28 mm and a mass flow-rate fraction of 0.66.

Abdelmagied [46] achieved that thermal and hydrodynamic characteristics of a new design heat exchanger called a triple spirally coiled tube heat exchanger (TSCTHE) were experimentally conducted and compared with a double spirally coiled tube heat exchanger (DSCTHE) as a particular reference. The new design was created by adding a third tube to a DSCTHE. The study carried out under consideration of turbulent fluid to fluid heat transfer condition. The research aims to present the TSCTHE thermo-hydraulic characteristics with different operating and design parameters. The experiments were carried out at four water inlet temperatures from 50°C to 80°C, four flow arrangements include parallel, counter, counter-parallel, and parallel-counter flow patterns with three coil inclination angles from 0° to 90°. The experimental runs applied at Dean number ranged from 500 to 6500 corresponding to Reynolds number from 3000 to 37000. The results obtained that the TSCTHE presents a significant enhancement of the Nusselt number compared to DSCTHE by 94.8% and 82.8% for both counter and parallel flow patterns, respectively. Also, the Nusselt number enhancement occurs with decreasing the hot water inlet

temperature from 80°C to 50°C by 40%, while the increment in pumping power was approximately neglected. Moreover, the highest values of Nusselt number occurred at counter flow patterns compared to other flow arrangements. In addition, the higher performance index was recorded at higher coil inclination angle of 90°. New correlations to predict the Nusselt number of hot water, friction factor, effectiveness, and performance index were presented.

Tanish et al.,[47] studied the heat exchangers performance was usually depending upon the physical characteristics of the fluid and the material. When a concentric tube was added in the intermediate space of a double pipe heat exchanger, they obtained a triple pipe heat exchanger. The performance of the triple was better than the double pipe, as it provided better heat transfer efficiencies. The results showed the comparison between double and triple concentric pipe, where the performance, LMTD and total effectiveness of the triple is better than the double pipe by 119.2 Watts, 0.5°C, 28.62% respectively. Basically, the additional pipe improves the heat transfer by providing an additional flow passage and a larger area for heat transfer area per unit length of the exchanger.

Arulkumar and Mathanraj [48] described the principle techniques of industrial importance as it deals with heat transfer analysis of concentric triple pipe heat exchanger employing blossom fins. Findings indicated that the use of fin arrangement was advantageous to enhance the performance of heat exchanger, LMTD, over all heat transfer and effectiveness was found to be increased. The additional fins improved the heat transfer by providing a larger area for heat transfer area per unit length of the exchanger. The net heat transfer, overall heat transfer, efficiency and effectiveness were calculated and compared for all the flow patterns and Counter flow 3 was found to have the best results among the flow patterns

with the maximum heat transfer, heat transfer coefficient, efficiency and effectiveness being 1642.09 watts, 1842.07 W/m^2 K, 0.57896 and 0.73 respectively.

2.3. Summary

It can be deduced that the most of the authors investigated the heat transfer performance of heat exchanger. Researches carried out double and triple concentric tube heat exchanger by using water as a heat transfer medium. It is observed that triple tube heat exchanger (TTHE) is very limited while comparing double tube heat exchanger (DTHE) due to its practical applications. Theoretically the researchers used different analytical and numerical methods as finite element, finite difference and finite volume. In addition, they used many techniques in CFD method, and different software package codes such as Fluent version, Ansys version and Solidworks version to solve this problem.

None of them were studied more than triple pipe heat exchanger. The present work designs four concentric pipe heat exchanger in order to cool the accessories systems for Al-Mussaib thermal power plant .In experimental study measured the parameters values of working fluid (water) in order to valid the performance for this new design of four concentric pipe heat exchanger(FCPHE) .In theoretical work used the Solidworks version (16) software in simulation the three-dimensions turbulent flow model to calculate these parameters such as temperature ,pressure , and velocity.

2.4. Originality Point

A new design of heat exchanger is achieved to solve the problem in Al-Mussaib thermal power plant. This new design consists of four copper pipes of diameter 1 inch (25.4 mm), 2 inch (50.8mm), 3 inch (76.2 mm)

and 4inch (101.6mm) and the length of the pipes are 2 m. The hot water is cooled at two stages. The first stage, the heat transfer is occurred between the hot water in first pipe and raw water in second pipe. While in the second stage, the heat transfer is occurred between the hot water in third pipe and raw water in second pipe and fourth pipe. The flow arrangement in first stage is counter flow while the flow arrangement in second stage is parallel.

Chapter Three

Experimental Work

Experimental Work

3.1. Introduction

A shell and tube heat exchanger type was used in the Al-Mussaib thermal power plant for cooling accessories of the power plant. This heat exchanger failed to reduce the hot water temperature to the required temperature for cooling.

In recent days, triple and double concentric tube heat exchangers are becoming popular because of more surface area. Heat transfer fluids play a major role in heat exchangers because they are based on the thermal conductivity of the fluid heat transfer.

In the present work, it is focused on designing, developing, and constructing a prototype rig as four concentric pipes heat exchanger (FCPHE) in order to improve its heat transfer and effectiveness of Al-Mussaib thermal power plant. In order to made and design this rig, it is needed to calculate all thermal physical properties and the limitation data of these properties for the working fluid which is flowing through this rig. Solidworks is used to simulate the design of the prototype. Also, a prototype module is designed for Al-Mussaib thermal power plant. As the initial step, obtain all the details of the existing heat exchanger such as number of tubes along with the relevant details of the masses flow rates, associated inlet and outlet temperatures, and selection of material pipe. Prototype was designed and constructed for all components depending upon these parameters as a reference function working of limitations parameters for Al-Mussaib thermal power plant. Appendix (A) is showed all these calculations for simulation design. The advantage of designs this prototype gives the mass flow rate value of working fluid with actual data for Al-Mussaib thermal power plant.

3.2. Fundamental of Rig Design

This rig is designed and fabricated as heat exchanger with four concentrated pipes (FCPHE). This rig is designed and fabricated in order to improve the cooling process in Al-Mussaib thermal power plant. The main components of the new design of heat exchangers are the four pipes which diameters are 1, 2, 3 and 4 inches. These pipes are collected together as annularly form. Raw water is used as working fluid.

The new design of this heat exchanger is depended upon the fundamental parameters which are calculated in design the prototype module as the data base function. These parameters are temperature and mass flow rate. This heat exchanger's function is to cool the hot water in two stages. As a first stage, heat transfer occurs between the hot water in the first pipe and the raw water in the second pipe to cool the hot water. The output hot water enters the third pipe in the second stage. Then, the heat transfer between the raw water in the second, third and fourth pipes to lower the temperature of hot water.

The limiting of input data are the mass flow rate and temperature of hot water. The pipes diameters and lengths are chosen by using the solidworks software tools depending upon the following steps of operation of designing in solidworks:

1. The main point in this design of heat exchanger is the diameter value of first pipe (hot water pipe).The selection diameter value of first pipe is depending upon the input values of mass flow rate and the inlet temperature of hot water which are feeding in solidworks program .Upon these input values the diameter value of first pipe is calculated .It was found the optimum diameter value of first pipe is 1 inch. This is the best value to reduce the hot water temperature from 40.8°C to 34.7 °C by two

stages of cooling in heat exchanger. Also, the temperature value of reduction exit hot water is calculated. Upon the selected of first pipe diameter another three pipes diameters are calculated by using annulus diameter ratio. These diameters values are 2, 3, and 4 inches,as shown in figure (3-1). When choosing, the diameter of the first pipe is 0.5 inches in design. Therefore, the diameter values of the second, third, and fourth pipes**,** are calculated using the equation of diameter ratios. Then, the temperature value of the exit hot water is 38.6°C. When trying to choose the diameter of the first pipe 2 inches .Then, the value of the exit hot water temperature is 37.5°C. These temperatures are not required in the design.

2. The mass flow rate and temperature of raw water in second pipe (60 l/min and 28°C) respectively. By using the annular diameter ratio that it is presented by **Van Zyl et al.[49]** . The diameter of the second pipe is chosen at 2 inches because it is the ideal diameter for providing adequate annular area for raw water. Because it is smaller than this diameter, it causes problems in the flow due to obstructions and other factors.

$$a = \frac{d_1}{d_2} \quad 0 < a < 1 \qquad \text{... (3.1)}$$

where

d_1 diameter of the first pipe

d_2 diameter of the second pipe

3. In the second stage, the hot water is cooled inside the third pipe, reducing the temperature from 38.5°C to 35 °C. According to equation (3.2), the third pipe has a diameter of 3 inches. This diameter gives a high total mass flow rate as well as a significant reduction in temperature.

$$a = \frac{d_2}{d_3} \quad 0 < a < 1 \qquad \text{... (3.2)}$$

where

d_3 diameter of the third pipe

4. To achieve the desired decrease in the temperature of the hot water, a fourth tube is inserted through which raw water with a temperature of 28°C is passed. The fourth pipe has a diameter of 4 inches. During the design process, it is estimated using the solidworks software program.

The length of the heat exchanger is determined by trial and error method using the solidworks program software. Where several lengths are chosen to get the appropriate length. Hot water with mass flow rate 40 l/min and temperature 40.8°C are taken as input data. Heat exchanger is designed to cool the hot water from 40°C to 35 °C. When designing and using flow simulation, it is found that the best length is 2 meters . This length has resulted in a significant reduction of hot water temperature to 35°C. This is the optimum length in designing to get the required cooling temperature.

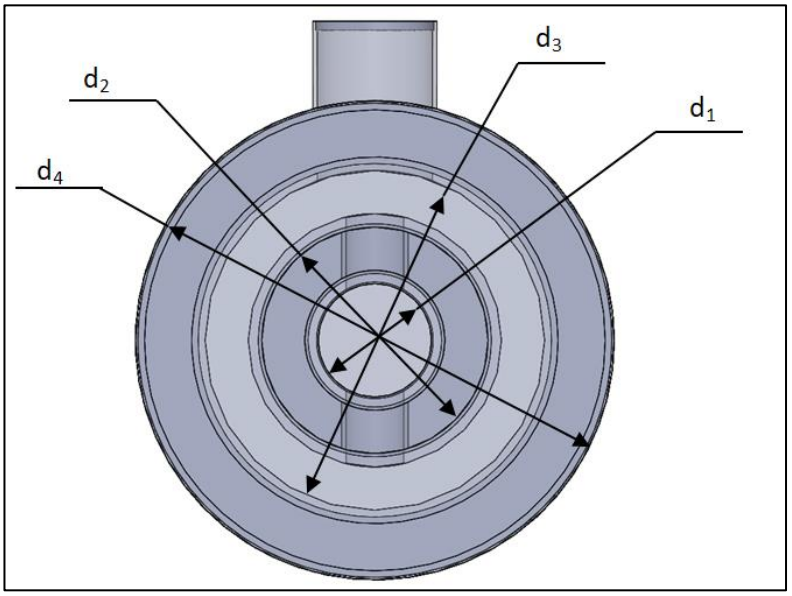

Figure (3-1) schematic of four concentric pipes heat exchanger (FCPHE)

3.3. Design consideration

A new design of a four-concentric-pipe heat exchanger is designed by using the steps in the Solidworks software program. All these steps are explained in appendix B.

3.4. Main Component of the Test Rig Design

The experimental rig is comprised of a heat exchanger, hot water rectangular tank, raw water rectangular tank, temperature data logger, thermocouples, three pumps, three flow meters, valves, and flexible tubes for connection ,as shown in figures(3-2)and (3-3). It is holed by metal frames and installed in the laboratory building of Mechanical Engineering Department, University of Babylon.

3.4.1. Heat exchanger (Test section)

The heat exchanger consisted of four concentric pipes. The outer pipe is made from plastic (PVC) with diameter 4 inch and length 2 m working as insulation for heat exchanger. The other three pipes are made from copper due to this material has a good a thermal conductivity **[50]** .The four pipes have dimensions of diameter 1 ,2,3,and 4 inch and fitted with length of 2 m , as shown in figures (3-4) and (3-5). Figure (3-4) shows the photograph of the four concentric four pipes heat exchanger. Figure (3-5) shows configuration of the four concentric pipes heat exchanger FCPHE with inserted support. The hot water is circulated through the first inner pipe to the third inner pipe as two stages. The raw water is circulated through the annulus second pipe as a counter-current flow with the first pipe through the first stage of cooling. The hot water in third pipe is cooled by raw water in fourth pipe and second pipe as second stage. The flow arrangement through the processing of cooling hot water in second stage is a parallel current flow. These parts have been fixed on the frame structure

which is designed to make both easy operation and maintenance through the heat exchanger. Table (3-1) gives the properties of pipes and the working fluid (water) that used in this test.

Figure (3-2) photograph of the experimental rig

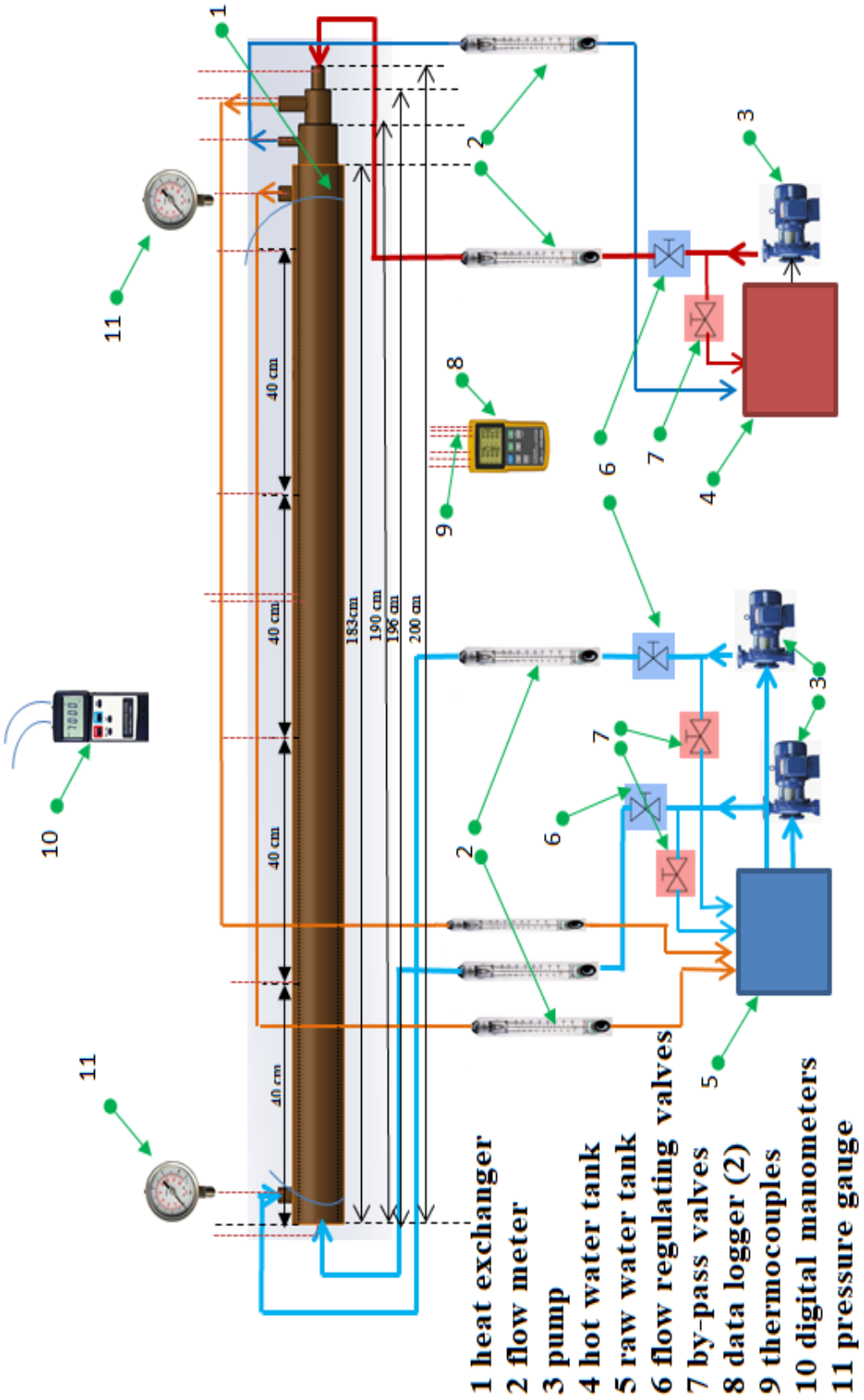

Figure (3-3) schematic diagram of the experimental set up.

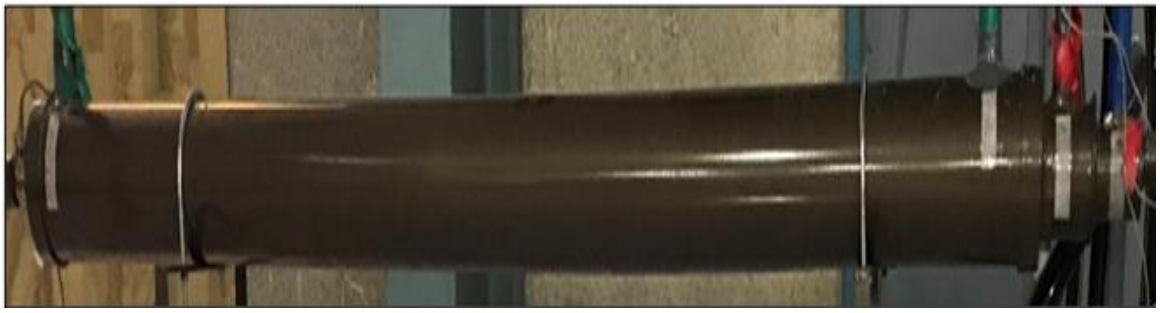

Figure (3-4) photograph of the four concentric pipes heat exchanger

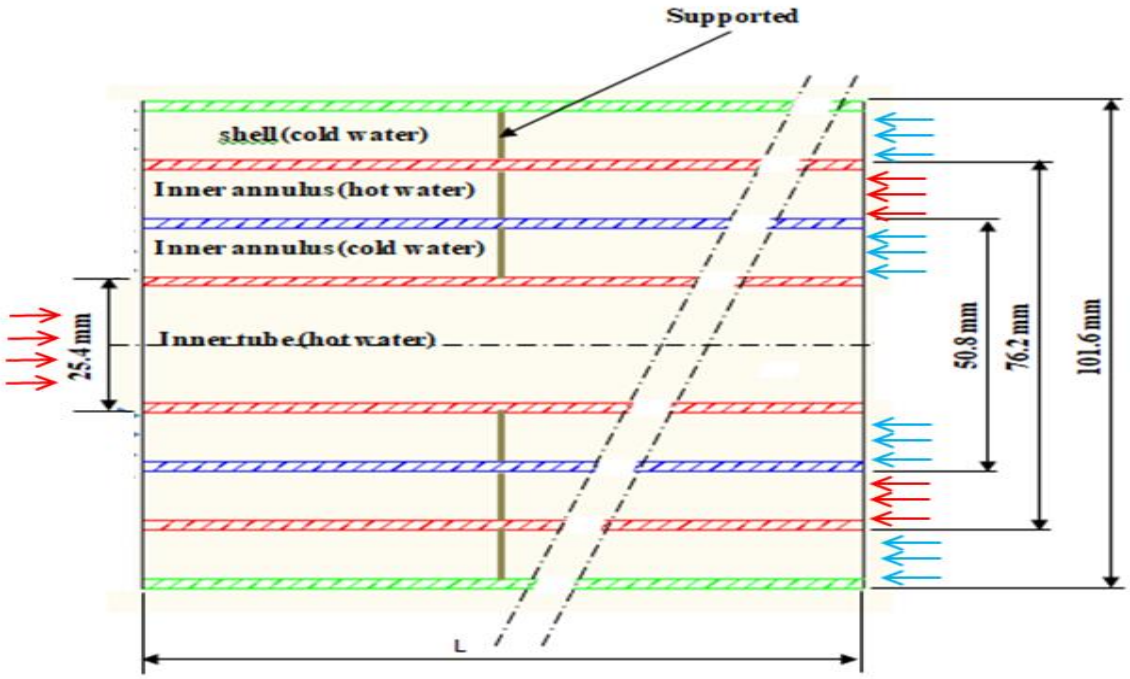

Figure (3-5) configuration of the four concentric pipes heat exchanger (FCPHE) with inserted support.

Table (3-1) thermo physical properties for materials and water.

Pipe properties			Water properties		
	Material of pipe	K W/m.°C		ρ kg/m^3	c_p J/kg. °C
First pipe	copper	401	Hot water	994.75	4178.375
Second pipe	copper	401	Raw water	996.1	4179.125
Third pipe	copper	401	Hot water	994.75	4178.375
Fourth pipe	Plastic	0.19	Raw water	996.1	4179.125

3.4.2. Water Tanks

Two water tanks are used and manufactured from galvanized steel sheet vessel as shown in figure (3-6). First tank with dimensions (1×0.75×0.75) m^3 is used to storage the raw water and supplies with two pumps in order to provide the raw water to second and fourth pipes. A second tank with dimensions (0.75×0.75×0.75) m^3 is used to storage the hot water by using heater with capacity (3000 W), it supplies desired temperature of the hot water which is controlled by the temperature controller to that supplied to first pipe. That heater is located in the bottom of the tank. This tank also provides with pump 0.37 kW.

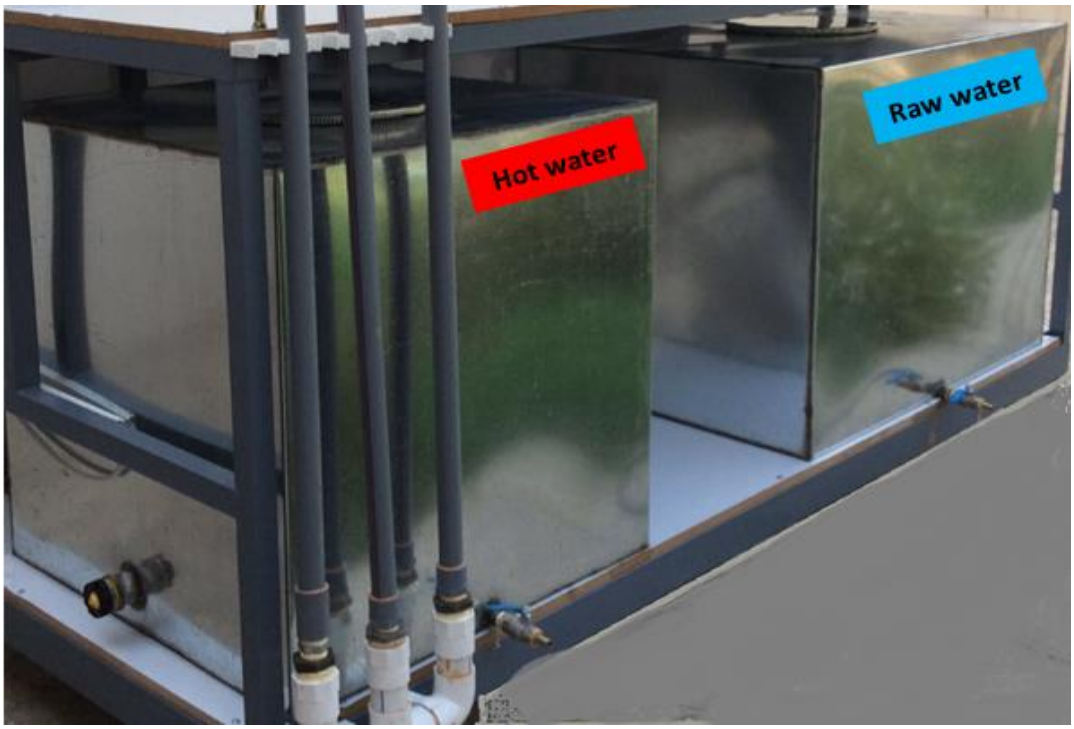

Figure (3-6) photograph of water tanks.

3.4.3. Water Pumps

Three centrifugal pumps are used in this experimental rig as shown in figure (3-7) and connected by series. First hot pump has a power 0.37 kW with maximum volumetric flow rate 50 l/min and maximum head 35 m. This pump supplies hot water to the inner pipe. Second pump has a power 0.75 kW with maximum volumetric flow rate 60 l/min and maximum head 50 m, which pumped raw water to second pipe. Third pump has a power 0.75kW with maximum volumetric flow rate 110 l/min and maximum head 30m, which pumped raw water to fourth pipe. Table (3-2) shows the specification of these water pumps.

Table (3-2) specification of water pumps

	Q_{max}(l/min)	Power(kW)	H_{max}(m)	Volt/Ampere
first pump	50	0.37	35	220/2.7
second pump	60	0.75	50	220/5
third pump	110	0.75	30	220/4.8

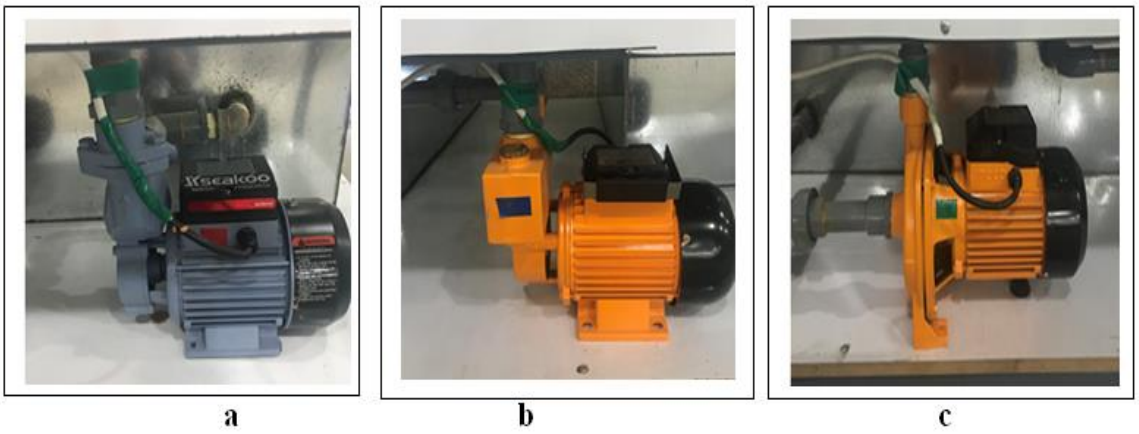

Figure (3-7) centrifugal pumps: a-first pump b-second pump c- third pump

3.5. Measurement Devices

3.5.1. Digital thermometer

Temperature recorder model (BTM-4208SD) with 12-channels is used to measure temperature after calibrating as shown in figure (3-8). It has SD card to save the temperature reading data with time, information into SD memory card and can be loaded to excel sheet. It uses for different sensor types of thermocouple such as J/K/T/R and S. It is worked as auto data logger or manual data logger sampling time range: (1 to 3600) seconds. The SD card capacity is 1 GB to 16 GB and it has Rs 232/USB computer interface, and the microcomputer circuit provides intelligent function with high accuracy.

In the present experimental work two devices are used in order to measure the temperature of 24 points over the domain of heat exchanger. Figure (3-9) shows the location of these thermocouples in different point of rig domain, and conducted by other side by two devices of temperature recorder. For (FCPHE), seven thermocouples are installed in the intake and exit of each pipe. On the other hand, seventeen thermocouples are fixed in various locations (0.2, 0.4, 0.8, 1, 1.2, 1.6) m along the pipe. The temperature measurement has been measured in all selected points using a date logger with SD ram that has been operated to read and save the temperature measurement during the time of device operation. These devices are working to catch the signal response, and transformation it to digital reading. Chromium-Aluminum thermocouple type -K is used for temperature measurements.

Figure (3-8) temperature recorder device

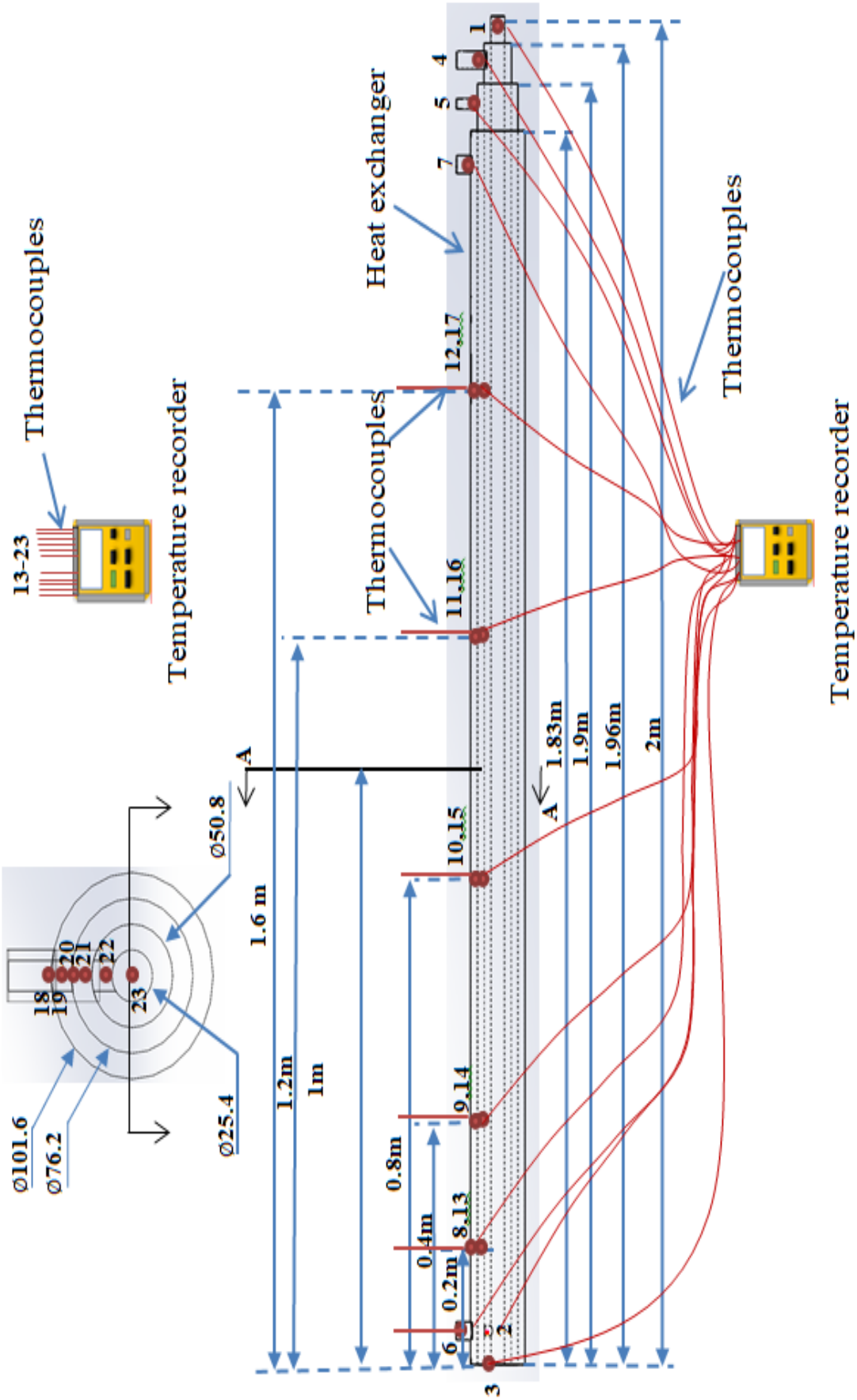

Figure (3-9) locations of thermocouples over the rig domain

3.5.1.1 Calibration of Temperature Reading

Temperatures reading by thermocouples are calibrated with a digital calibration device type (PROVA 123) as shown in figures (3-10). Thermocouple a chromium-aluminum type (K) is used for temperature measurement with range -200˚C to 1250 ˚C **[51]**. The process of calibration is done by reading the temperature values by two devices with varying temperature range from 28 to 45 ˚C.

The steps of the calibration apparatus are summarized in the following points as shown in figure (3-11):

1- Turn the power on and wait until the symbol disappears about 2 min

2- Plug the corresponding connector K type connector with thermocouple K type into TC terminals of calibrator and thermometer to be calibrated move the sliding switch to C, F position

3- Press the keypad (including the minus – button) to enter the value of temperature directly.

4- Enter the temperature value from 28 to 45˚C

5- Then, draw the relation between the temperatures reading for two devices. A polynomial equation is obtained to correct the temperature measurement readings as shown in figure (3-12):

$$T_{calibration} = 0.0002T_{read}^{3} - 0.0262T_{read}^{2} + 1.922T_{read} - 10.488 \quad \text{.....(3.3)}$$

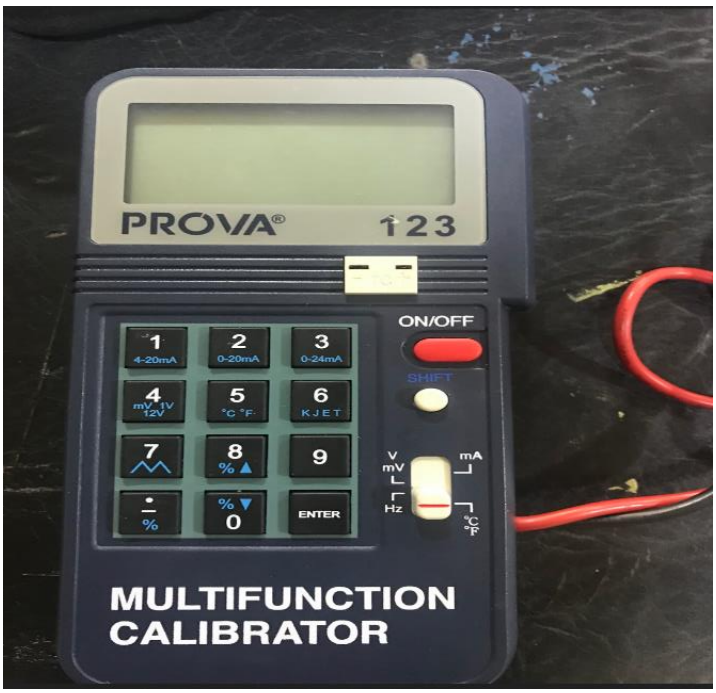

Figure (3-10) calibration device of temperature

Figure (3-11) photograph of calibration of temperature recorder

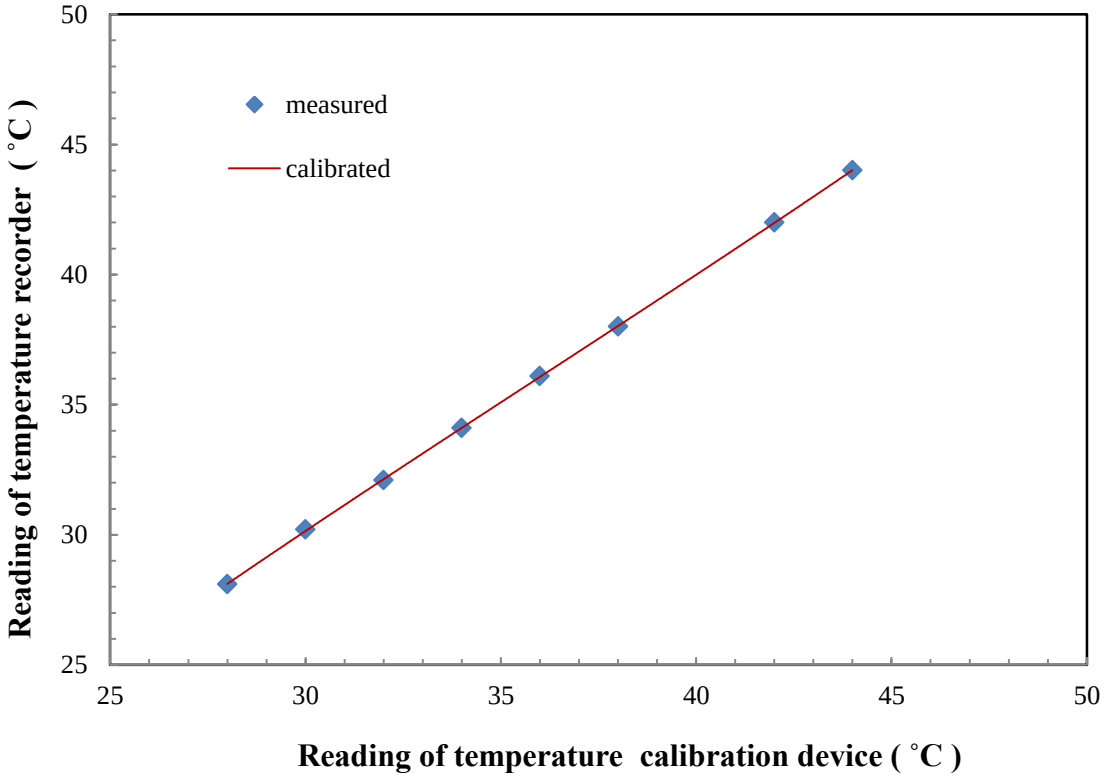

Figure (3-12) calibration curve of temperature recorder readings

3.5.2. Water Flow Meter

Seven flow meters are used to measure water flow rate as shown in figure (3-13). The volume flow of liquids can be calculated using this water flow meter. The flow meters' measuring ranges for hot water in the first and third pipes are 10 to 70 (l/min), raw water in the second pipe is 10 to 70 (l/min), and raw water in the fourth pipe is 10 to 130 (l/min). The flow meter (a) is vertically connected in inlet and outlet of pipe to measure the hot water flow rate in the first and third pip. The flow meter (b) is vertically connected in inlet and outlet of pipe to measure the raw water flow rate in the second pipe. The flow meter(c) that is attached vertically in inlet and outlet to measure the water flow rate in fourth pipe.

Figure (3-13) photograph of flow meter: a- using for hot water b-using for raw water c-using for raw water

3.5.2.1 Calibration of Flow meter

The calibration of the flow meters is performed by using a scaling volumetric flask and a stop watch to measure the time required to fill a specified volume of flask. Volumetric flask filled with the water that exits from the pipe of heat exchanger for each flow rate, and the time required for each flow rate is recorded. This process is repeated for each flow meter five times. Figures (3-14) and (3-15) show the polynomial equations are obtained to correct the flow rate measurement readings as:

For hot water flow meter (a) and raw water flow meter (b):

$$\dot{m}_{calibration}^{\circ} = 0.00005\ \dot{m}_{read}^{\circ 3} - 0.0023\ \dot{m}_{read}^{\circ 2} + 0.956\ \dot{m}_{read}^{\circ} + 0.244 \quad \ldots.(3.4)$$

For raw water flow meter (c):

$$m^{\circ}_{calibration} = 0.00006\, m^{\circ 3}_{read} + 0.0032\, m^{\circ 2}_{read} + 0.6243\, m^{\circ}_{read} + 1.0959 \quad ...(3.5)$$

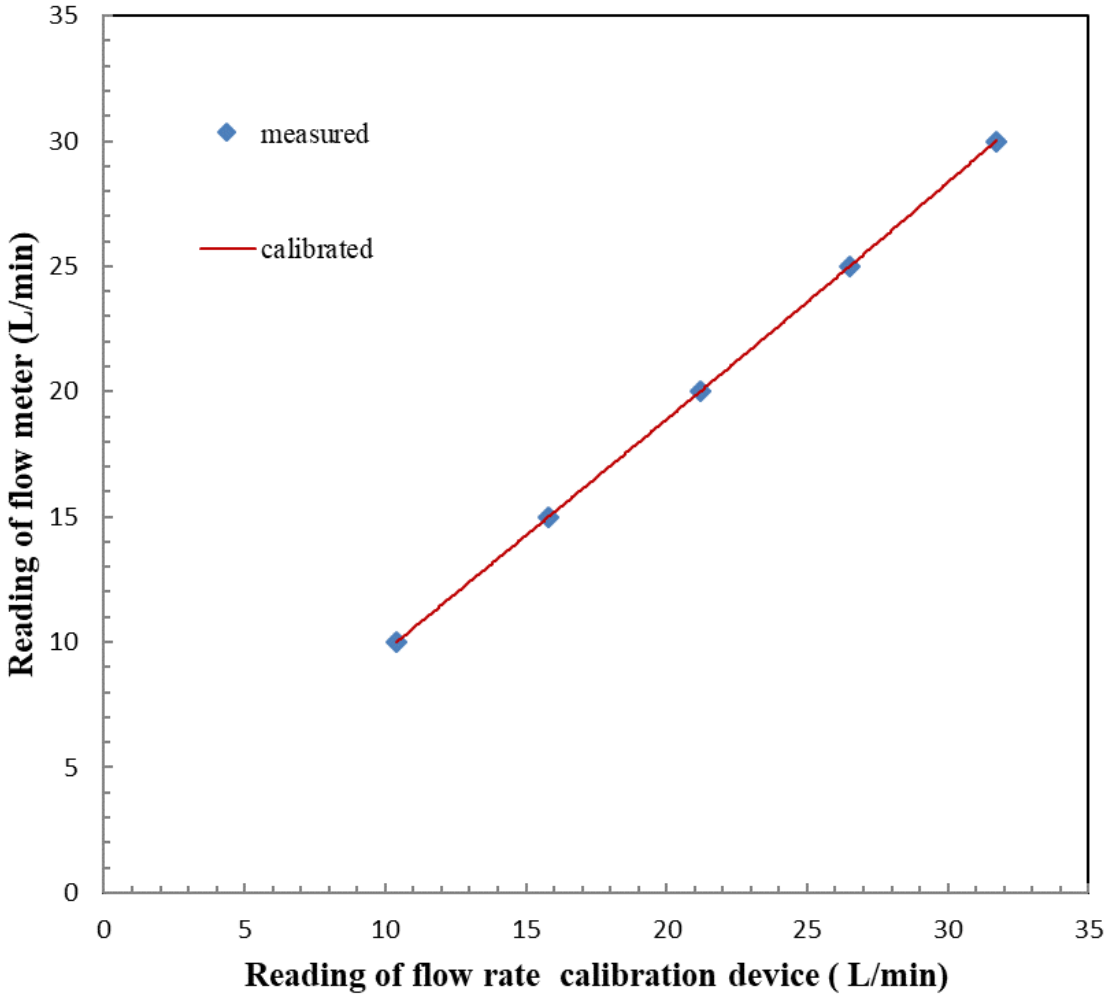

Figure (3-14) calibration curve of flow meter readings for flow meter (a) and flow meter (b)

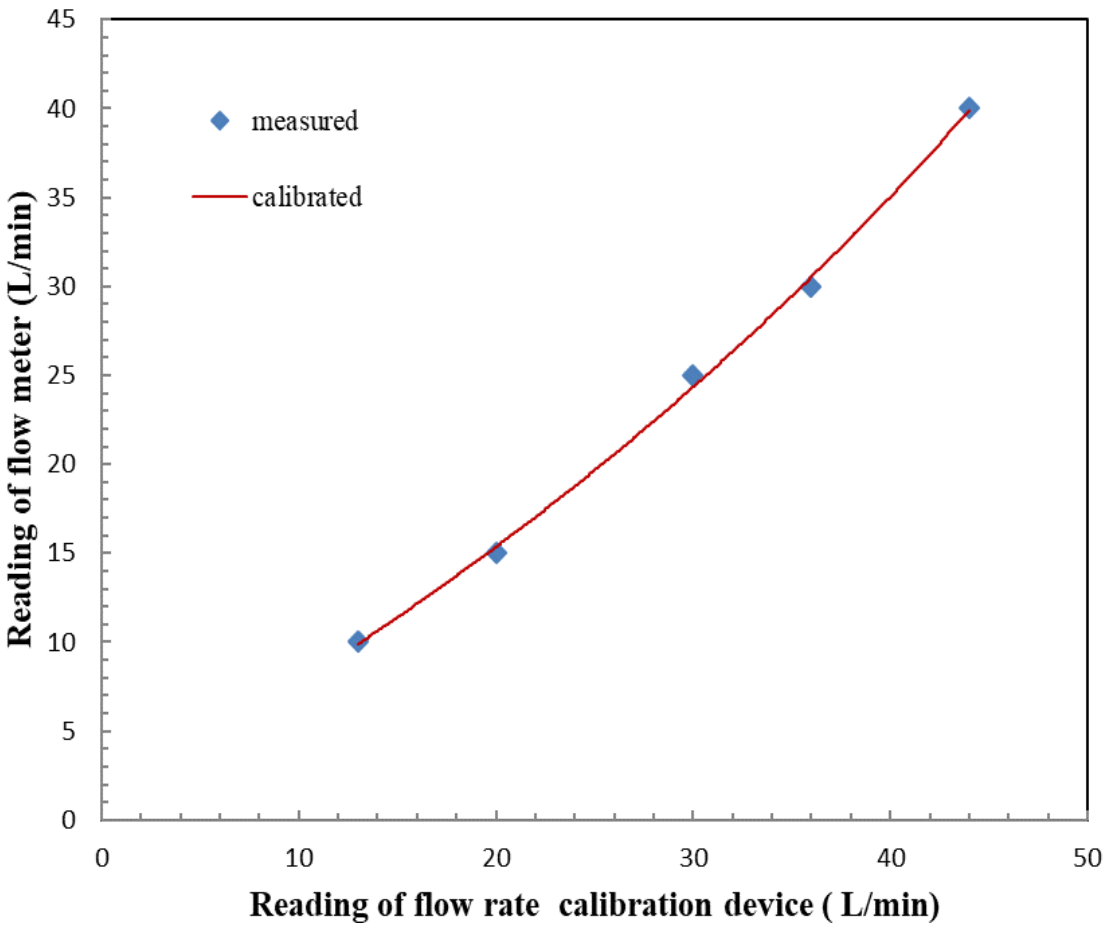

Figure (3-15) calibration curve of flow meter readings for flow meter(c)

3.5.3. Pressure Device

Digital pressure different manometer type Lutron PM-9107, as shown in figure (3-16). This device is used to measure the pressure difference between the inlet and the exit of the pipe. Digital pressure manometer can be measured the static pressure in range 0 to 7000 mbar (7 bar). Digital pressure manometer connects at inlet and outlet of each pipe of FCPHE to measure the pressure difference between the inlet and the exit of the pipe at these locations.

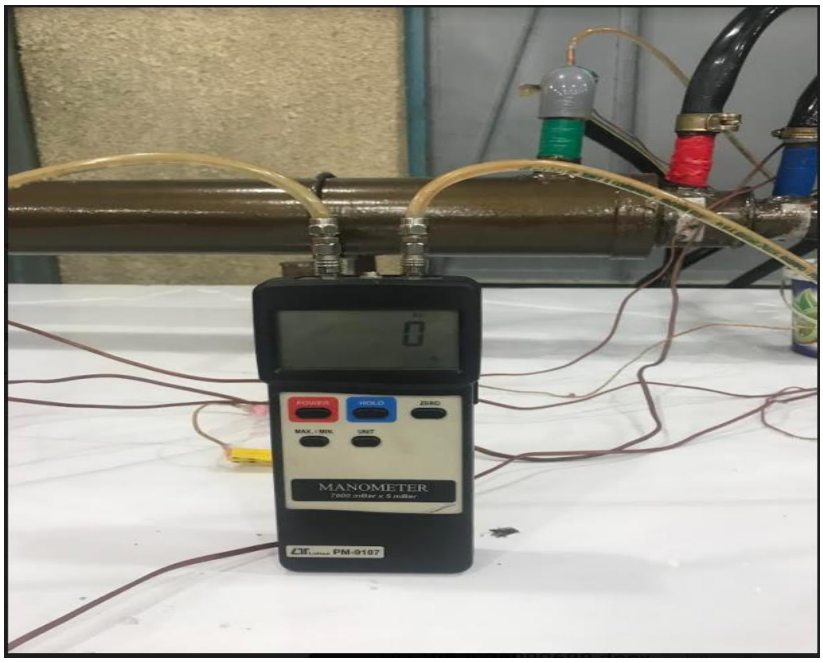

Figure (3-16) photograph of pressure recorder device

3.5.3.1 Calibration of Pressure

The readings of digital pressure different manometer are calibrated with Bourdon gauge pressure as shown in figure (3-17). Bourdon gauge pressure is used to measure the pressure of water, with a range of (0 to 4 bar). Bourdon gauge pressure connects at inlet and outlet of each pipe of FCPHE to measure the pressure at these locations. Equation (3-6) is used to compute the pressure drop for each pipe as follows:

$$\Delta P = P_{inlet} - P_{outlet} \quad \ldots (3.6)$$

The results of pressure drop for Bourdon gauge and digital pressure manometer are compared and represented by calibration curve in figure (3-18). A polynomial equation for this relation is obtained to correct these readings of pressure drop as:

$$\Delta P_{calibration} = 10.417\ \Delta P_{read}^{3} - 7.8125\ \Delta P_{read}^{2} + 2.8271\ \Delta P_{read} - 0.1262 \quad \ldots (3.7)$$

Figure (3-17) Bourdon gauge pressure

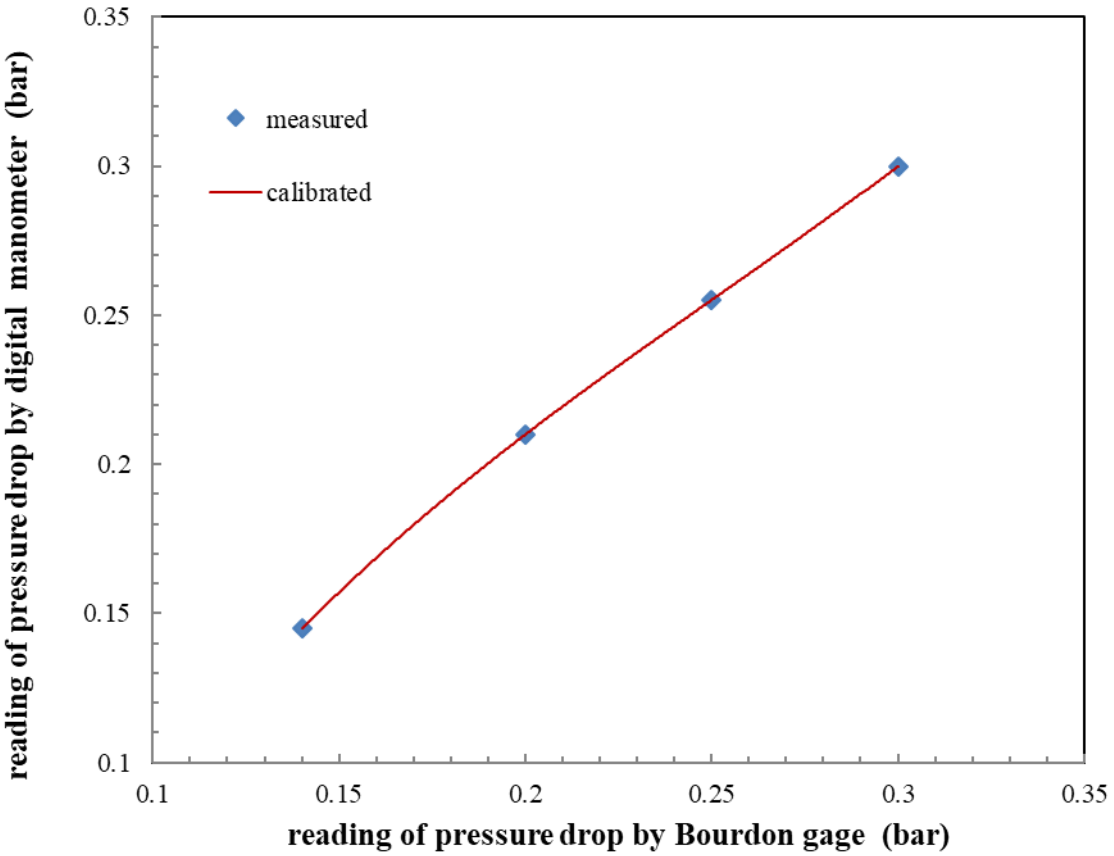

Figure (3-18) calibration curve of pressure device reading

3.6. Experimental Procedures

The experimental procedure starts by following steps:

1- Filling the two tanks by water and check the leakage from any point in the pipes and the tanks.

2- Switching on the circuit to supply power to the system when all valves of the water cycle are opened.

3- Turning on the heater which is fixed inside the hot water tank by setting the heater controller to the required temperature.

4- Adjusting the water flow rate in water cycle by the control valves of the water flow through main and bypass pipes before the test pipe and flow meter.

5- Turning on the water pumps and adjusts it at a certain water flow rate.

6- Recording the temperature in different point in the system after the steady state condition reached about two minutes. In the meantime, connect thermocouples with data loggers.

7- When steady state condition is reached after two minutes. Then, take the following readings:

- Water temperatures of inlet and outlet of each pipe
- The surface temperature of the third and fourth pipes
- Water temperature distribution at different distance along the pipes
- Pressure drop in each pipe
- Flow rate for working fluid for each pipe.

8- The date logger with SD ram are operated to read and save the temperature readings, through the time of device operating has been

measured in all selected points as in tables (3-5) to (3-10) after calibrated by equation (3.3).

9- The pressure drop is measured of four pipes of heat exchanger by digital pressure manometer. The measurements explain in tables (3-5) to (3-10) at different mass flow rate after calibrated by equation (3.7).

10- Repeating step 7 with a volume flow rate of (40) l/min for hot water in the first pipe, and using different values of mass flow rate for raw water in pipes two and four as shown in tables (3-5) to (3-10). These is done in order to see which mass flow rate of raw water in two pipes gives better performance of heat exchanger. That gives six cases of experimental tests.

3.7. Experimental Analysis

The following equations are used to calculate the effectiveness of the design four concentric pipe heat exchanger (FCPHE) that cools the Al-Mussaib thermal power plant to the appropriate temperature.

1. Heat Transfer Rates

Heat transfer rates of water in four pipes are calculated according to **Cengel [52]** as follows:

$$\dot{Q} = \dot{m}\, C_p \Delta T \quad \text{... (3.8)}$$

Then, the heat transfer rate of hot water in pipe one is calculated as:

$$\dot{Q}_{h1} = \dot{m}_{h1} C_{p_{h1}} (T_{h1\,in} - T_{h1\,out}) \quad \text{... (3.9)}$$

Heat transfer rate of raw water in pipe two is calculated as:

$$\dot{Q}_{n2} = \dot{m}_{n2} C_{p_{n2}} (T_{n2\,in} - T_{n2\,out}) \quad \text{... (3.10)}$$

Heat transfer rate of hot water in pipe three is calculated as:

$$\dot{Q}_{h3} = \dot{m}_{h3} C_{p_{h3}} (T_{h3\,in} - T_{h3\,out}) \quad \text{... (3.11)}$$

Heat transfer rate of raw water in pipe four is calculated as:

$$\dot{Q}_{n4} = \dot{m}_{n4} C_{p_{n4}} (T_{n4\,in} - T_{n4\,out}) \quad \text{... (3.12)}$$

2. Hydraulic diameter

According to the definition of the hydraulic diameter; for circular inner pipe the hydraulic diameter is the inside diameter of the pipe, while the hydraulic diameter for the inner annulus is computed by **Batmaz and Sandeep [21]** as follows:

$$d_{hy} = 4 \cdot \frac{\frac{\pi}{4}(d_{out}^2 - d_{in}^2)}{\pi(d_{out} + d_{in})} = (d_{out} - d_{in}) \quad \text{... (3.13)}$$

3. Velocity

Velocity of water in four pipes are calculated according to **Cengel [52]** as follows:

$$v = \frac{\dot{m}}{\rho\, A_c} \quad \text{… (3.14)}$$

Then, velocity of hot water in pipe one is calculated as:

$$v_1 = \frac{4\dot{m}_1}{\pi\, \rho_1\, d_1^2} \quad \text{… (3.15)}$$

Velocity of raw water in pipe two is calculated as:

$$v_2 = \frac{4\, \dot{m}_2^{\circ}}{\pi\, \rho_2\, (d_2^2 - d_1^2)} \quad \text{… (3.16)}$$

Velocity of hot water in pipe three is calculated as:

$$v_3 = \frac{4\,\dot{m_3}}{\pi\,\rho_3\,(d_3^2 - d_2^2)} \quad \ldots (3.17)$$

velocity of raw water in pipe four is calculated as:

$$v_4 = \frac{4\,\dot{m_4}}{\pi\,\rho_4\,(d_4^2 - d_3^2)} \quad \ldots (3.18)$$

4. Reynolds Number

Reynolds number is estimated for four pipes of heat exchanger by **Gomaa et al. [31]** as follows:

$$Re = \frac{\rho\,v\,d_h}{\mu} \quad \ldots (3.19)$$

5. Prandtl numbers

Prandtl numbers of water in four pipes are calculated according to **Vocale et al. [53]** as follows:

$$Pr = \frac{\mu\,C_p}{k_w} \quad \ldots (3.20)$$

6. Nusselt number

Nusselt number can be calculated for different flows. Through the inner pipe the flow was turbulent with Reynolds number between $3000 \leq Re \leq 5 \times 10^6$, so Nusselt number calculated by **Gnielinski [54]** as follows:

$$Nu_1 = \frac{(f_t/2)(Re_1 - 1000)Pr}{1 + 12.7(f_t/2)^{0.5}(Pr^{0.67} - 1)} \quad \ldots (3.21)$$

where

f_t is friction factor which was calculated as:

$$f_t = (1.58\ln(Re_1) - 3.28)^{-2} \quad \ldots (3.22)$$

While annular Nusselt numbers calculated by **Davis [55]** as follows:

$$Nu_{hy} = 0.038\, a^{0.15}(a-1)^{0.2} Re_{hy}^{0.8} Pr^{0.33} \quad \ldots (3.23)$$

where

a is the annular diameter ratio

Re_{hy} is the hydraulic Reynold number

7. Friction factor coefficient in annular space

The friction factor coefficient in annular space was presented by **Gnielinski [56]** as follows:

$$f_t = (1.8 \log(Re_{hy}^{*}) - 1.5\ )^{-2} \quad \ldots (3.24)$$

where

$$Re_h^{*} = Re_h \frac{(1+a_1^2)\ln a_1 + (1+a_1)}{(1-a_1)^2 \ln a_1} \quad \ldots (3.25)$$

$$a_1 = 1/a \quad \ldots (3.26)$$

8. Heat transfer coefficient

From definition of Nusselt number, heat transfer coefficient calculated as:

$$h = \frac{Nu\, k_w}{d_h} \quad \ldots (3.27)$$

where

k_w is the thermal conductivity of water

d_h is the hydraulic diameter for pipe

Nu is the nusselt number

9. Effectiveness of the heat exchanger

The overall effectiveness of the heat exchanger which is calculated by **Cengel [52]** as:

$$\varepsilon = \frac{\dot{Q}_{av}}{\dot{Q}_{max}} = \frac{\dot{Q}_{av}}{\dot{m} Cp\ (T_{h\,in} - T_{n\,in})} \quad \ldots (3.28)$$

Where the average rate of heat transfer rate $\dot{Q}_{av}$ is determined between the three fluid sides which is determine by **Gomaa et al.[57]** as:

$$\dot{Q}_{av} = \frac{\dot{Q}_h + \dot{Q}_n}{2} \quad \ldots (3.29)$$

where

$$\dot{Q}_h = \dot{m}_h\ Cp_h\ (T_{h\,in} - T_{h\,out}) \quad \ldots (3.30)$$

The heat balance between the hot water and raw water is calculated as:

$$\dot{Q}_h = \dot{Q}_n + \dot{Q}_{loss} \quad \ldots (3.31)$$

Where $\dot{Q}_{loss} \cong zero$ (neglected)

10. Overall heat transfer coefficient

There are four overall heat transfers coefficient. Two is for inner annular space and another is for outer annular space.

$$\frac{1}{U_{o1}} = \frac{d_{o1}}{d_{i1}\ h_1} + \frac{d_{o1} \ln(d_{o1}/d_{i1})}{2K_{copper}} + \frac{1}{h_2} \quad \ldots (3.32)$$

$$\frac{1}{U_{i2}} = \frac{d_{o2}}{d_{i2}\ h_3} + \frac{d_{o2} \ln(d_{o2}/d_{i2})}{2K_{copper}} + \frac{1}{h_2} \quad \ldots (3.33)$$

$$\frac{1}{U_{o2}} = \frac{d_{o2}}{d_{i2}\ h_2} + \frac{d_{o2} \ln(d_{o2}/d_{i2})}{2K_{copper}} + \frac{1}{h_3} \quad \ldots (3.34)$$

$$\frac{1}{U_{i3}} = \frac{d_{o3}}{d_{i3}\ h_4} + \frac{d_{o3} \ln(d_{o3}/d_{i3})}{2K_{copper}} + \frac{1}{h_3} \quad \ldots (3.35)$$

$$\frac{1}{U_{total}} = \frac{1}{U_{o1}} + \frac{1}{U_{i2}} + \frac{1}{U_{o2}} + \frac{1}{U_{i3}} \quad \dots (3.36)$$

$$U_{total} = \frac{1}{R_{th}} \quad \dots (3.37)$$

Where total thermal resistance can be calculated by **Cengel [52]** as :

$$R_{th} = \frac{1}{h_1 A_1} + \frac{\ln d_{o1}/d_{i1}}{2\pi K_{copper} L_1} + \frac{1}{h_2 A_2} + \frac{\ln d_{o2}/d_{i2}}{2\pi K_{copper} L_2} + \frac{1}{h_3 A_3} + \frac{\ln d_{o3}/d_{i3}}{2\pi K_{copper} L_3} + \frac{1}{h_4 A_4} \quad \dots (3.38)$$

11. Logarithmic Mean Temperature Difference (LMTD)

The log-mean temperature difference is presented by **Gomaa et al. [31]** as shown in figure (3-33):

$$LMTD_{av.} = \frac{LMTD_1 + LMTD_2 + LMTD_3}{3} \quad \dots (3.39)$$

Where $LMTD_1$ is the log-mean temperature difference between hot water which it flows in inner pipe and raw water which it flows in pipe two.

$$LMTD_1 = \frac{(T_{1in} - T_{2out}) - (T_{1out} - T_{2in})}{\ln(\frac{T_{1in} - T_{2out}}{T_{1out} - T_{2in}})} \quad \dots (3.40)$$

$LMTD_2$ is the log-mean temperature difference between hot water which it flows in pipe three and raw water which it flows in pipe two.

$$LMTD_2 = \frac{(T_{3in} - T_{2in}) - (T_{3out} - T_{2out})}{\ln(\frac{T_{3in} - T_{2in}}{T_{3out} - T_{2out}})} \quad \dots (3.41)$$

$LMTD_3$ is the log-mean temperature difference between hot water which it flows in pipe three and raw water which it flows in pipe four.

$$LMTD_3 = \frac{(T_{3in} - T_{4in}) - (T_{3out} - T_{3out})}{\ln(\frac{T_{3in} - T_{4in}}{T_{3out} - T_{4out}})} \quad \dots (3.42)$$

12. Rate of heat transfer

Rate of heat transfer for four concentric pipe heat exchanger FCPHE is determined as follows:

$$Q = U_{total}\, A_{total}\, LMTD_{av.} \quad \ldots (3.43)$$

where A_{total} is the total cross section area for FCPHE

$$A_{total} = \pi\, d\, L \quad \ldots (3.44)$$

13. Fouling factor

Heat exchanger performance typically degrades over time due to the deposition of deposits on heat transfer surfaces. The layer of deposits adds to the heat transfer resistance and slows down the rate of heat transmission in a heat exchanger. As a result, after accounting for the fouling factor, the total thermal resistance is calculated by **Cengel [52]** as:

$$R_{th1} = R_{th} + R_f \quad \ldots (3.45)$$

where R_f is the fouling factor

$$R_f = \frac{R_{fi}}{A_{i1}} + \frac{R_{fo}}{A_{o1}} + \frac{R_{fi}}{A_{i2}} + \frac{R_{fo}}{A_{o2}} + \frac{R_{fi}}{A_{i3}} + \frac{R_{fo}}{A_{o3}} \quad \ldots (3.46)$$

Where A_i and A_o are the areas of inner and outer surfaces for the pipes.

$$A_i = \pi d_i\, L \quad \ldots (3.47)$$

$$A_o = \pi d_o\, L \quad \ldots (3.48)$$

R_{fi} and R_{fo} have values 0.0001 presented by Tubular Exchange Manufacturers Association Appendix C shows the experimental data and the results of the experimental analysis.

3.8. Uncertainty Analysis

The error in measurement is defined as the difference between its true and measured value. However, this definition is not easy to know which the true quantity of these values is. Therefore, it is necessary to compute the uncertainty when presenting an experimental result. Generally, the uncertainty of measurement is described as the amount of errors or doubts in taking measurement. These errors or doubts are mainly due to measuring instrument, measuring process, human error (operator skills), and operating condition. For any set data, the standard uncertainty (SU) can be calculated by equation detailed by Bell as:

$$Su = \frac{S.D}{\sqrt{N}} \quad \ldots (3.49)$$

Where,

N is the total number of measurements in each pipe.

$S.D$ is the standard deviation which is calculated as:

$$S.D = \sqrt{\frac{\sum_{i=1}^{N}(X_i - X_{average})^2}{(N-1)}} \quad \ldots (3.50)$$

$X_{average}$ is the average readings of temperature or any function in pipe. The average experimental values of readings in each pipe which were repeating N times. The value of average readings is calculated as:

$$X_{average} = \frac{1}{N} \sum_{i=1}^{N} X_i \ \ldots\ldots \quad \ldots (3.51)$$

Where X_i is represented the values for measurements data of temperature or any function measured in each pipe. Then, all experimental analysis depending on measuring values are uncertain. Table (3-3), indicates the uncertainty for all parameter measurement.

Then the uncertainty in the results (U_R) can be written as Equation (3.52), whereU_1,U_2,…. to U_n are the uncertainty of independent variables[58].

$$U_R = \left[\left(\left(\frac{\partial R}{\partial x_1}\right) * U_1\right)^2 + \left(\left(\frac{\partial R}{\partial x_2}\right) * U_2\right)^2 + \cdots + \left(\left(\frac{\partial R}{\partial x_n}\right) * U_n\right)^2\right]^{0.5} \quad \ldots\ldots\ldots(3.52)$$

Appendix (D) gives a detailed calculation of the uncertainties of Nusselt number and heat transfer coefficient.

Table (3-3) temperature, mass flow rate and pressure drop uncertainty

Description	S.U. value (pipe1)	S.U. value (pipe2)	S.U. value (pipe 3)	S.U. value (pipe4)
T_{in} °C	0.065	0.085	0.104	0.155
T_{out} °C	0.104	0.132	0.129	0.165
$T_{0.2}$ °C			0.111	0.165
$T_{0.4}$ °C			0.085	0.075
$T_{0.8}$ °C			0.104	0.132
T_1 °C	0.125	0.121	0.091	0.118
$T_{1.2}$ °C			0.065	0.158
$T_{1.6}$ °C			0.119	0.189
$\dot{m}$ (l/min)	0.155	0.155	0.194	0.190
Δp(bar)	0.003	0.003	0.005	0.021

Chapter Four

MATHEMATICAL MODEL AND NUMERICAL ANALYSIS

Mathematical model and numerical analysis

4.1 Introduction

Four concentric pipe heat exchanger FCPHE which is developed from double and triple pipes heat exchanger. Computational fluids dynamic approach is used to determine output temperature, temperature distribution, velocity distribution, and pressure distribution for each fluid. It argues that turbulence models, in which the magnitudes of two turbulence quantities, the turbulence kinetic energy k and its dissipation rate ε, were calculated from transport equations solved simultaneously with those governing mean flow behaviors. The width of applicability of the model was demonstrated by reference to numerical computations of nine substantially different kinds of turbulent flow.

In this present work, the computational fluid dynamics (CFD) used to predict water flow and temperature fields in four concentric pipe heat exchanger (FCPHE). This is accomplished numerically by solving the partial differential governing equations for mass, momentum and energy. These equations are linearized, discretized, and applied to finite volume in the solver to obtain a detailed solution, including velocity and temperature fields. A commercially available CFD code (Solidwork Flow Simulation-Ver.2016) has been used to carry out the numerical calculations for the studied geometries. A three dimensional geometrical model of the problem with SOLIDWORKS software is used and mesh generation is done. The physical model is presented. The simulation is solved to predict the heat transfer and fluid flow characteristics by using k-ε.

4.2 Physical Geometry Model Description

The geometry in the present work consists from a four concentric pipes, where working fluids are hot water and cold water. Hot water enters

through the first and third pipe, while cold water enters through the second and fourth pipe. The modeled of 2D structure using the CAD solidwork ver.16 systems as shown in table (4-1) and figure (4-1) . The domain of the physical geometry is presented in figure (4-2). The pipes material is Copper for pipe1, pipe2 and pipe 3, while the material of pipe 4 is PVC. The physical properties of copper and thermal properties of water are taken from the SOLIDWORKS database as shown in table (4-2).

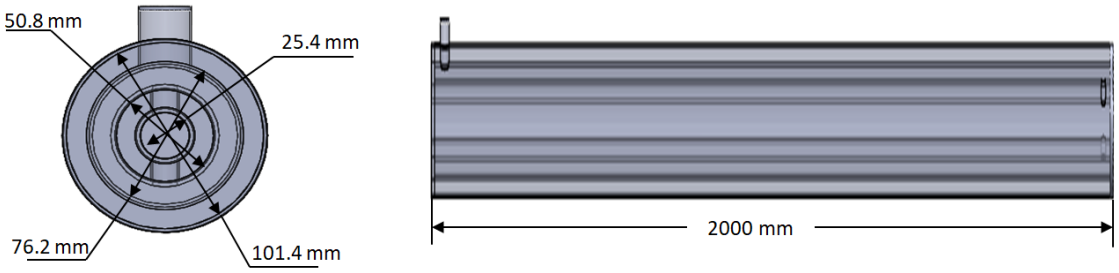

Figure (4-1) physical model of FCPHE

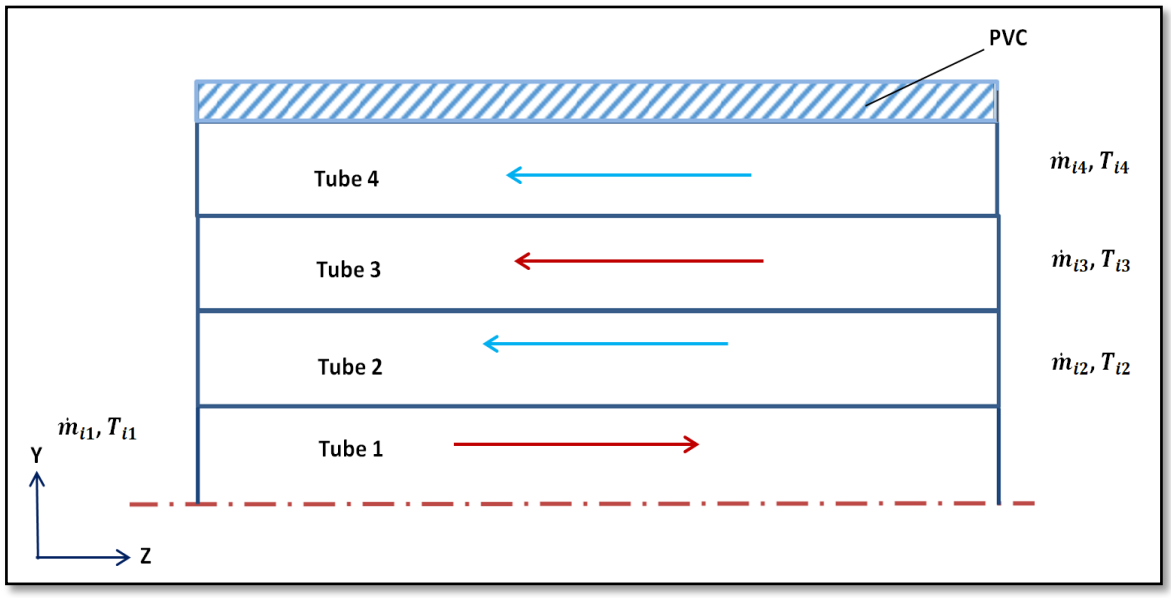

Figure (4-2) domain of FCPHE

Table (4-1) geometrical dimensions of FCPHE

No. of pipe	diameter (mm)	length (mm)	material
Pipe1	25.4	2000	copper
Pipe2	50.8	2000	copper
Pipe3	76.2	2000	copper
Pipe4	101.4	2000	PVC

Table (4-2) thermo-physical properties of pipes and working fluid in FCPHE

	k W/m.°C	μ mPa.sec	c_p J/kg.°C	ρ kg/m^3
Water	0.613	0.856	4179	997.1
Copper	401	-	385	8960
PVC	0.19	-	840	130

4.3 Mesh Generation

SOLIDWORKS Flow Simulation uses the finite volume method (FVM) to represent fluid and solid volumes with a mesh of three-dimensional rectangular cells. During solution of the Navier-Stokes fluid flow equations, the FVM establishes a balance of mass, energy and momentum at every fluid cell and at the extent of the fluid volume under consideration (the computational domain boundaries). A good finite volume mesh is a must to accurately capture the solid/fluid boundary and the fluid within the domain. The right and front views mesh for the FCPHE

are shown in figure (4-3). The detailed computational mesh for FCPHE is described in Table (4-3).

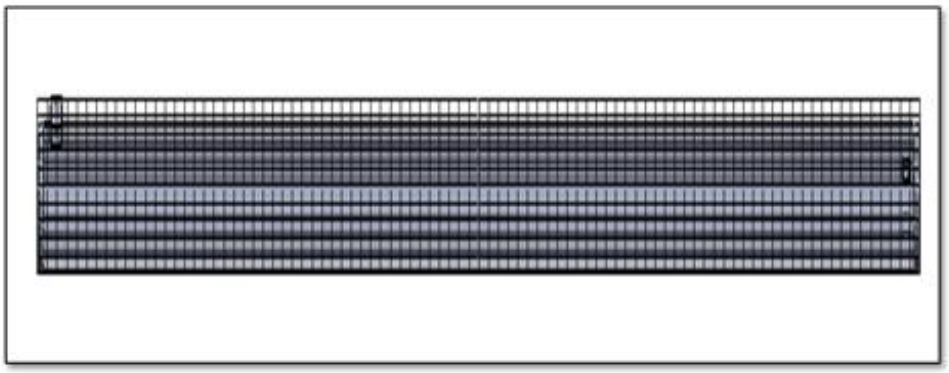

Figure (4-3) meshing of FCPHE by Solidworks

Table (4-3) Number of cells in the computational mesh

No. of Fluid cells	117754
No. of solid cells	124478
No. of partial cells	90054

4.4 Grid Independent Test

The grid independence test is a process used to find the optimal grid condition that has the smallest number of grids without generating a difference in the numerical results based on the evaluation of various grid conditions. In this case, the level is selected “level = 2”, which means that each cell in the mesh may be refined up to two times. As shown in figure (4-4).

The best way to check for a mesh independent solution is to plot a graph of the Nusselt number value vs the number of fluid cells, as shown in figure (4-5). From this test it can be concluded that the baste mesh value is at number of total cell 117754 with 0.5 % error for Nu.

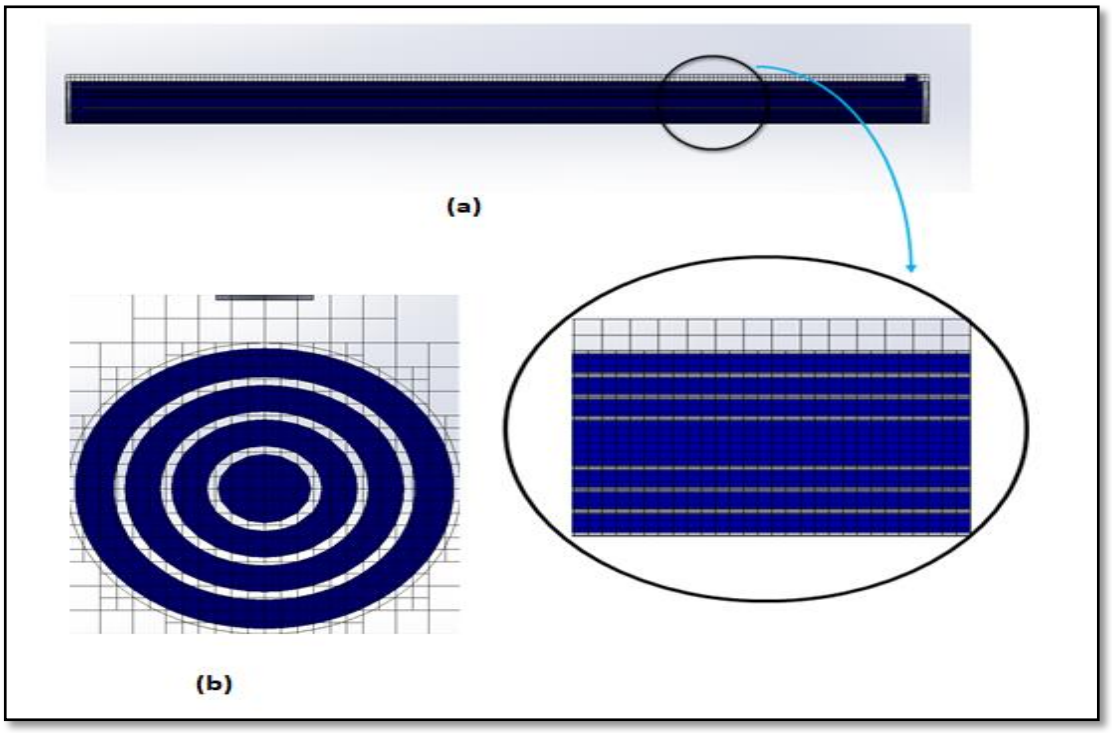

Figure (4-4) mesh refinement of FCPHE (a) right view of FCPHE (b) front view of FCPHE.

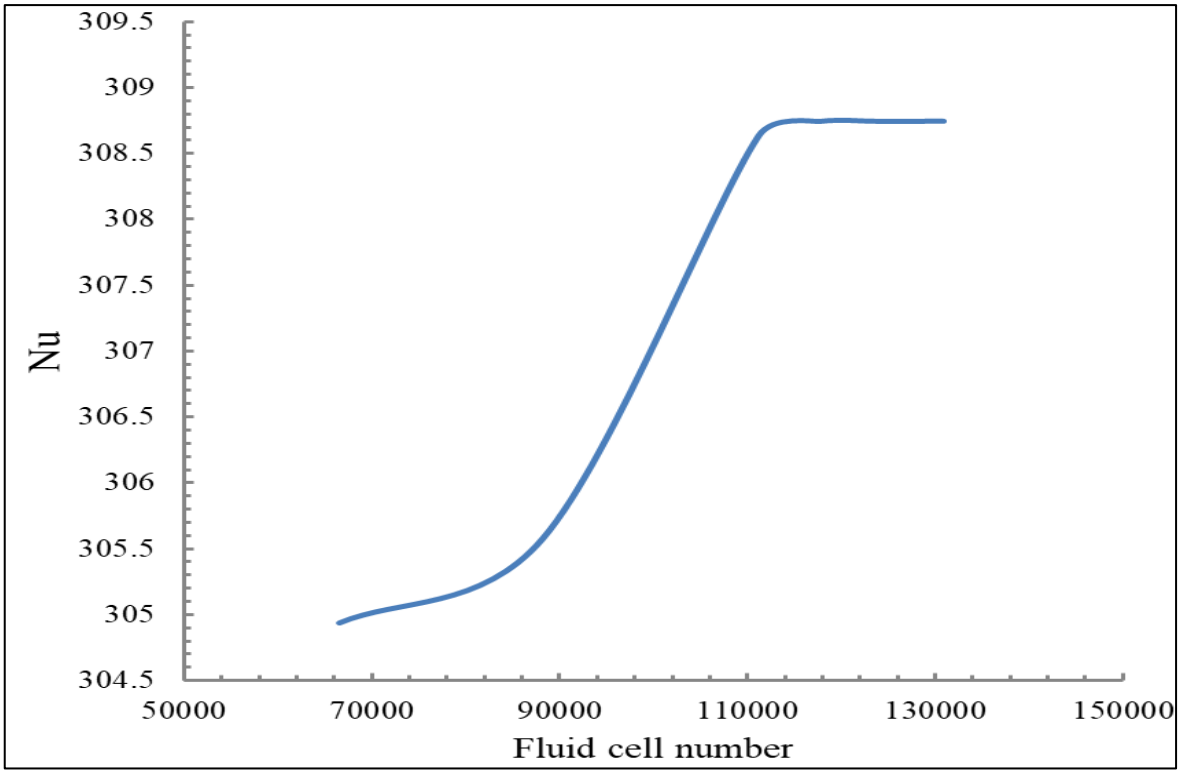

Figure (4-5) grid independent test.

4.5 Assumptions and Boundary Conditions

The following assumptions are supported to simplify numerical simulation:

1. Constant physical properties for working fluid.

2. No heat generation within the heat exchanger.

3. Incompressible and Newtonian fluid.

4. Steady state and turbulent flow.

5. No phase change for water (homogenous fluid).

6. No-slip condition.

As shown in Table (4-4) the boundary condition of FCPHE, as well as figure (4-6) shows physical geometry for four concentric pipe heat exchanger (FCPHE).

Table (4-4) input data for different cases study.

	Pipe 1		Pipe 2		Pipe 3		Pipe 4	
	$\dot{m}$ kg/sec	T_{in} °C	$\dot{m}$ kg/sec	T_{in} °C	$\dot{m}$ kg/sec	T_{in} °C	$\dot{m}$ kg/sec	T_{in} °C
Case 1	0.667	40.8	1	28	0.667	From solution	1.167	28
Case 2	0.667	40.8	0.833	28	0.667	From solution	1	28
Case 3	0.667	40.8	0.667	28	0.667	From solution	0.833	28

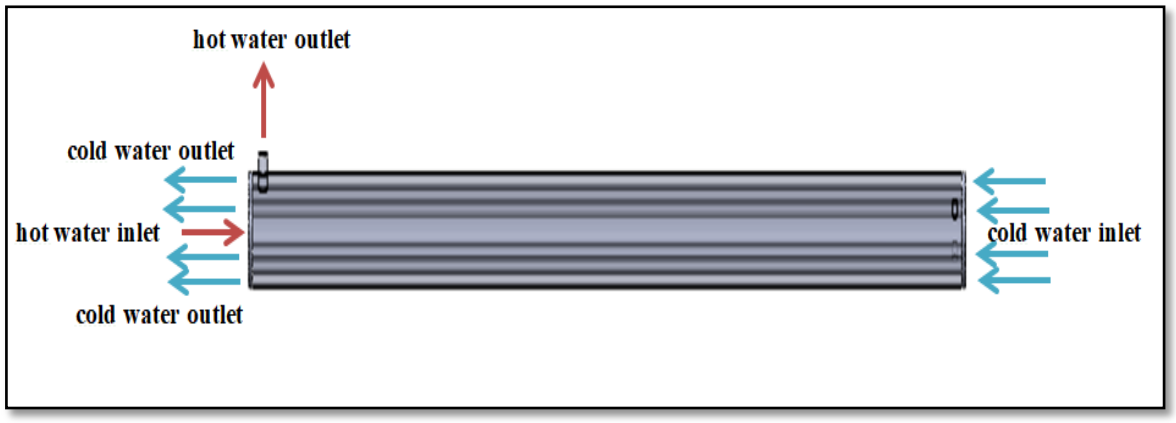

Figure (4-6) physical geometry for four concentric pipe heat exchanger (FCPHE)

4.6 Mathematical Model

For turbulent flow modelling, the *k-ε* turbulence model is adopted for calculation process. The governing equations for continuity, momentum, energy, k and ε in the computational domain which are showed by **Versteeg and Malalasekera [59]** as follows:

Continuity equation

The continuity equation is part of Euler's equations in fluid dynamics. Steady flow, incompressible fluid, ideal fluid and frictionless

$$\frac{\partial}{\partial x}(\rho u) + \frac{\partial}{\partial y}(\rho v) + \frac{\partial}{\partial z}(\rho w) = 0 \qquad \ldots (4.1)$$

Navier–Stokes equations

Nonlinear equations that describe the motion of Newtonian fluids, for viscous incompressible, Newtonian fluids may be written in the following form:

X. momentum equation:

$$\frac{\partial}{\partial x}(\rho uu)+\frac{\partial}{\partial y}(\rho uv)+\frac{\partial}{\partial z}(\rho uw)=-\frac{\partial p}{\partial x}+\frac{\partial}{\partial x}\left(\mu\frac{\partial u}{\partial x}\right)+\frac{\partial}{\partial y}\left(\mu\frac{\partial u}{\partial y}\right)+\frac{\partial}{\partial z}\left(\mu\frac{\partial u}{\partial z}\right)+\frac{1}{3}\frac{\partial}{\partial x}\left[\mu\left(\frac{\partial u}{\partial x}+\frac{\partial v}{\partial y}+\frac{\partial w}{\partial z}\right)\right]+\frac{\partial}{\partial x}\left(-\rho\overline{u'u'}\right)+\frac{\partial}{\partial y}\left(-\rho\overline{u'v'}\right)+\frac{\partial}{\partial z}\left(-\rho\overline{u'w'}\right) \quad \dots (4.2)$$

Y. momentum equation:

$$\frac{\partial}{\partial x}(\rho uv)+\frac{\partial}{\partial y}(\rho vv)+\frac{\partial}{\partial z}(\rho vw)=-\frac{\partial p}{\partial y}+\frac{\partial}{\partial x}\left(\mu\frac{\partial v}{\partial x}\right)+\frac{\partial}{\partial y}\left(\mu\frac{\partial v}{\partial y}\right)+\frac{\partial}{\partial z}\left(\mu\frac{\partial V}{\partial z}\right)+\frac{1}{3}\frac{\partial}{\partial y}\left[\mu\left(\frac{\partial u}{\partial x}+\frac{\partial v}{\partial y}+\frac{\partial w}{\partial z}\right)\right]+\frac{\partial}{\partial x}\left(-\rho\overline{u'v'}\right)+\frac{\partial}{\partial y}\left(-\rho\overline{v'v'}\right)+\frac{\partial}{\partial z}\left(-\rho\overline{v'w'}\right) \quad \dots (4.3)$$

Z. momentum equation:

$$\frac{\partial}{\partial x}(\rho uw)+\frac{\partial}{\partial y}(\rho vw)+\frac{\partial}{\partial z}(\rho ww)=-\frac{\partial p}{\partial z}+\frac{\partial}{\partial x}\left(\mu\frac{\partial w}{\partial x}\right)+\frac{\partial}{\partial y}\left(\mu\frac{\partial w}{\partial y}\right)+\frac{\partial}{\partial z}\left(\mu\frac{\partial w}{\partial z}\right)+\frac{1}{3}\frac{\partial}{\partial Z}\left[\mu\left(\frac{\partial u}{\partial x}+\frac{\partial v}{\partial y}+\frac{\partial w}{\partial z}\right)\right]+\frac{\partial}{\partial x}\left(-\rho\overline{u'w'}\right)+\frac{\partial}{\partial y}\left(-\rho\overline{v'w'}\right)+\frac{\partial}{\partial z}\left(-\rho\overline{w'w'}\right) \quad \dots (4.4)$$

Where the terms ($\rho\overline{v'w'}$, $-\rho\overline{w'w'}$, $\rho\overline{u'v'}$, $\rho\overline{v'w'}$, $\rho\overline{u'w'}$) are the turbulent Reynolds shear stress (τ_t) .

Conservation of thermal energy:

The energy equation per unit volume for steady, 3D flow is presented by **Li et al. [60]** as :

$$\frac{\partial}{\partial x}(\rho uT)+\frac{\partial}{\partial y}(\rho vT)+\frac{\partial}{\partial z}(\rho wtT)=\frac{\partial}{\partial x}\left(\Gamma\,\rho\frac{\partial T}{\partial x}\right)+\frac{\partial}{\partial y}\left(\Gamma\,\rho\frac{\partial T}{\partial y}\right)+\frac{\partial}{\partial z}\left(\Gamma\,\rho\frac{\partial T}{\partial z}\right)+\frac{\partial}{\partial x}\left(-\rho\overline{u'T'}\right)+\frac{\partial}{\partial y}\left(-\rho\overline{v'T'}\right)+\frac{\partial}{\partial z}\left(-\rho\overline{w'T'}\right)+S_t \quad \dots\dots(4.5)$$

Where Γ is diffusivity, the term (St) is source term and term $(-\rho\overline{u'T'}, -\rho\overline{v'T'}$ and$-\rho\overline{w'T'})$ are the turbulent heat fluxes respectively

4.7 Turbulence models

The *k-ε* turbulence model is presented by **Arani and Moradi [61]** as follows:

Turbulent kinetic energy:

$$\frac{\partial}{\partial x_i}(\rho u_i k) = \frac{\partial}{\partial x_i}\left(\left(\mu + \frac{\mu_t}{\sigma_k}\right)\frac{\partial k}{\partial x_i}\right) + S_k \quad \ldots (4.6)$$

Turbulent dissipation energy:

$$\frac{\partial}{\partial x_i}(\rho u_i \varepsilon) = \frac{\partial}{\partial x_i}\left(\left(\mu + \frac{\mu_t}{\sigma_\varepsilon}\right)\frac{\partial \varepsilon}{\partial x_i}\right) + S_\varepsilon \quad \ldots (4.7)$$

where the source terms S_k and S_ε are defined as:

$$S_k = \tau_{ij}^R \frac{\partial u_i}{\partial x_j} - \rho\varepsilon + \mu_t P_B \quad \ldots (4.8)$$

$$S_\varepsilon = C_{\varepsilon 1}\frac{\varepsilon}{k}\left(f_1 \tau_{ij}^R \frac{\partial u_i}{\partial x_i} + \mu_t C_B P_B\right) - C_{\varepsilon 2} f_2 \frac{\rho\varepsilon^2}{k} \quad \ldots (4.9)$$

Where P_B represents the turbulent generation due to buoyancy forces and can be written as

$$P_B = -\frac{g_i}{\sigma_B}\frac{1}{\rho}\frac{\partial \rho}{x_i} \quad \ldots (4.10)$$

Where g_i is the component of gravitational acceleration in directionx_i, the constants σ_B = 0.9, and constant C_B is defined as: C_B= 1 when $P_B > 0$, and 0 otherwise; and, following the Boussinesq assumption, the Reynolds stress tensor for Newtonian fluids has the following form:

$$\tau_{ij}^{R} = \mu\left(\frac{\partial u_i}{\partial x_j} + \frac{\partial u_j}{\partial x_i} - \frac{2}{3}\delta_{ij}\frac{\delta u_k}{\delta x_k}\right) - \frac{2}{3}\delta_{ij}\rho\, k \quad \ldots (4.11)$$

Where $\delta_{ij}$is referring to the Kronecker delta function (it is equal to unity when i = j, and zero otherwise), μ is the dynamic viscosity coefficient, k is the turbulent kinetic energy andμ_t is the turbulent eddy viscosity coefficient, which is determined from:

$$\mu_t = f_\mu \frac{c_\mu \rho k^2}{\varepsilon} \quad \ldots (4.12)$$

where f_μ is a turbulent viscosity factor represented as follows:

$$f_\mu = (1 - e^{-0.0165\, R_y})\left(1 + \frac{20.5}{R_T}\right) \quad \ldots (4.13)$$

The distance from the point to the wall is y and Lam and Bremhorst's damping functions are calculated as follows:

$$f_1 = 1 + \left(\frac{0.05}{f_\mu}\right)^3 \quad \ldots (4.14)$$

$$f_2 = 1 - \exp(-R_T^2) \quad \ldots (4.15)$$

The constants *Cμ*, *Cε1*, *Cε2, σk, σε* are defined empirically. In Flow Simulation the following typical values are used:

Cμ = 0.09, *Cε1* = 1.44, *Cε2* = 1.92, *σk* = 1, *σε* = 1.3

Where Lewis number Le = 1 the diffusive heat flux is defined as:

$$q_i = \left(\frac{\mu}{\mathrm{Pr}} + \frac{\mu_t}{\sigma_c}\right)\frac{\partial h}{\partial x_i}, i = 1,2,3 \quad \ldots (4.16)$$

Here the constant *σc* = 0.9, Pr is the Prandtl number, and *h* is the thermal enthalpy.

4.8 Analysis Procedure

The solid works flow simulation approach is based on two main principles which is presented by ***Sobachkin and Dumnov [62]*** as :

1. Direct use of native CAD as the source of geometry information

2. Combination of full 3D CFD modelling with simpler engineering methods in the cases where the mesh resolution is insufficient for full 3D simulation.

Therefor the numerical analysis requires the following steps:

1. A grid of points at which to store the variables calculated by CFD.

2. Boundary conditions required for defining all the conditions at the boundaries of the flow domain and which enable the boundary values of all variables to be calculated.

3. Physical fluid properties.

4. For turbulent flow modelling, the $k-\varepsilon$ turbulence model is adopted for the calculation process.

5. Initial conditions used to provide an initial guess of the solution variables in a steady state and transient simulations.

6. Solver control parameters required to control the behavior of the numerical solution process.

4.9 CFD solvers

The standard wall functions were employed for the near wall region to accurately simulate the thermos-hydraulic performance. The governing equations mentioned above were discretized by the finite volume method with SIMPLE pressure velocity coupling algorithm as shown in figure (4-7).

By using the Quadratic Upwind Interpolation for Convective Kinematics (QUICK) scheme for both the convective and diffusive terms in the numerical simulation, which is presented by **Nishikawa [63]**. The convergence criterion was taken as 10^{-4} for the flow equations and 10^{-8} for the energy equation.

4.10 Finite volume solution methods

The finite volume solution method can either use a "segregated" or a "coupled" solution procedure. With segregated methods an equation for a certain variable is solved for all cells, and then the equation for the next variable is solved for all cells, etc. With coupled methods, for a given cell equation for all variables are solved, and that process is then repeated for all cells. The segregated solution method is the default method in most commercial finite volume codes. As shown in figure (4-8) the segregated solution procedure and figure (4-9) shows the coupled solution procedure. Appendix (E) described the numerical procedure for finite volume.

4.11 The multigrid solver

The algebraic equation (4.20) can be solved by sweeping through the domain cell-by-cell in an iterative manner. This method reduces local errors quickly and speed up convergence for Large number of cells, Large cell aspect ratios (e.g. $\Delta z/\Delta y > 9$), and Large differences in thermal conductivity such as in conjugate heat transfer problems. The multigrid

solver uses a sequence of grids going from fine to coarse. The solution on the coarser meshes is used as a starting point for solutions on the finer meshes. This accelerates convergence on the fine mesh. Coarse mesh calculations only accelerate convergence and do not change the final answer.as shown in figure (4-10)

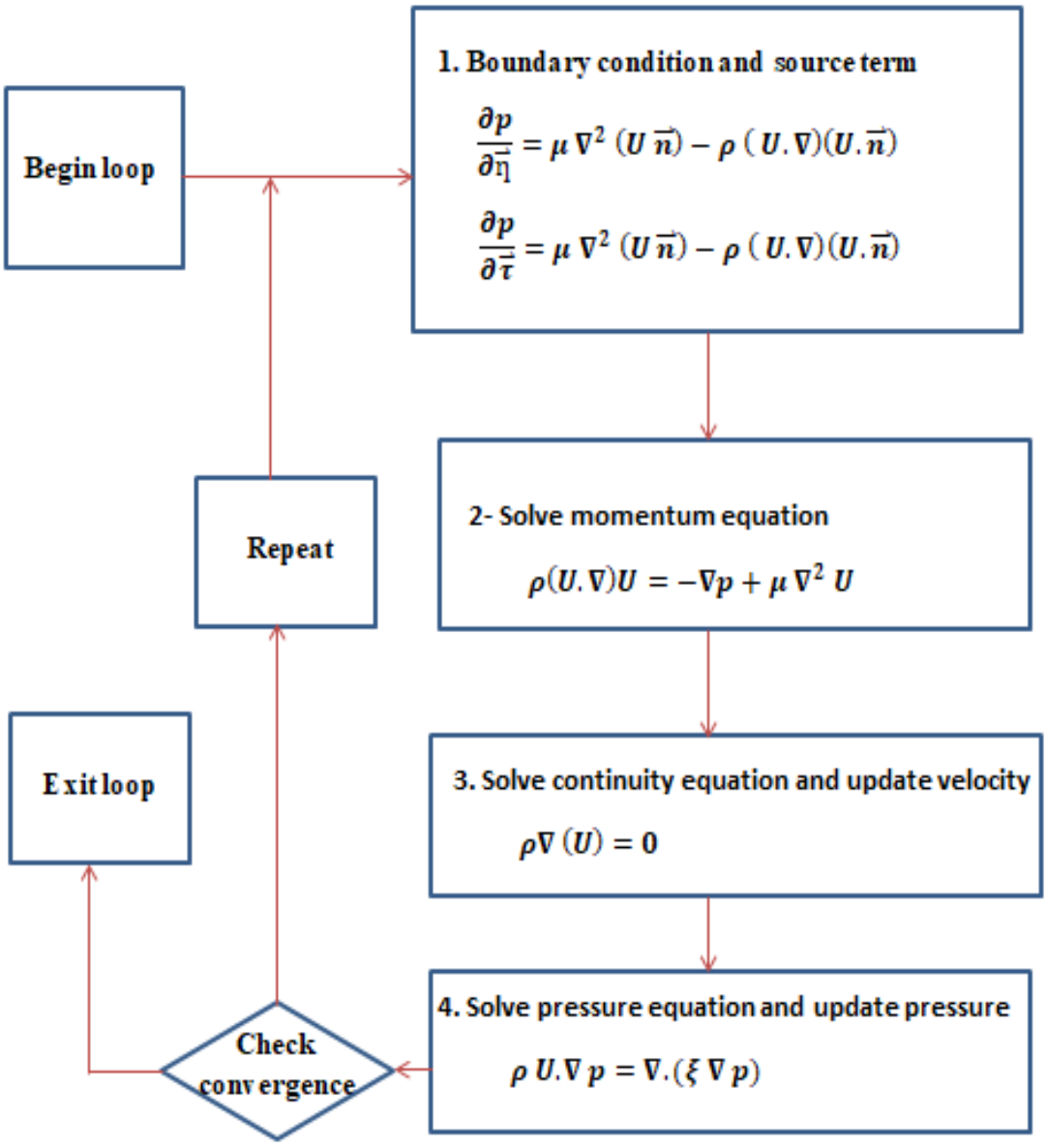

Figure (4-7) flowchart for SIMPLE pressure-velocity coupling method. Ref. [64].

.

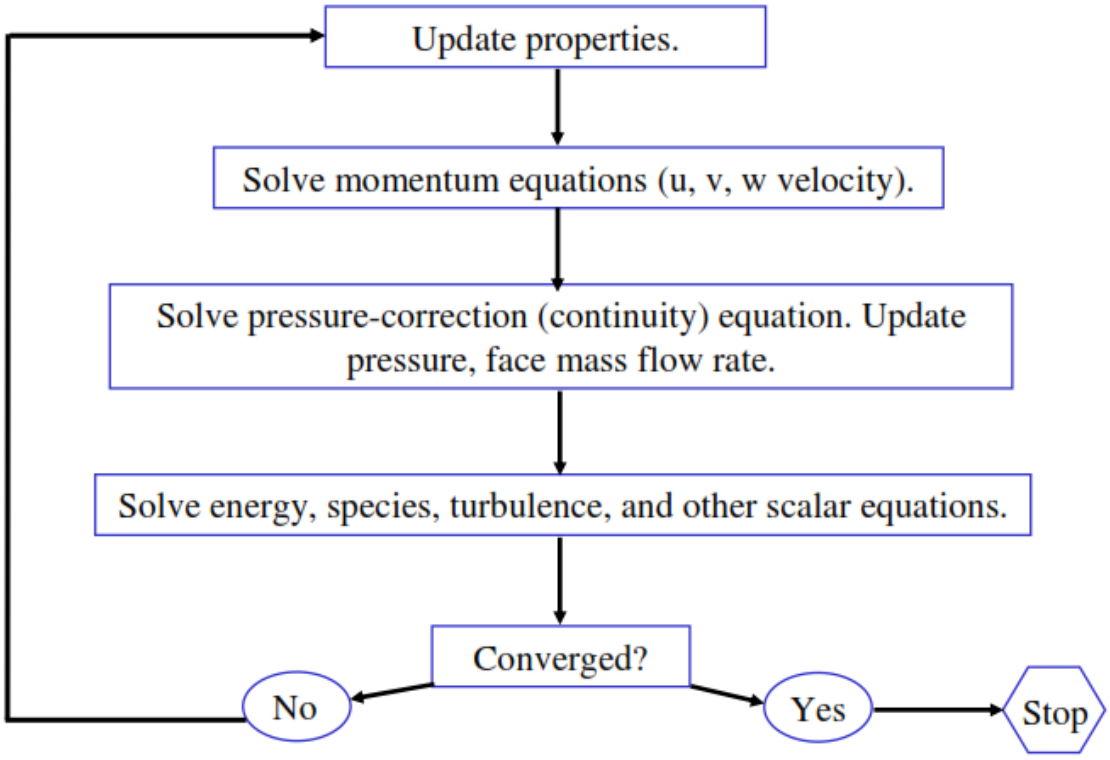

Figure (4-8) flowchart of segregated solution procedure

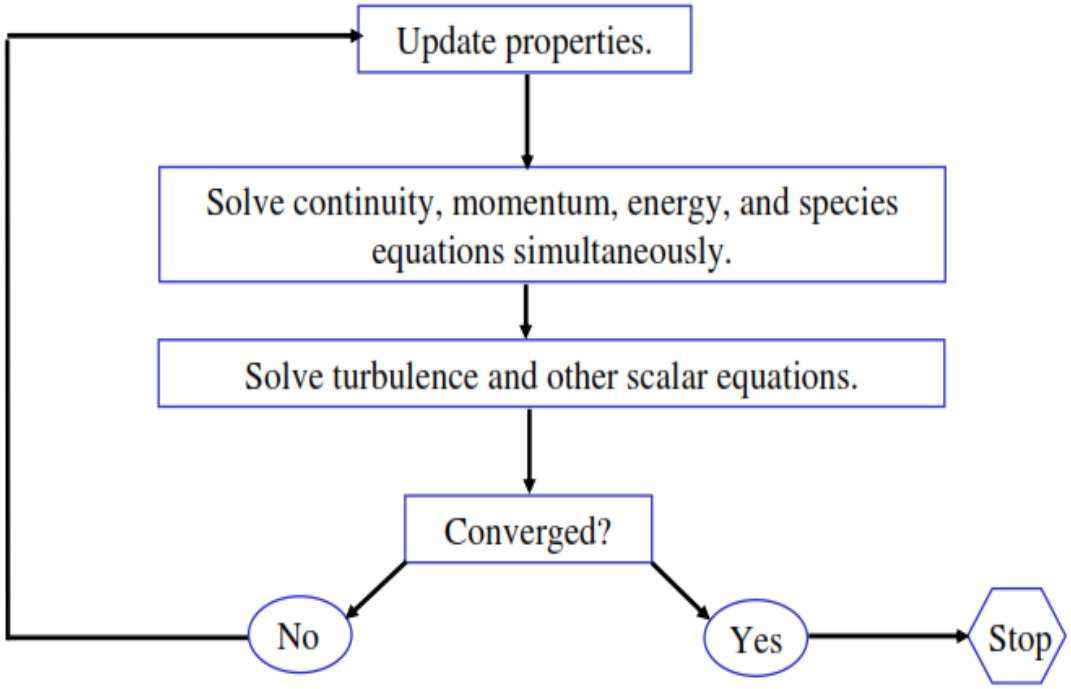

Figure (4-9) flowchart of coupled solution procedure

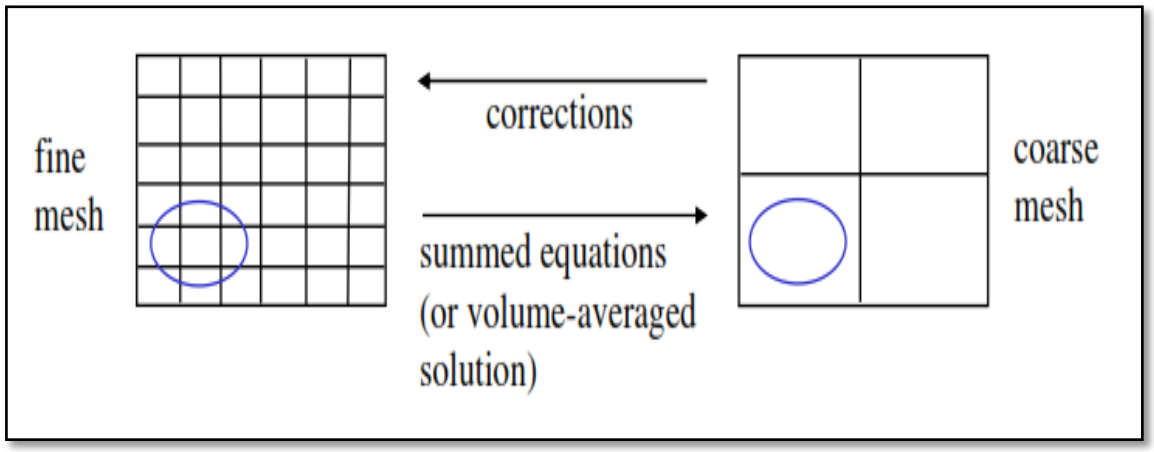

Figure (4-10) rectangular mesh

4.12 Residual errors

Number of iterations is the highest digit of iterations done before the solver terminates. The CFD technique requires iterating the solution of the fluid flow equations till it is converged. The iterations are stopped when the solution remains the same within the accuracy of the selected convergence criteria. The solution is said to be converged when the residuals are below a tolerance limit of 10^{-6} for all the fluid flow equations. Figure (4-11) shows the convergence history for temperature, velocity and pressure of the fluid flow. The goals are being checked for convergence between the 60st iteration and the 160st iteration.

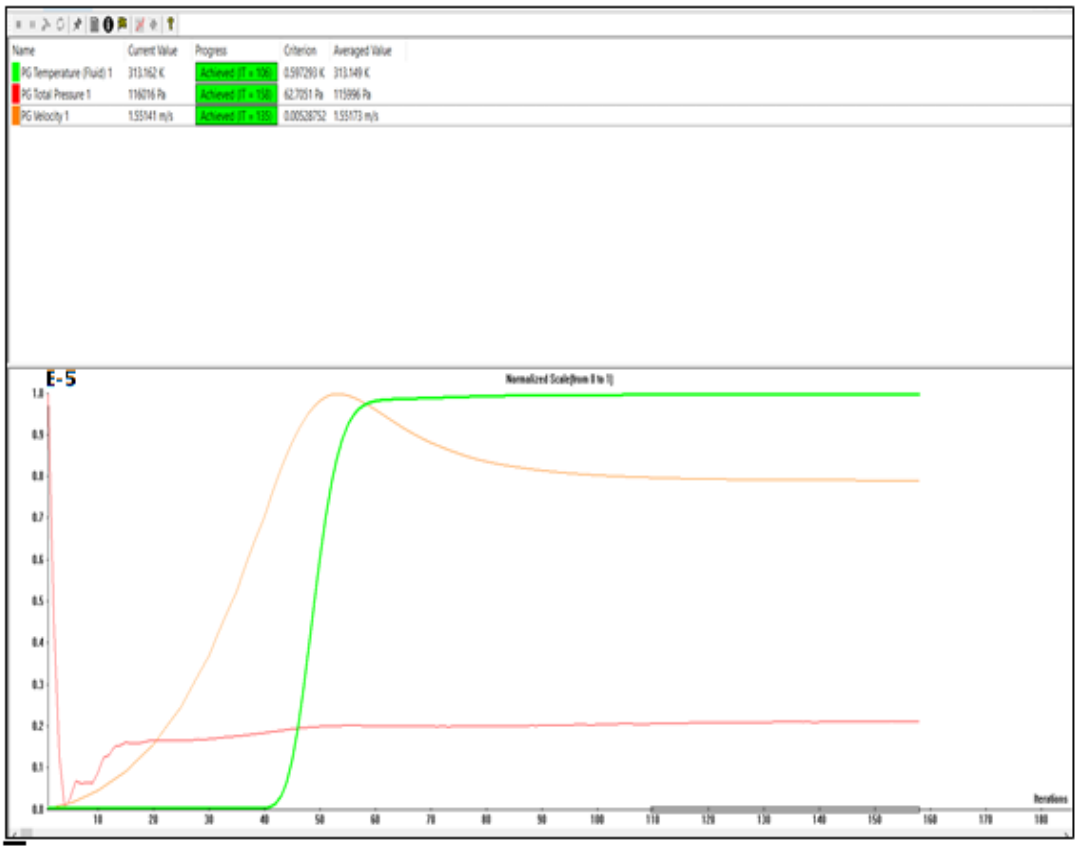

Figure (4-11) residuals of numerical simulation

Chapter Five

Results and Discussion

Results and discussion

5.1. Experimental Results

As mention in chapter three the heat exchanger is designed to work by two stages in order to cool the temperature of hot water in Al- Mussaib thermal power plant to 35 °C. The experimental work is carried out with different values of mass flow rate of raw water which were used to cool the hot water as illustrated in below table (5-1).

Table (5-1) mass flow rate of raw water at different cases

Cases No.	$\dot{m}_2$ (l/min) through pipe2	$\dot{m}_4$ (l/min) through pipe4
Case1	60	70
Case2	50	70
Case3	40	70
Case4	40	60
Case5	40	50
Case6	50	60

Figure (5-1) demonstrates the temperature distribution along the length of FCPHE for case1 and stage 1. In this stage the flow through first pipe and second pipe is counter flow. The value of mass flow rate of hot water enters the first pipe is 40 l/min, this value of mass flow rate is limited by Al-Mussaib thermal power plant. The temperature of hot water decreases about 2 °C in first stage**.** While the mass flow rate of raw water enters second pipe with value of 60 l/min. It shows that the heat transfers from first pipe to second pipe and temperature decreases from 40.8°C to 38.5°C in first pipe. While the temperature of raw water in the second pipe

increases from 28°C to 31.8°C.The log mean temperature difference between hot water and raw water in this stage is 9.73 °C, where the pattern is counter flow. This value is the maximum due to the large difference between temperature of hot water and raw water. The LMTD represents the analysis of heat exchanger in this stage.

Figure (5-2) shows the temperature distribution along the length of FCPHE for case1and stage 2. In this stage the hot water in third pipe was cooled by the raw water in two around pipes. These are the second and fourth pipes. The mass flow rate of raw water in the second pipe and forth pipe is 60 l/min and 70 l/min, respectively. The heat transfers from third pipe to the second pipe and fourth pipe. This figure illustrates that temperature of hot water in third pipe decreases from 38.5°C to 34.7°C.It is observed that mass flow rate of raw water in second pipe and fourth pipe (60 and 70)l/min respectively , are significant to reduce the temperature of hot water to required value. Therefor the parallel flow arrangement in this stage led to reduce hot water temperature to the required temperature by Al-Mussaib thermal power plant. If the counter flows arrangement used in this stage the temperature of hot water decreasing less than the required temperature. In this stage there are two log mean temperature difference. The log mean temperature difference between hot water in third pipe and raw water in second pipe is 5.91 **°C,** that the pattern is parallel flow, while the log mean temperature difference between hot water in third pipe and raw water in fourth pipe is 7.88 °C also that the pattern is parallel flow.

Figure (5-3) represents the case 1 which including the two stages of cooling the hot water with selecting two values of mass flow rate of raw water in second and fourth pipes. These values give a good required temperature for cooling the system of Al-Mussaib thermal power plant. The

average log mean temperature in this case is 7.84 °C. This value produces a good sizing of heat exchange.

Figure (5-4) illustrates case 2 with two stages of hot water cooling and two values of raw water mass flow rate in the second and fourth pipes. In the first stage, the flow arrangement in the first pipe and second pipe is counter flow. The mass flow rate of raw water in the second pipe is 50 l/min. It shows that the heat transfers from the first pipe to the second pipe and the temperature decreases from 40.8°C to 39.3°C in the first pipe. It is observed that the hot water temperature is reduced by 1.5 °C, due to the mass flow rate of raw water decreasing to 50 l/min. While the temperature of raw water in the second pipe increases from 28°C to 31.5°C. The log mean temperature difference between hot water and raw water in this stage is 10.27 °C, which means that the pattern is counter flow. That is, the temperature difference increases in this case due to the mass flow rate of raw water decreasing. This figure illustrates that the temperature of hot water in the third pipe decreases from 39.3°C to 35.3°C.It is noted that the temperature of hot water is reduced by 4 ° C because the mass flow rate of raw water in the second pipe is 50 l/min, which produces more time for heat transfer than 60 l/min in case 1. The log mean temperature difference between hot water in the third pipe and raw water in the second pipe is 6.88 °C which means the pattern is parallel flow, while it is 9.73 °C between hot water in the third pipe and raw water in the fourth pipe, that the pattern is parallel flow. In spite of that, the mass flow rate of raw water in the fourth pipe is as case1 ,the temperature difference increases due to the decreasing mass flow rate of raw water in the second pipe.The average log mean temperature in this case is 8.96 °C. The LMTD average represents the analysis of the heat exchanger in this case.

Figure (5-5) promotes the case 3 which including the two stages of cooling the hot water with selecting two values of mass flow rate of raw water in second and fourth pipes. It indicates that heat is transferred from the first pipe to the second pipe, and the temperature in the first pipe decreases from 40.8 °C to 39.4 °C. It can be seen that the hot water temperature is reduced by 1.4 °C, when the mass flow rate of raw water decreases to 40 l/min. Therefore, this value of mass flow rate in the second pipe is not significant enough to reduce the hot water temperature by 2 °C as a first stage. The temperature of the raw water in the second pipe rises from 28 to 31.1°C. The log mean temperature difference between hot water and raw water at this stage is 10.5 °C, when the pattern is counter flow. That is, the temperature difference increases in this case due to the mass flow rate of raw water decreasing from 50 l/min to 40 l/min in the second pipe. The temperature of the hot water in the third pipe decreases from 39.4°C to 35. 9°C.It is noted that the temperature of hot water is reduced by 3.5 ° C due to the amount of mass flow rate for raw water in the second pipe not being enough to decrease the hot water temperature to 35 °C. The log mean temperature difference between hot water in the third pipe and raw water in the second pipe is 7.58 °C, which means the pattern is parallel flow, while it is 15.51 °C between hot water in the third pipe and raw water in the fourth pipe, which means parallel flow. Despite the fact that the raw water mass flow rate in the fourth pipe is the same as in cases 1 and 2, the temperature difference increases due to the decrease in raw water mass flow rate in the second pipe to 40 l/min.Therefore the mass flow rate of raw water in second pipe 40 l/min is not a significant amount to decrease temperature of hot water to 35 °C in spite of low velocity in this mass flow rate. The average log mean temperature in this case is 11.19 °C.

Figure (5-6) promotes case 4 with two stages of hot water cooling and two values of raw water mass flow rate in the second and fourth pipes. It shows that heat is transported from the first pipe to the second pipe, and the temperature in the first pipe decreases from 40.8 °C to 39.5 °C. It is illustrated that the mass flow rate for raw water in the second pipe is the same as in case 3 but the temperature of the hot water decreases to 39.5 °C. This is due to the mass flow rate of raw water in the third pipe decreasing to 60 l/min. In the second pipe, the raw water temperature increases from 28°C to 30°C. Therefore, since the mass flow rate of raw water in the fourth pipe decreases to 60 l/min in this case, the log mean temperature difference increases at this stage. The log mean temperature difference between hot water and raw water at this stage is 11.15 °C, which means that the pattern is counter flow. The third pipe transfers heat to the second and fourth pipes. As seen in this figure, the temperature of the hot water in the third pipe declines from 39.5°C to 36.3°C. It can be seen that the temperature of hot water was reduced by 3.2 ° C due to the amount of mass flow rate for raw water in the fourth pipe, which was not enough to decrease the hot water temperature to 35 °C. The log mean temperature difference between hot water in the third pipe and raw water in the second pipe is 8.64 °C that the pattern is parallel flow, while it is 14.06 °C between hot water in the third pipe and raw water in the fourth pipe, that the pattern is parallel flow. Despite the fact that the mass flow rate of raw water in the second pipe is the same as in case 3, the temperature difference increases as the mass flow rate of raw water in the fourth pipe is reduced to 60 l/min.In this case the average log mean temperature difference is 14.06°C.

Figure (5-7) depicts case 5, which includes two stages of cooling hot water by selecting two values for the raw water mass flow rate in the

second and fourth pipes. It demonstrates that heat is transferred from the first to the second pipe, and the temperature in the first pipe decreases from 40.8 °C to 39.8 °C. The raw water temperature rises from 28°C to 30.3°C in the second pipe. At this stage, the mass flow rate of raw water in the second pipe is the same as in case 3 and case 4 but the temperature of the hot water drops to 39.8°C .This is because of the effect of the decreasing mass flow rate of raw water in the fourth pipe. The log mean temperature difference between hot water and raw water at this stage is 11.14 °C, which means that the pattern is counter flow. It is noted that the log mean temperature difference in this case less than the log mean temperature difference in case 4 by 0.09%. This is because of the effect of the decreasing mass flow rate of raw water in the fourth pipe. Also, the temperature of the hot water in the third pipe decreases from 39.8 °C to 36.9 °C. This is because the mass flow rate of raw water in the fourth pipe is not significant enough to decrease the temperature of hot water to 35 °C. The log mean temperature difference between hot water in the third pipe and raw water in the second pipe is 8.95 °C that the pattern is parallel flow, while it is 22.11 °C between hot water in the third pipe and raw water in the fourth pipe, which means parallel flow, it is noted that the maximum value. This is because the maximum temperature difference.In this case, the average log mean temperature difference is 14.07°C, which is the maximum value.

Figure (5-8) illustrates case 6, which includes the two stages of cooling the hot water by selecting two values of mass flow rate of raw water in the second and fourth pipes. It shows that heat is transported from the first to the second pipe, with the temperature in the first pipe descending from 40.8 to 39.3 °C. This is as in case 2. In the second pipe, the raw water temperature rises from 28°C to 30.5°C. The log mean

temperature difference between hot water and raw water in this stage is 10.79 °C, when that the pattern is counter flow. It is noted that the log mean temperature difference in this case larger than log mean temperature difference in case 2 by 4.7%. This is because the temperature difference increases as the mass flow rate of raw water in the fourth pipe decreases. As indicated in this figure, the temperature of the hot water in the third pipe decreases from 39.3°C to 35.6°C. When comparing this case with case 2 the temperature of hot water decreases less than in case 2 due to the effect of the decreasing mass flow rate for raw water in the fourth pipe. The log mean temperature difference between hot water in the third pipe and raw water in the second pipe is 7.79 °C that the pattern is parallel flow, while it is 8.61 °C between hot water in the third pipe and raw water in the fourth pipe, that the pattern is parallel flow. The average log mean temperature difference is larger than case2, that it is 9.07°C.

Figures (5-9), (5-10), (5-11), (5-12), (5-13), and (5-14) indicate the variation of pressure along the length of the FCPHE for cases 1, 2, 3, 4, 5, and 6, respectively. It can be seen that as the mass flow rate increases, the pressure drop increases significantly for the entire pipe. The reason for this is that the flow rate (square of inlet flow velocity) has a greater impact on the pressure drop than other parameters. The mass flow rate of hot water in the first pipe and in the third pipe is constant. Therefore, the pressure drop is 3 KPa and 1.3 KPa in the first pipe and third pipe, respectively, for six cases.

Figures (5-9), (5-10), and (5-11) depict the pressure variation along the length of the FCPHE at various mass flow rates of raw water in the second pipe. It is noted that the pressure drop by (1.2, 0.8, and 0.13) KPa in cases 1, 2, and 3, respectively. It is observed that the pressure drop in the second pipe decreases when the mass flow rate of raw water decreases.

While the pressure drops by 0.3 KPa in the fourth pipe for case1, 2, and 3, due to the mass flow rate of raw water, it is constant in the fourth pipe in these cases.

Figures (5-12) and (5-13) indicate the pressure variation along the length of the FCPHE at various mass flow rates of raw water in the fourth pipe. It is noted that the pressure drop by (0.25 and 0.21) KPa in the fourth pipe at cases 4 and 5, respectively, It is observed that the pressure drop in the fourth pipe decreases when the mass flow rate of raw water decreases.

Figure (5–14) shows the pressure variation along the length of the FCPHE in case 6. It is noted that the pressure drops by (3, 0.8, 1.3, and 0.25) KPa in the first, second, third, and fourth pipes, respectively. Because the variance in temperature is so minimal, pressure drops relatively slightly.

Figure (5-15) induces variation between Nusselt numbers and Reynolds number for FCPHE. The relationship between Nusselt number and Reynolds number is direction. It is observed that the Nusselt number of the inner pipe is larger than the other pipes. It reaches up to 260 at Reynolds number 46712. This can be attributed to the highly cooling process of the inner pipe, which causes an enhancement in the heat transfer coefficient and hence in the Nusselt number. The maximum Nusselt number is (192.7 and 93.13) in case 1 for the second and fourth pipes, respectively. This is due to the maximum mass flow rate of raw water in case 1.

Figure (5-16) induce variation between friction factor versus Reynolds number for FCPHE. Friction factor decreases with an increase in Reynolds number. It is observed that the friction factor for the second pipe; third pipe, and fourth pipe are very close. The friction factor of the first pipe is the lowest; it reaches 0.005. This is due to the high Reynolds number in the

first pipe. Therefore, the measuring values of friction factors are the lowest for hot water in the inner pipe and the highest for raw water in the outer annulus. It is due to the fact that the relative roughness of the outer pipe is greater than that of the inner pipe. These results agree with the experimental results of Gomaa et al.[31] .

Figure (5-17) observes the variation of the pipe side heat transfer coefficient with Reynolds number. The pipe side heat transfer coefficient proportional with the Reynolds number due to increasing turbulence introduced by increasing the mass flow rate of water through the pipes. This figure illustrates that the heat transfer coefficient of the first pipe is the highest value when compared with other pipes. At a given water flow rate, the pipe side heat transfer coefficient for higher inlet water temperature is higher than that for the lower ones, i.e., the pipe side heat transfer coefficient increases with increasing inlet water temperature. This is due to the increase in the surface temperature and the temperature difference between the water temperature and the surface tube temperature that led to an increase in the overall heat transfer coefficient.

Figure (5-18) moderates the relation between logarithmic mean temperature difference (LMTD) and mass flow rate of raw water. Log mean temperature difference (LMTD) is a vital parameter as it determines the temperature driving force for heat transfer in a heat exchanger. It shows that the LMTD decreases with increasing of mass flow rate of raw water. $LMTD_1$ represents the temperature difference in first stage of heat exchanger; therefor the flow is counterflow between first pipe and second pipe. While $LMTD_2$ and $LMTD_3$ indicate the temperature difference in parallel flow arrangement for second pipe, third pipe and fourth pipe. It can be seen that the larger value of $LMTD_{average}$ a t (40,40,40 and70)l/min mass

flow rate at first pipe, second pipe , third pipe and fourth pipe ,respectively . These results agree with the experimental results of Prasanna et al [65].From this figure can be seen that the maximum LMTD between third pipe and fourth pipe due to the large size of heat exchanger .

Figure (5-19) shows the variation of the overall heat transfer coefficient with the Reynolds number of raw water. It is observed that overall heat transfer coefficients increase with the mass flow rate of raw water. The maximum overall heat transfer coefficient between hot water in the first pipe and raw water in the second pipe is found to be 2343.37 (W/m2.°C at a 60 L/min mass flow rate of raw water in the second pipe . While the maximum overall heat transfer coefficient measured between the hot water of the third pipe and the raw water of the second pipe is 1365.39 W/m2.°C. The maximum overall heat transfer coefficient between hot water in the third pipe and raw water in the fourth pipe is 889.3 W/m^2.°C at a mass flow rate of raw water of 70 l/min in the fourth pipe. These results agree with the experimental results of Hossain [37].

Figure (5-20) perceives the variations in heat transfer rates with respect to the Reynolds number of raw water in six cases. The mass flow rate of hot water is 40 l/min. It is found that the heat transfer rate increases as the mass flow rate of raw water increases. It can also be seen that the larger the inlet mass flow rate, the higher the magnitude of the Reynolds number. A higher heat transfer rate from the FCPHE can be achieved when the inlet mass flow rate of raw water is 70 L/min in the fourth pipe and the inlet mass flow rate of raw water is 60 L/min in the second pipe. At this mass flow rate of raw water, the exit temperature of hot water reaches the required temperature of 34.7 °C. There is an elementary equation from basic thermodynamics that states that the rate of heat transfer equals the mass flow rate times a constant (the specific heat of water) times the delta

T (fluid temp out minus fluid temp in).Therefore, when the mass flow rate of raw water increases, the heat transfer rate also increases.

Figure (5–21) presents the relationship between the effectiveness of FCPHE and the Reynolds number of raw water. The effectiveness is used to estimate the performance of the FCPHE. It can be clearly seen from this figure that the effectiveness of the FCPHE increases with the increase in the mass flow rate of raw water. The effectiveness reaches its maximum value of 0.76 at a mass flow rate of raw water of 60 l/min in the second pipe and 70 l/min in the fourth pipe. It has been shown that increasing the mass flow rate of raw water will increase the effectiveness according to equation (3-28) . The minimum thermal capacity is for hot water and it is constant at 40 l/min, so increasing the mass flow rate of raw water will increase the average heat transfer, which increases the effectiveness.

Figure (5-22) explains the relationship between the Nusselt number and annular diameter ratio for a cooled annulus. It is observed that the Nusselt number increases with increasing the annular diameter ratio until reaches peak point at annular diameter ratio 2. Then, the Nusselt number drops after maximum point. For a cooled annulus, a maximum Nusselt number is seen in the mid-range of annular diameter ratios, which decreases as the annular diameter ratio moves from the mid-range. Due to the large scatter in the LMTD results, an averaging scheme is used through the points to provide an accurate data point at the respective Reynolds numbers.

Figure (5-23) demonstrates the relationship between the Nusselt number and annular diameter ratio of heated annulus ratio. It is showed that the Nusselt number increases with increasing the annular diameter ratio and reaches maximum value, after that the Nusselt number decreases. From

figures (5-22) and (5-23), the diameters of four pipes for heat exchanger have been selected with saving the other conditions of design.

Figure (5-24) imposes the variation of Nusselt number with Reynolds number at different diameter ratio for second pipe. It has been shown that the Nusselt number increases with increasing the Reynolds number for all diameter ratios. The experimental results show that the best diameter ratio equal 1.89 to achieve a good agreement with theoretical results.

Figure (5-25) shows the variation of Nusselt number with Reynolds number at different diameter ratio for third pipe. For all diameter ratios, it has been demonstrated that the Nusselt number rises as the Reynolds number rises. The optimal diameter ratio, according to the experimental data, is 1.47, which is in good agreement with theoretical predictions.

Figure (5-26) depicts the fluctuation of Nusselt number with Reynolds number at various diameter ratios in fourth pipe. For all diameter ratios, it has been demonstrated that the Nusselt number rises as the Reynolds number rises. The experimental results suggest that the best diameter ratio is 1.36, which agrees well with theoretical diameter ratio 1.33 values.

Figures (5-27),(5-28) and (5-29) moderate friction factor as a function of Reynolds number for four pipe concentric heat exchanger at different diameter ratio. Friction factor decreases with increasing Reynolds number. The rate of decrease in friction factor is higher at lower range of Reynolds number compared to that at higher range of Reynolds number. It can be show the same response in figures (5-27) to (5-29). It is found that is no significant impact by comparing the different diameter ratio on friction factor.

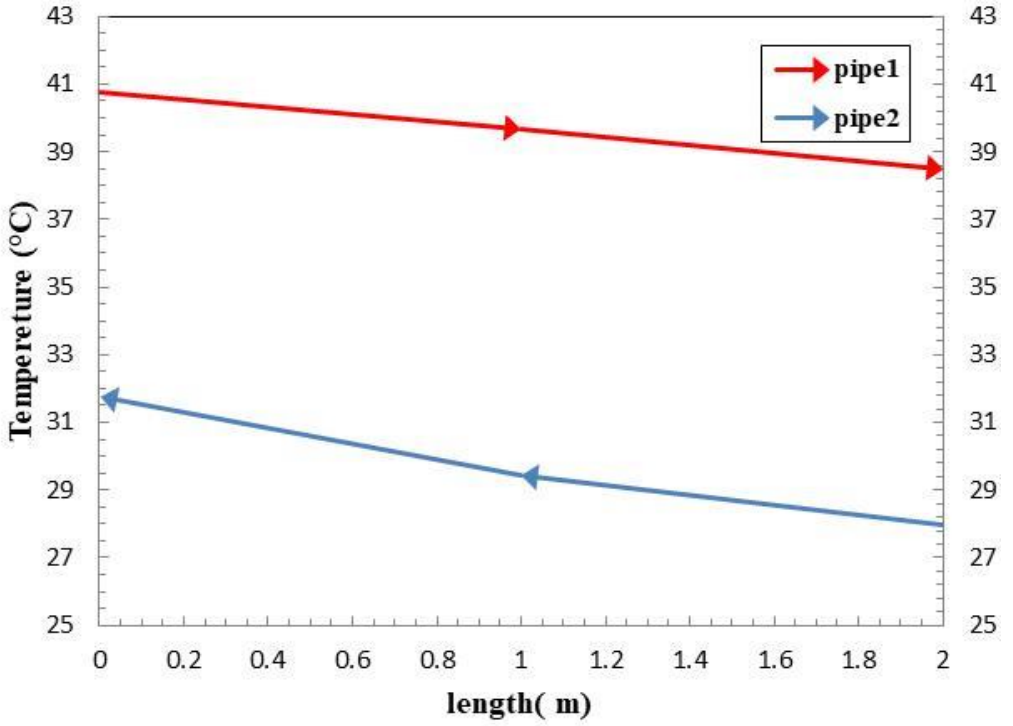

Figure (5-1) variation of temperatures along the length of pipe for stage1 at case1

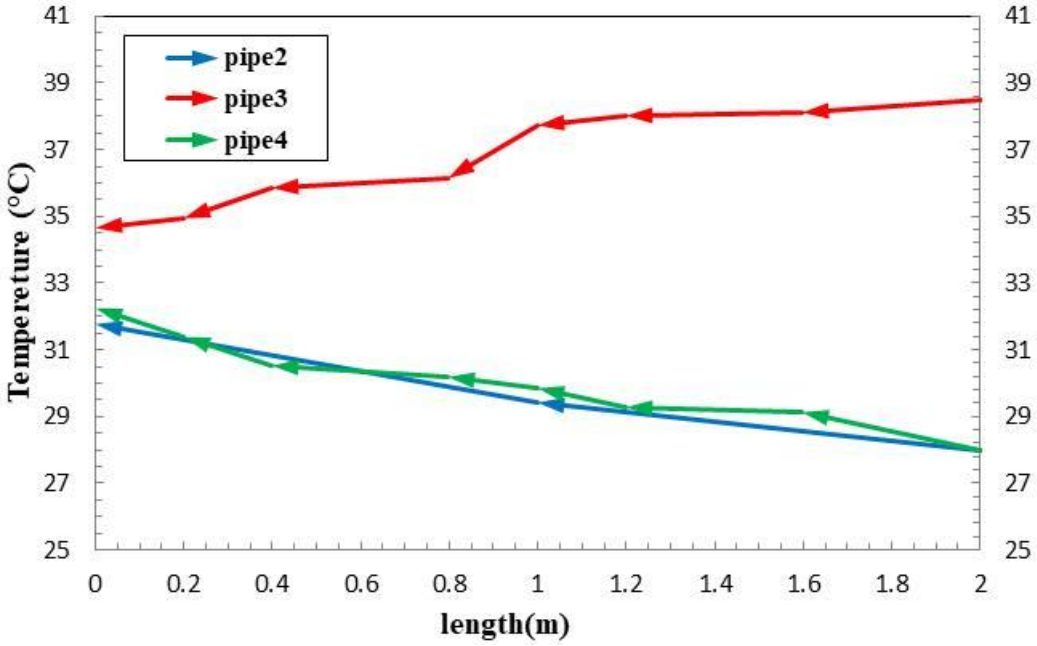

Figure (5-2) variation of temperatures along the length of pipe for stage2 at case1

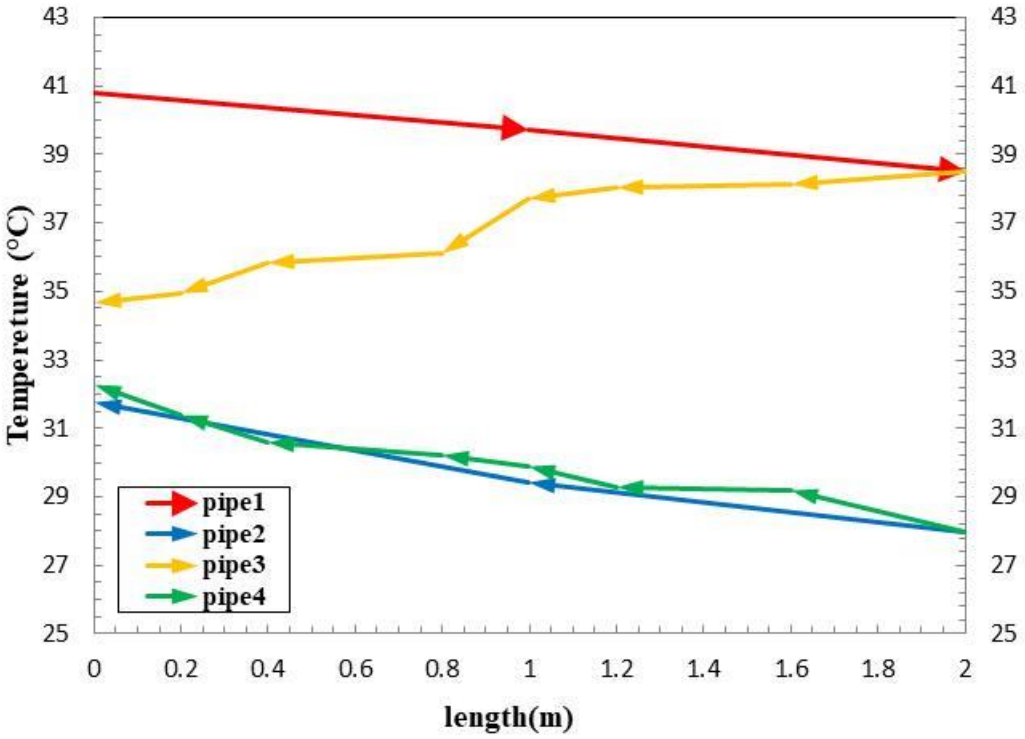

Figure (5-3) variation of temperatures along the length of FCPHE at case1

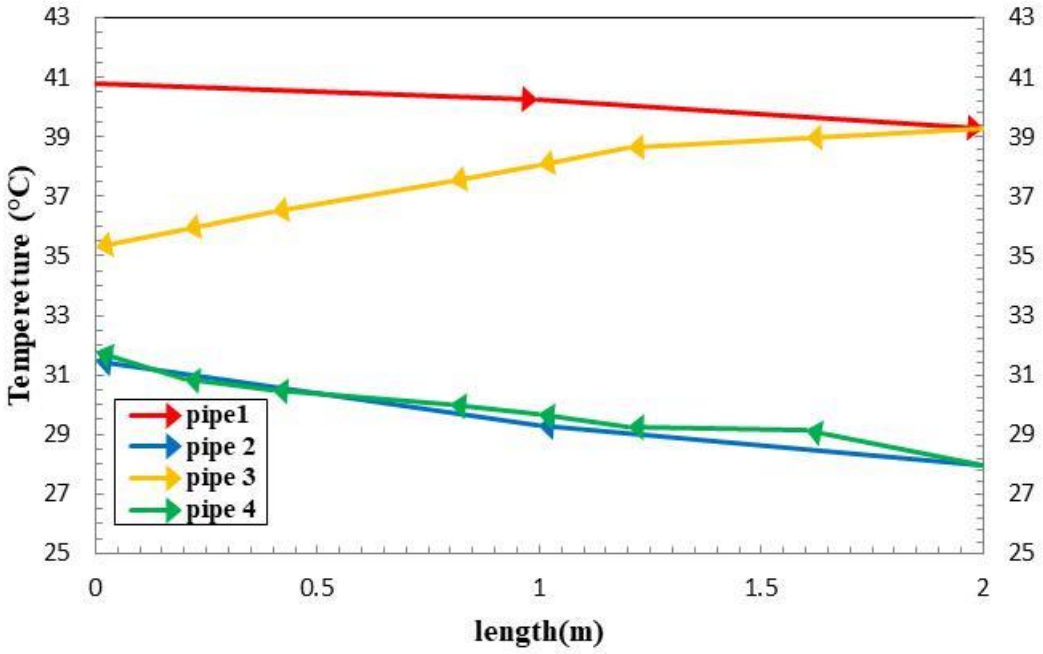

Figure (5-4) variation of temperatures along the length of FCPHE at case2

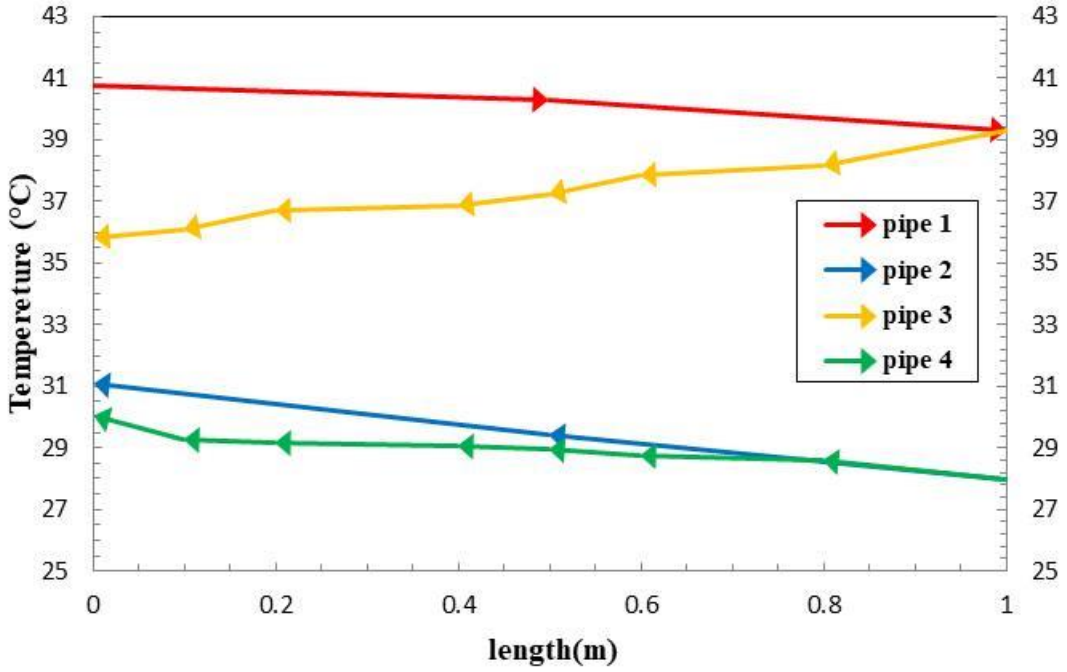

Figure (5-5) variation of temperatures along the length of FCPHE at case3

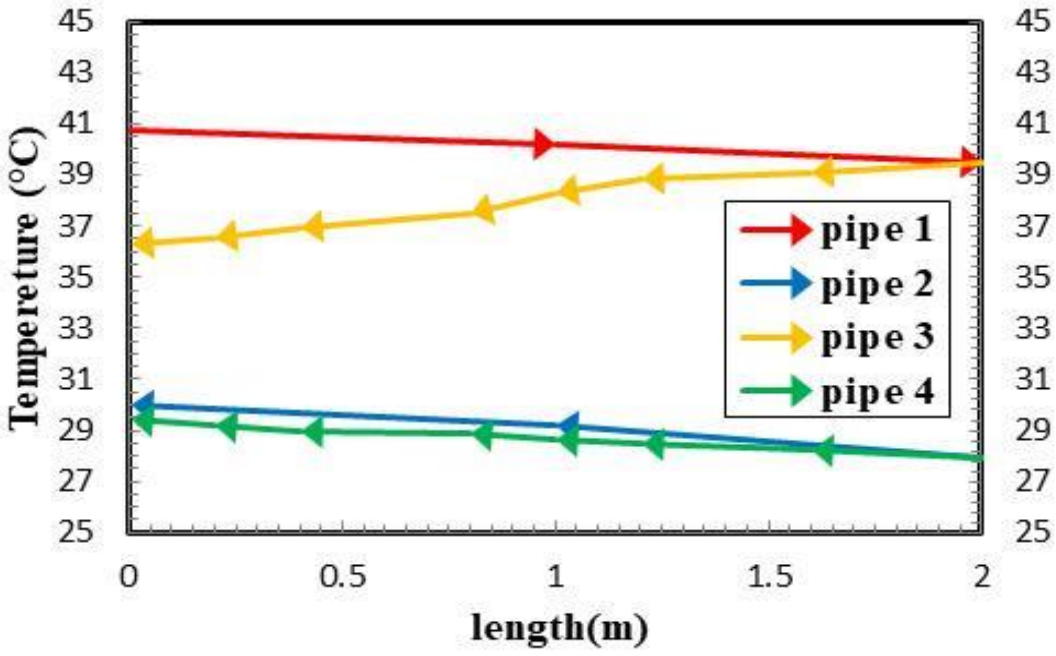

Figure (5-6) variation of temperatures along the length of FCPHE at case4

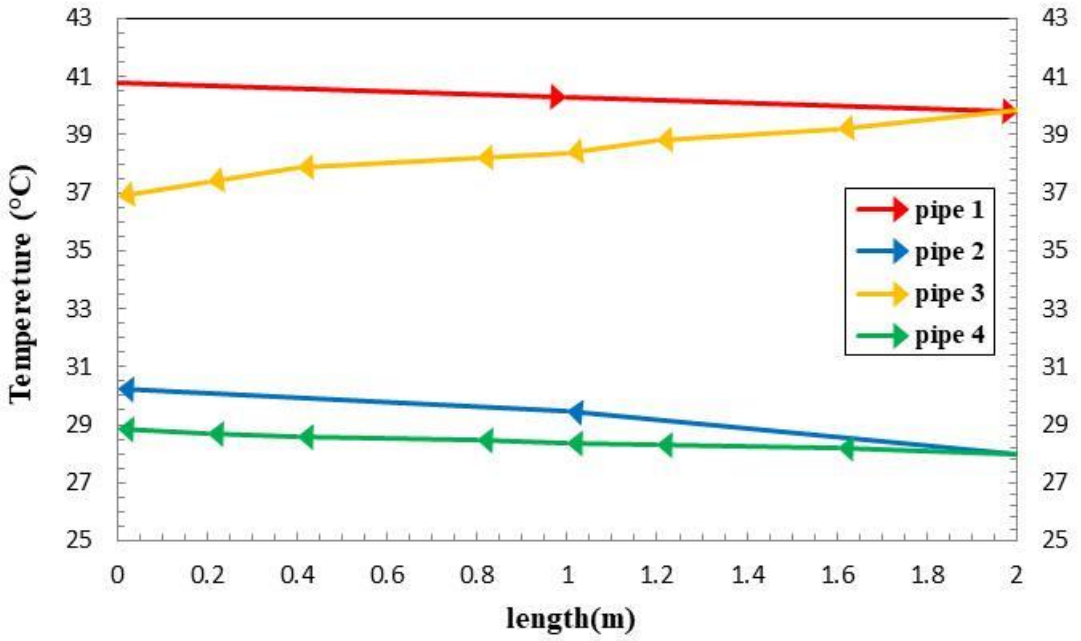

Figure (5-7) variation of temperatures along the length of FCPHE at case5

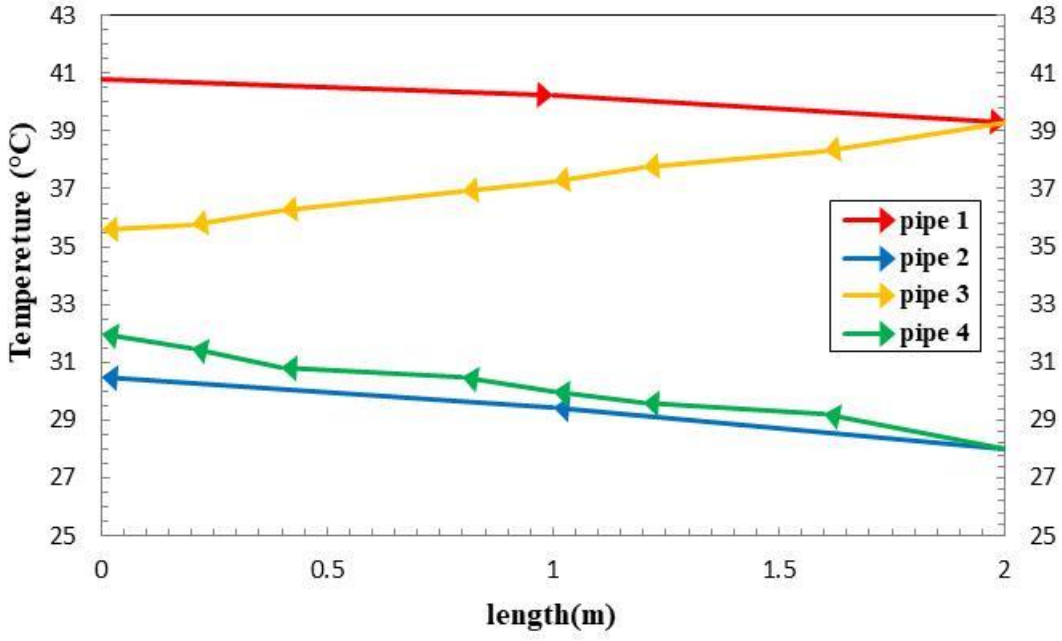

Figure (5-8) variation of temperatures along the length of FCPHE at case6

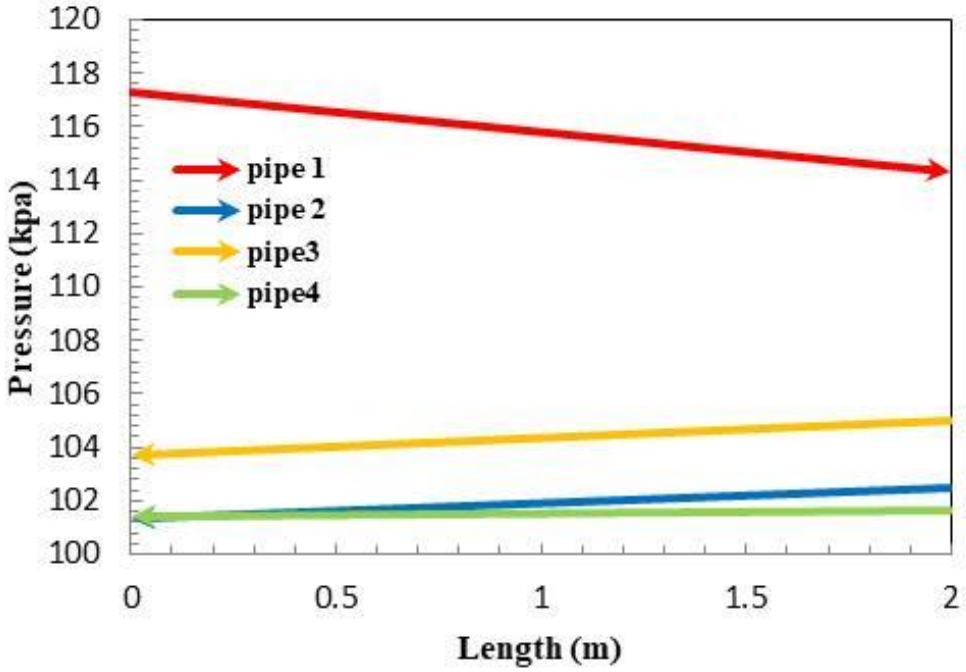

Figure (5-9) variation of pressure along the length of FCPHE at case1

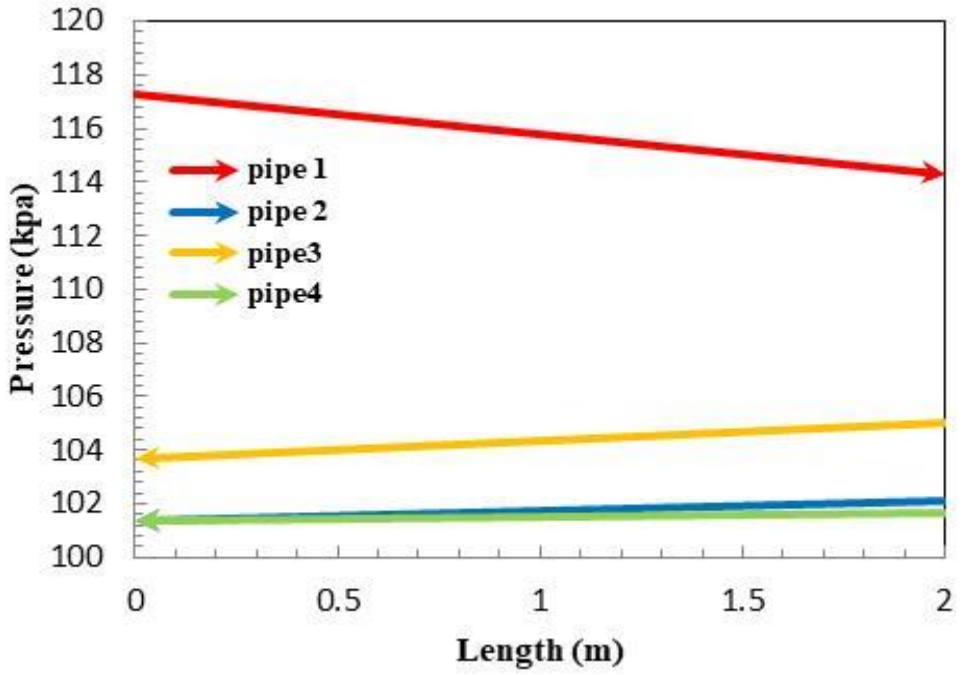

Figure (5-10) variation of pressure along the length of FCPHE at case2

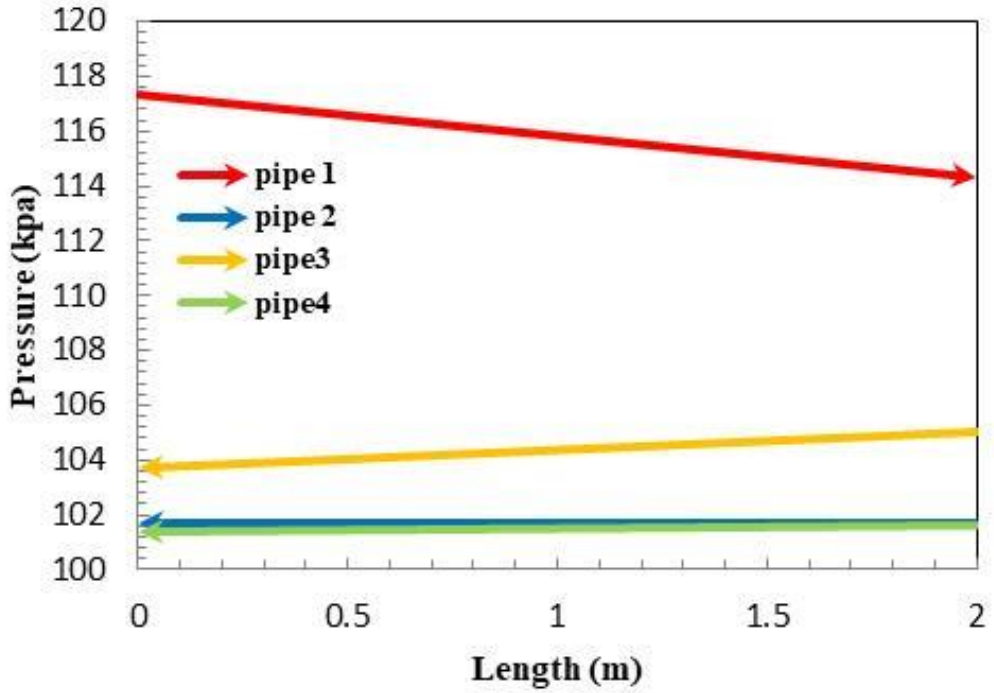

Figure (5-11) variation of pressure along the length of FCPHE at case3

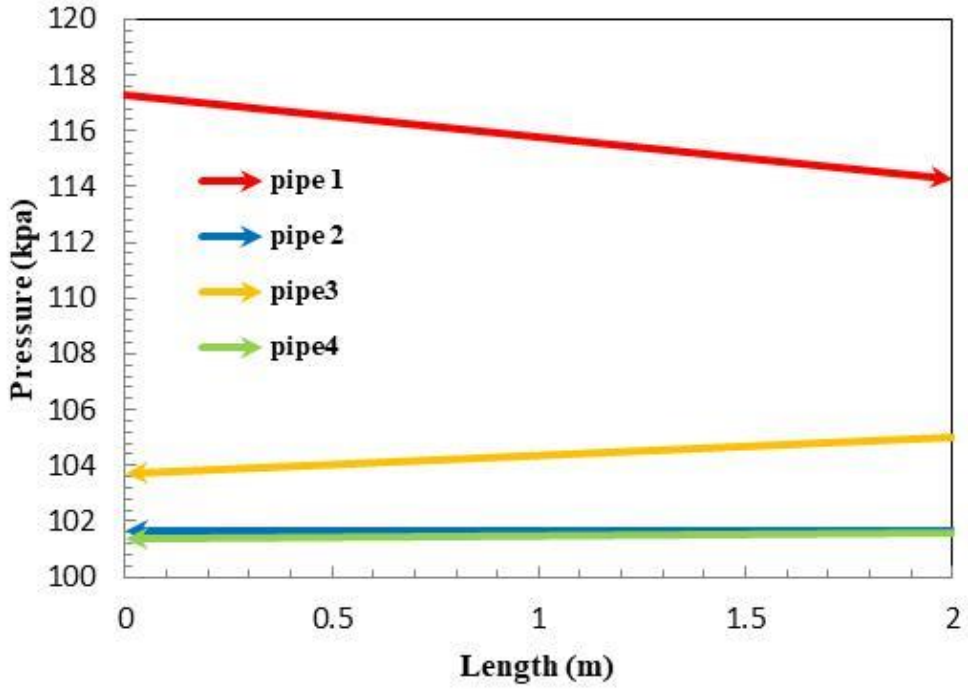

Figure (5-12) variation of pressure along the length of FCPHE at case4

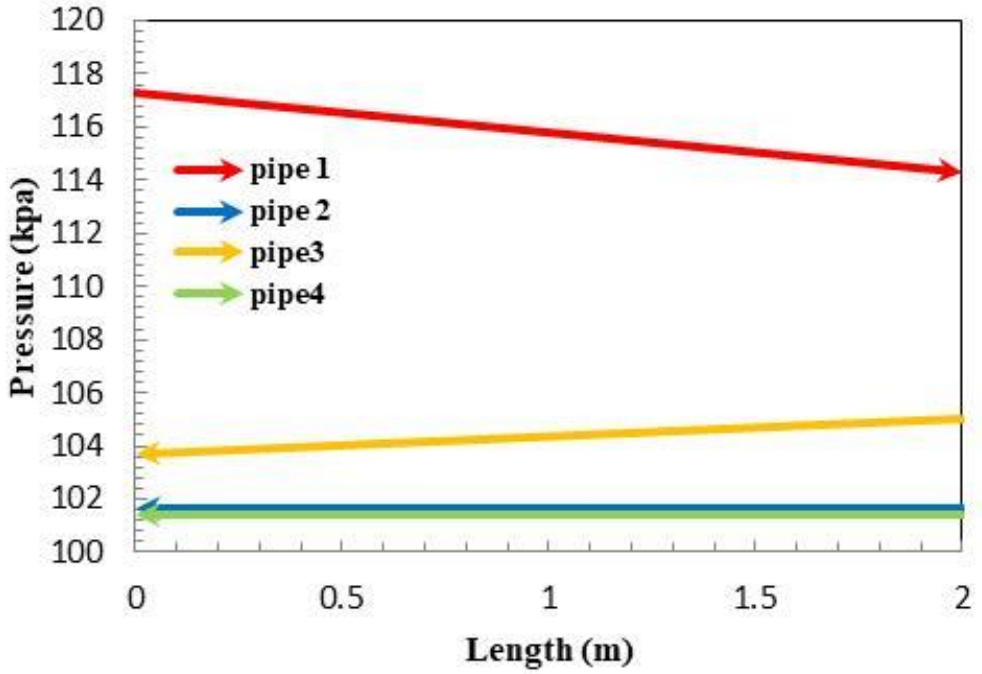

Figure (5-13) variation of pressure along the length of FCPHE at case5

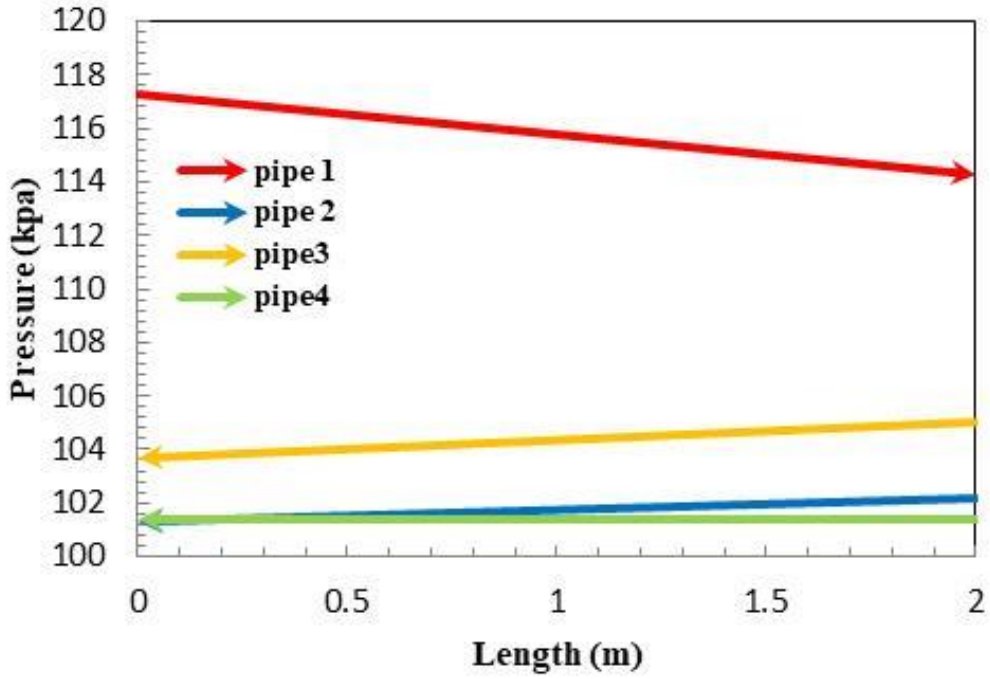

Figure (5-14) variation of pressure along the length of FCPHE at case6

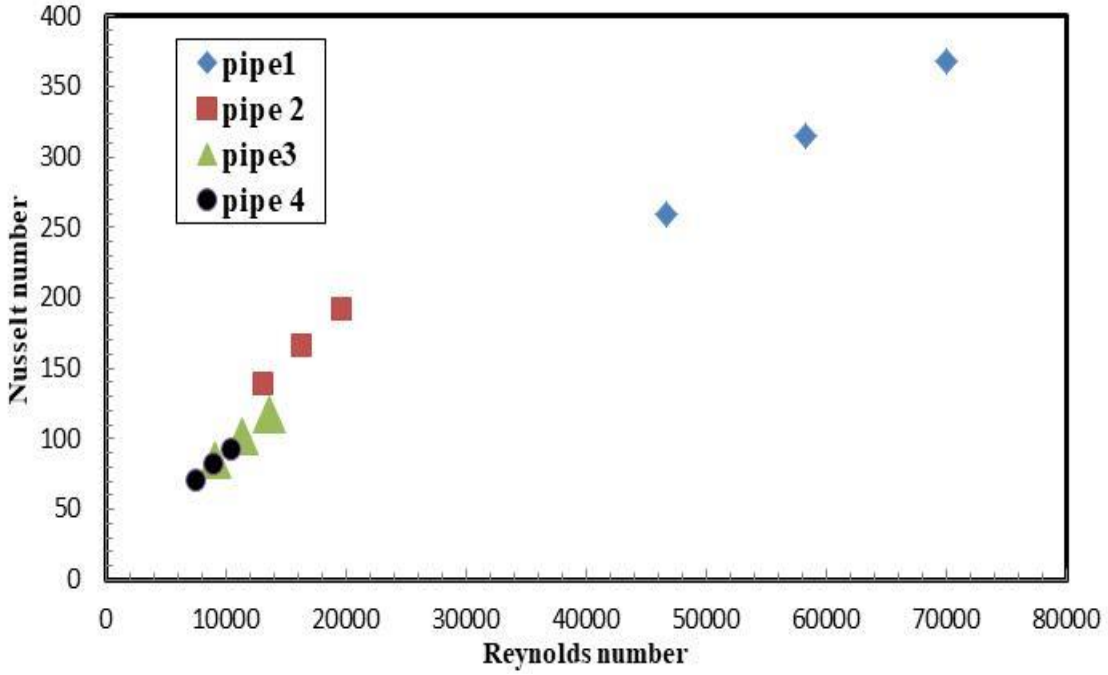

Figure (5-15) variation Nusselt numbers versus Reynolds number of FCPHE

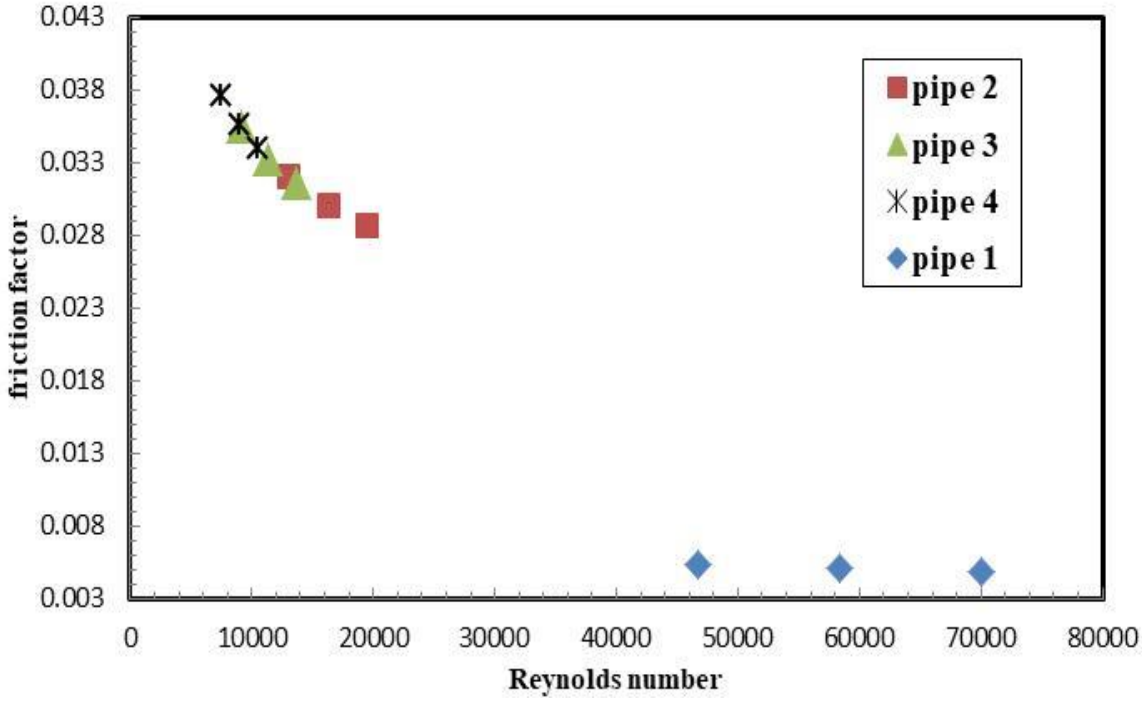

Figure (5-16) variation friction factors versus Reynolds number of FCPHE

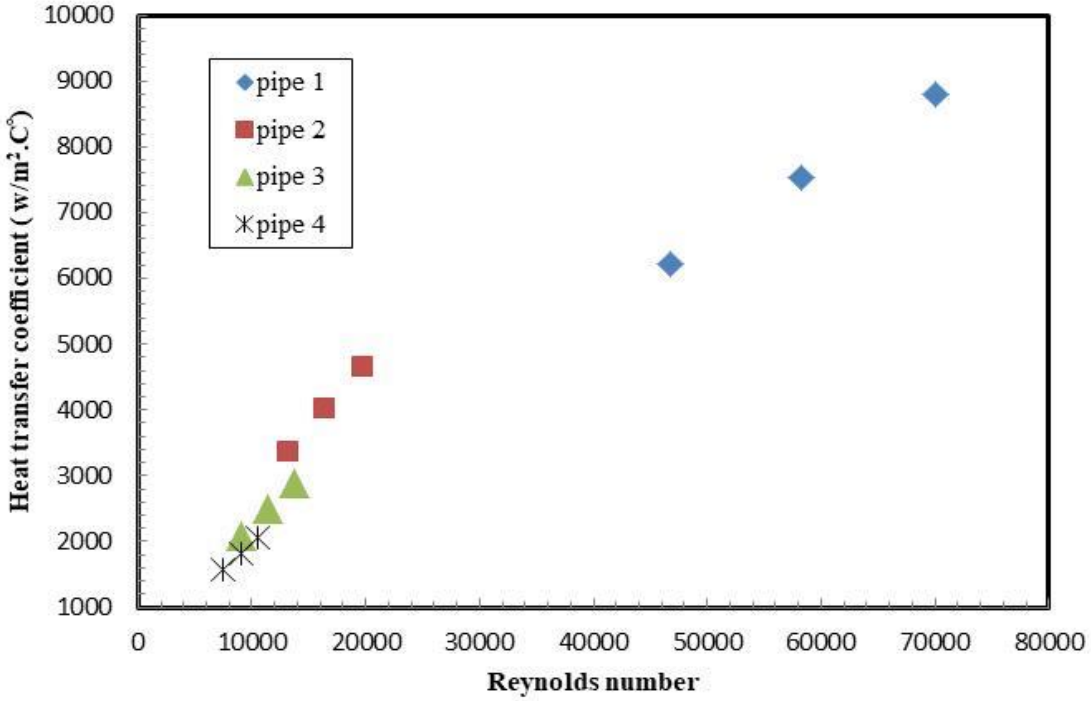

Figure (5-17) variation heat transfer coefficients versus Reynolds number of FCPHE

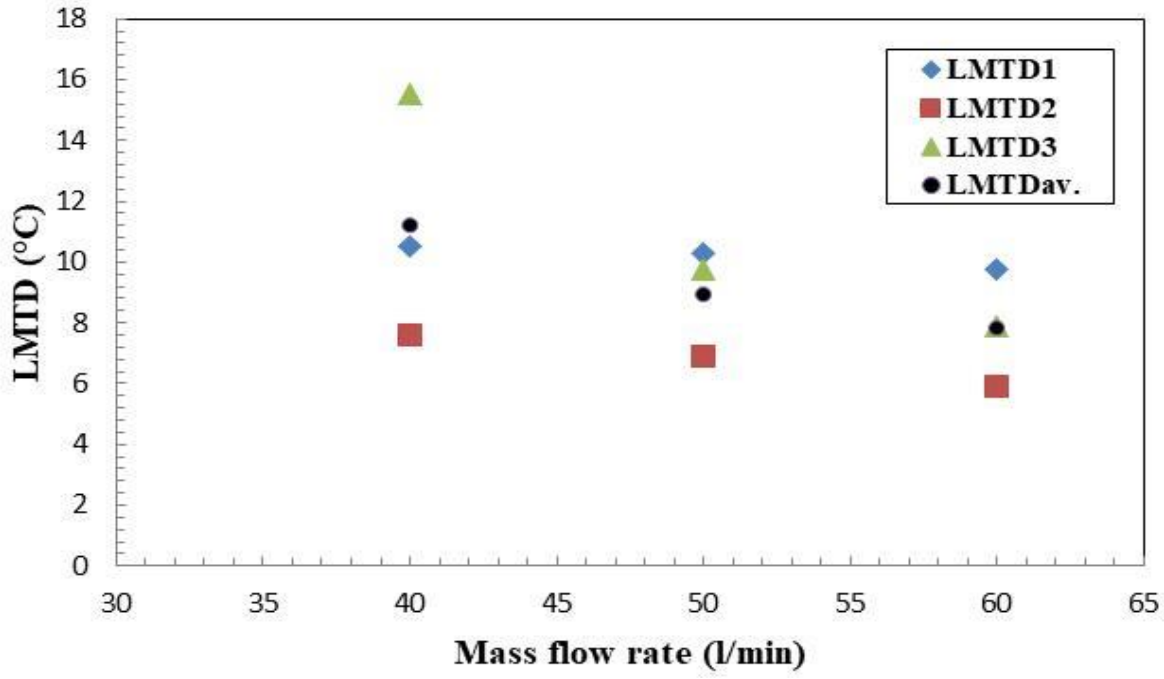

Figure (5-18) variation log mean temperature difference with different mass flow rate of raw water

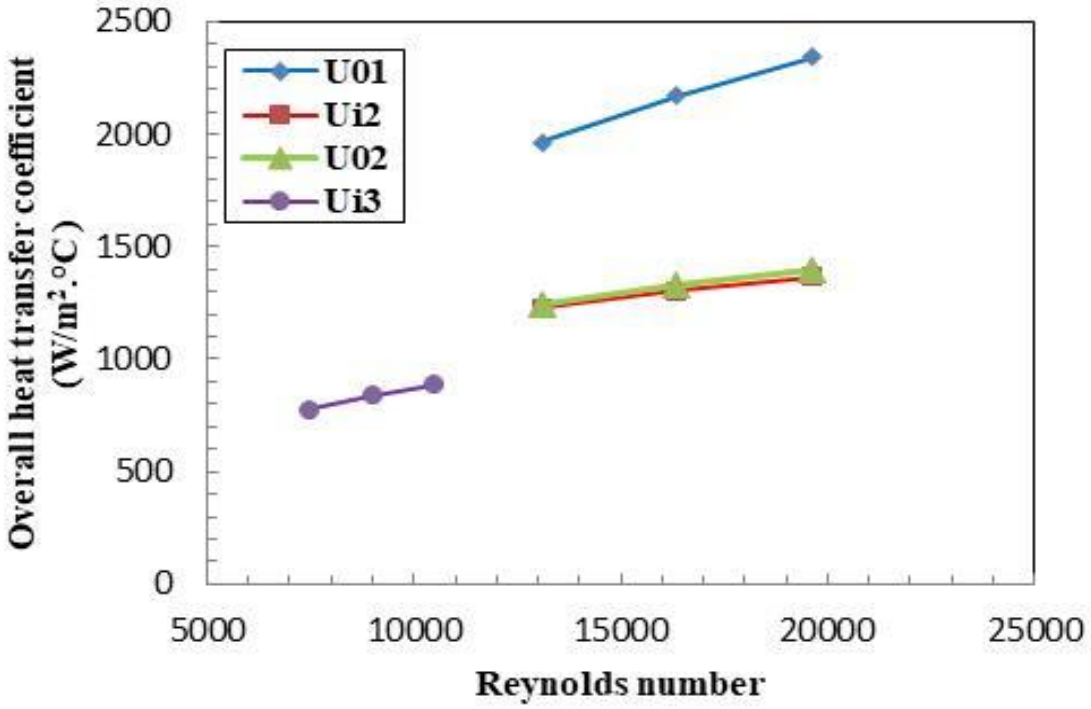

Figure (5-19) variation of overall heat transfer coefficient at different Reynolds number of raw water

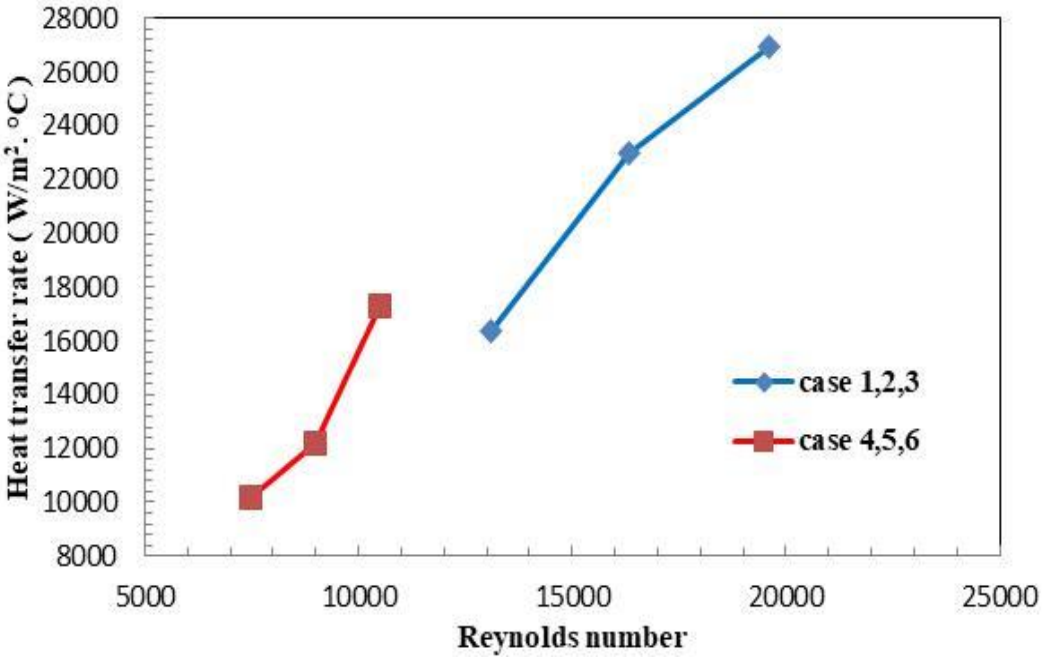

Figure (5-20) heat transfer flow rate of the FCPHE with Reynolds number of raw water

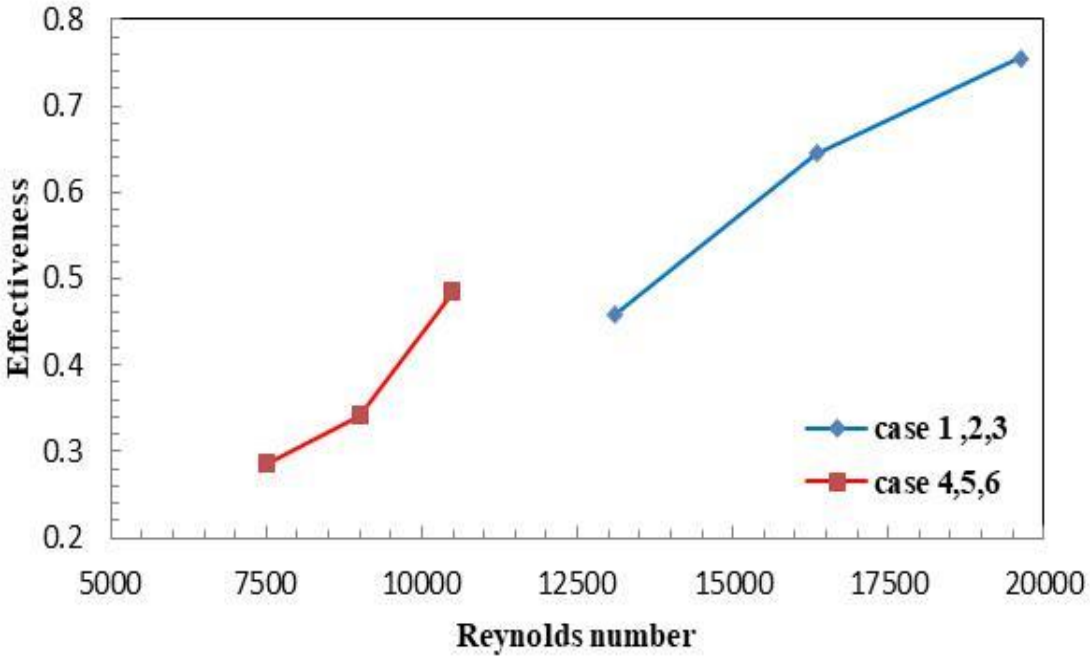

Figure (5-21) effectiveness variation with Reynolds number of raw water

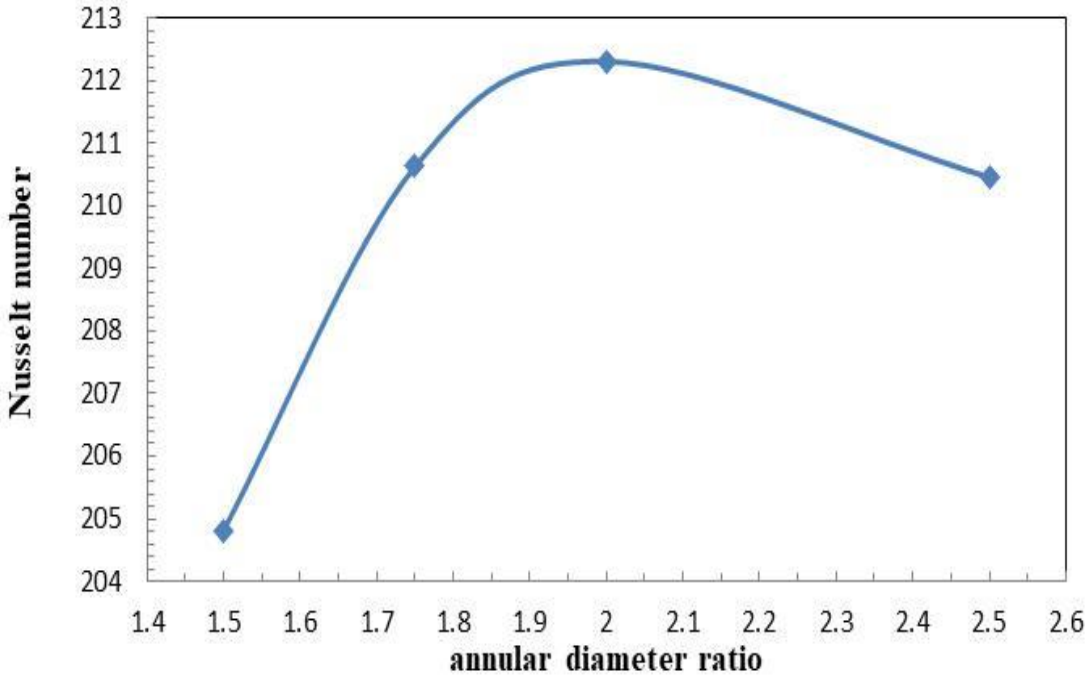

Figure (5-22) Nusselt numbers for cooled annulus at different annular diameter ratios

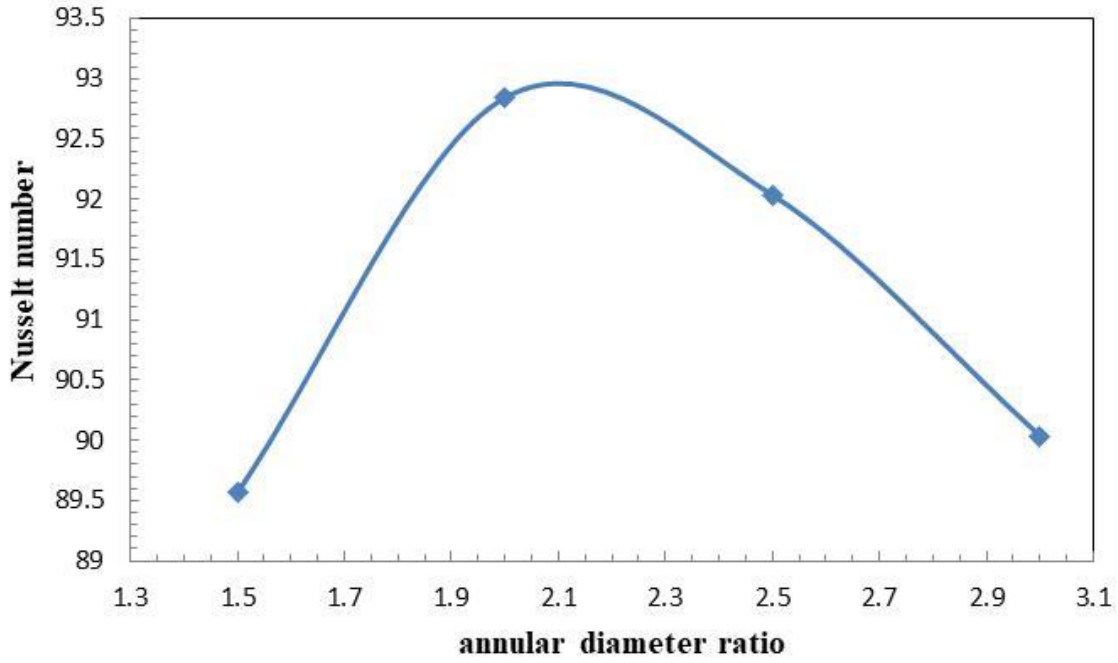

Figure (5-23) Nusselt numbers for heated annulus at different annular diameter ratios

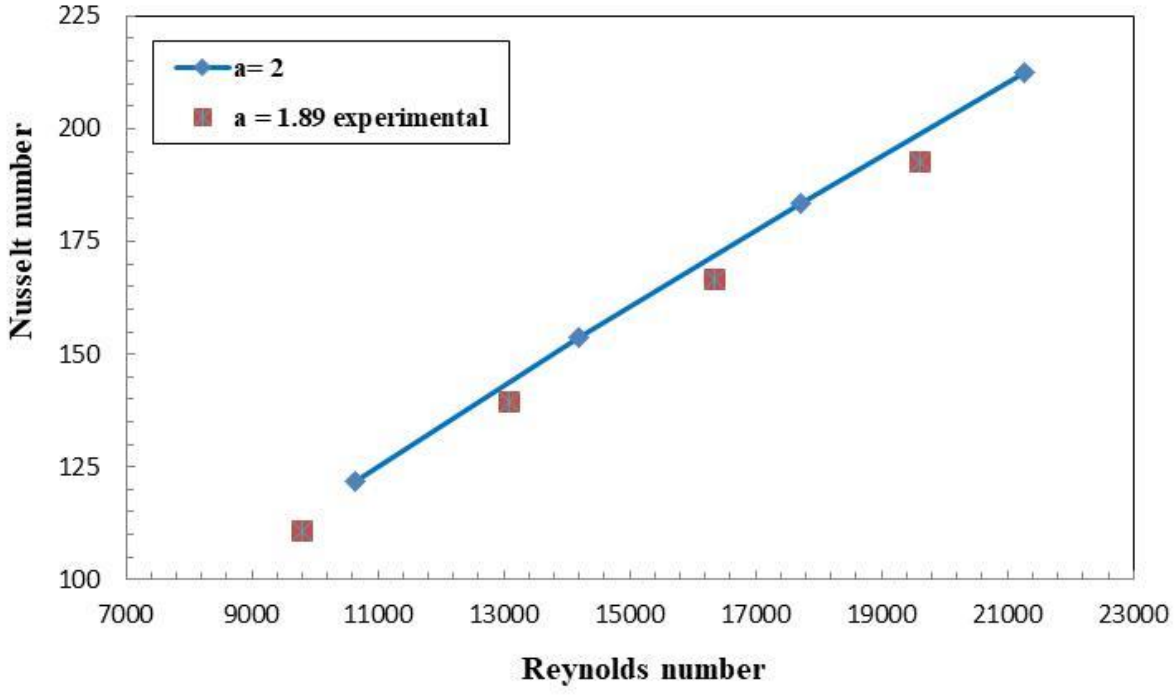

Figure (5-24) Nusselt numbers variation with Reynolds number for a cooled annulus (second pipe) at different diameter ratio

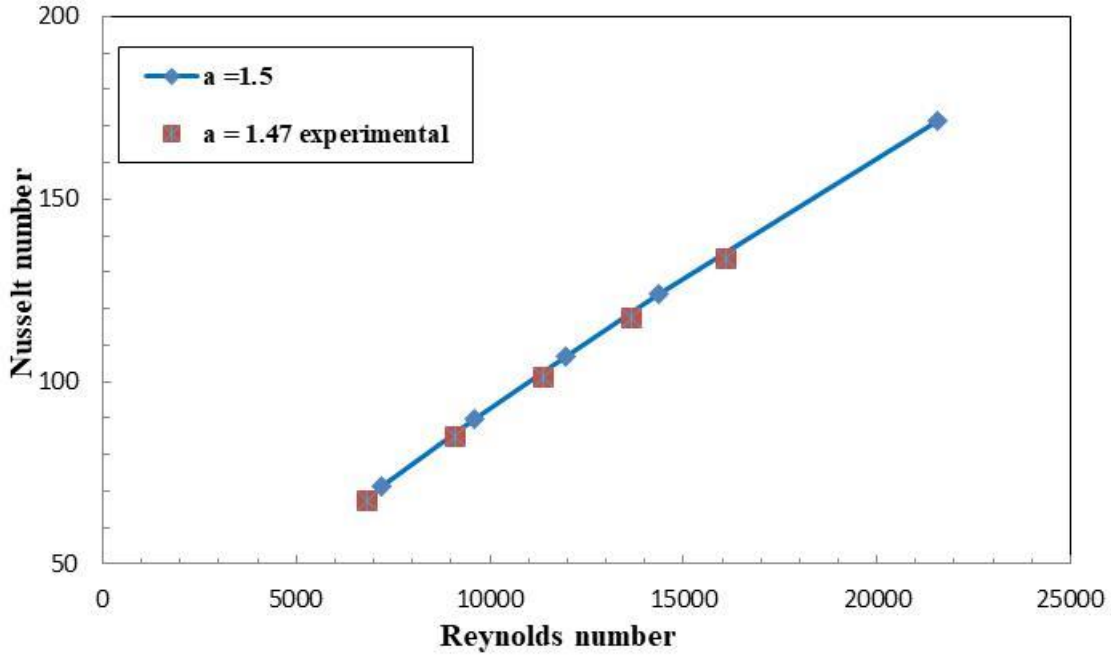

Figure (5-25) Nusselt numbers variation with Reynolds number for a heated annulus (third pipe) at different diameter ratio

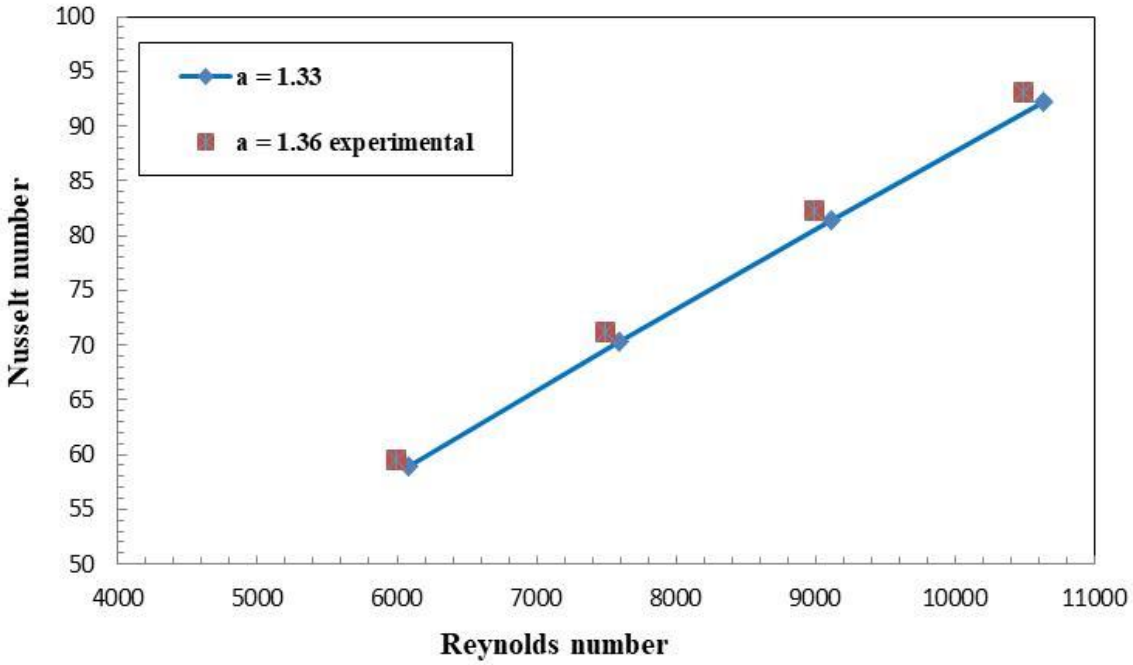

Figure (5-26) Nusselt numbers variation with Reynolds number for a cooled annulus (fourth pipe) at different diameter ratio

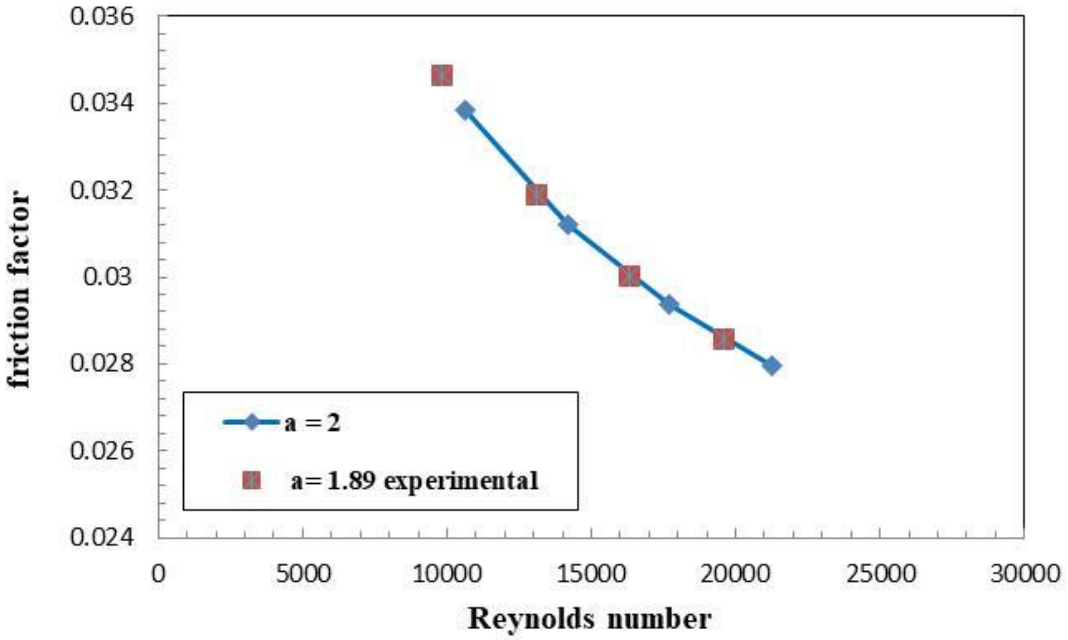

Figure (5-27) Friction factor variation with Reynolds number for inner annulus (second pipe) at different diameter ratio

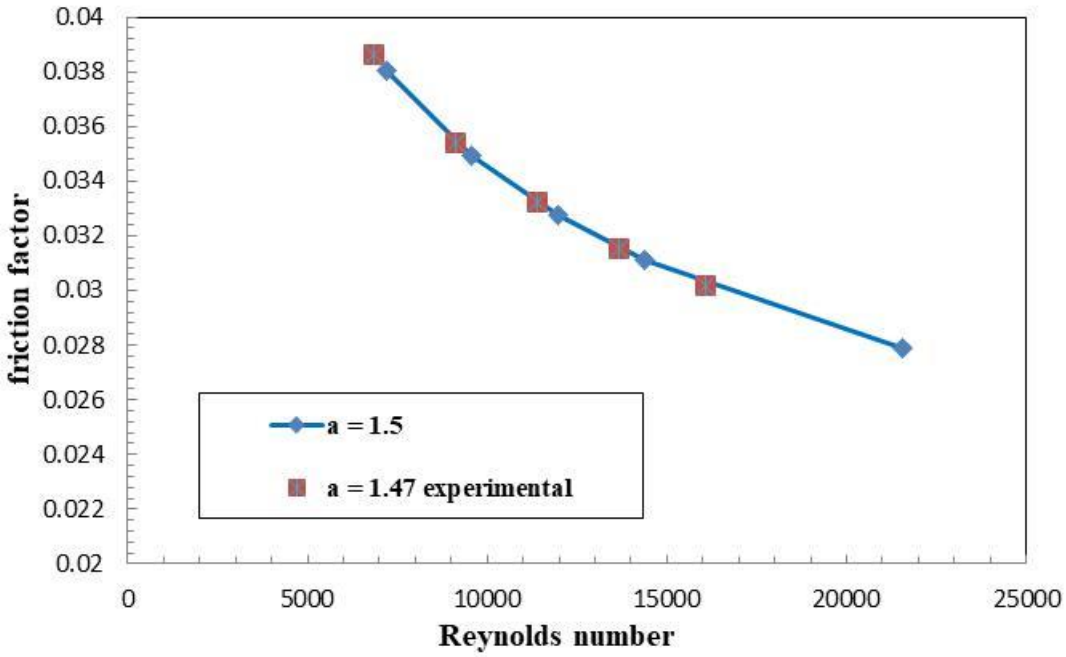

Figure (5-28) friction factor variation with Reynolds number for heated annulus (third pipe) at different diameter ratio

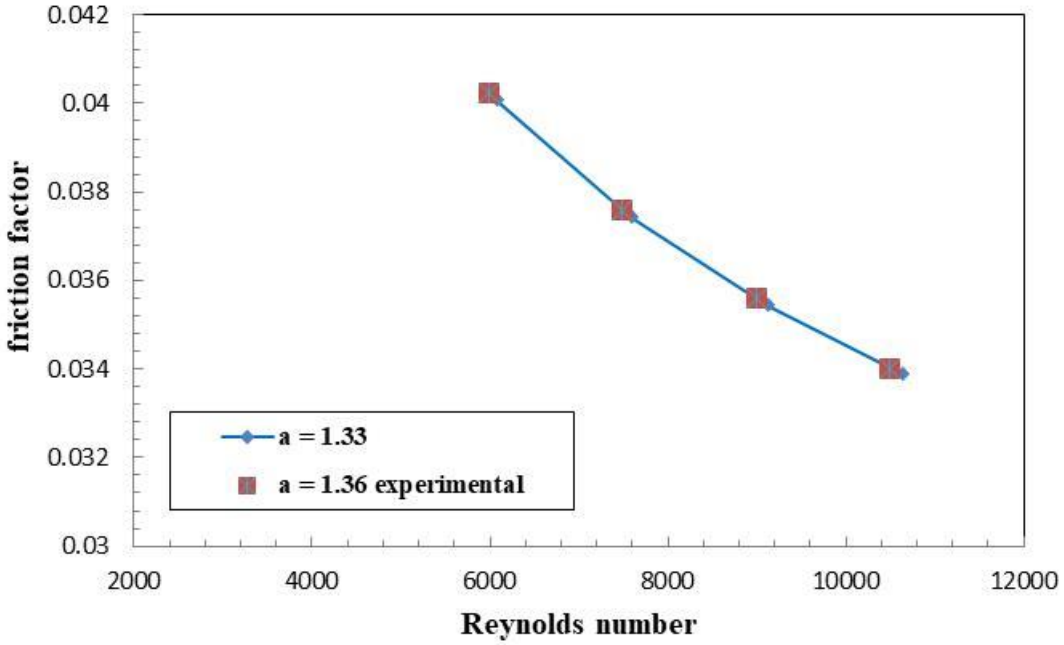

Figure (5-29) friction factor variation with Reynolds number for cooled annulus (fourth pipe) at different diameter ratio

5.2. Numerical Results

In this study, the numerical results obtained from using finite volume method single-phase model by CFD software program solidworks ver. 16, package are presented to show both the flow, heat transfer and interaction characteristics in form of path lines, velocity vectors and contours for the present models. Numerical results of temperature distribution, pressure distribution and velocity vectors are presented for turbulent flow. The results show the same behavior of temperature, pressure and velocity as that in the experimental result.

Figure (5-30) demonstrates the temperature distribution along the length of FCPHE of stage 1 at case1.In this stage the hot water in first pipe was cooled by the raw water in the around second pipe only. The flow of hot water arrangement in first pipe is counter flow with raw water in second pipe, due to that counter flow heat exchangers are inherently more efficient than parallel flow heat exchangers. The mass flow rate of raw water is 60 l/min in second pipe. It is noted the temperature decreasing along the first pipe and it reaches to 39.6 ℃ at x equal to 1 m. The decreasing of temperature continuous until reaches to 38.8 ℃.The log mean temperature difference represents the analysis of heat transfer inside heat exchanger. Therefore, the log mean temperature difference between hot water and raw water in this stage is 10.08 ℃, where that the pattern is counter flow.

Figure (5-31) shows the temperature distribution along the length of FCPHE of stage 2 at case1. In this stage the hot water in third pipe was cooled by the raw water in two pipes. These are the second and fourth pipes. The flow are arranged in parallel flow pattern. The value of mass flow rate of raw water is 60 l/min and 70 l/min in second and fourth pipes,

respectively. In this figure illustrates that temperature of hot water in third pipe decreases along the length. At the middle of the third pipe, the temperature decreases to 36.4 °C. After that the temperature decreases to 35 °C at x equal to 2 m. Therefore, the parallel flow arrangement in this stage led to reduce hot water temperature to required temperature of AL-Mussaib thermal power plant to 35 °C. In this stage there are two log mean temperature difference. The log mean temperature difference between hot water in third pipe and raw water in second pipe is 6.6 °C, that the pattern is parallel flow. While the log mean temperature difference between hot water in third pipe and raw water in fourth pipe is 9.06 °C, that the pattern is parallel flow.

Figure (5-32) represents the temperature distribution along the length of FCPHE at case1.In this figure it is noted that cooling of hot water accrued at two stages. In first stage the flow is counter current flow. The hot water in first pipe was cooled by raw water in second pipe. After that the hot water in third pipe was cooled by raw water in second and fourth pipes at second stage, where the flow pattern is parallel flow .In this case that the mass flow rate of raw water in second and fourth pipes are 60 l/min and 70 l/min, respectively. These values of masses flow rate of raw water are satisfied to cool the exit hot water temperature in AL-Mussaib thermal power plant to 35 °C. The average log mean temperature difference is 8.5 °C.

Figure (5-33) moderates the temperature distribution along the length of FCPHE for case2. The hot water cooling process takes place in two stages . In the first stage the flow is counter current flow. The hot water in first pipe was cooled by raw water in second pipe . The mass flow rate of raw water is 50 l/min in second pipe. It is noted the temperature decreasing along the first pipe and it reaches to39.4°C. The log mean temperature

difference is 10.4 in this stage. In the second stage the hot water in third pipe was cooled by the raw water in two pipes. These are the second and fourth pipes. The flow are arranged in parallel flow pattern .The value of mass flow rate of raw water is 50 l/min and 70 l/min in second and fourth pipes, respectively. In this figure illustrates that temperature of hot water in third pipe decrease from 39.4°C to 35.5°C.It is noted that the temperature of hot water higher than the temperature of hot water in case 1 ,due to the decreasing in mass flow rate of raw water in second pipe. In this stage there are two log mean temperature difference .The log mean temperature difference between hot water in third pipe and raw water in second pipe is 7.2 °C, that the pattern is parallel flow. While the log mean temperature difference between hot water in third pipe and raw water in fourth pipe is 10.2 °C, that the pattern is parallel flow. In this case, the average log mean temperature difference is 9.3 °C.

Figure (5-34) perceive the temperature distribution along the length of FCPHE for case3. There are two stages to the hot water cooling process. The flow is counter-current in the first stage. Raw water in the second pipe cooled the hot water in the first pipe. In the second pipe, the mass flow rate of raw water is 40 l/min. The temperature is recorded to be decreasing throughout the first pipe, reaching 39.5°C. In this stage, the log mean temperature difference is 10.6. The hot water in the third pipe was cooled in the second stage by the raw water in the two pipes. These are the second and fourth pipes. The flow is arranged in a parallel flow pattern. The mass flow rate of raw water in the second and fourth pipes is 40 l/min and 70 l/min, respectively. The temperature of hot water in the third pipe drops from 39.5°C to 36.09°C, as seen in this figure. The temperature of hot water was reduced by 3.41 ° C because the mass flow rate of raw water in the second pipe was insufficient to reduce the hot water temperature to 35 °

C. There are two log mean temperature differences at this stage. The LMTD between hot water in the third pipe and raw water in the second pipe is 7.9 ℃, indicating that the flow pattern is parallel. The LMTD between hot water in the third pipe and raw water in the fourth pipe is 16.6 ℃, showing that the flow pattern is parallel. In this case, the average log mean temperature difference is 11.7 °C.

Figure (5-35) indicates the temperature distribution along the length of FCPHE for case4. The hot water cooling process takes place in two stages . In the first stage the flow is counter current flow. The hot water in first pipe was cooled by raw water in second pipe . The mass flow rate of raw water is 40 l/min in second pipe. It is noted the temperature decreasing along the first pipe and it reaches to39.59°C. The log mean temperature difference is 10.9 in this stage. In the second stage the hot water in third pipe was cooled by the raw water in two pipes. These are the second and fourth pipes. The flow are arranged in parallel flow pattern .The value of mass flow rate of raw water is 40 l/min and 60 l/min in second and fourth pipes, respectively. In this figure illustrates that temperature of hot water in third pipe decreases from 39.59°C to 36.8°C. In this stage there are two log mean temperature difference .The log mean temperature difference between hot water in third pipe and raw water in second pipe is 8.7 °C, that the pattern is parallel flow. While the log mean temperature difference between hot water in third pipe and raw water in fourth pipe is 16.5 °C, that the pattern is parallel flow. In this case, the average log mean temperature difference is 12.03 °C. It is noted that the temperature of hot water higher than the temperature of hot water in case 3 ,due to the decreasing in mass flow rate of raw water in fourth pipe.

In figure (5-36), the temperature distribution along the length of FCPHE for case 5 has been tempered. There are two stages to the hot water cooling process. The flow is counter-current in the first stage. Raw water in the second pipe cooled the hot water in the first pipe. In the second pipe, the mass flow rate of raw water is 40 l/min. The temperature is recorded to be decreasing throughout the first pipe, reaching 39.85°C. In this stage, the LMTD is 11.16℃. The hot water in the third pipe was cooled in the second stage by the raw water in the two pipes. These are the second and fourth pipes. The flow is arranged in a parallel flow pattern. The mass flow rate of raw water in the second and fourth pipes is 40 l/min and 50 l/min, respectively. The temperature of hot water in the third pipe drops from 39.85°C to 37.12°C, as seen in this figure. The temperature of hot water was reduced by 2.73 ° C because the mass flow rate of raw water in the fourth pipe was insufficient to reduce the hot water temperature to 35 ° C. There are two log mean temperature differences at this stage. The LMTD between hot water in the third pipe and raw water in the second pipe is 9.1 ℃, indicating that the flow pattern is parallel. The LMTD between hot water in the third pipe and raw water in the fourth pipe is 22.9 ℃, showing that the flow pattern is parallel. In this case, the average log mean temperature difference is 14.4 ℃.

Figure (5-37) illustrates the temperature distribution along the length of FCPHE for case6.The mass flow rate of raw water is (50 and 60)l/min at second pipe and fourth pipe ,respectively. There two stages in this case to cool the hot water. In the first stage, the flow arrangement is counter flow between hot water in first pipe and raw water in second pipe. The temperature decreases along the first pipe and it reaches to 39.44°C. Therefore, the LMTD is 10.97°C.After that the cooling of hot water accrues in second stage. In the second stage the hot water in third pipe was cooled

by the raw water in second and fourth pipes. In this stage demonstrates the temperature of hot water in third pipe decreasing from 39.44°C to 35.8°C. The LMTD between hot water in third pipe and raw water in second pipe is 8.13 °C, that the pattern is parallel flow. While the LMTD between hot water in third pipe and raw water in fourth pipe is 9.42 °C, that the pattern is parallel flow. In this case, the average log mean temperature difference is 9.51 °C. It is noted that the temperature of hot water higher than the temperature of hot water in case 2 ,due to the decreasing in mass flow rate of raw water in fourth pipe.

Figure (5-38) indicates isothermal contour of temperature distribution of FCPHE at (z-y) plane .The inlet temperature of hot water and raw water are 40.8 °C and 28°C, respectively. It is noted from this figure, that the hot water was cooled in two stages. In the first stage the hot water in first pipe was cooled by the raw water in the second pipe. Therefore, the temperature decreases from 40.8 °C to 38.8 °C. It is observed the flow of hot water arrangement in first pipe is counter flow with raw water in second pipe .Therefore, the temperature decreasing from left to right in first pipe and from right to left in second pipe. In the second stage the hot water in third pipe was cooled by the raw water in second and fourth pipes. The temperature of hot water decreases from 38.8°C to 35 °C,in this stage .The temperature colors are graduated from right to left for raw water in second pipe, hot water in third pipe and raw water in fourth pipe, due to that the flow is parallel in the second stage.

Figure (5-39) shows a focused view of isothermal contours of temperature at the portion A of heat exchanger at (z-y) plane. It is observed the temperature of hot water at inlet of the first pipe is 40.8°Cthat has red

color and it decreases to minimum value 35 °C at the exit of third pipe that it has yellow color.

Figure (5-40) moderates a focused view of isothermal contours of temperature at the portion B of heat exchanger at (z-y) plane. The inlet temperature of raw water is 28°C.The mass flow rate of raw water in second and fourth pipes are (60 and 70) l/min ,respectively. It shows that the heat transfers from the hot water in first pipe to the raw water in second pipe by convection and across the pipe wall by conduction .After that the heat transfer from hot water in the third pipe to the raw water in the second and fourth pipes by convection and through the pipes wall by conduction .Therefore the fourth pipe is made of PVC to insulated the heat exchanger.

Figures (5-41), (5-42) and (5-43) present isothermal contours of temperatures distribution for the FCPHE at x-y plane and z = 0, 1,2 m respectively. Figure (5-41) shows that the inlet temperature of hot water in the first pipe is 40.8 °C and decreases to 35 °C at the outlet of the third pipe. In the same time the temperature of raw water in the second and fourth pipe is (31.4 and 31.8) °C, respectively. It is noted at z=0, the inlet of hot water in first pipe and outlet of hot water from third pipe. While the exit of raw water from second and fourth pipes. Figure (5-42) presents isothermal contours of temperatures distribution for the FCPHE at x-y plane and z =1(middle of the heat exchanger).It is showed that temperature of hot water in the first pipe is 39.6 °C and temperature of hot water in the third pipe 36.4 °C. Figure (5-43) shows isothermal contours of temperatures distribution for the FCPHE at x-y plane and z =2.It is indicated how the hot water followed from the first pipe to the third pipe. The counter flow arrangement between hot water in the first pipe and hot water in the second pipe can be seen.

Figure (5-44) details the velocity vector map for the FCPHE.It is observed that the flow is counter current flow arrangement in the first stage. While the flow is in a parallel flow arrangement in the second stage. It shows that the velocity in the inner tube is larger than other velocities because of the small cross section area of the tube. Also, this figure shows that the velocity decreases when the diameter of the tube increases.

There is an irregular motion of fluid in directions transverse to the direction of the main flow. The pressure drop caused by friction and turbulent flow depends on the roughness of the pipe. Therefore, figures (5-45), (5-46), (5-47), (5-48), (5-49), and (5-50) indicate the pressure drop in each pipe of the heat exchanger.

Figure (5-45) illustrates the pressure distribution along the heat exchanger at case 1. When a flow is disturbed, a pressure drop is created, that is the flow pressure at the beginning of a passage is higher than at its end. It is noted that the pressure drop by (1.38, 0.82, 1.02 and 0.198) % at first pipe and second pipe, third pipe and fourth pipe, respectively.

The pressure distribution along the heat exchanger in case 2 is depicted in figure (5-46). A pressure drop occurs when a flow is disrupted; meaning the flow pressure at the beginning of a passage is higher than at the end. At the first pipe, second pipe, third pipe, and fourth pipe, the pressure drops by (1.44, 0.59, 1.07, and 0.198) %, respectively.

Figure (5- 47) represents the pressure distribution along the heat exchanger in case 3. When a flow is disturbed, a pressure drop occurs, indicating the flow pressure at the beginning of a passage is higher than at the end. The pressure reduces by (1.41, 0.32, 1.29, and 0.199) % at the first, second, third, and fourth pipes, respectively.

Figure (5-48) depicts the pressure distribution along the heat exchanger in case 4. A pressure drop happens when a flow is disrupted, showing that the flow pressure at the beginning of a passage is higher than the flow pressure at the end. At the first, second, third, and fourth pipes, respectively, the pressure drops by (1.39, 0.41, 0.25, and 0.121) %.

Figure (5-49) shows the pressure distribution along the heat exchanger in case 5. When a flow is disturbed, a pressure drop occurs, indicating that the flow pressure at the beginning of a passage is higher than the flow pressure at the end. The pressure reduces by (1.4, 0.412, 0.89, and 0.06) % at the first, second, third, and fourth pipes, respectively.

In case 6, figure (5-50) depicts the pressure distribution along the heat exchanger. A pressure drop happens when a flow is disrupted, showing that the flow pressure at the start of a passage is higher than the flow pressure at the end. At the first, second, third, and fourth pipes, the pressure drops by (1.39, 0.59, 1.31, and 0.12) %, respectively.

Figure (5-51) shows the static pressure drop distribution contour map of FCPHE. There are two stages to cool the hot water. In the first stage, the flow arrangement is a counter current flow between the hot water in the first pipe and raw water in the second pipe. It is observed that pressure drops inside the first pipe and the second pipe .In the second stage, the flow arrangement is a parallel flow between the raw water in the second pipe, hot water in the third pipe, and raw water in the fourth pipe. From the figure, it is noted that the higher pressure in the first pipe and the lower pressure in the fourth pipe.

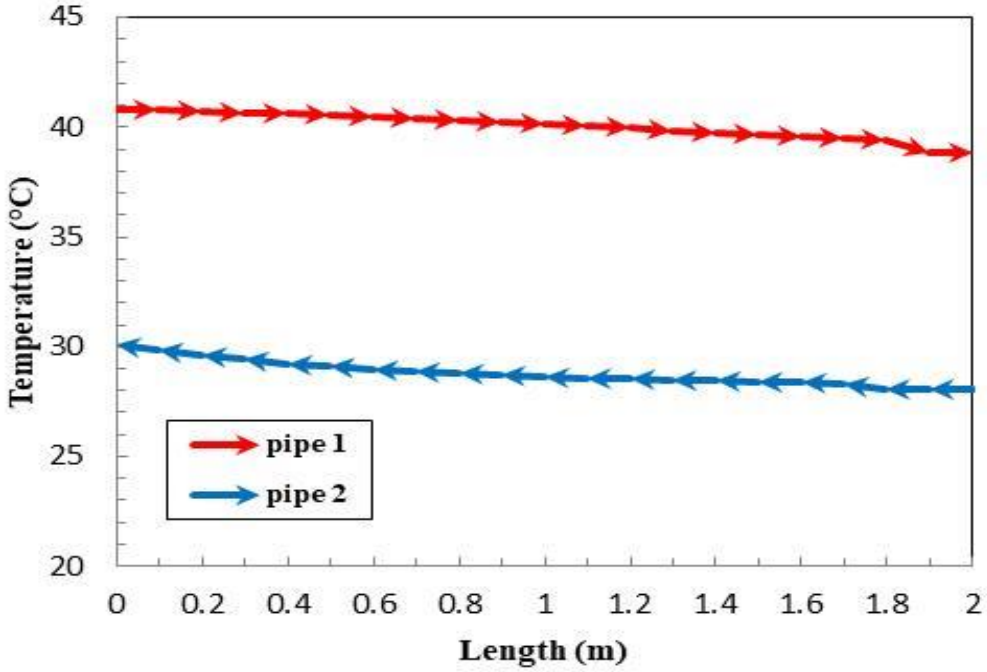

Figure (5-30) variation of temperatures along the length of FCPHE for stage 1 at case1

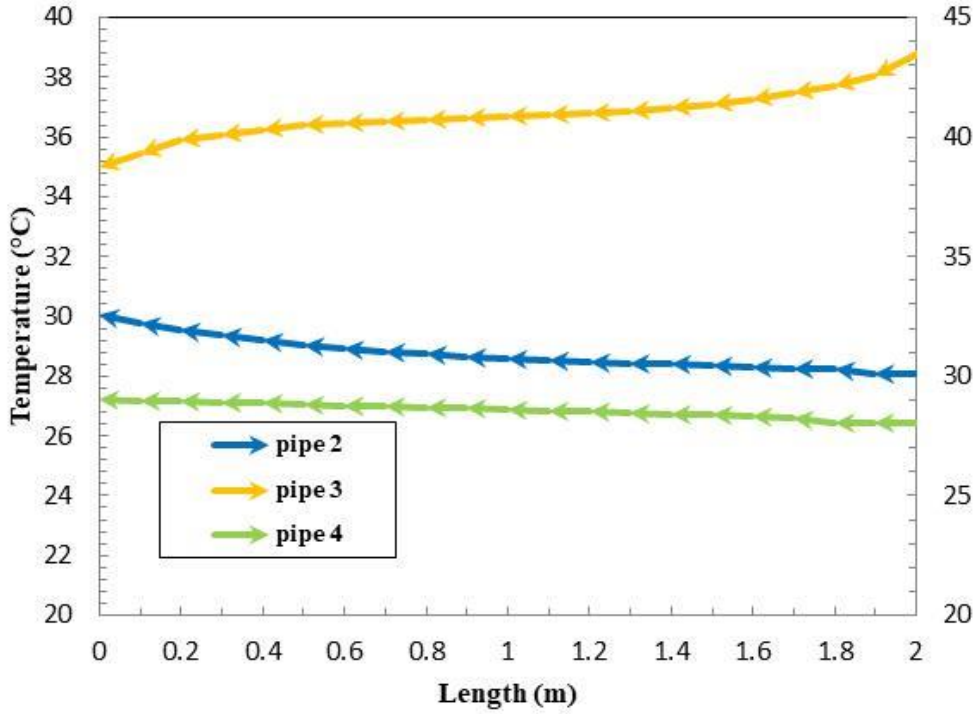

Figure (5-31) variation of temperatures along the length of FCPHE for stage 2 at case1

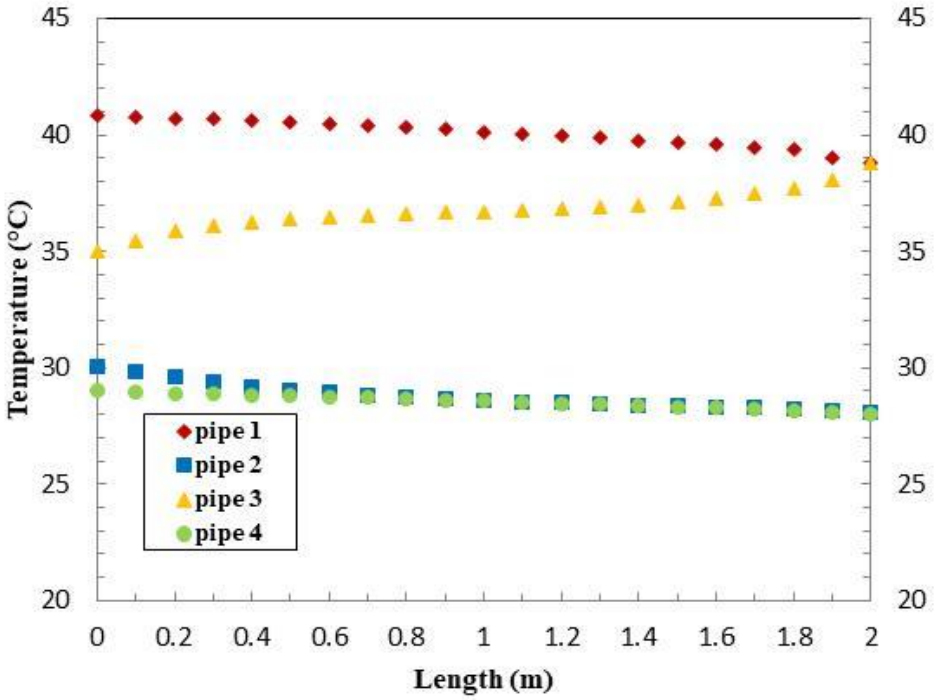

Figure (5-32) variation of temperatures along the length of FCPHE at case1

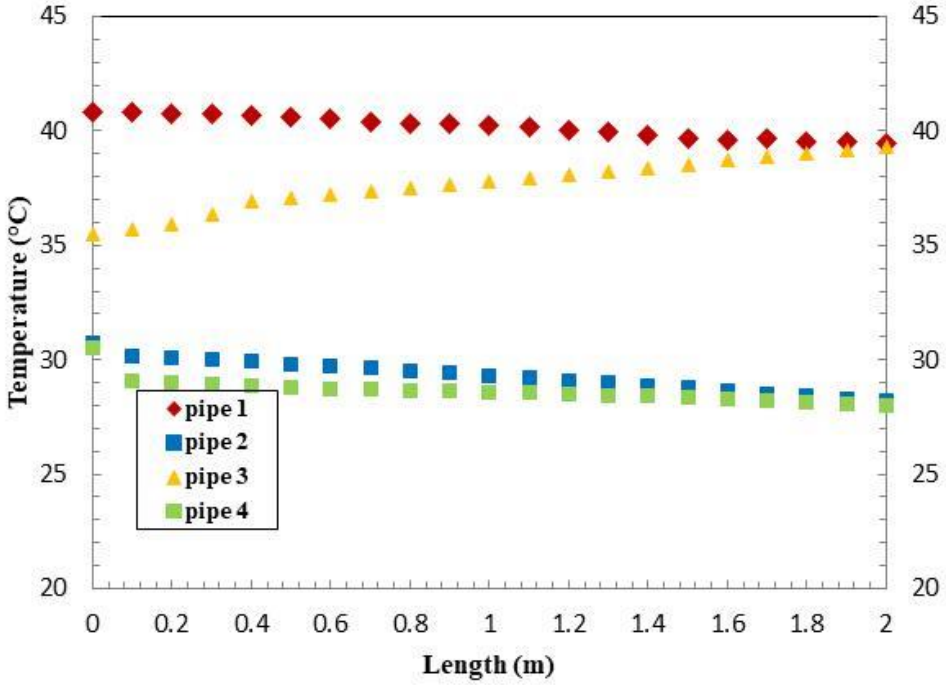

Figure (5-33) variation of temperatures along the length of FCPHE at case2

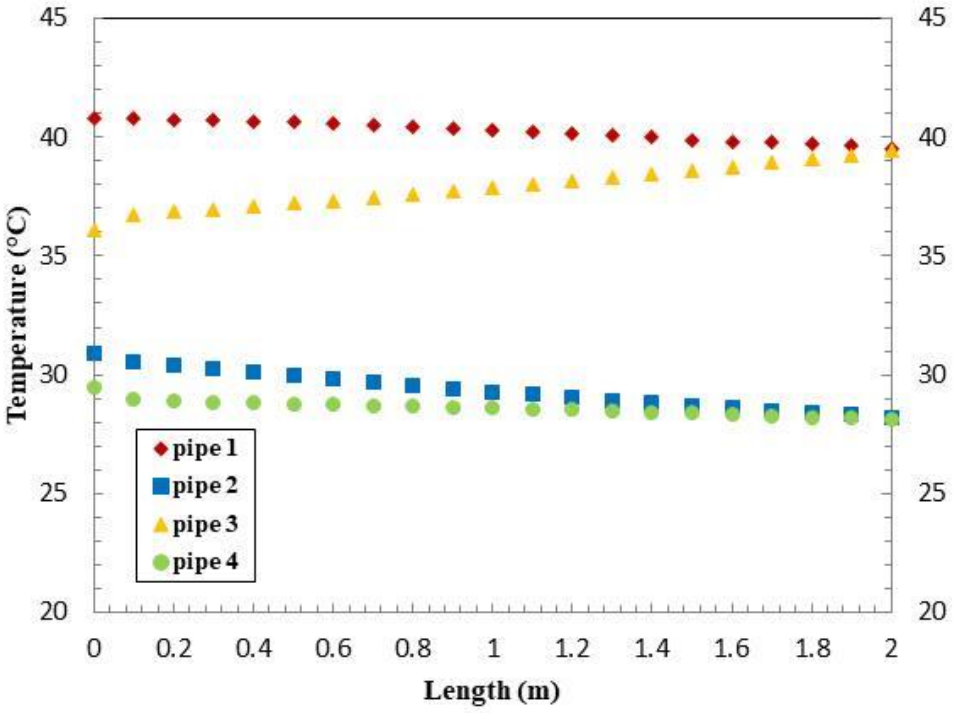

Figure (5-34) variation of temperatures along the length of FCPHE at case3

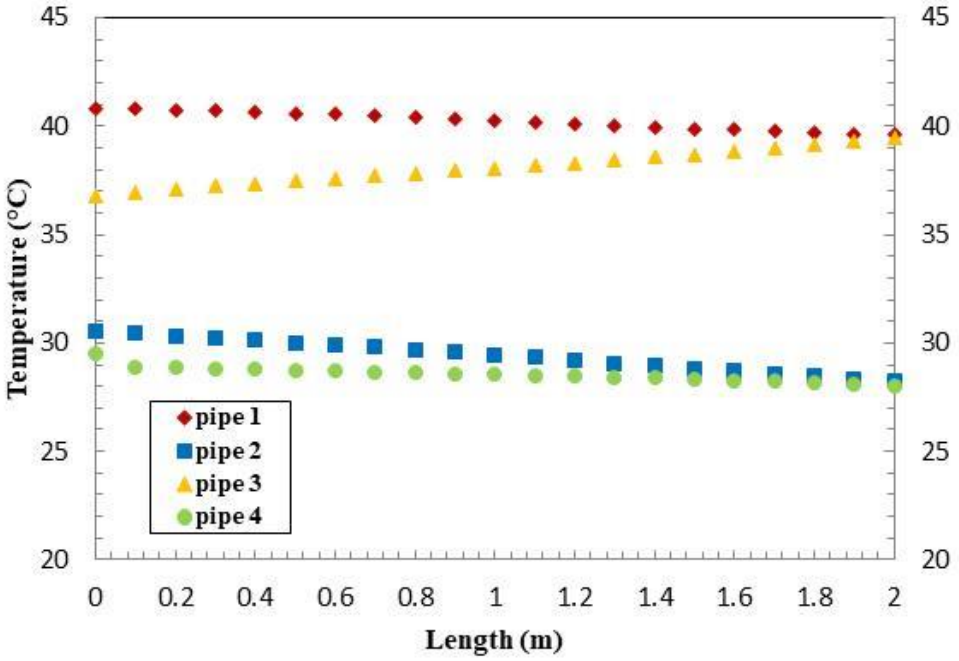

Figure (5-35) variation of temperatures along the length of FCPHE at case4

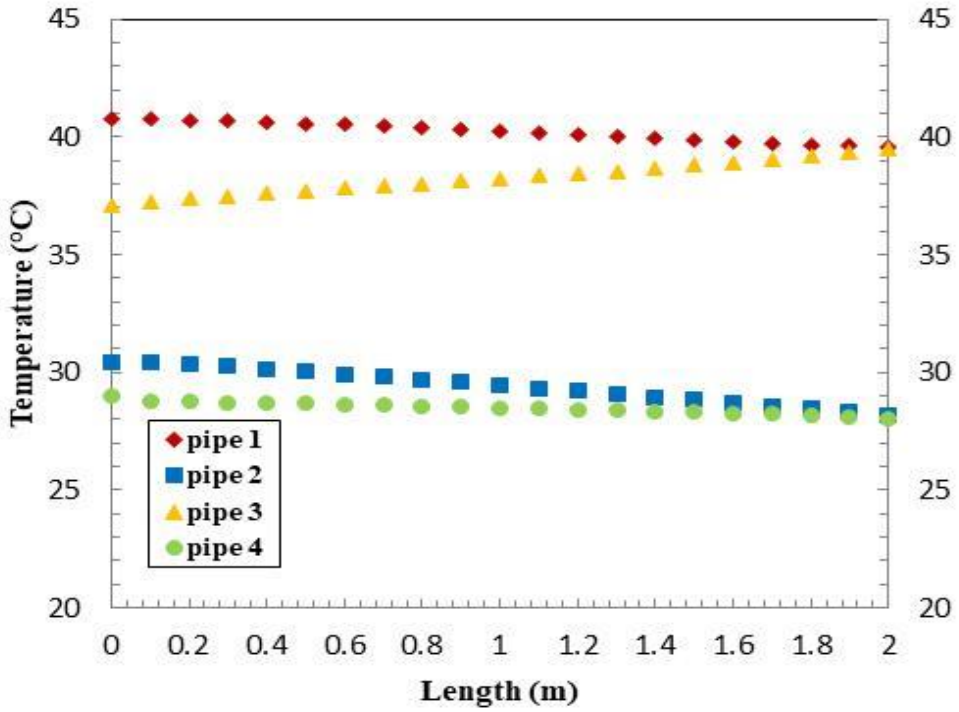

Figure (5- 36) variation of temperatures along the length of FCPHE at case5

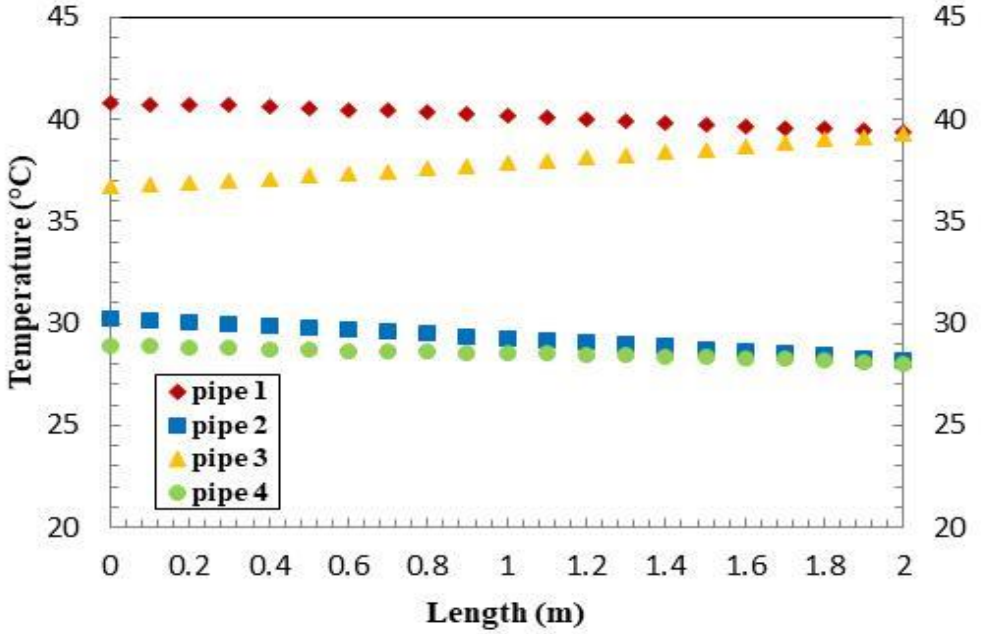

Figure (5- 37) variation of temperatures along the length of FCPHE at case6

Figure (5-38) isothermal contour of temperature distribution for FCPHE

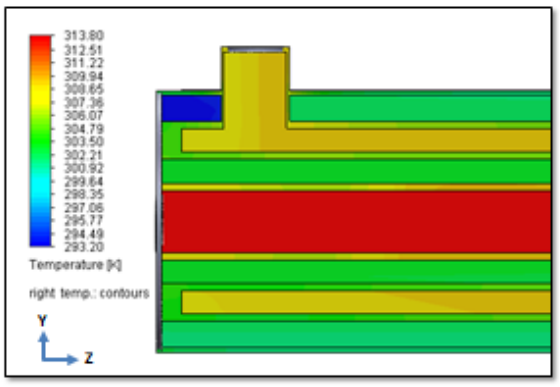

Figure (5-39) isothermal contour of temperature distribution for FCPHE, at position A

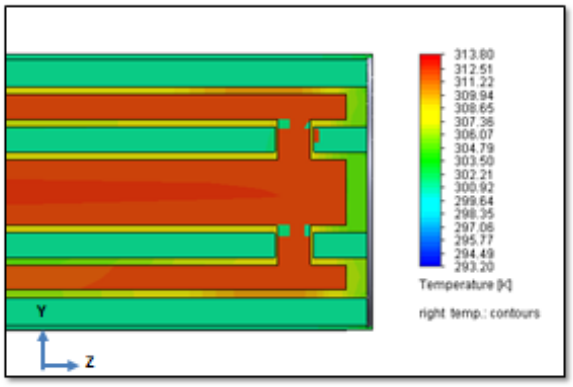

Figure (5-40) isothermal contour of temperature distribution for FCPHE, at position B

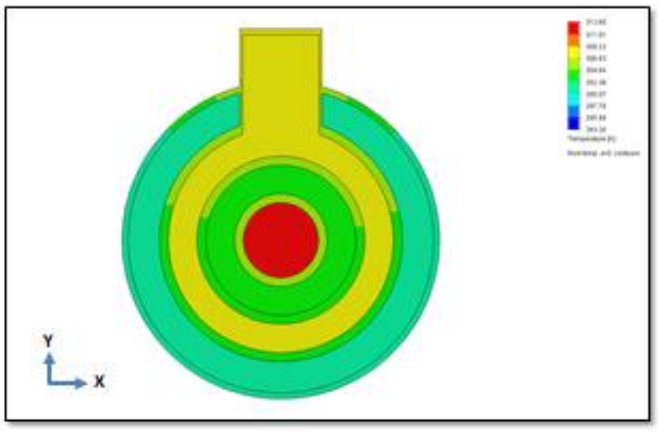

Figure (5-41) isothermal contours of temperature for (FCPHE) of plane x-y at z=0

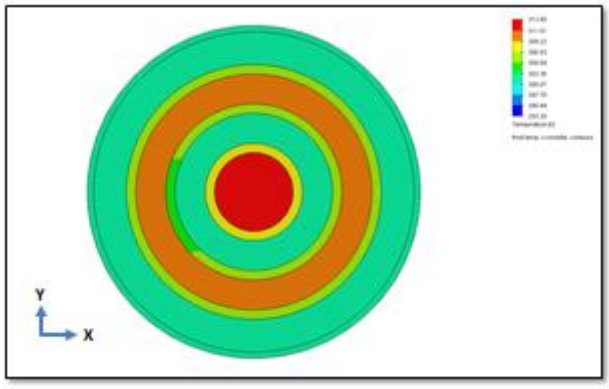

Figure (5-42) isothermal contours of temperature for (FCPHE) of plane x-y at z=1

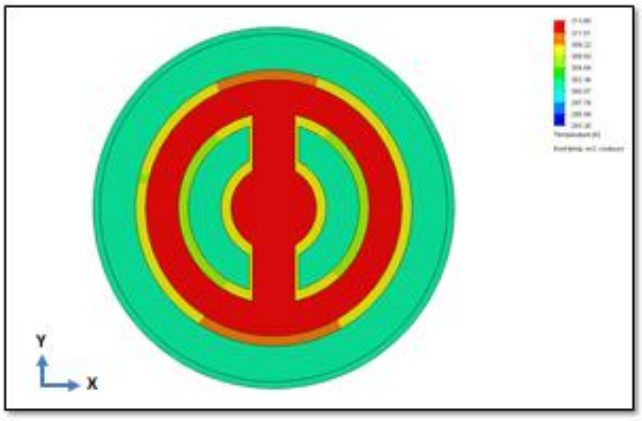

Figure (5-43) isothermal contour of temperature for (FCPHE) of plane x-y at z=2m

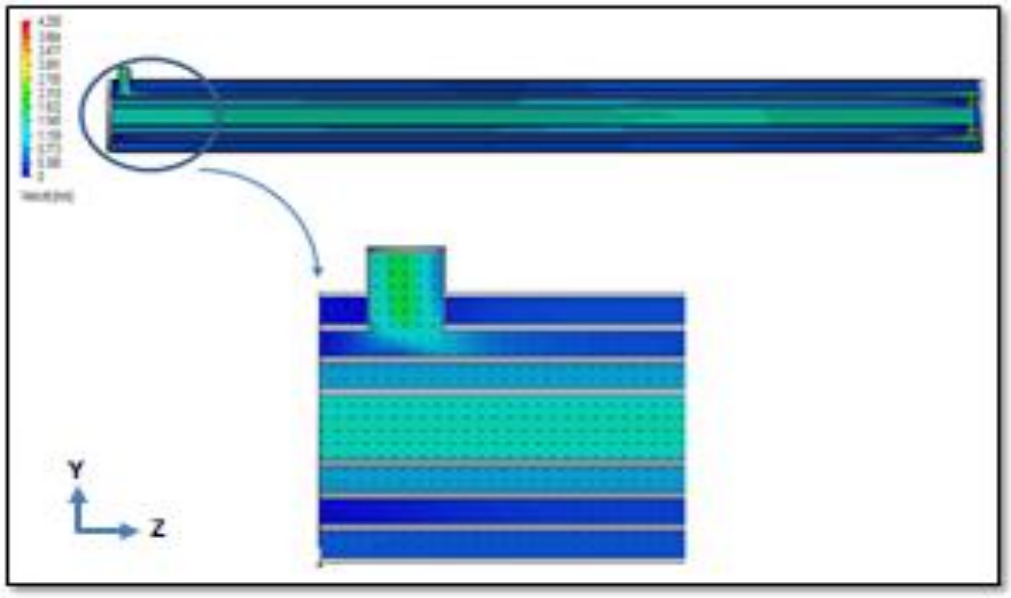

Figure (5- 44) vector map of velocity for FCPHE

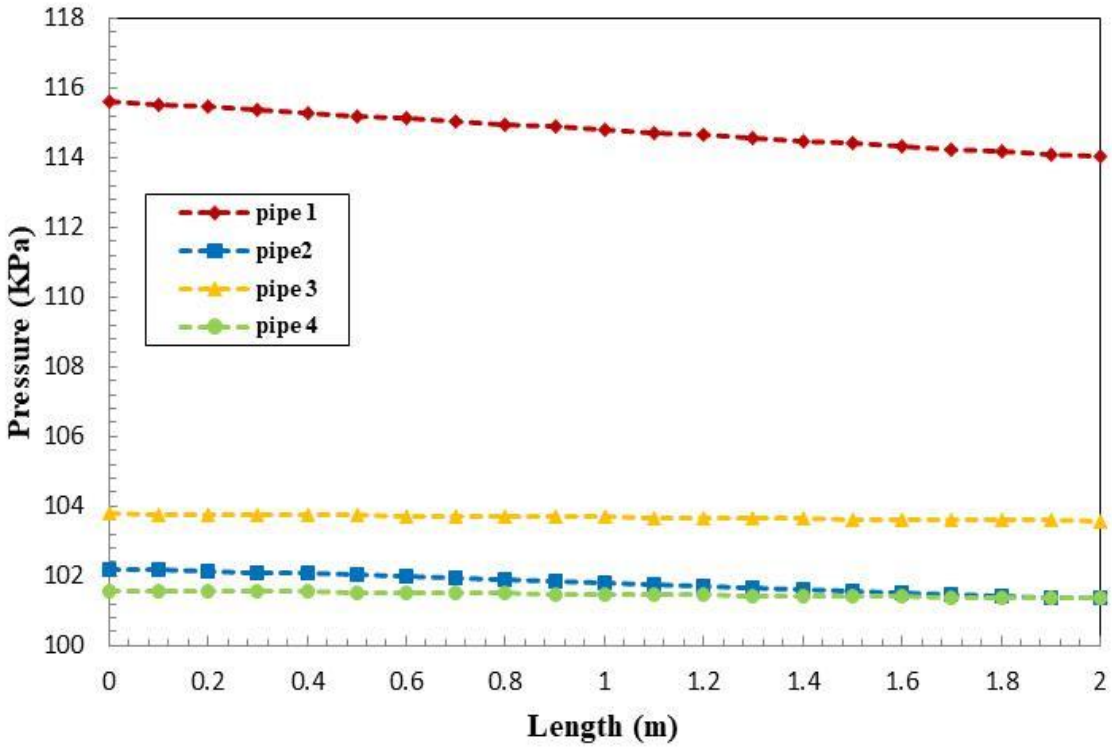

Figure (5-45) variation of pressure along the length of FCPHE at case1

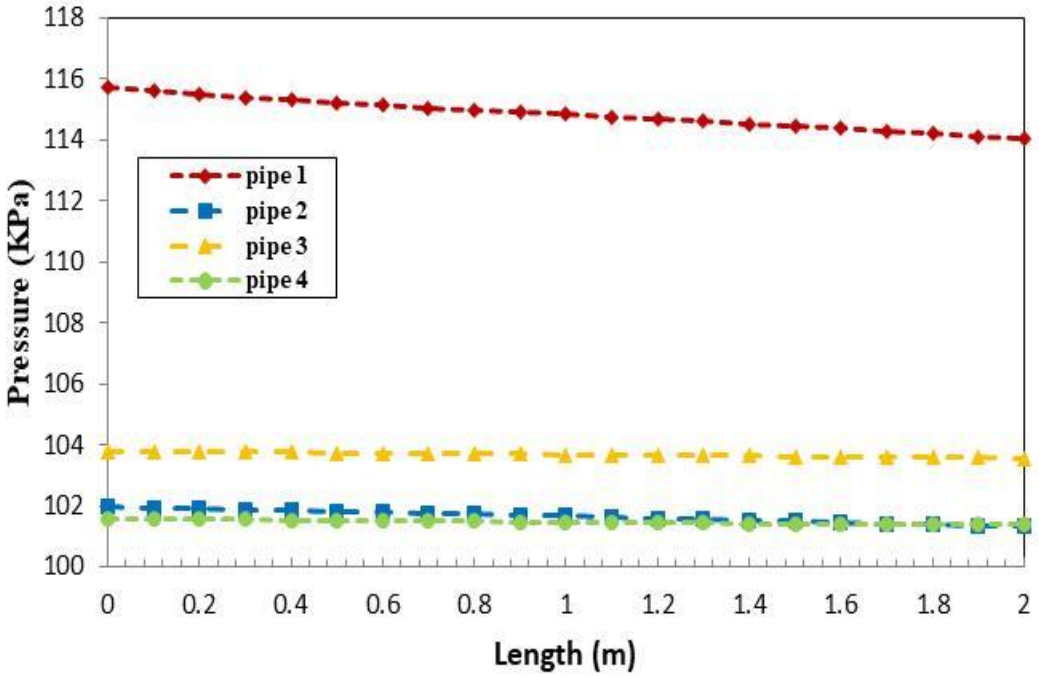

Figure (5-46) variation of pressure along the length of FCPHE at case2

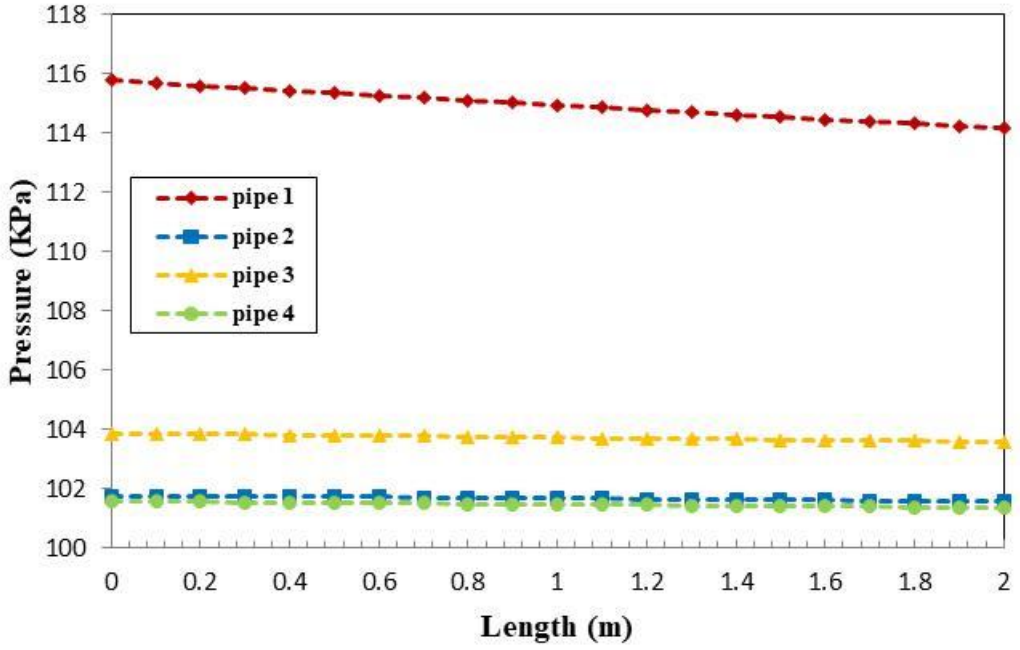

Figure (5-47) variation of pressure along the length of FCPHE at case3

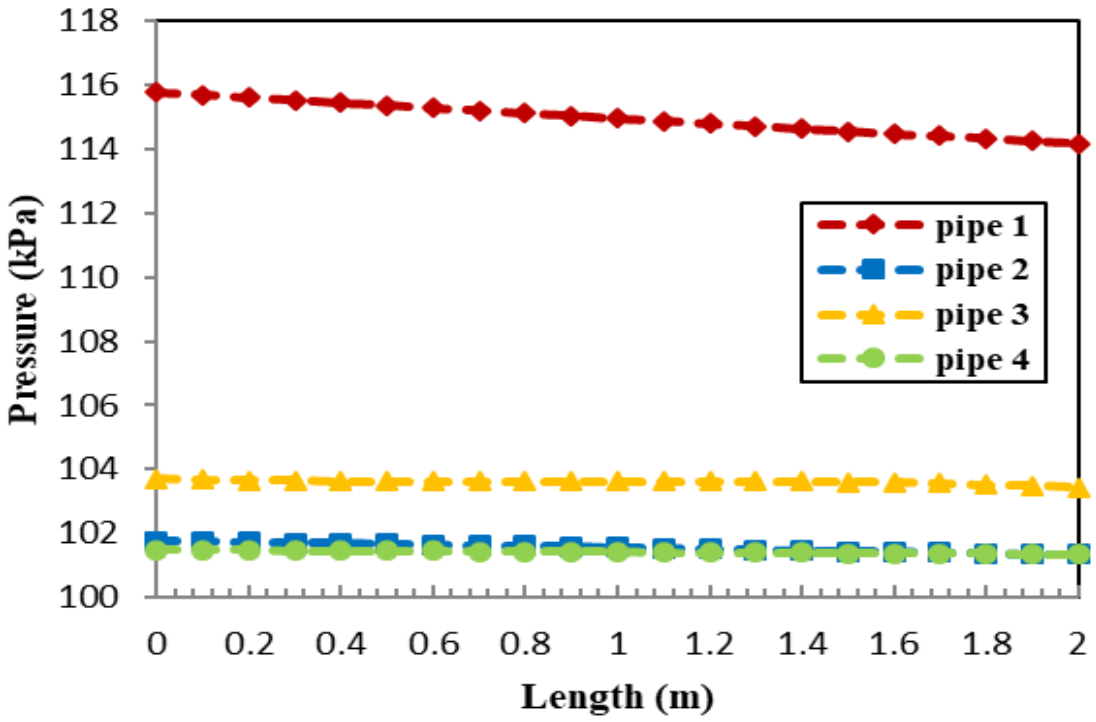

Figure (5-48) variation of pressure along the length of FCPHE at case4

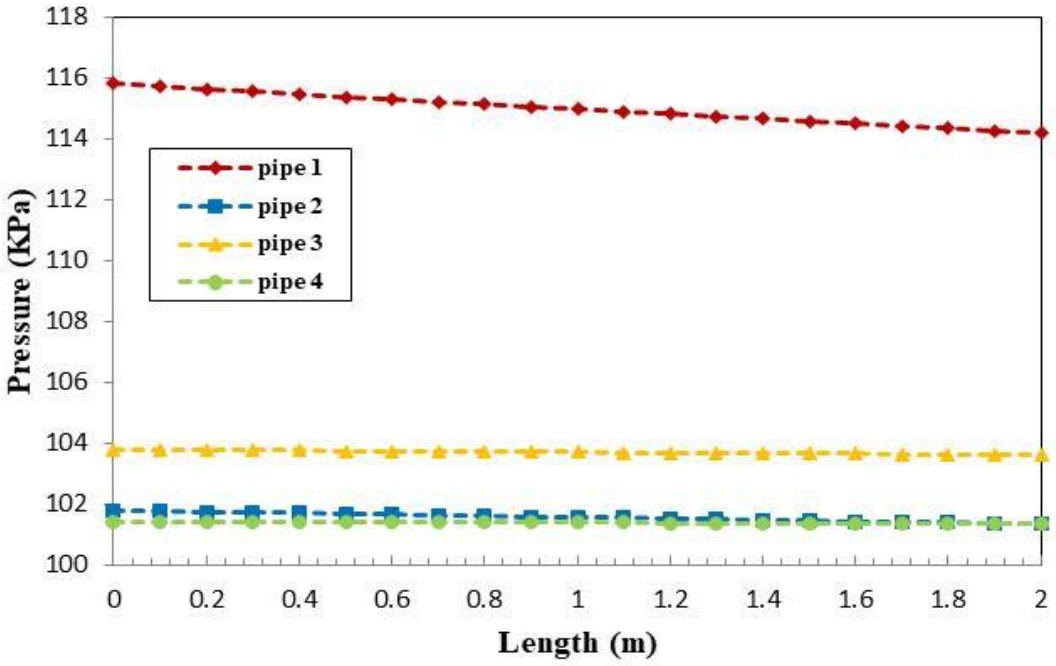

Figure (5-49) variation of pressure along the length of FCPHE at case5

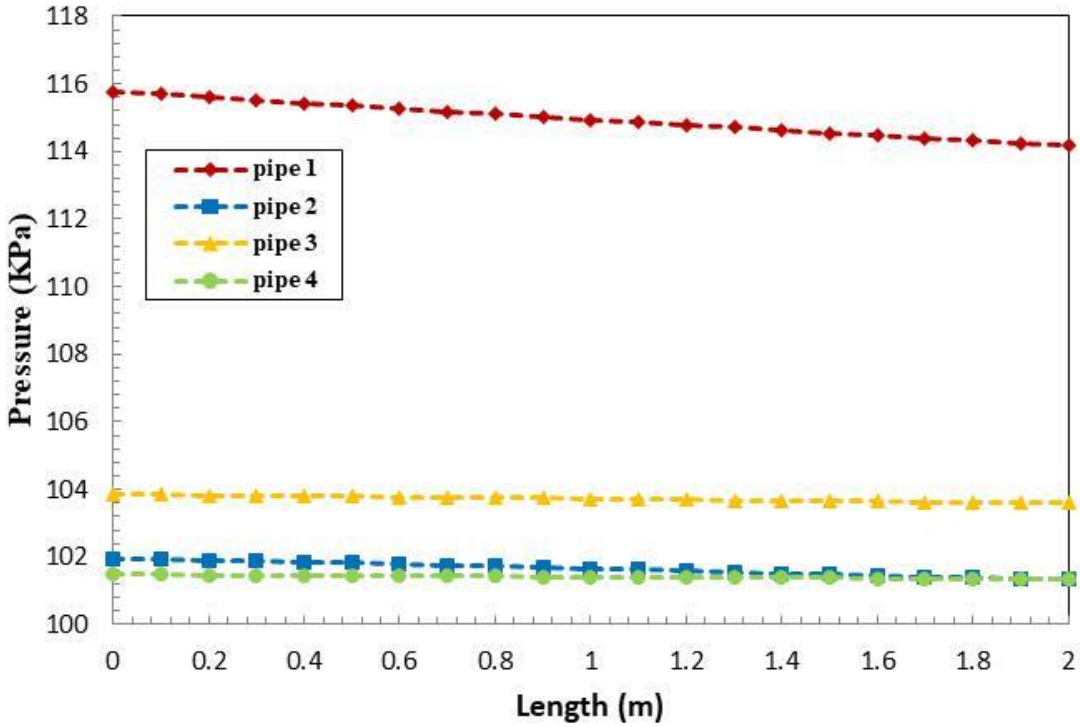

Figure (5-50) variation of pressure along the length of FCPHE at case6

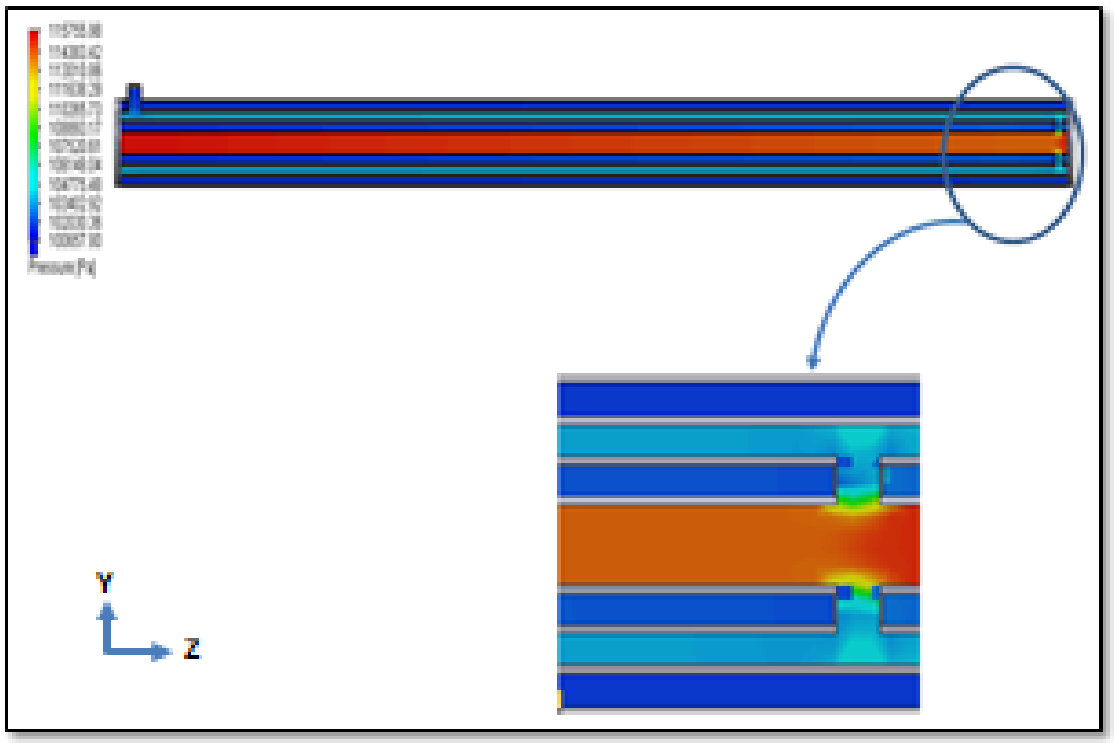

Figure (5- 51) contour map of pressure for FCPHE

5.3. Comparison between Experimental and Theoretical Results

Figures (5-52) to (5- 57) illustrates the experimental and the numerical temperature distributions along the length of the four concentric pipe heat exchanger. In these figures, it is noted that cooling of hot water accrued at two stages. In first stage the flow is counter current flow. The hot water in first pipe was cooled by raw water in second pipe. After that the hot water in third pipe was cooled by raw water in second and fourth pipes at second stage, where the flow pattern is parallel.

Figure (5-52) indicates experimentally and numerically the local temperature distributions along the length of the four pipe heat exchanger in case 1. In this case, the mass flow rates (40, 60, 40, and 70) l/min for the first pipe, the second pipe, the third pipe, and the fourth pipe, respectively. At the first stage, the temperature of hot water decreased to 38.5 °C and 38.8 °C experimentally and numerically, respectively. After that, the temperature of hot water decreased to 34.7°C and 35°C experimentally and numerically, respectively, at the second stage. The experimental results show good agreement with the theoretical results. The deviation error between experimental and theoretical work is 0.86 % at the exit of hot water.

Figure (5-53) illustrates experimentally and numerically the local temperature distributions along the length of the four pipe heat exchanger in case 2. The temperature of hot water dropped to 39.3 °C and 39.4 °C experimentally and numerically in the first stage. The temperature of hot water then dropped to 35.3°C and 35.5°C, respectively, in the second stage, both experimentally and numerically. The experimental and theoretical results are in good agreement. At the exit of hot water, the deviation error between experimental and theoretical work is 0.57 %.

Figure (5-54) represents experimentally and numerically the local temperature distributions along the length of the four pipe heat exchanger in case 3. In the first stage, the temperature of hot water reduced to 39.3 °C and 39.5 °C, respectively, experimentally and numerically. Both experimentally and numerically, the temperature of hot water declined to 35.8°C and 36.09°C in the second stage. The deviation error between experimental and theoretical work at the hot water outlet is 0.81 %.

Figure (5-55) reports experimentally and numerically the local temperature distributions along the length of the four pipe heat exchanger in case 4. Experimentally and numerically, the temperature of hot water was decreased in the first stage to 39.5 °C and 39.6 °C, respectively. The temperature of hot water fell to 36.3°C and 36.8°C in the second stage, according to experimental and numerical. At the hot water exit, there is a 1.38 % discrepancy between experimental and theoretical work.

Figure (5-56) shows the local temperature distributions along the length of the four-pipe heat exchanger in case 5 both experimentally and numerically. The temperature of hot water was decreased to 39.8 °C and 39.6 °C, respectively, in the first stage, both experimentally and numerically. According to experimental and numerical data, the temperature of hot water dropped to 36.9°C and 37.12°C in the second stage. There is a 0.59 %divergence between experimental and theoretical work at the hot water outlet.

In case 6, Figure (5-57) demonstrates the local temperature distributions over the length of the four pipe heat exchanger, as experimentally and numerically. In the first stage, the temperature of hot water was reduced to 39.3 °C and 39.42 °C, respectively, as experimentally and numerically. According to experimental and numerical results, the

temperature of hot water decreased to 35.6°C and 36.72°C in the second stage. There is a 3.15 %change between experimental and theoretical work at the hot water outlet.

Figures (5-58), (5-59), (5-60), (5-61), (5-62), and (5-63) represent the pressure distribution along the heat exchanger for two stages of six cases, experimentally and theoretically. It is noted that the pressure drops in four pipes. In the first stage, the deviation error between experimental and theoretical at the first pipe is (1.46 to 0.25) % for all cases. In the second stage, the deviation error between experimental and theoretical at the third pipe is (0.77 to 0.55) % for all cases. . While the pressures drop in the second and fourth pipes, experimental and theoretical, is very close.

The comparison of the present experimental and theoretical results is shown in figure (5-64) for Nusselt number versus Reynolds number. Agreement between the results is noticed, and the maximum division was 2.76% at the first pipe .It can be seen that the Nusselt number increases with increasing the Reynolds number.

Figure (5-65) depicts a comparison of the present experimental and theoretical results for friction factor against Reynolds number. The highest difference was 8 % at the first pipe, indicating that the findings were in agreement. Experimentally and theoretically, the friction factor for the second, third, and fourth pipes is fairly close.

Figure (5-66) depicts a comparison of the present experimental and theoretical results for heat transfer coefficient against Reynolds number. The largest difference in the first pipe was 0.15%, indicating that the results were consistent. Experimentally and mathematically, the heat transfer coefficients for the second, third, and fourth pipes are quite similar.

Figure (5-67) moderates the relation between logarithmic mean temperature difference (LMTD) and mass flow rate of raw water. It shows that the LMTD decreases with increasing of mass flow rate of raw water. In this figure the comparison shows agreement with LMTD with maximum difference 7.2 % for mass flow rate 40 l/min.

The relationship between heat transfer rate and Reynolds number is shown in Figure (5-68). For cases 1, 2, 3, and 4, the experimental and numerical deviations are (10.11, 16.6, 14.56, and 11.39 %, respectively). In cases 5 and 6, however, the results are extremely close.

Figure (5-69) reports the comparison between the experimental and theoretical results of effectiveness at different values of raw water mass flow rate. The effectiveness increases with increasing the raw water mass flow rate until it reaches its peak point at (60 and 70) l/min in the second and fourth pipes, respectively. The percentage error between the experimental effectiveness and theoretical effectiveness is 10.2% at maximum value.

Figure (5-70) reports the local temperature distributions along the length of shell and tube heat exchanger(STHE) for Al-Mussaib thermal power plant and four concentric pipe heat exchanger(FCPHE) at the same inlet hot water temperature and raw water temperature .Counter flow arrangements in the shell and tube heat exchanger. While, the four concentric pipe heat exchanger the flow arrangements counter flow in first stage and parallel flow in second stage. When compared between the two heat exchangers, it was found that the temperature of hot water decreased from 40°C to 38.5°C at the shell and tube heat exchanger. While the temperature of hot water decreased from 40 °C to 34.7°C in the four concentric pipe heat exchanger. Therefore, the shell and tube heat

exchanger cannot decrease the temperature of hot water to the required temperature of the Al-Mussaib thermal power plant.

The experimental and numerical investigations of the triple concentric-tube heat exchanger were presented by **Gomaa et al.[31]** . Three fluids being considered which are chilled water in inner tube, hot water in inner annulus, and normal tap water in outer annulus. Numerical CFD model is developed using a finite volume discretization method .The comparison between TTHE which was presented by Gomaa and FCPHE in this work, is carried out**.** Figure (5-71) shows the local temperature distributions along the dimensionless length of triple tube heat exchanger (TTHE) .Counter flow arrangements in the triple tube heat exchanger. It can be seen from the figure that the hot water temperature decreases from 70°C to 48.7°C. It can be observed that the TTHE function used two fluids, raw water and chilled water, to reduce the temperature of hot water. The FCPHE, on the other hand, uses raw water in two stages to reduce the temperature of hot water to 45°C.

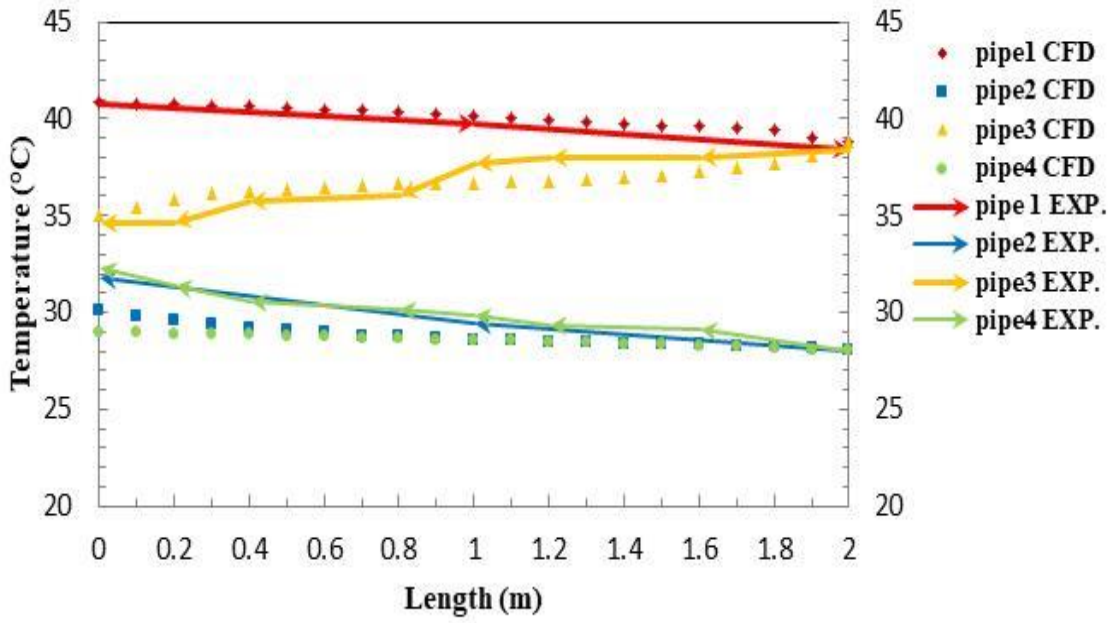

Figure (5-52) variation of temperature along the length of FCPHE at case1

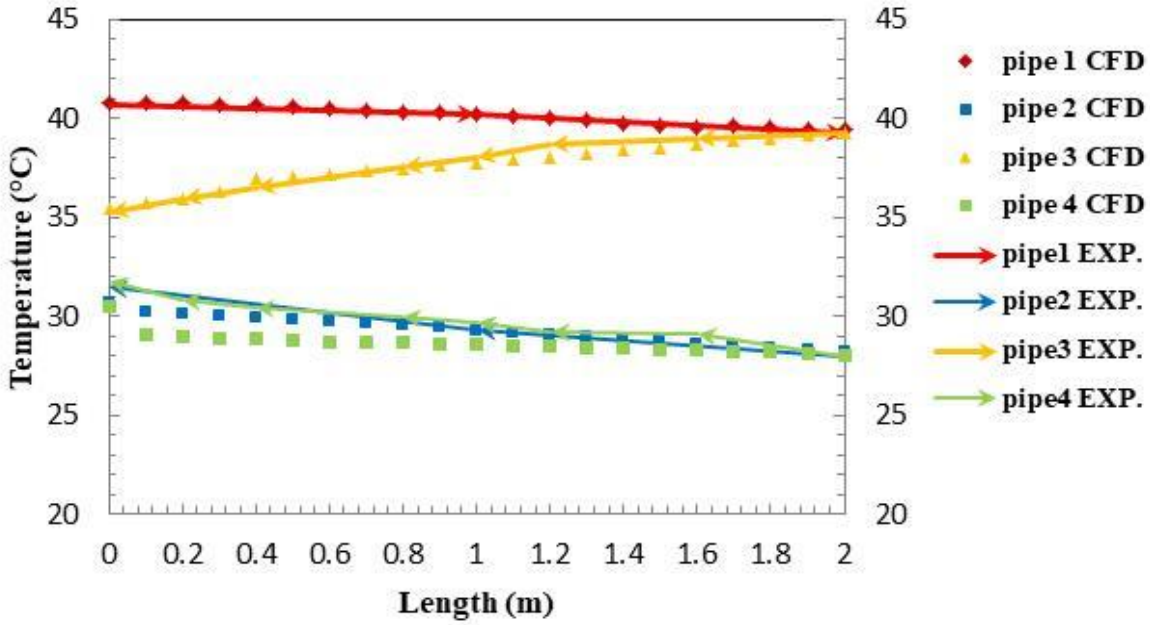

Figure (5-53) variation of temperature along the length of FCPHE at case2

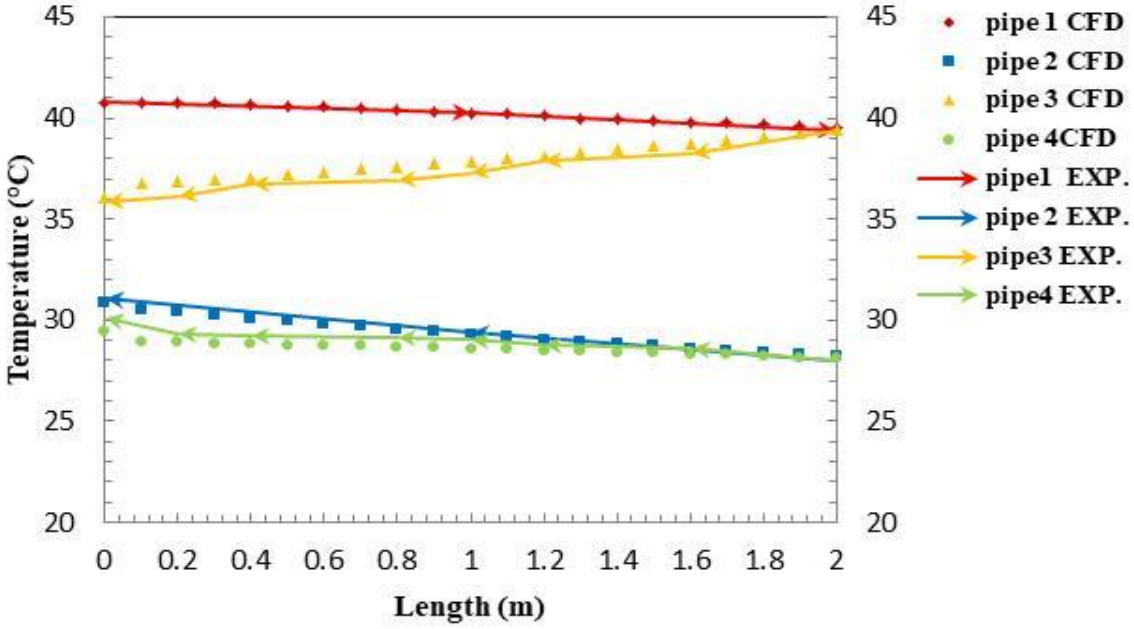

Figure (5-54) variation of temperature along the length of FCPHE at case3

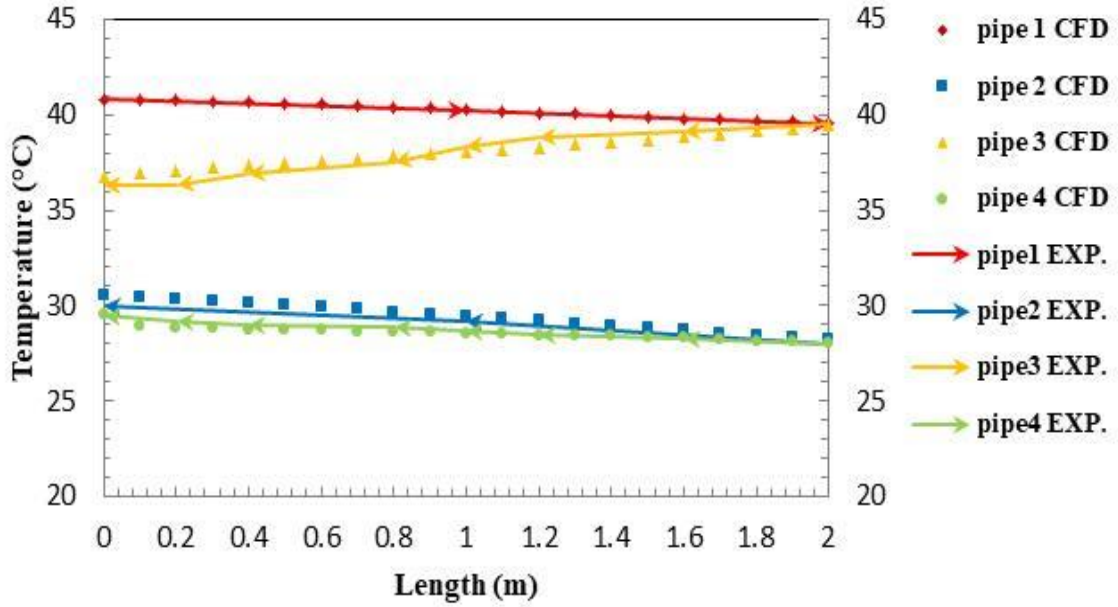

Figure (5-55) variation of temperature along the length of FCPHE at case4

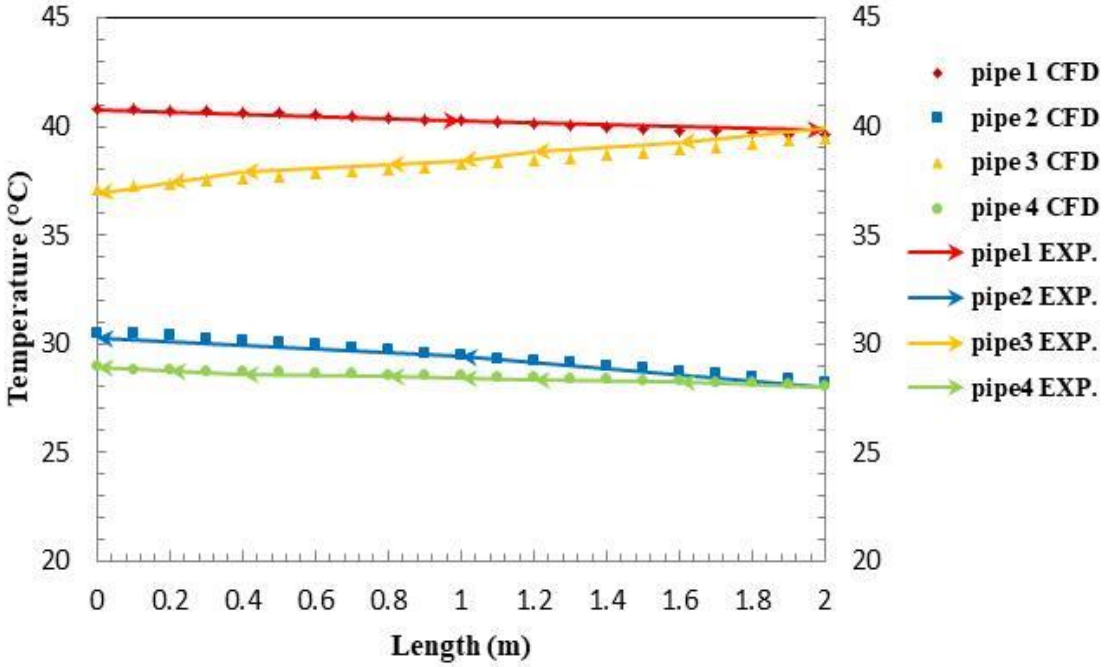

Figure (5-56) variation of temperature along the length of FCPHE at case5

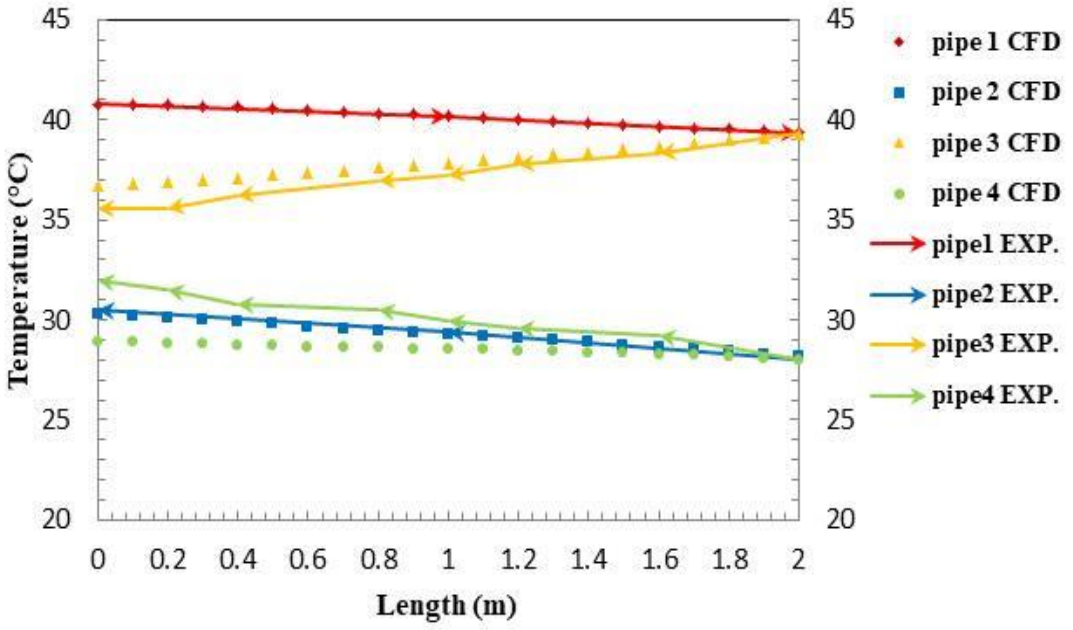

Figure (5-57) variation of temperature along the length of FCPHE at case6

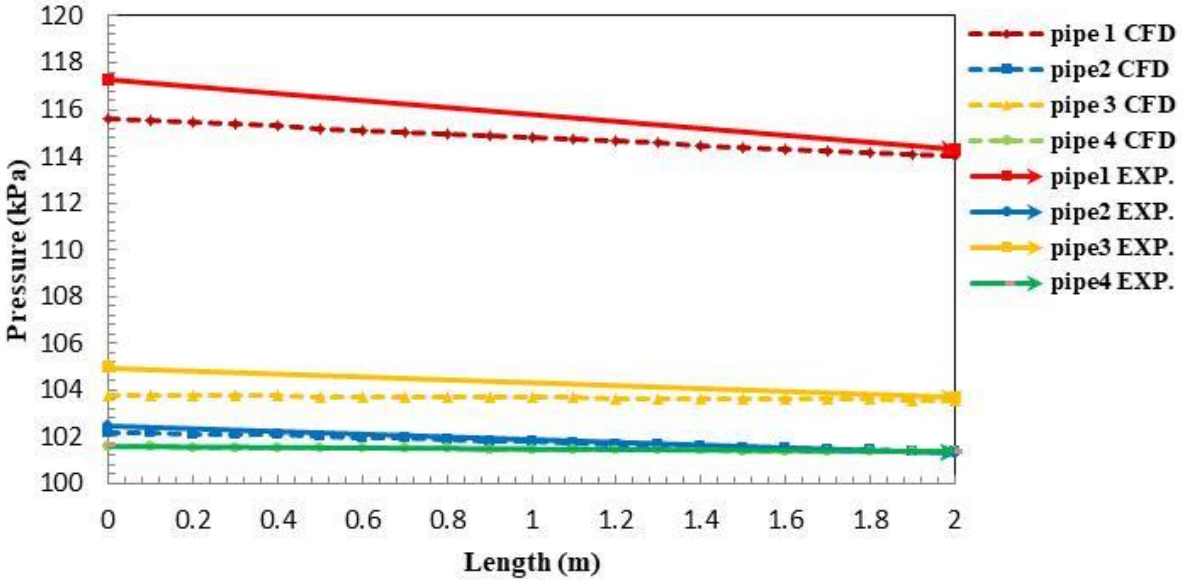

Figure (5-58) variation of pressure along the length of FCPHE at case1

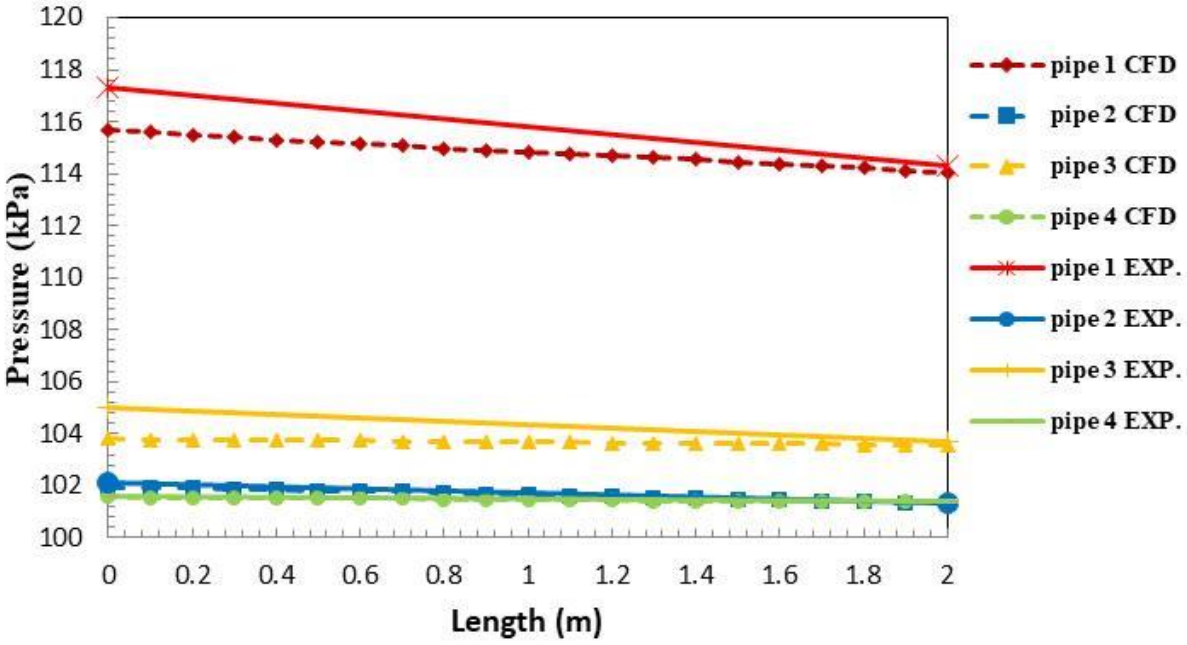

Figure (5-59) variation of pressure along the length of FCPHE at case2

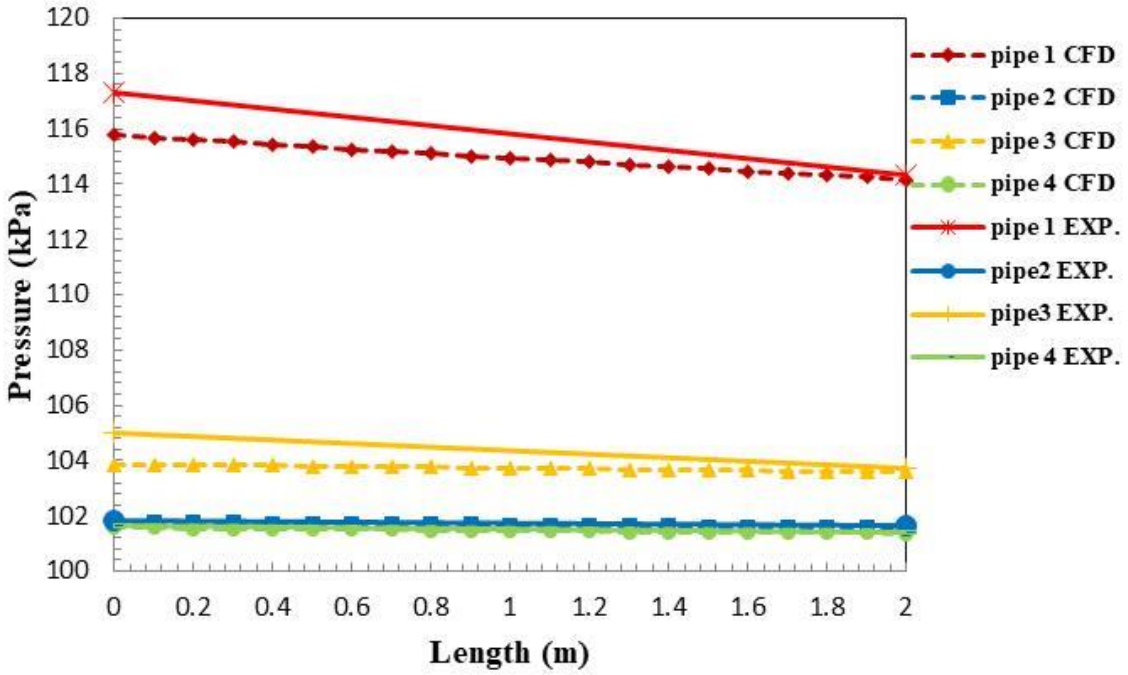

Figure (5-60) variation of pressure along the length of FCPHE at case3

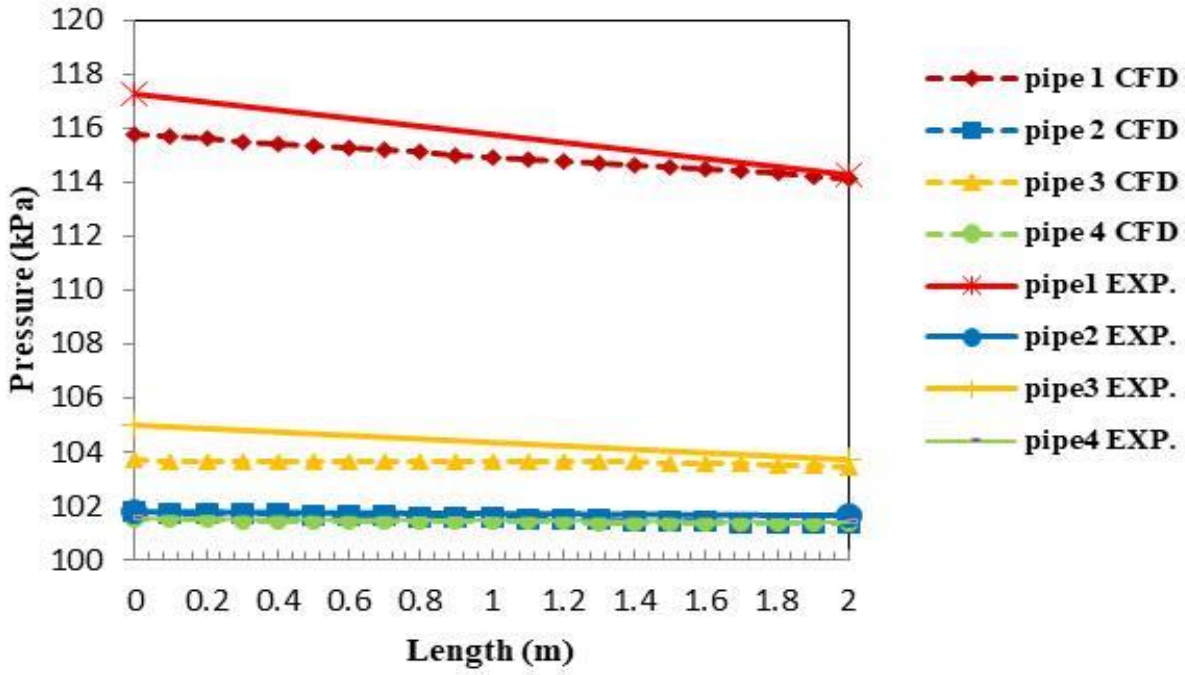

Figure (5-61) variation of pressure along the length of FCPHE at case4

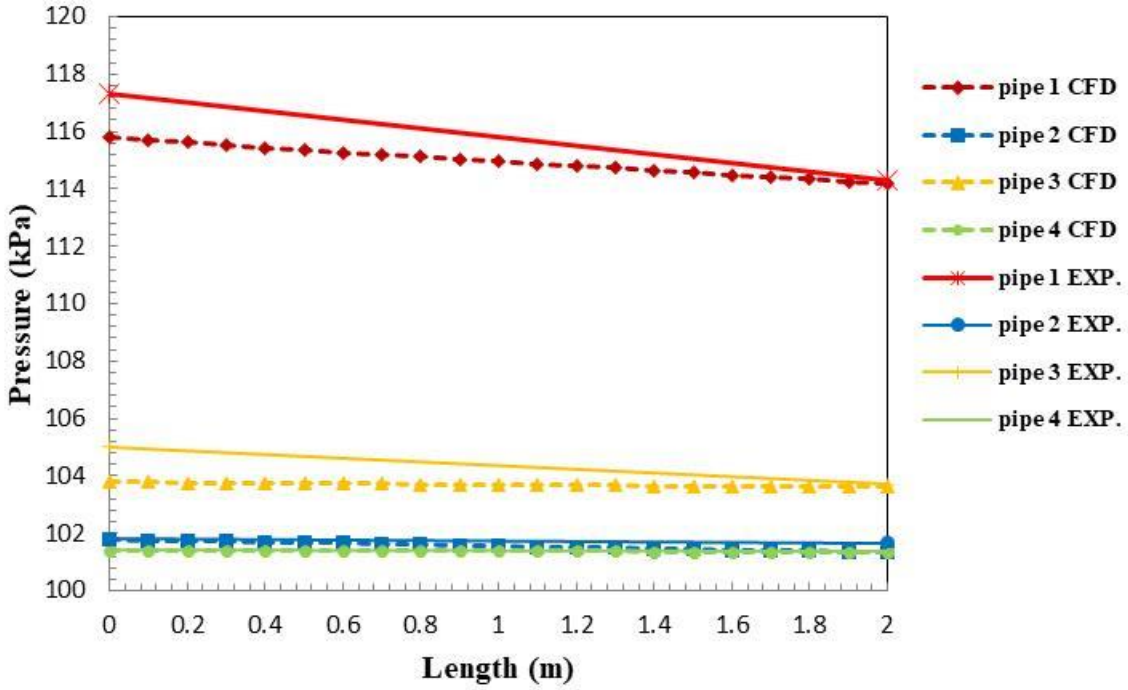

Figure (5-62) variation of pressure along the length of FCPHE at case5

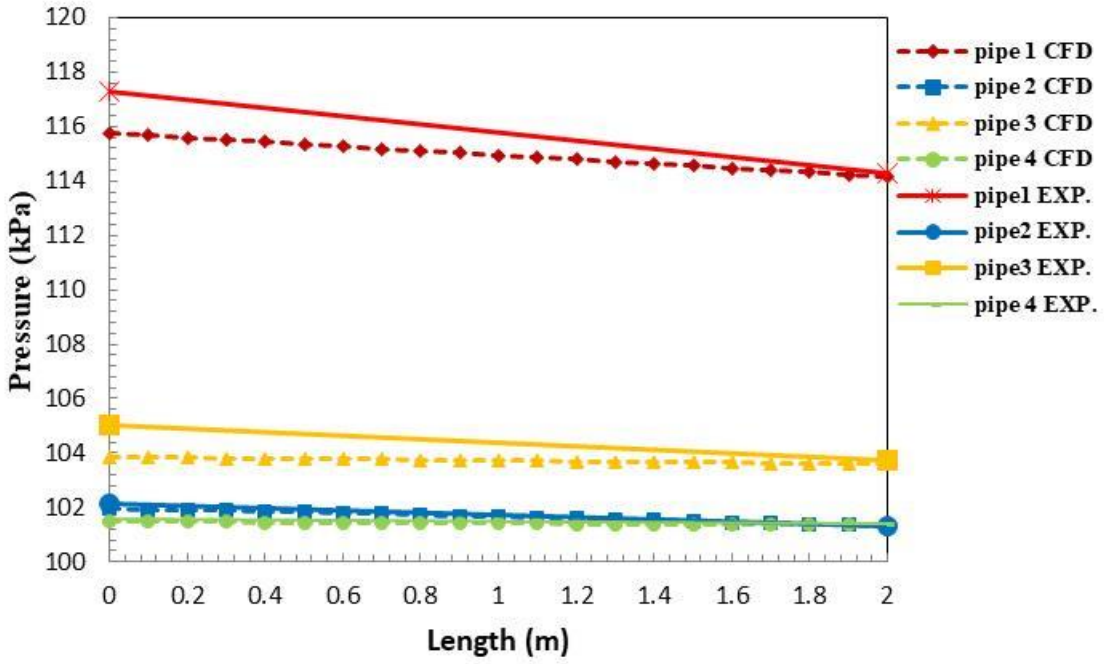

Figure (5-63) variation of pressure along the length of FCPHE at case6

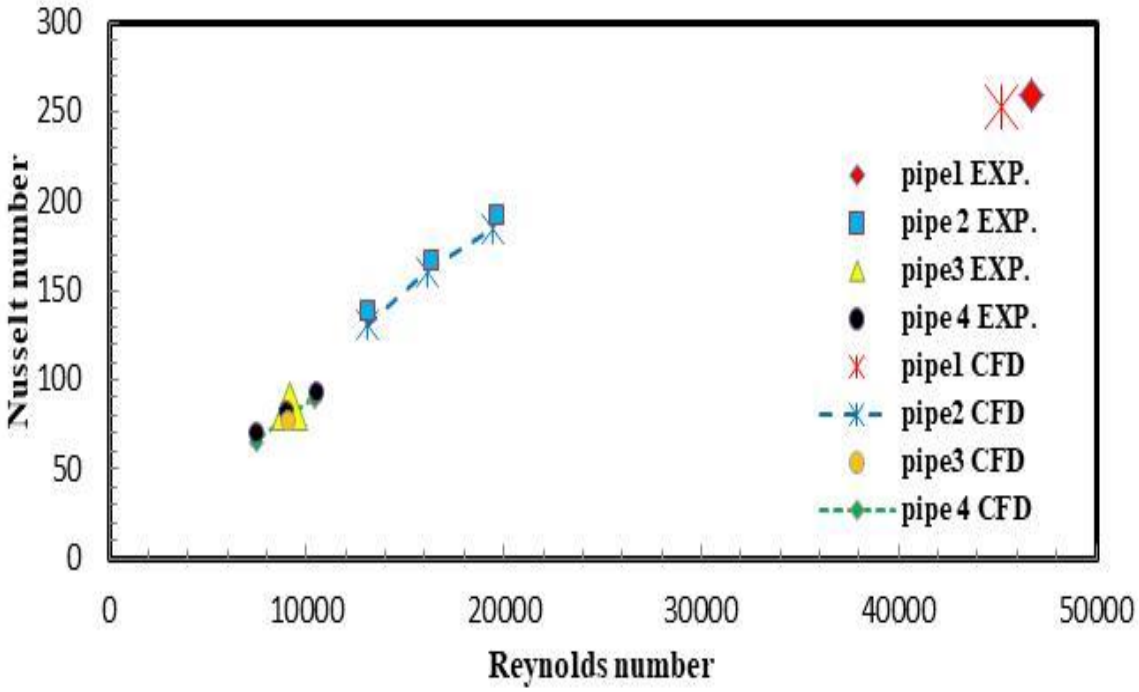

Figure (5-64) variation Nusselt number with Reynolds number

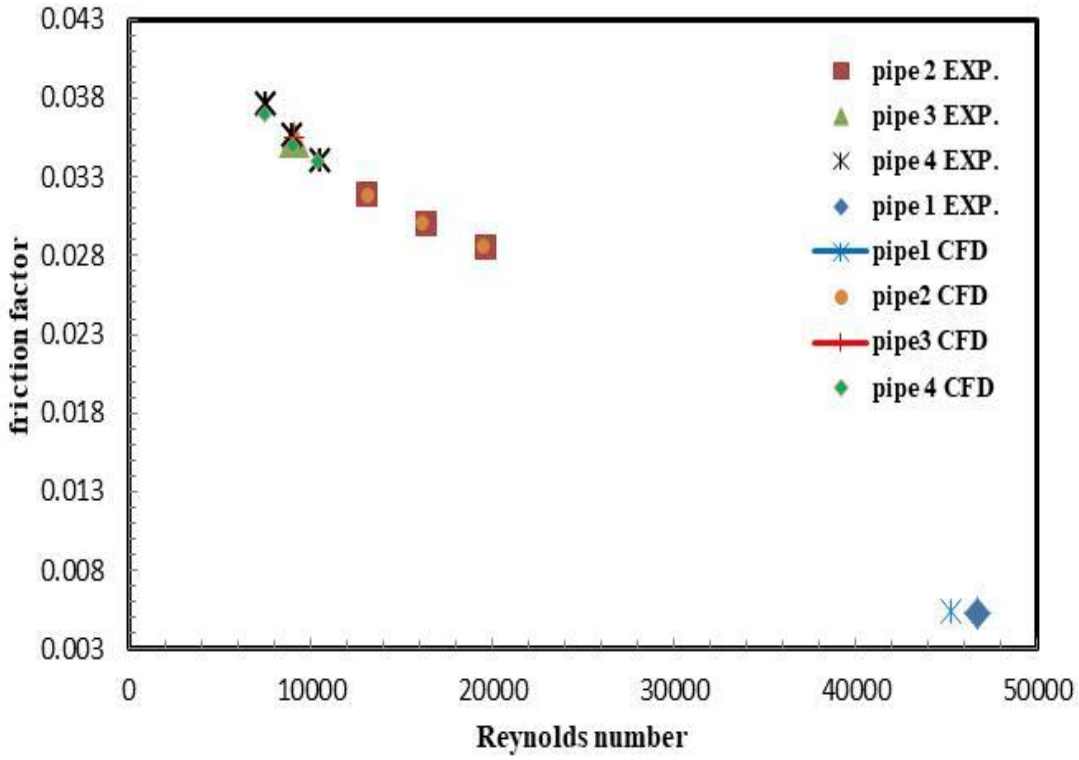

Figure (5-65) variation friction factor with Reynolds number

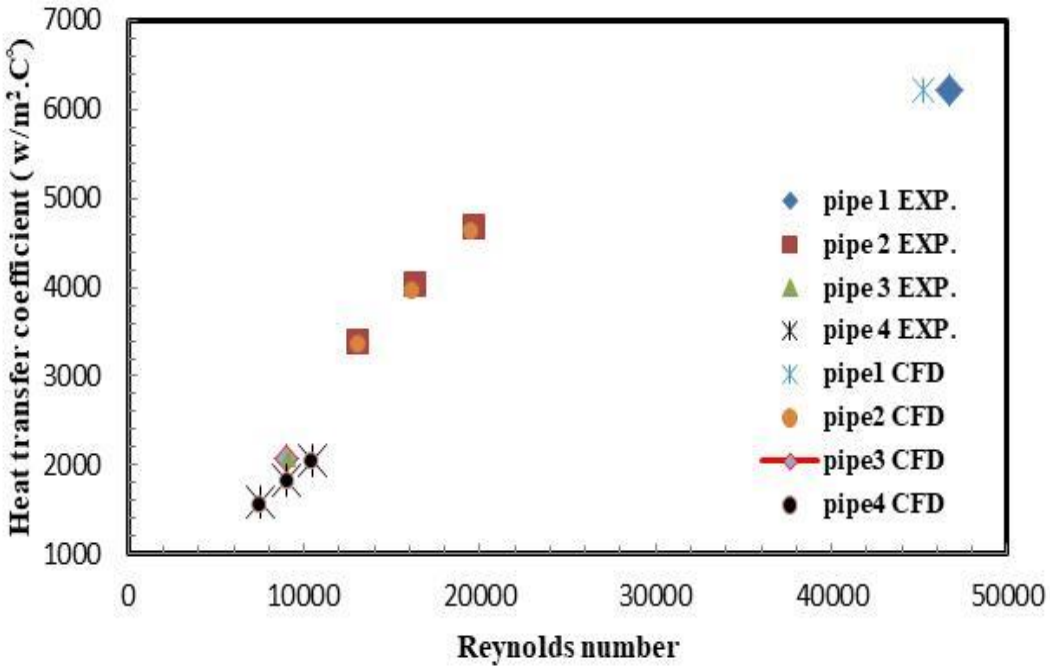

Figure (5-66) variation heat transfer coefficients versus Reynolds number of FCPHE

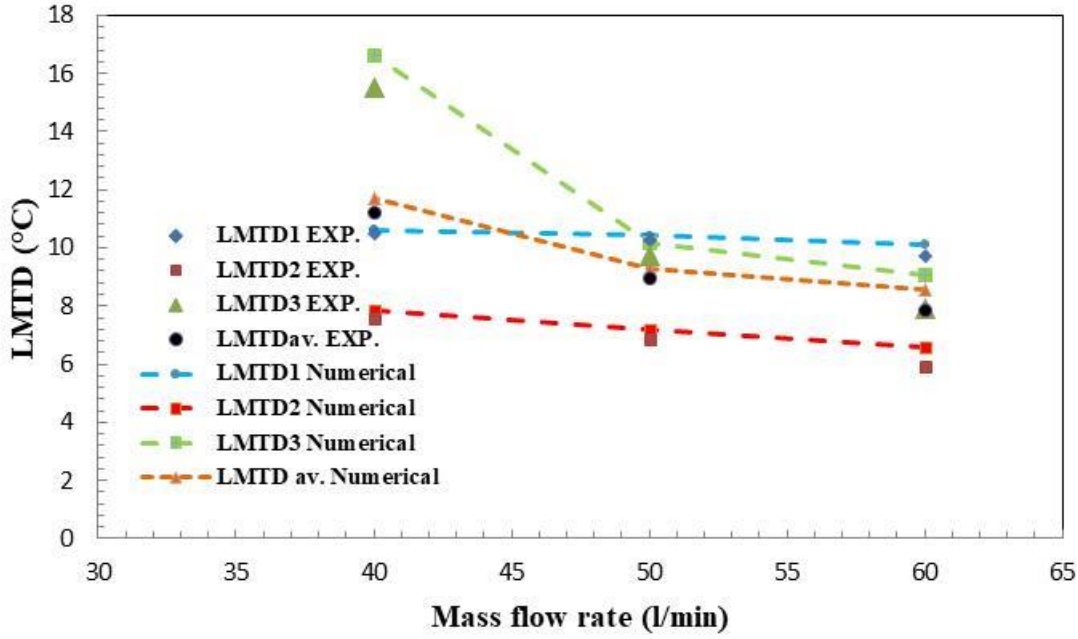

Figure (5-67) variation log mean temperature difference with different mass flow rate of raw water

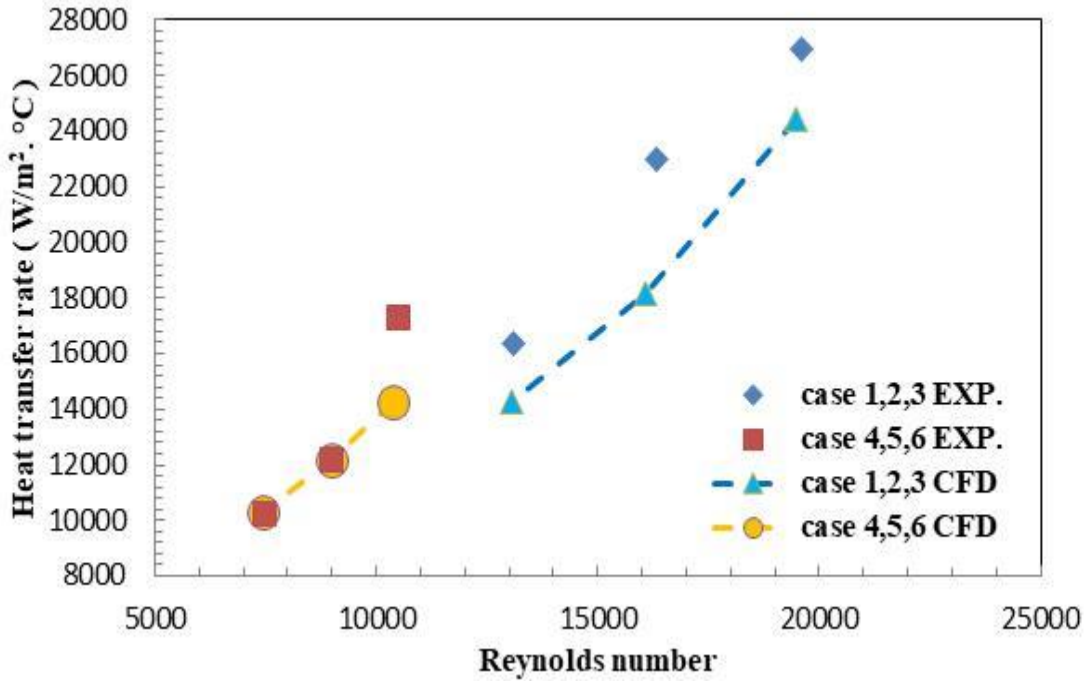

Figure (5-68) heat transfer flow rate of the FCPHE with different Reynolds number of raw water

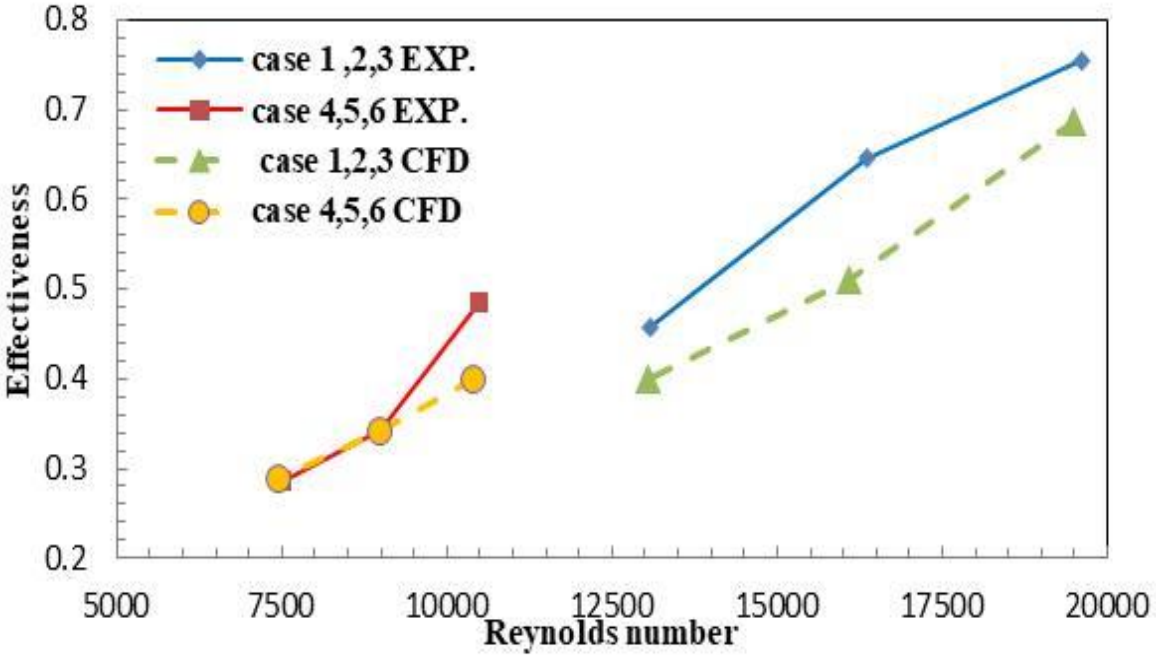

Figure (5-69) effectiveness variation with different Reynolds number of raw water

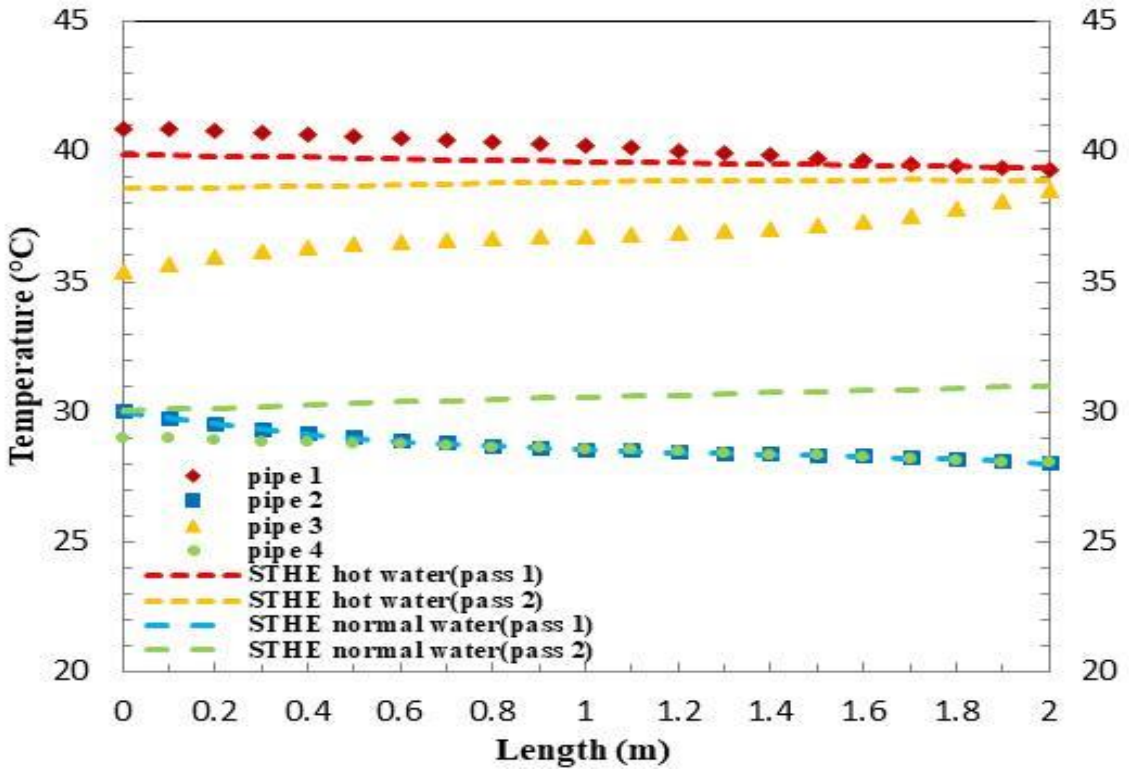

Figure (5-70) local temperature variation along the length of STHE and FCPHE

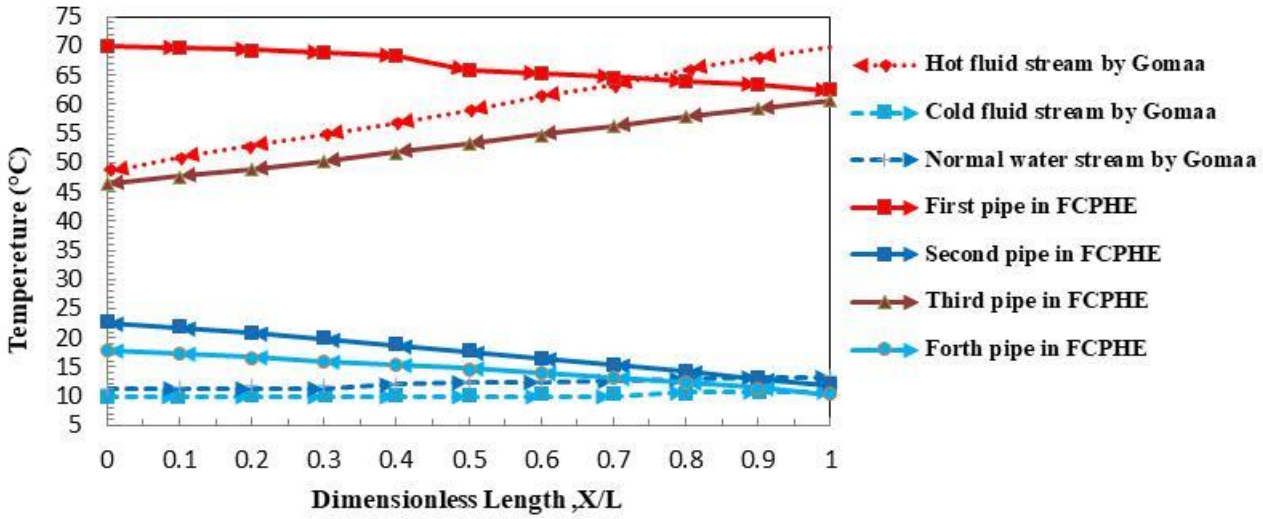

Figure (5-71) local temperature variation of the three water streams along the dimensionless length of TTHE and FCPHE

Chapter six

Conclusions and Suggestions for Future Work

Conclusions and Suggestions for Future Work

6.1. Conclusions

In this study, the following conclusions have been gained:

1. Optimal diameters ratio of a new design for four concentric pipe heat exchanger (FCPHE) are (1.89, 1.47 and 1.36) of second pipe, third pipe and fourth pipe respectively.

2. The effectiveness is directly proportional to the raw water flow rate, which means effectiveness increases with increasing the raw water flow rate. At raw water mass flow rates of 60 and 70 l/min in the second and fourth pipes, respectively, the effectiveness is 76%.

3. The experimental results indicate that the temperature of hot water was decreased by increasing mass flow rate of raw water in second pipe and fourth pipe. Therefore, the temperature of hot water was decreased to minimum value 34.7°C for raw water mass flow rate (60 and 70) l/min in second pipe and fourth pipe respectively.

4. The LMTD decreases with the increasing in mass flow rate of raw water. The maximum LMTD occurred at raw water mass flow rate 40 l/min.

5. It was concluded that the four concentric pipe heat exchanger gives a good enhancement of heat transfer compared with the shell and tube heat exchanger. It was noted hot water temperature decreased 5.75% in STHE. While hot water temperature decreased 15% in FCPHE .

6. The percentage error between the experimental effectiveness and theoretical effectiveness is 9.27 % at maximum value.

7. It is found the best flow arrangement in the first stage is counter flow, while in the second stage is parallel through the working function of the new heat exchanger.

6.2. Suggestions for Future Research

The following suggestion are recommended for future work

1. Studying the effect of using a different fluid on a heat exchanger effectiveness.

2. Studying the effect of nano fluids on heat exchanger effectiveness.

4-inserting ribs inside pipes in order to increase the surface area of heat transfer and turbulent flow.

5-Using corrugated tubes for four concentric pipe heat exchanger

References

References

[1] **Wang, Y. H.**, "An Optimization Design of the Efficient Tubular Heat Exchanger Structure," J. *Applied Mechanics and Materials*, Vol.197, pp. 83-88., **2012**

[2] **T. K. Hou, S. N. Kazi, A. B. Mahat, C. B. Teng, A. Al-Shamma'a, and A. Shaw, "**Industrial Heat Exchanger: Operation and Maintenance to Minimize Fouling and Corrosion," *Heat Exchangers–Advanced Features and Applications*, 2017
.

[3] **Zare, M. K. B., Kanchan, M. D., and Patel, M. N.** "Design of Double Pipe Heat Exchanger.", J. *International Journal of Science Technology and Management*, Vol.5, Issue.12, **2016.**

[4] **Rădulescu, S., Negoiţă, L., and Onuţu I.**, "Analysis of The Heat Transfer in Double and Triple Concentric Tube Heat Exchangers," *IOP Conference Series: J. Materials Science and Engineering*, p. 012148, **2016**.

[5] **Amanuel, T. and Mishra, M.**, "Thermohydraulic Optimization of Triple Concentric-Tube Heat Exchanger: A Multi-Objective Approach," J. *Proceedings of the Institution of Mechanical Engineers, Part E: Journal of Process Mechanical Engineering*, Vol. 233, pp. 589-600, **2019.**

[6] **Zheng, H. F., Bai, J., Wei, J., and Huang, L. Y.,** "Numerical Simulation About Heat Transfer Coefficient for The Double Pipe Heat Exchangers," J. *Applied Mechanics and materials*, Vol.1 pp. 2577-2580, **2011.**

[7] **Baadache, K. and Bougriou, C.**, "Optimisation of The Design Of Shell And Double Concentric Tubes Heat Exchanger Using The Genetic Algorithm," J. *Heat and Mass Transfer*, vol. 51, pp. 1371-1381, **2015**.

[8] **Han, H.-Z., Li, B.-X., Wu, H., and Shao, W.**, "Multi-Objective Shape Optimization of Double Pipe Heat Exchanger with Inner Corrugated Tube Using RSM Method," J. *International Journal of Thermal Sciences*, vol. 90, pp. 173-186, **2015.**

[9] **Sheikholeslami M., Gorji-Bandpy M., and Ganji D. D.,** "Experimental study on turbulent flow and heat transfer in an air to water heat exchanger using perforated circular-ring," J. *Experimental Thermal and Fluid Science*, vol. 70, pp. 185-195, **2016.**

[10] **Dirker J., Meyer J. P., and Kohlmeyer B. W.**, "Local heat transfer coefficients at the inlet of an annular flow passage," J. *International Journal of Heat and Mass Transfer*, vol. 113, pp. 268-280, **2017.**

[11] **Verma T. N., Nashine P., Singh D. V., Singh T. S., and Panwar D.,** "ANN: Prediction of an experimental heat transfer analysis of concentric tube heat exchanger with corrugated inner tubes," J. *Applied Thermal Engineering*, vol. 120, pp. 219-227, **2017.**

[12] **Sreedhard N. and Varghese G.**, "Analysis of Longitudinal Fin Patterns in a Concentric Double Tube Heat Exchanger using LMTD and CFD Techniques”," J. *International Journal of Applied Engineering Research*, vol. 12, pp. 6471-6479, **2017**.

[13] **Mashoofi N., Pourahmad S., and Pesteei S.**, "Study the effect of axially perforated twisted tapes on the thermal performance enhancement factor of a double tube heat exchanger," J. *Case studies in thermal engineering*, vol. 10, pp. 161-168, **2017**.

[14] **Hosseinian A. and Isfahani A. M**., "Experimental study of heat transfer enhancement due to the surface vibrations in a flexible double

pipe heat exchanger," J. *Heat and Mass Transfer*, vol. 54, pp. 1113-1120, **2018**.

[15] **Bahmani M. H., Sheikhzadeh G., Zarringhalam M., Akbari O. A., Alrashed A. A., Shabani G. A. S.,** "Investigation of turbulent heat transfer and nanofluid flow in a double pipe heat exchanger," J. *Advanced Powder Technology*, vol. 29, pp. 273-282, **2018**.

[16] **Hamzah J. A. and Nima M. A**., "Experimental study of heat transfer enhancement in double-pipe heat exchanger integrated with metal foam fins," *Arabian Journal for Science and Engineering*, vol. 45, pp. 5153-5167, **2020.**

[17] **Córcoles J., Moya-Rico J., Molina A., and Almendros-Ibáñez J**., "Numerical and experimental study of the heat transfer process in a double pipe heat exchanger with inner corrugated tubes," J. *International Journal of Thermal Sciences*, vol. 158, p. 106526, **2020**.

[18] **Zuritz, C. A.,** " Design of Triple Concentric-Tube Heat Exchangers ", J. *Journal of Food Process Engineering*, Vol. 12, pp. 113-130, **1990.**

[19] **Dirker, J., and Meyer, J. P.**, "Heat Transfer Coefficients in Concentric Annuli," *J. Heat Transfer*, Vol. 124, pp. 1200-1203, **2002.**

[20] **García-Valladares, O.**, "Numerical Simulation of Triple Concentric-Tube Heat Exchangers," J. *International journal of thermal sciences*, Vol. 43, pp. 979-991, **2004**.

[21] **Batmaz, E., and Sandeep, K.,** "Overall Heat Transfer Coefficients and Axial Temperature Distribution in A Triple Tube Heat Exchanger," J. *Journal of food process engineering*, Vol. 31, pp. 260-279, **2008.**

[22] **Zhao, M. and Li, Y.,** "New Integral-Mean Temperature Difference Model for Thermal Design and Simulation of Parallel Three-Fluid Heat Exchanger," J. *International journal of thermal sciences*, Vol. 59, pp. 203-213, **2012.**

[23] **Radulescu, S., Negoita, I. L., and Onutu, I.**, "Heat Transfer Coefficient Solver for A Triple Concentric-Tube Heat Exchanger in Transition Regime," J. *Rev Chim (Buchar)*, Vol. 8, pp. 820-824, **2012.**

[24] **Quadir, G., Jarallah, S. S., Ahmed, N. S., and Badruddin, I. A.,** "Experimental Investigation of the Performance of a Triple Concentric Pipe Heat Exchanger," J. *International Journal of Heat and Mass Transfer*, Vol. 62, pp. 562-566, **2013.**

[25] **Başal, B. and Ünal, A.,** "Numerical Evaluation of a Triple Concentric-Tube Latent Heat Thermal Energy Storage,"J. *Solar Energy*, Vol. 92, pp. 196-205, **2013**.

[26] **Quadir, G., Badruddin, I. A., and Ahmed, N. S.**, "Numerical Investigation of the Performance of a Triple Concentric Pipe Heat Exchanger," J. *International Journal of Heat and Mass Transfer*, Vol. 75, pp. 165-172, **2014.**

[27] **Pătrăşcioiu, C. and Rădulescu, S.,** "Prediction of The Outlet Temperatures in Triple Concentric—Tube Heat Exchangers in Laminar Flow Regime: Case Study," J. *Heat and Mass Transfer*, Vol. 51, pp. 59-66, **2015.**

[28] **Patel Dharmik, A., Dhiman, V., Patel, J. J., and Engineer R.**, "CFD Analysis of Triple Concentric Tube Heat Exchanger," J. *University Journal of Research*, vol. 1, pp. 30-44, **2015**.

[29] **Singh, S. K., Mishra, M., and Jha, P**., "Experimental Investigations On Thermo-Hydraulic Behaviour of Triple Concentric-Tube Heat Exchanger,", J. *Proceedings of the Institution of Mechanical Engineers, Part E: Journal of Process Mechanical Engineering* vol. 229, pp. 299-308, **2015**.

[30] **Wafelkar, G. V. and Kamble, L.**, "Experimental Performance Analysis of Triple Tube Heat Exchanger with Dimple Tubing," J. *International Journals of Advance Research in Science and Engineering (IJARSE)*, ISSN (O), Vol. 20. pp. 2319-8354, **2016.**

[31] **Gomaa A., Halim M., and Elsaid A. M.**, "Experimental and Numerical Investigations of a Triple Concentric-Tube Heat Exchanger," J. *Applied Thermal Engineering*, vol. 99, pp. 1303-1315, **2016.**

[32] **Sahoo, M., Behera, V., Das, S., and Das, H**., "Experimental Investigation and Performance Analysis of Triple Concentric Helical Tube Heat Exchanger," J. *International Journal of Engineering and Technology (IJET)*, ISSN (Print),Vol. 22. pp. 2319-8613, **2016.**

[33] **Dilpak Saurabh, P., Khond, H., and Lele, M. M**., "CFD Analysis of a Triple Concentric Tube Heat Exchanger having water flowing at three different temperatures," J. *International Journal of Current Engineering and Technology*, vol. 80, pp. 185-195, **2016.**

[34] **Boultif N. and Bougriou C**., "Steady and Unsteady State Thermal Behaviour of Triple Concentric-Tube Heat Exchanger," J. *Heat and Mass Transfer*, vol. 53, pp. 849-863, **2017.**

[35] **Wafelkar G. and Raut A.**, "Experimental study of heat transfer enhancement in triple tube heat exchanger with CuO and Al_2O_3 Nano

fluids," J. *International Research Journal of Engineering and Technology*, Vol.33. pp. 2594-2596, **2017.**

[36] **Giovannoni V., Sharma R. N., and Raine R. R.,** "Numerical prediction of thermal performances in a concentric triple tube heat exchanger," J. *International Journal of Thermal Sciences*, vol. 120, pp. 86-105, **2017**.

[37] **Hossain A., Uddin M. A., Hossen R., and Afroz H**., "Experimental analysis of a triple concentric tube heat exchanger," *Int J Mod Stud Mech Eng*, vol. 3, pp. 1-10, **2017**.

[38] **Gomaa A., Halim M., and Elsaid A. M**., "Enhancement of cooling characteristics and optimization of a triple concentric-tube heat exchanger with inserted ribs," J. *International Journal of Thermal Sciences*, vol. 120, pp. 106-120, **2017**.

[39] **Zeeshan M., Duggal R., Tated M., and Singh M**., "Numerical and experimental investigation of bi-annulus heat exchanger for different alternative materials," *IOP Conference Series: Materials Science and Engineering*,Vol. 66. p. 012017. **2018.**

[40] **Touatit A., and Bougriou C**., "Optimal diameters of triple concentric-tube heat exchangers," J. *International Journal of Heat and Technology*, vol. 36, pp. 367-375, **2018**.

[41] **Saraireh M. A.,** "Experimental and Numerical Thermal Study of Triple Pipe Heat Exchanger," *International Journal of Simulation--Systems, Science & Technology*, vol. 19, **2018.**

[42] **Afzal A., Rk A. R., Ad M. S., Kareemulla M., Km Y., and Raju S.,** "Heat transfer analysis of triple tube heat exchanger using water and

titanium-dioxide nanofluid," *ICTEA: International Conference on Thermal Engineering*, vol. 36, pp. 367-375 **2019.**

[43] **Lubis Z., Manik T., Rinkanto M., and Sitorus T.,** "Design of a heat exchanger of three concentric tube layer on contrary flow," *IOP Conference Series: Materials Science and Engineering*, vol. 36, pp. 367-365 p. 012091, **2019**.

[44] **Memon M. A., Unar I. N., and Abassi A. F.**, "Modeling and Simulation of Triple Concentric Tube Heat Exchanger Using Different Materials," J. *Engineering Science and Technology International Research Journal*, Vol. 20. **2020**.

[45] **Tuyen V., Van Hap N., and Phu N. M.,** "Thermal-hydraulic characteristics and optimization of a liquid-to-suction triple-tube heat exchanger," J. *Case Studies in Thermal Engineering*, vol. 19, p. 100635, **2020.**

[46] **Abdelmagied M**., "Experimental study of a triple spirally coiled tube heat exchanger thermo-fluid characteristics," J. *Applied Thermal Engineering*, vol. 180, p. 115803**, 2020.**

[47] **Tanish P., Ramanathan N., Balasekhar C., and Manikandaraja G.,** "Experimental Study of Heat Transfer in Concentric Triple Pipe Heat Exchanger," *IOP Conference Series: Materials Science and Engineering*, p. 012048**, 2021**.

[48] **Arulkumar S. and Mathanraj V.**, "Experimental Investigation of Heat Transfer of Concentric Triple Pipe Heat Exchanger Coupled with Blossom Fins," *IOP Conference Series: Materials Science and Engineering*, p. 012068**, 2021**.

[49] **Van Zyl W. R., Dirker J., and Meyer J. P.**, "Single-phase convective heat transfer and pressure drop coefficients in concentric annuli," J. *Heat Transfer Engineering*, vol. 34, pp. 1112-1123, **2013.**

[50] **Permatasari R. and Yusuf A. M.**, "Material selection for shell and tube heat exchanger using computational fluid dynamics method," *AIP Conference Proceedings*, p. 060005**, 2018**.

[51] **Omega**, "The temperature hand book," Book, Publish by *Omega Engineering* Inc., Standard,, **1998**.

[52] **Cengel Y. A. and Pérez H.**, "Heat transfer: a practical approach". Book Publish by *transferencia de calor*, **2004.**

[53] **Vocale P., Malavasi M., Cattani L., Bozzoli F., Pelacci M., and Rainieri S**., "Thermal characterisation of Triple Concentric Tube Heat Exchangers by applying parameter estimation: direct problem implementation," *Journal of Physics: Conference Series*, p. 012022**, 2021**.

[54] **Bergman T. L., Incropera F. P., DeWitt D. P., and Lavine A. S**., "Fundamentals of heat and mass transfer", Book Publish by *John Wiley & Sons*, **2011**.

[55] **Davis E. S.**, "Heat transfer and pressure drop in annuli," Book Publish by *Trans. Asme*, vol. 65, p. 755-760, **1943**.

[56] **Gnielinski V.**, "Heat transfer coefficients for turbulent flow in concentric annular ducts," J. *Heat transfer engineering*, vol. 30, pp. 431-436, **2009**.

[57] **Abdalla G., Halim M., and Ashraf M**., "Enhancement of cooling characteristics and optimization of a triple concentric-tube heat

exchanger with inserted ribs" *Journal of Thermal Sciences*, vol. 120, pp. 106-120, **2017**.

[58] Holman, J. P. (2002). Heat Transfer-Si Units-Sie. Tata McGraw-Hill Education.

[59] **Versteeg H.and Malalasekera W.**, "Computational fluid dynamics," Book Publish by *The finite volume method*, pp. 1-26, **1995**.

[60] **Li C., Bai F., and Gou F.,** "Analysis of Heat Exchange Performance of Heat Exchange Tubes of Evaporative Heat Exchanger Based on Fluent," *IOP Conference Series: Earth and Environmental Science*, , p. 012006, **2020**.

[61] **Arani A. A. A. and Moradi R**., "Shell and tube heat exchanger optimization using new baffle and tube configuration," J. *Applied Thermal Engineering*, vol. 157, p. 113736, **2019.**

[62] **Sobachkin A., and Dumnov G.**, "Numerical basis of CAD-embedded CFD," *Book publish by NAFEMS World Congress*, pp. 9-12**, 2013**.

[63] **Nishikawa H**., "The QUICK scheme is a third-order finite-volume scheme with point-valued numerical solutions," J. *International Journal for Numerical Methods in Fluids*, vol. 93, pp. 2311-2338, **2021**.

[64] **Xiao H. and Liu W.**, "A Solution to Pressure Equation with Its Boundary Condition of Combining Tangential and Normal Pressure Relations," J. *Energies*, vol. 14, p. 1507, **2021.**

[65] **Prasanna M., Kumar P. R., Emmanuel B., and Prasad K. L.,** "Experimentation on Augmenting Heat Transfer Characteristics of

(Ethylene Glycol+ Water) Mixture in A Combined (Pipe in Pipe and Shell & Tube) Heat Exchanger." J. *International Journal of Recent Technology and Engineering*, vol. 8, pp. 4442- 4449, **2019.**

Appendices Reference

[66] **A. Sadikin, N. Khian, Y. Hwey, H. Al-Mahdi, I. Taib, A. Sadikin, *et al.***, "Effect of number of baffles on flow and pressure drop in a shell side of a shell and tube heat exchangers," *Journal of Advanced Research in Fluid Mechanics and Thermal Sciences*, vol. 48, pp. 156-164, 2018.

[67] **HoSung Lee**, "Thermal Design Heat Sinks, Thermoelectrics, Heat Pipes, Compact Heat Exchangers, and Solar Cells. ", Published by John Wiley & Sons, Inc., Hoboken, New Jersey, 2010.

[68] **A. Ş. Şahin, B. Kılıç, and U. Kılıç,** "Design and economic optimization of shell and tube heat exchangers using Artificial Bee Colony (ABC) algorithm," *Energy Conversion and Management*, vol. 52, pp. 3356-3362, 2011.

[69] **R. Sinnott**, *Chemical Engineering Design: Chemical Engineering Volume 6*: Elsevier, 2005.

[70] **J. Holman**, "Heat Transfer tenth edition, ser," ed: McGraw-Hill Series in Mechanical Engineering. McGraw Hill Higher Education, 2009.

[71] **S. Kakac, H. Liu, and A. Pramuanjaroenkij**, *Heat exchangers: selection, rating, and thermal design*: CRC press, 2020.

[72] **A. A. Abd and S. Z. Naji,** "Analysis study of shell and tube heat exchanger for clough company with reselect different parameters to improve the design," *Case Studies in Thermal Engineering*, vol. 10, pp. 455-467, 2017.

[73] **F.Edition and R.Sinnott**, "Coulson Richardson&# 039; s Chemical Engineering Vol. 6 Chemical Engineering Design 4th Edition."

[74] **H. Kücük, M. Ünverdi, and M. S. Yılmaz**, "Experimental investigation of shell side heat transfer and pressure drop in a mini-channel shell and tube heat exchanger," *International Journal of Heat and Mass Transfer*, vol. 143, p. 118493, 2019.

[75] **A. A. Shrikant, R. Sivakumar, and M. Vivekanandan**, "Comparison of Shell and Tube Heat Exchanger Using Theoretical Methods, HTRI, ASPEN and SOLIDWORKS Simulation Soft Wares," *International Journal of Engineering Research and Application,* vol. 6, pp. 99-107, 2016.

[76] **O. A. Mohsen, M. A. R. Muhammed, and B. O. Hasan**, "Heat Transfer Enhancement in a Double Pipe Heat Exchanger Using Different Fin Geometries in Turbulent Flow," *Iranian Journal of Science and Technology, Transactions of Mechanical Engineering*, 2020.

[77] **W. M. Kays and A. L. London, "Compact heat exchangers**," Book Published by Krieger Publishing Company,.1984.

[78] **S. A. Marzouk, M. M. Abou Al-Sood, E. M. S. El-Said, and M. K. El-Fakharany**, "Effect of wired nails circular–rod inserts on tube side performance of shell and tube heat exchanger: Experimental study," *Applied Thermal Engineering*, vol. 167, p. 114696, 2020.

[79] **LeVeque R. J**., "Finite volume methods for hyperbolic problems" vol. 31: Book Publish by Cambridge university press, **2002**.

[80] **Marshall E. M. and Bakker A.**, "Computational fluid mixing," *Handbook of industrial mixing*, Book publish by *science and practice* by pp. 257-343, **2004**.

APPENDICES

Appendix (A): Design consideration for prototype thermal power plant for Al-Mussaib

1. Baffle Spacing

Inter-baffle spacing effected the response of the heat and mass transfer and pressure drop on the shell side of a shell and tube heat exchanger where the pressure drop is strongly affected by the baffle spacing that was presented by Sadikin et al.,[66].Lee[67] explained the equation of calculating the baffle spacing as:

$$B = \frac{L_t}{N_b+1} \quad \text{..... (A.1)}$$

where

L_t is the length of tubes assumed 2000mm as validating with actual length with Al- Mussaib thermal power plant

N_b is the number of baffles equal 11 for one pass which takes the same number of Al- Mussaib thermal power plant

2. Equivalent Diameter

Sahin et al. [68] described how to calculate the equivalent diameter for the triangular pitch layout as:

$$D_e = \frac{4\left(\frac{\sqrt{3}\,P_t^2}{4} - \frac{\pi d_0^2}{8}\right)}{\pi d_0/2} \quad \text{..... (A.2)}$$

Where tube pitch P_t is calculating by equation as:

$$P_t = P_r . d_0 \quad \text{..... (A.3)}$$

P_r is the pitch ratio, this value between $1.25 < P_r < 1.5$ as noted by Sinnott [69], the P_r value was taken 1.48 .This is due to the tubes are

too close to each other tube sheet becomes too weak for proper rolling of the tubes and cause leak joints. The sketch of the tube pitch details in figure (A-1).

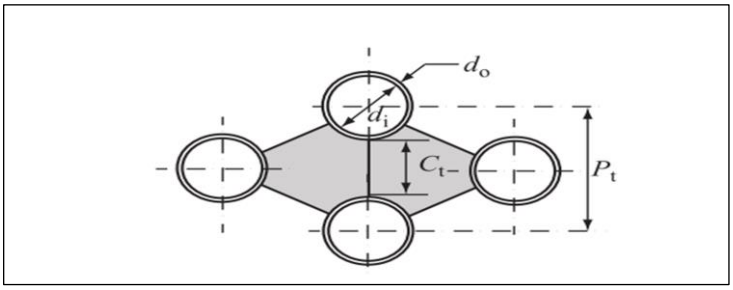

Figure (A-1) triangular-pitch layout. Ref. [1]

3. Cross-Flow Area of the Shell

Lee [67] showed the cross flow area calculated as:

$$A_c = \frac{D_s C_t B}{P_t} \quad \text{..... (A.4)}$$

where

D_s is the shell diameter which assume 154.4 mm .

Ct is the tube clearance was calculated as:

$$C_t = P_t - d_0 \quad \text{..... (A.5)}$$

4. Number of Tubes

The number of tubes can be predicted in fair approximation with the shell inside diameter. Sinnott [69] expressed the number of tubes as:

$$N_t = \frac{\pi}{4}\left(\frac{CTP}{CL}\right)\frac{D_s^2}{P_r^2 d_0^2} \quad \text{..... (A.6)}$$

where

CTP is the tube count pass which accounts for the incomplete coverage of the shell diameter by the tubes due to necessary clearances between the shell and the outer tube circle, the value of CTP equal 0.85

for a four tubes pass and CL is the tube layout constant equal 0.866 for a triangle tube layout reported in reference.[67].

5. Logarithmic Mean Temperature Difference

The *LMTD* method will be used to evaluate the required equipment's area. Analysis will start by first calculating the mean temperature, for fluids will be used in counter-flow to maximize the log mean temperature difference. Holman [70]expressed the calculation as:

$$LMTD1 = \frac{(T_{si}-T_{to})-(T_{so}-T_{ti})}{ln\frac{(T_{si}-T_{to})}{(T_{so}-T_{ti})}} \quad \text{..... (A.7)}$$

where *LMTD* expressed as:

$$LMTD=F\ LMTD1 \quad \text{.....(A.8)}$$

For a two shell and four tubes passes the geometry correction factor *F* equal 0.95 as noted by Holman [70].

6. Overall Heat Transfer Coefficient

The overall heat transfer coefficient U_0without fouling according to the tube outer diameter. Cengel [52]showed the overall heat transfer coefficient calculated as:

$$U_0 = \frac{1/A_0}{\frac{1}{h_t A_i}+\frac{ln\left(\frac{d_0}{d_i}\right)}{2\pi k_t L_t}+\frac{1}{h_s A_0}} \quad \text{..... (A.9)}$$

where

$$A_i = \pi d_i N_t L_t \quad \text{..... (A.10)}$$

$$A_0 = \pi d_0 N_t L_t \quad \text{..... (A.11)}$$

k_t is the thermal conductivity of the metal tube.

h_t and h_s are the heat transfer coefficient of the tube and shell respectively.

6.1. Calculating Tube side heat transfer coefficient

From dimensionless number (Nusselt number), heat transfer coefficient of the tube showed by Cengel [52] as:

$$h_t = \frac{Nu_t\, k_{tf}}{d_i} \quad \text{..... (A.12)}$$

where

k_{tf} is the thermal conductivity of tube water

Nu_t the Nusselt number in turbulent flow is related to the friction factor which was calculated by Gnielinski [54, 71]as:

$$Nu_t = \frac{(f_t/2)(Re_t - 1000)Pr}{1+12.7(f_t/2)^{0.5}(Pr^{0.67}-1)} \quad \text{..... (A.13)}$$

Then, the Re_t was estimated as:

$$Re_t = \frac{\dot{m_t} d_i}{A_{ct}\mu} \quad \text{..... (A.14)}$$

A_{ct} is the cross section area of the tube which was calculated as:

$$A_{ct} = \frac{\pi}{4} d_i^2 \quad \text{..... (A.15)}$$

Prandtl number which was calculated as:

$$Pr = \frac{\mu c_p}{k} \quad \text{..... (A.16)}$$

The values of the Prandtl number between $0.5 \leq Pr \leq 2000$ and Reynolds number value between $3000 \leq Re \leq 5 \times 10^6$ .This due to the flow is turbulent .Then f_t is friction factor which was calculated as:

$$f_t = (1.58 \ln(Re_t) - 3.28)^{-2} \quad \text{..... (A.17)}$$

Then , the average Nusselt number correlation calculated by Abd and Naji [72] as:

$$Nu_t = j_h \, Re \, Pr^{0.33} \quad \text{..... (A.18)}$$

where

j_h is the dimensionless of thermal factor. Edition and Sinnott [73] showed this value was calculated by using Kern method from curve as shown in figure(A-2).

6.2. Calculating Shell side heat transfer coefficient

From definition of Nusselt number, Shell side heat transfer coefficient calculated as:

$$h_s = \frac{Nu_s \, k_{sf}}{D_e} \quad \text{..... (A.19)}$$

where

k_{sf} is the thermal conductivity of shell water

Nu_s is the nusselt number of shell water ,where McAdam's[74] showed the correlation for turbulent flow is:

$$Nu_s = 0.36 \, Re^{0.55} Pr^{0.33} \quad \text{..... (A.20)}$$

$$Re_s = \frac{\rho_s \, D_s v_s}{\mu_s} \quad \text{..... (A.21)}$$

The correlation obtained using the proposed curve for baffles with a 28% baffle cut from the graphs prepared by Kern [75] based on experimental studies on shell side heat transfer is as follows:

$$Nu_s = j_h \, Re \, Pr^{0.33} \quad \text{..... (A.22)}$$

where

j_h is the dimensionless shell side heat transfer factor which is evaluated from curve as shown in figure (A-3).

7. Pressure Drop

Pressure drop is an essential criterion in shell and tube heat exchanger.

7.1. Calculating Pressure Drop in Tube Side

The tube side pressure drop can be calculated by Shrikant et al. [75].

$$\Delta P=4\left(\frac{f_t.L_t}{d_i}+1\right)N_p\,\frac{1}{2}\rho.v_t^2 \qquad \text{..... (A.23)}$$

Where

N_p is the number of tube passes

v_t^2 is the mean fluid velocity inside the tube

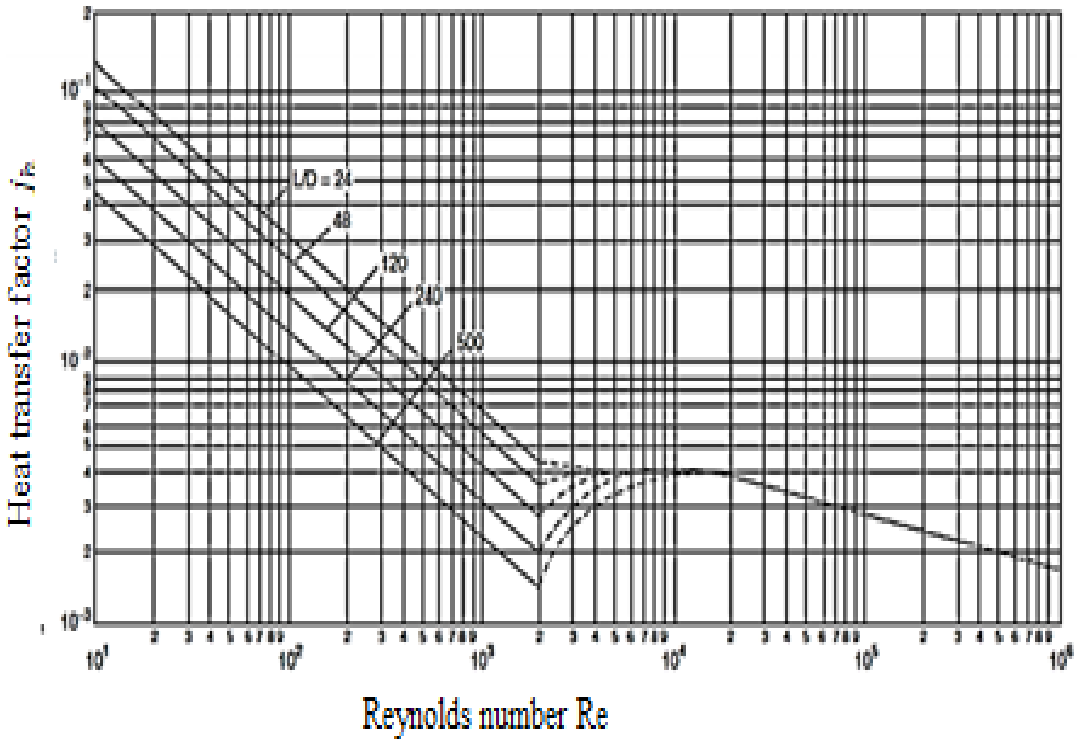

Figure (A-2) tube-side heat-transfer factor .Ref. [75]

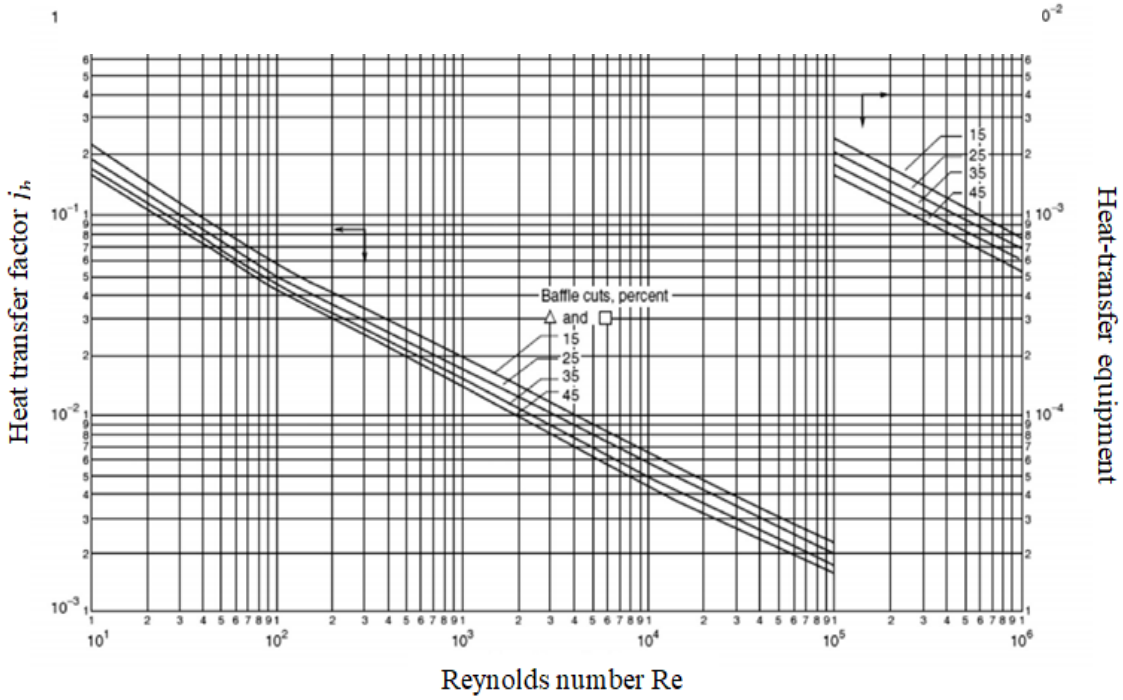

Figure (A-3) shell-side heat-transfer factor.Ref. [75]

7.2. Calculating Pressure Drop in Shell Side

The shell-side pressure drop depends on the number of tubes the fluid passes through in the tube bundle between the baffles as well as the length of each crossing. A correlation has been obtained using the product of distance across the bundle, taken as the inside diameter of the shell and the number of times the bundle calculated by Shinde and Chavan [76] .

$$\Delta P = f_s \frac{D_S}{D_e} (N_b + 1)_{\frac{1}{2}} \rho . v_s^2 \quad \text{..... (A.24)}$$

Where

v_s is the mean fluid velocity inside the shell,and f_s Shell side friction coefficient includes the entrance and exit losses which was calculated by Shinde and Chavan [76]as:

$$f_s = \exp(0.576 - 0.19 \ln(Re_s)) \quad \text{..... (A.25)}$$

8. Calculation Methods for Heat Exchanger Performance

The performance of heat exchanger by using two methods, Kays and London came up with a method in 1955 called the effectiveness–NTU method, which greatly simplified heat exchanger analysis[77].

8.1. Calculating Performance by using

The number of transfer units NTU is specified as a fraction of overall thermal sizing (UA_0) to the minimum storage capability $(m^0 c_p)_{min}$,which was reported by by Cengel [52]as:

$$NTU = \frac{UA_0}{(m^0 c_p)_{min}} \quad \text{..... (A.26)}$$

8.2. Calculating Performance by using Effectiveness

Effectiveness of STHE, in steady state is defined as the actual heat transferred divided by the maximum possible heat transfer, which was presented by by Cengel [52] as:

$$\varepsilon = \frac{q}{q_{max}} = \frac{(m_t^0 c_{pt})(T_{ti}-T_{to})}{(m^0 c_p)_{min}(T_{ti}-T_{si})} = \frac{(m_s^0 c_{ps})(T_{so}-T_{si})}{(m^0 c_p)_{min}(T_{ti}-T_{si})} \quad \text{..... (A.27)}$$

Effectiveness for two passes shell was presented by Holman [70] as:

$$\varepsilon = \frac{[\,(1-\varepsilon_1 C_r)/(1-\varepsilon_1)\,]^2-1}{[\,(1-\varepsilon_1 C_r)/(1-\varepsilon_1)\,]^2-C_r} \quad \text{..... (A.28)}$$

where

C_r is the capacity ratio calculated as:

$$C_r = \frac{(m^0 c_p)_{min}}{(m^0 c_p)_{max}} \quad \text{..... (A.29)}$$

ε_1 is the effectiveness one shell-one pass showed by Kays and London [77] as:

$$\varepsilon_1 = 2\left[1 + C_r + (1+C_r^2)^{1/2}\,\frac{1+\exp[-NTU\ \ (1+C_r^2)^{1/2}}{1-\exp[-NTU\ (1+C_r^2)^{1/2}}\right]^{-1} \quad \text{..... (A.30)}$$

9. Heat balance deviation

The difference of heat transfer rates between the hot water and cold water should be less than 5.0%.It was presented by Marzouk et al.[78]as:

$$q_{dev.} = \frac{|q_s-q_t|}{q_{ave}} \times 100\% \quad \text{..... (A.31)}$$

where

q_s is the heat exchange rate of shell-side fluid calculated as:

$q_s = m_s^0 c_p (T_{si} - T_{so})$ ….. (A.32)

q_t is the heat exchange rate of tube-side fluid calculated as:

$q_t = m^0 c_p (T_{ti} - T_{to})$ ….. (A.33)

q_{ave} is the average heat exchange rate is defined as

$q_{ave} = \frac{q_s + q_t}{2}$ ….. (A.34)

10. Fundamentals Results for prototype module design

The used many assumptions for fluid flow and heat transfer simulation are summarized as follows:

1. The heat transfer between the water and the baffles is neglected.
2. The fluid temperature is kept constant at the shell side inlet.
3. The walls of tubes have the thermal boundary condition of coupling heat transfer.
4. The inlet to the shell and tube are set as mass flow inlet.
5. The properties of working fluid which was used in design selected and assumed as input data. These values are reported in table (A-1)

Table (A-1) data for design of heat exchanger

Shell Side Fluid-Hot Water		
Property	**Unit**	**Value**
T_{hi}	°C	40
Density	kg/m3	994.75
Specific Heat Capacity	J/kg °C	4178.375
Viscosity	mPa .s	0.698
Conductivity	W/m °C	0.624
Mass flow rate	Kg/sec	0.5-2.5

Tube Side Fluid-Cold Water		
T_{ci}	°C	30
Density	kg/m3	996.1
Specific Heat Capacity	J/kg °C	4179.125
Viscosity	mPa .s	0.786
Conductivity	W/m °C	0.616
Mass flow rate	Kg/sec	0.5-2.5

6. To complete the designed it should be assume the dimensions of prototype module compared with Al- Mussaib thermal power plant, these values were presented in table(A-2).

Table (A-2) geometrical dimensions of prototype shell and tube heat exchanger

Geometry	Size
Shell diameter	154.4 mm
Tube diameter	25.4 mm
Number of tube	12
Heat exchanger length	2000 mm
Baffle cut	28 %
Central baffle spacing	157 mm
No. of baffle	22
No. of shell pass	2
No. of tube pass	4
Tube Layout	Triangle

7. Table (A-3) showed the calculation dimensionless parameters (Nusselt number and Reynolds number) at different mass flow rate of shell and tube side in prototype module.

Table (A-3) dimensionless properties of prototype shell and tube heat exchanger

Tube side				Shell side			
m° kg/sec	Re	Nu (Eq.13)	Nu (Eq.18)	m° kg/sec	Re	Nu (Eq.20)	Nu (Eq.22)
2.448	51803.6	302.625	297.2326	2.45	16289.24	124.77	131.478
2	42323.2	254.466	242.837	2	13297.34	111.592	118.118
1.5	31742.4	198.7	182.128	1.5	9973.005	95.2615	101.473
1	21161.6	139.852	121.419	1	6648.67	76.2197	81.917
0.5	10580.8	75.538	60.7093	0.5	3324.335	52.0596	56.8107

8. Table (A-4) explained the effectiveness with different value of mass flow rate in tube and shell side.

Table (A-4) effectiveness variation with mass flow rate of shell and tube

m_s^0 (kg/sec)	ε	m_t^0 (kg/sec)	ε
0.5	0.512206	0.5	0.793525
1	0.657462	1	0.629142
1.5	0.726955	1.5	0.514503
2	0.76826	2	0.433516
2.45	0.793585	2.448	0.379423

Many sketches from figures (A-4) to (A- 9) were given for design prototype module which was isolated the shape and element number of tubes and all these element.

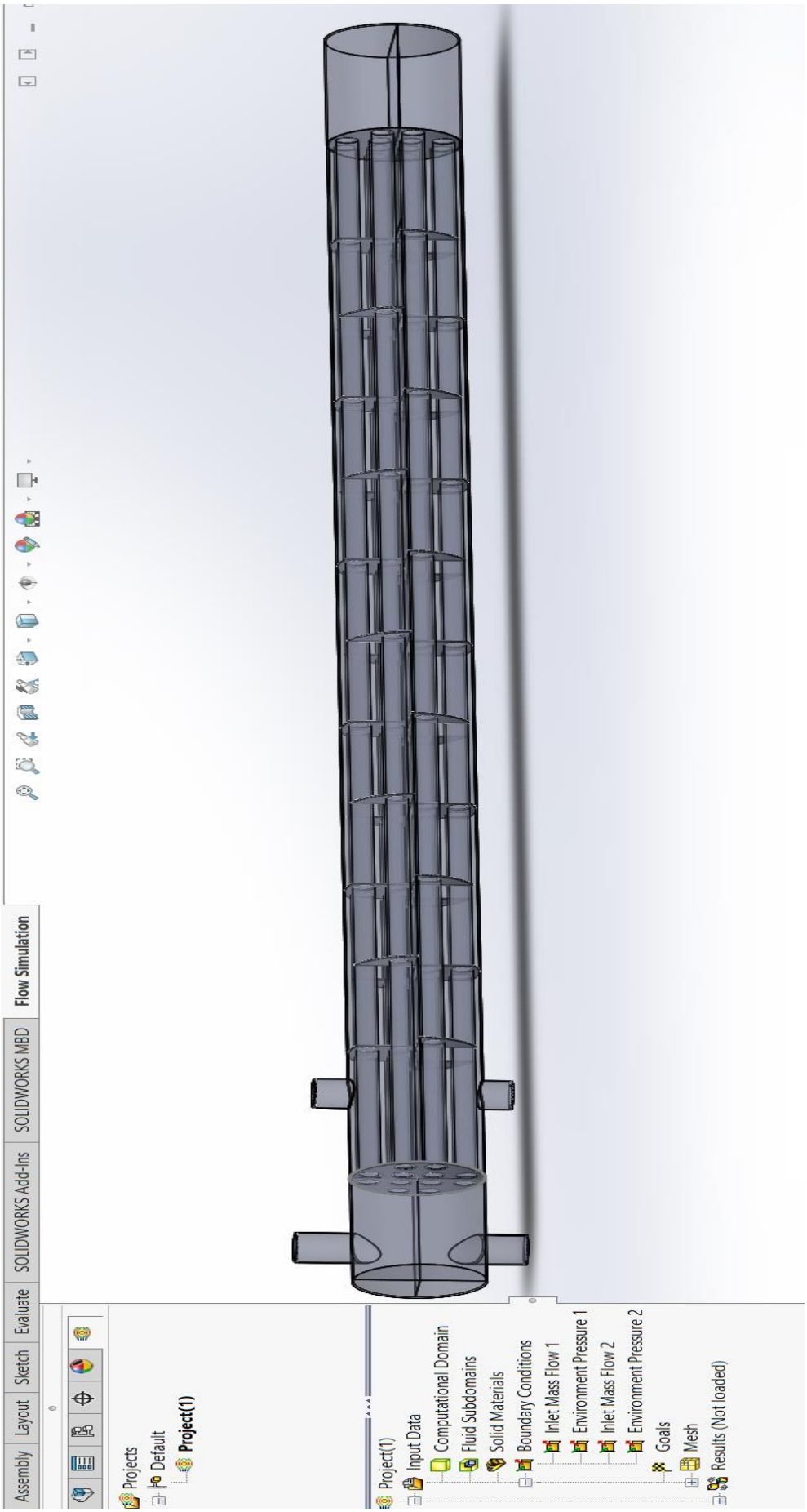

Figure (A-4) 3D sketch of the prototype heat exchanger

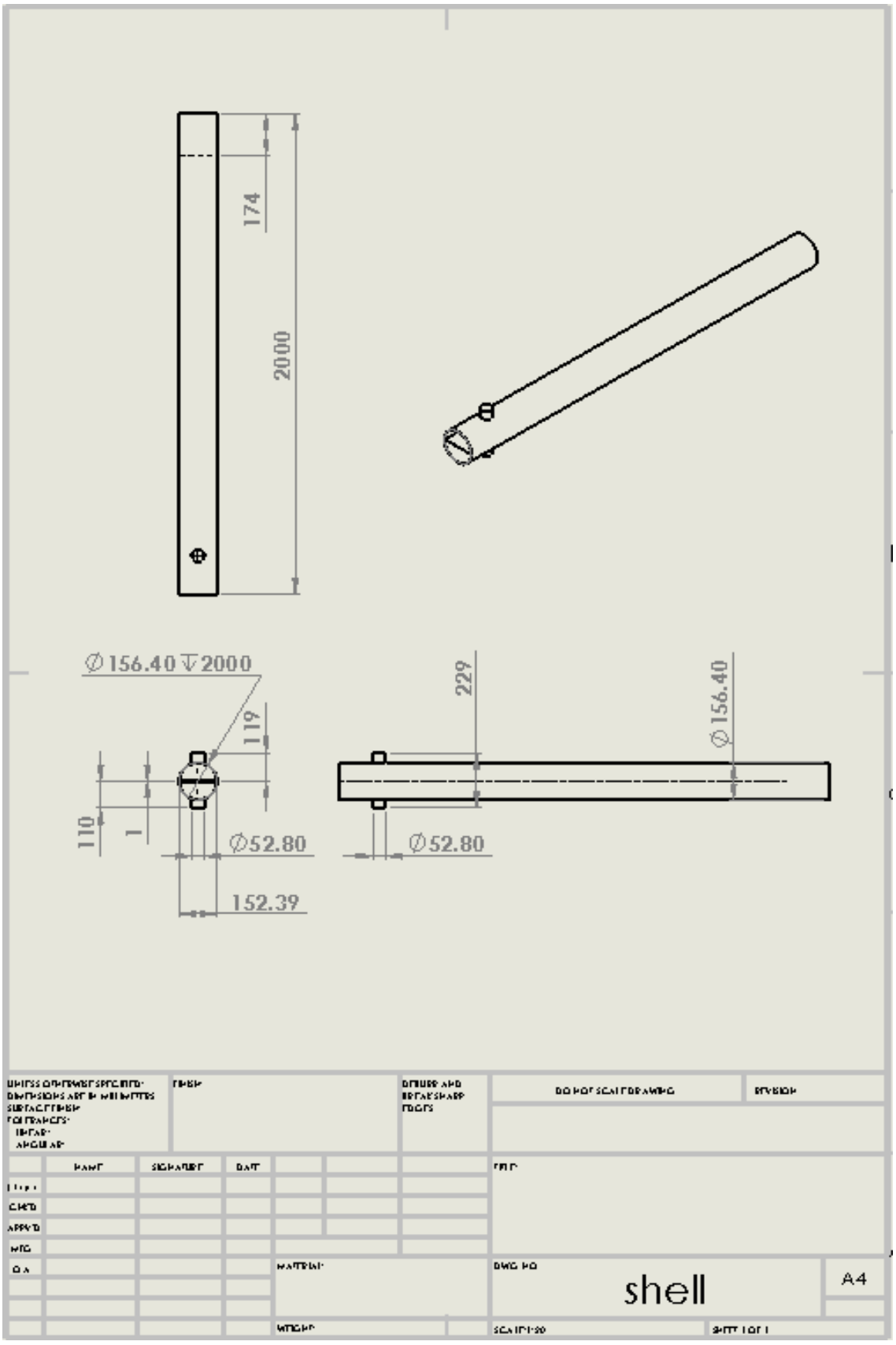

Figure (A-5) 2 D sketch of shell body of the prototype conventional heat exchanger (mm)

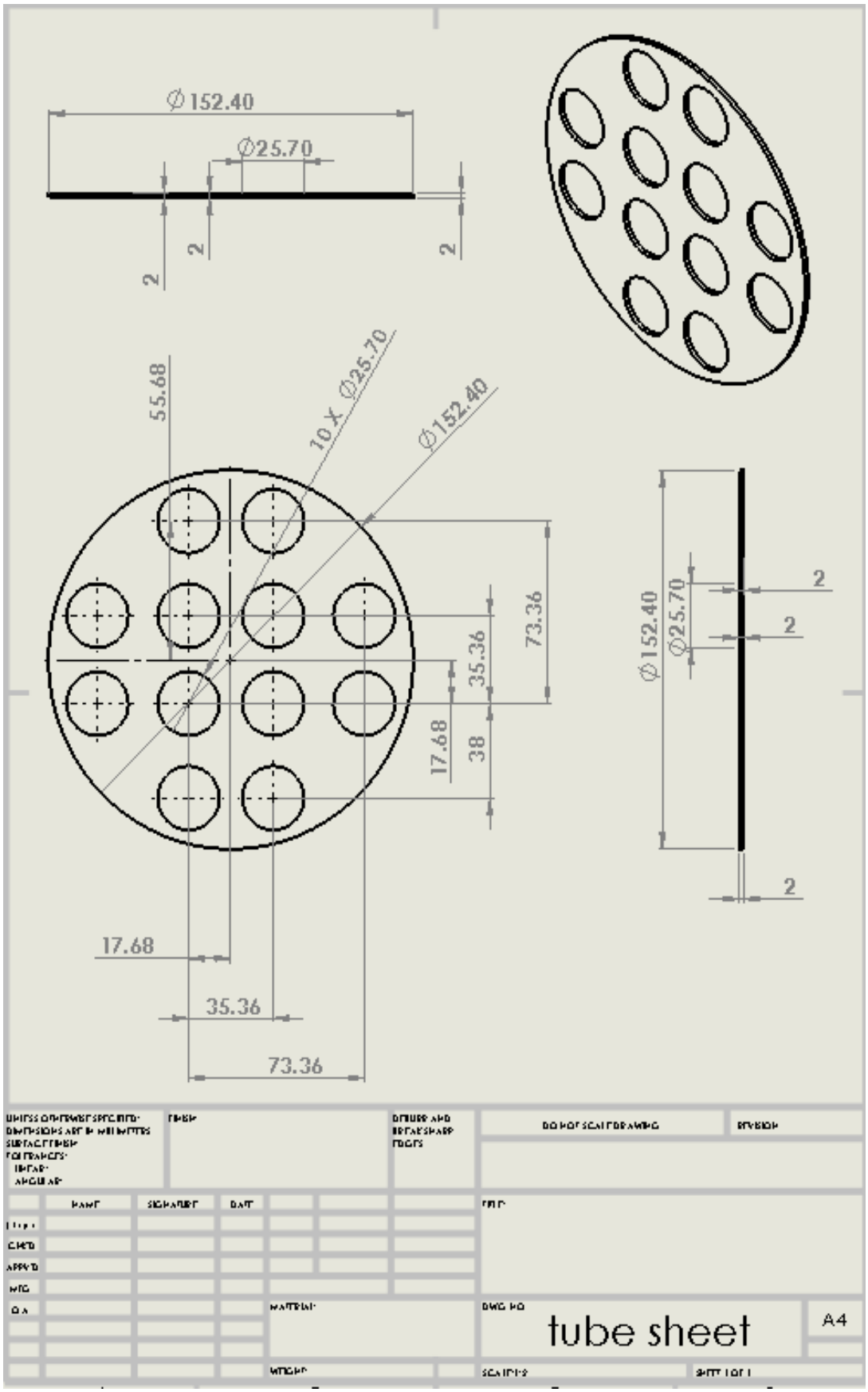

Figure (A-6) 2D sketch of the tube sheet (mm)

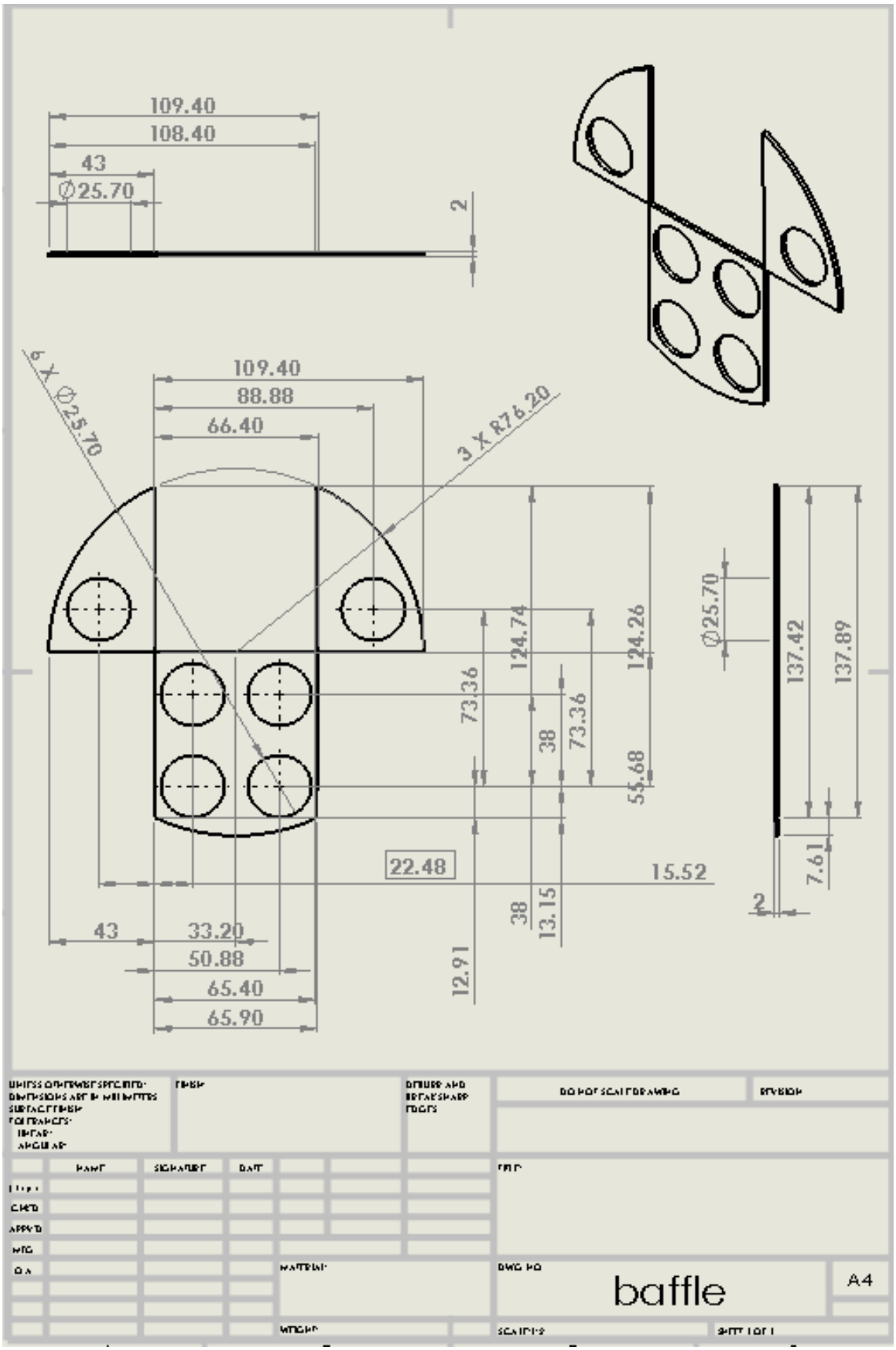

Figure (A-7) 2D sketch of the baffle (mm)

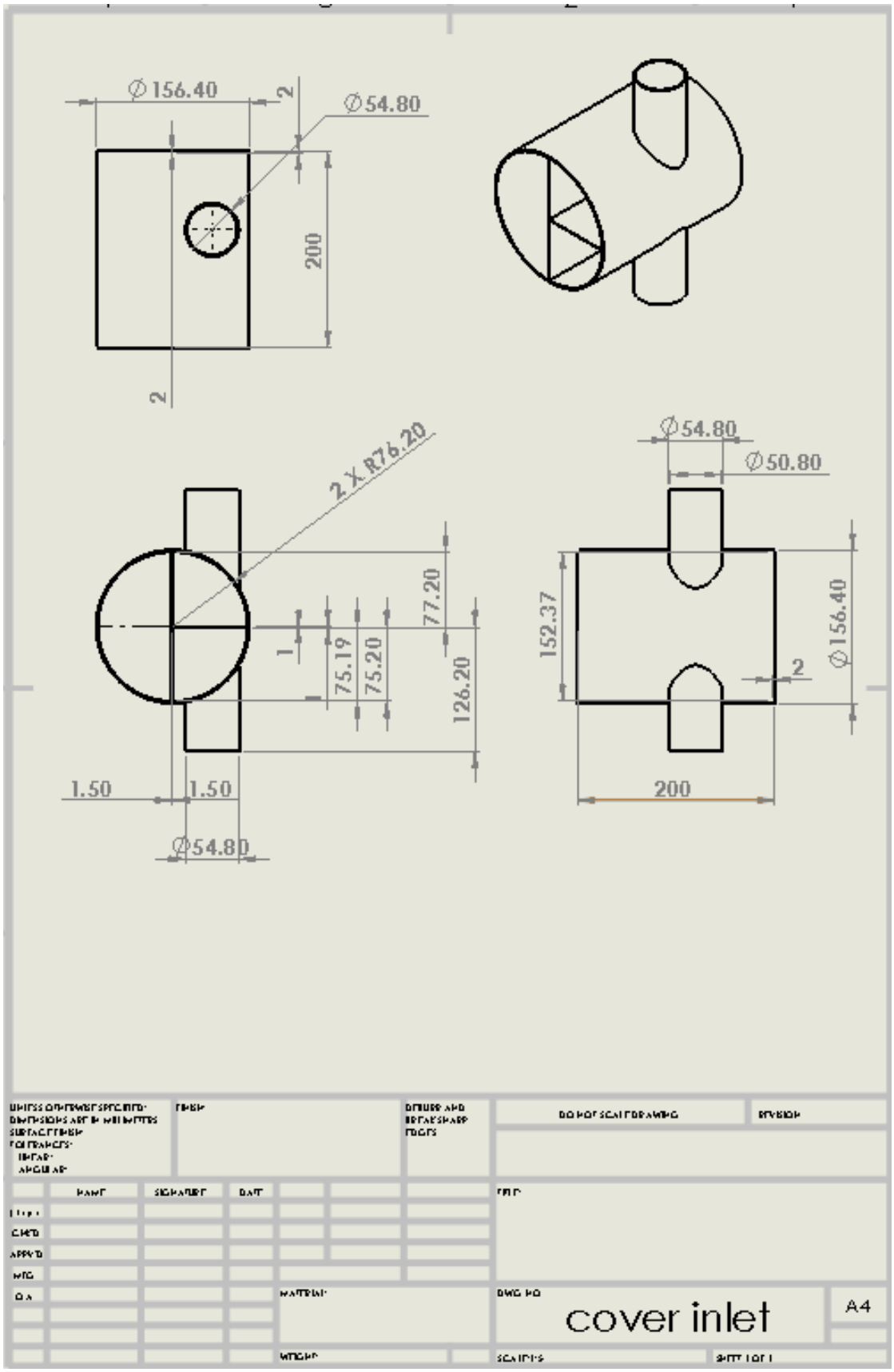

Figure (A-8) 2D sketch of the inlet cover (mm)

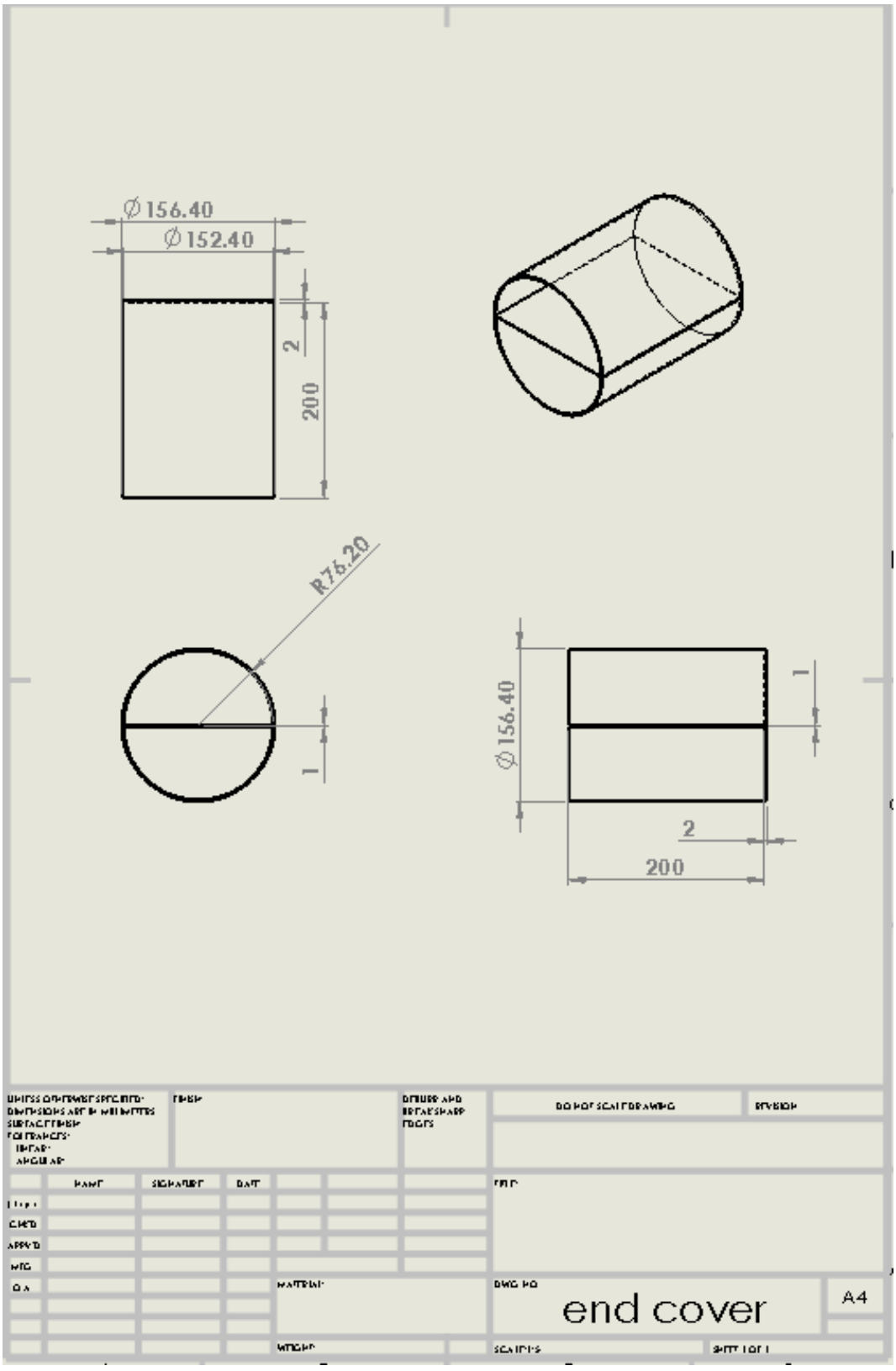

Figure (A-9) 2D sketch of the end cover (mm)

Appendix (B): Presimulation by using solidworks

A new design of a four-concentric-pipe heat exchanger is designed by using the following steps in the Solidworks software program.

1. Creating the solidworks model of the (FCPHE)

a. Start by creating a new part in solidworks. Click on Front Plane in the Feature Manager design tree and select Front from the View Orientation drop down menu in the graphics window as shown in figure (B-1).

b. Select the Sketch tab and click on Circle as shown in figure (B-2).

c. Click at the origin in the graphics window and create a circle with diameters 25.4, 50.8, 76.2 and 101.4 mm for first pipe, second pipe, third pipe and fourth pipe, respectively as shown in figure (B-3).

d. Select the Features tab and the Extruded Boss. Enter 2000 mm for the depth of the extrusion in direction 1, as shown in figures (B-4) and (B-5).

e. Repeat steps a to d to create inlet flow and outlet flow for each pipe, as shown in figure (B-6).

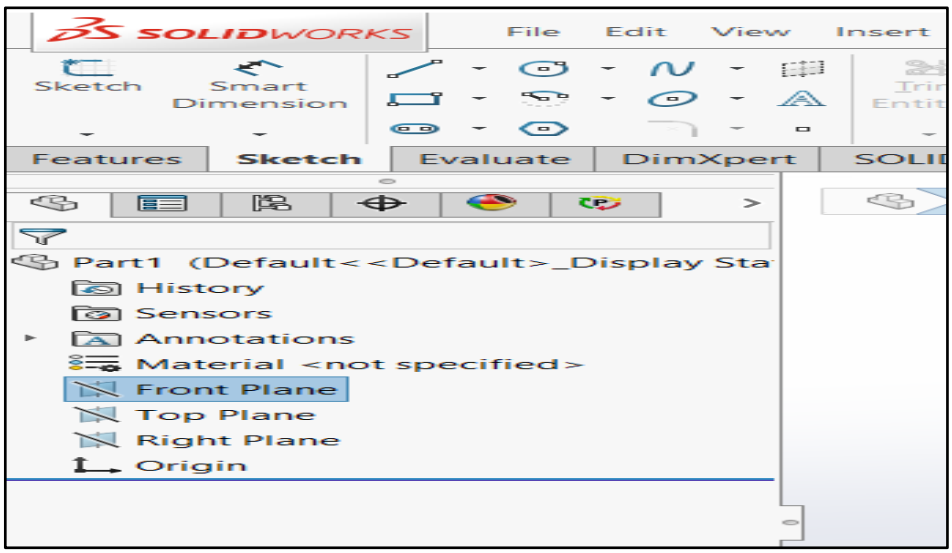

Figure (B-1) selection of front plane

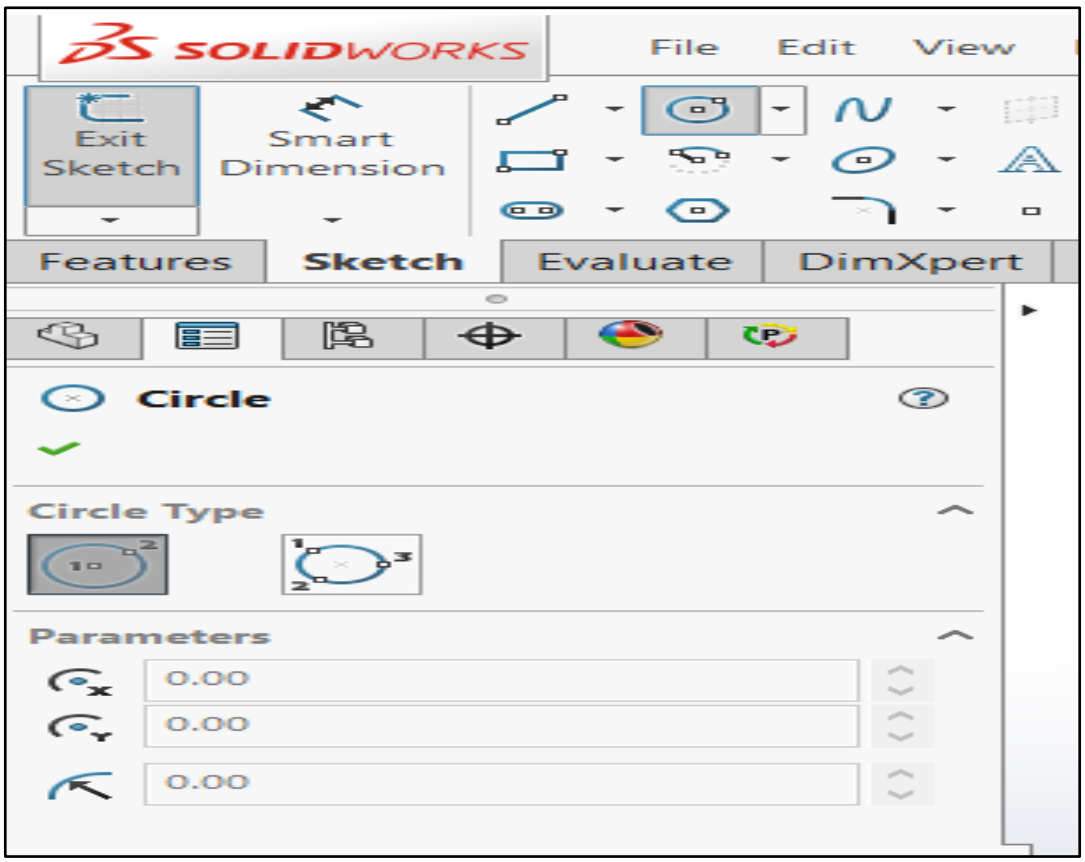

Figure (B-2) selecting a sketch tool

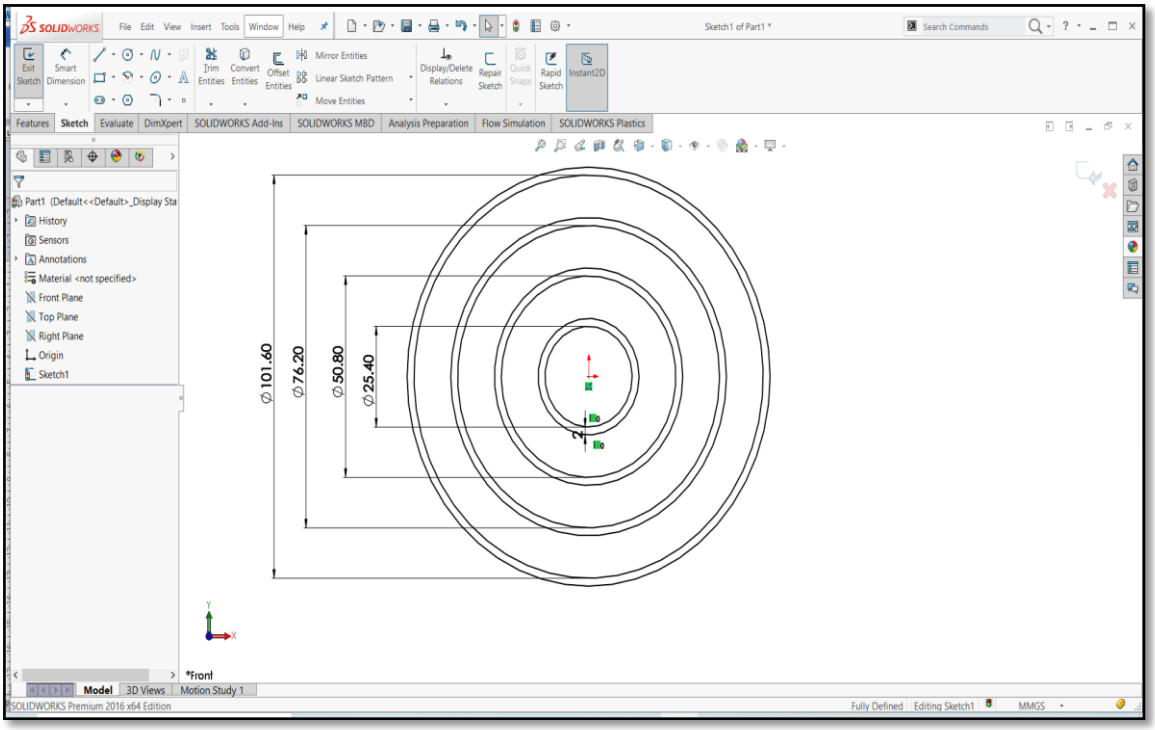

Figure (B-3) diameters selection of FCPHE

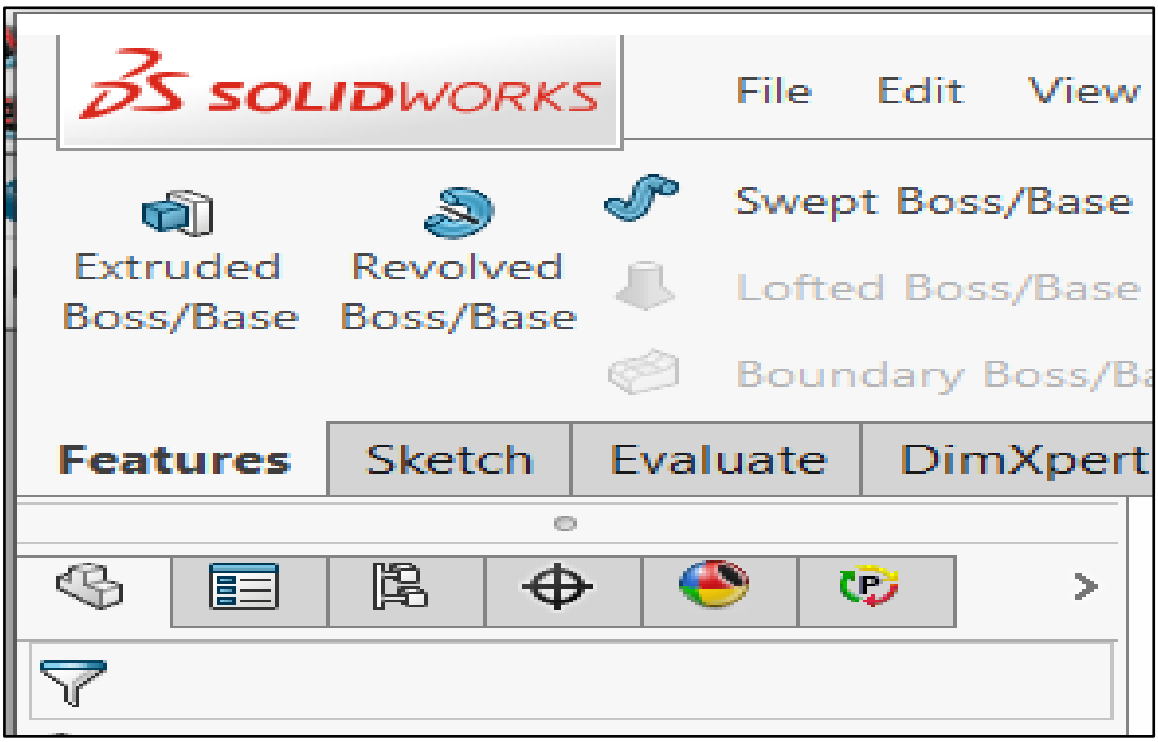

Figure (B-4) selection of extruded boss

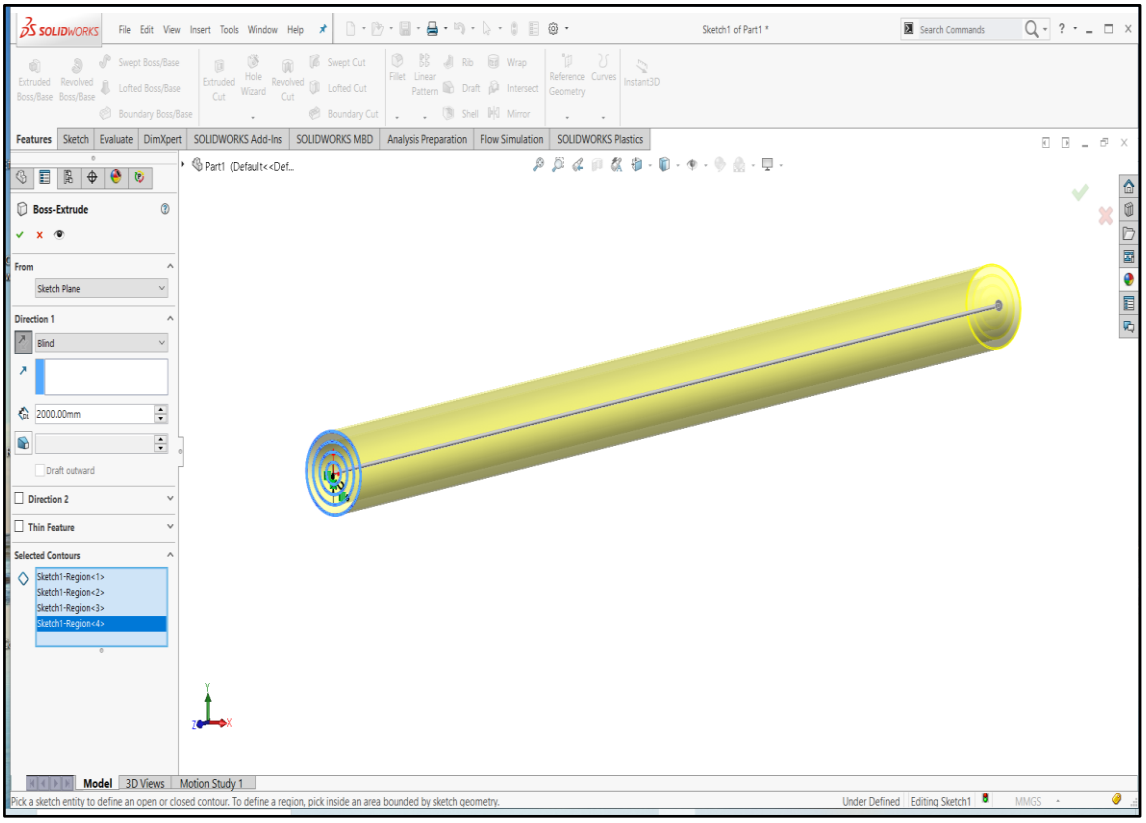

Figure (B-5) extruding the sketch

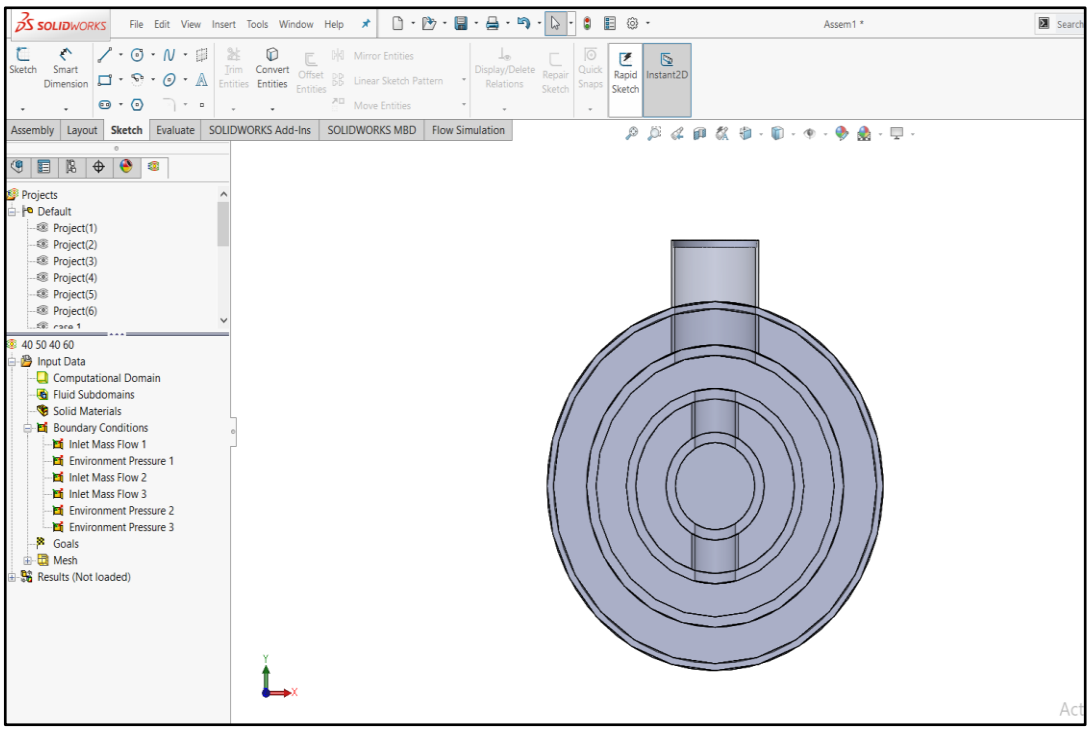

Figure (B-6) front view of (FCPHE)

2. Setting up Flow Simulation projects

a. Select Tools >> Flow simulation >> Project >> Wizard to create a new flow simulation project, as shown in figure (B-7).

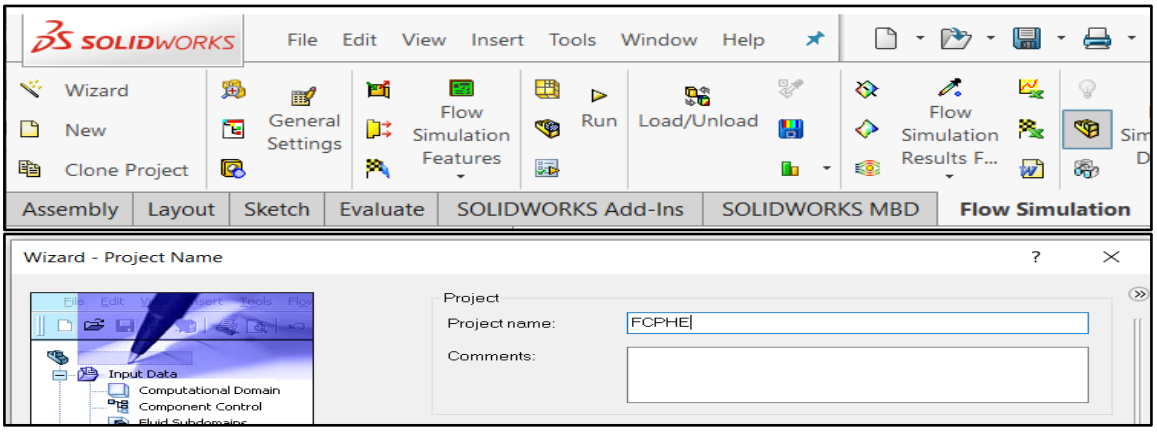

Figure (B-7) creating a name for the project

b. Use the default Internal Analysis type and check the heat conduction in solids box, as shown in figure (B-8).

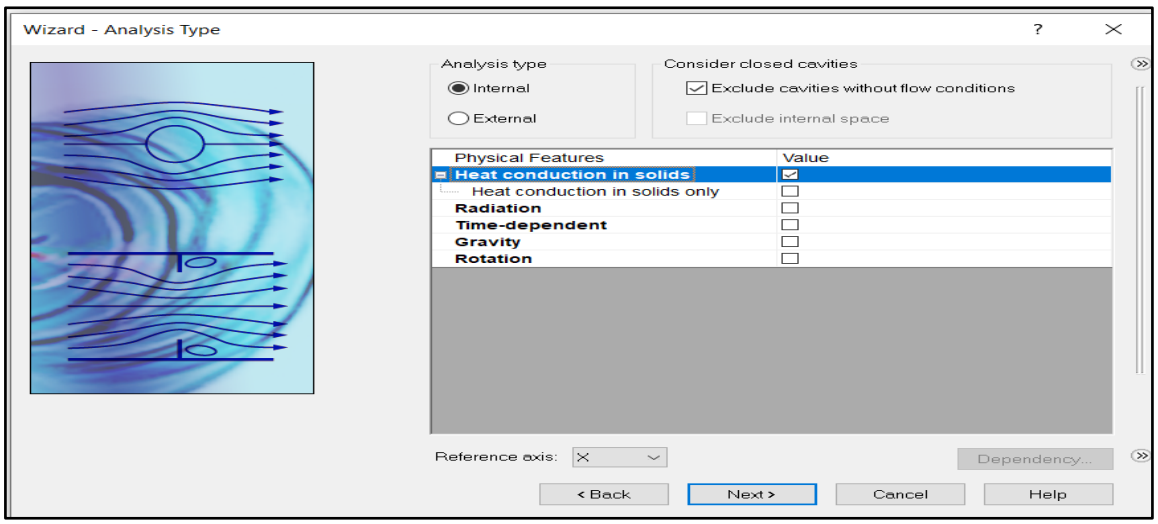

Figure (B-8) internal analysis type with heat conduction in solids

c. Add water from liquids as the project fluid, as shown in figure (B-9). Select alloys copper as the default solid, as shown in figure (B-10).

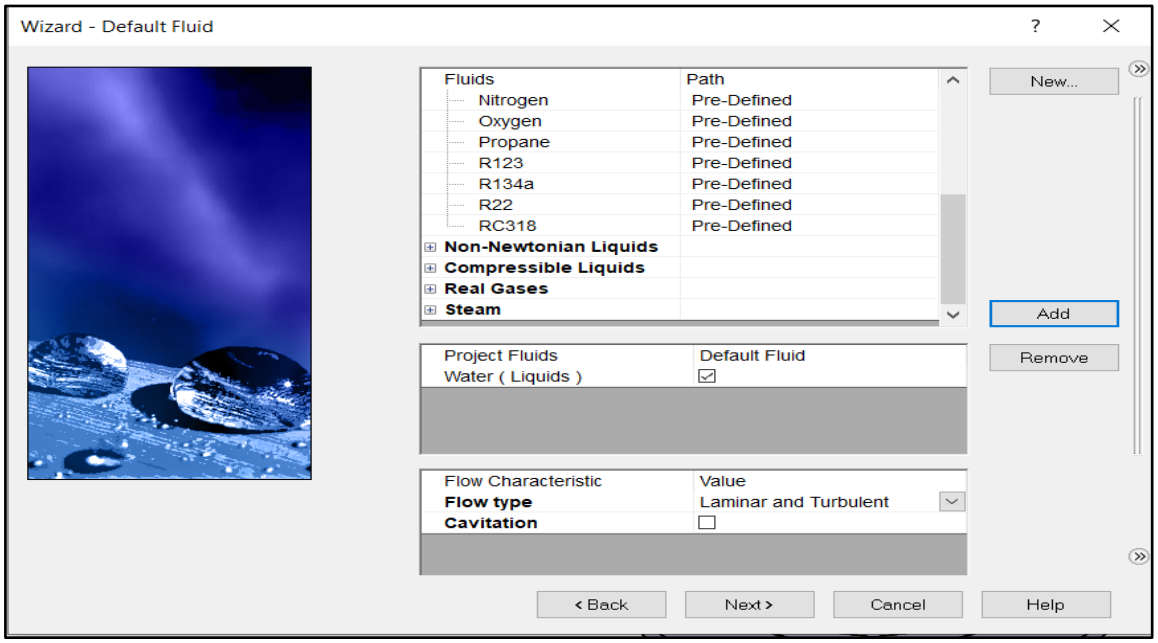

Figure (B-9) adding water as the project fluid

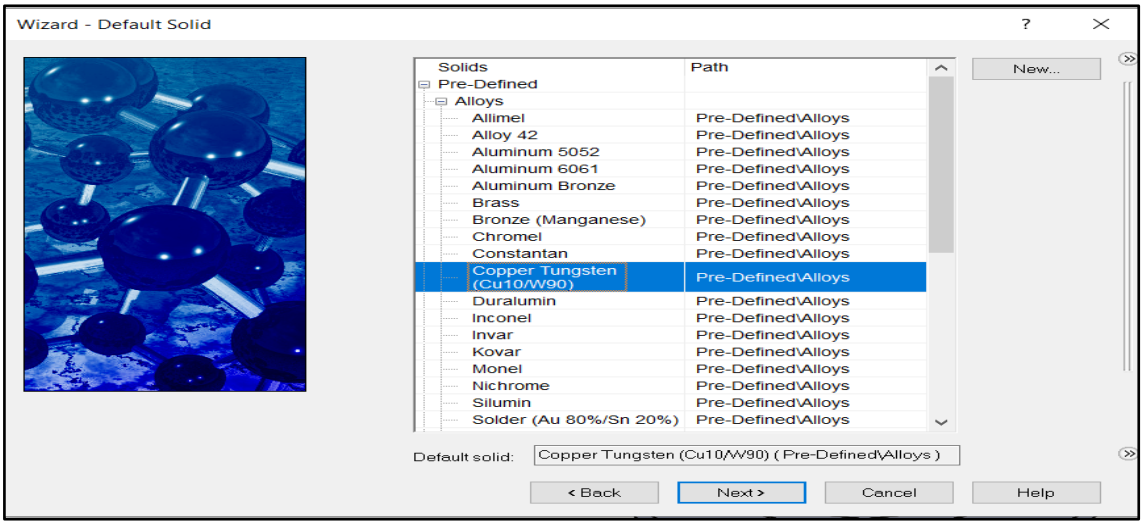

Figure (B-10) selecting copper as the default solid

3. Creating lids for the model

Select the face and create lids as shown in figure (B-11). Select Tools Flow Simulation Tools Create Lids from the solidworks menu.

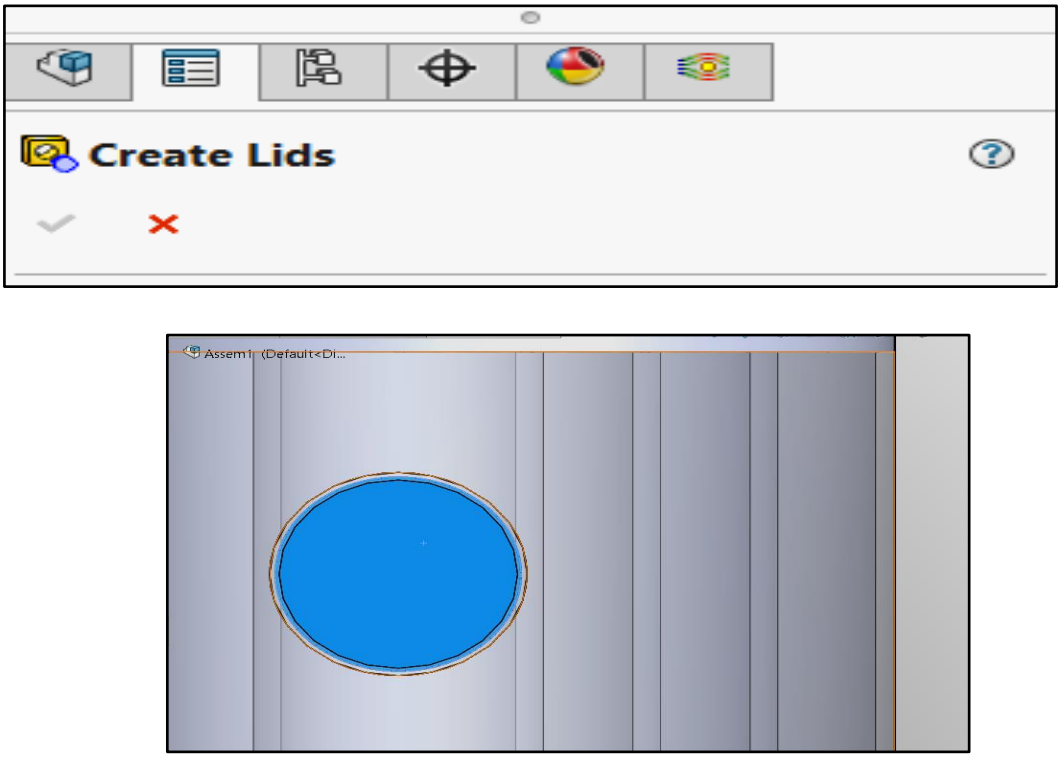

Figure (B-11) selection of the face for the lid

4. Inserting Boundary Conditions

a. Click on the plus sign next to the input data folder in the flow simulation analysis tree. Right click on boundary conditions and select insert boundary condition. Select the inner surface of the all input lids. Set the inlet mass flow and the temperature for hot water and raw water, as shown in figure (B-12).

b. Right click on boundary condition and select insert boundary condition. Right click on the pipes outflow region and click on select other. Select the inner surface of the lids, see figure (B-13). Click on the pressure opening button and select environment pressure.

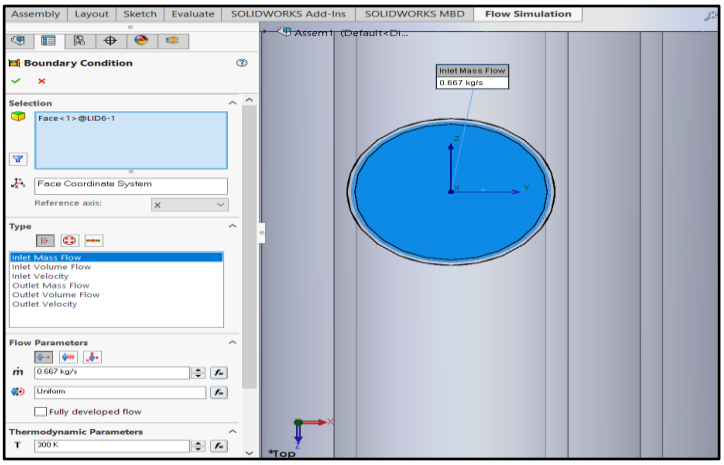

Figure (B-12) pipe input data parameters

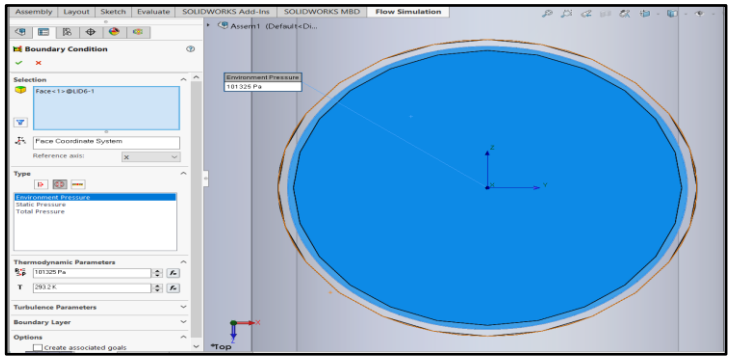

Figure (B-13) pipe outflow parameters

5. Running the calculations for heat exchanger

Select Tools >>Flow Simulation>>Solve>>Run to start calculations, see figure (B-14).

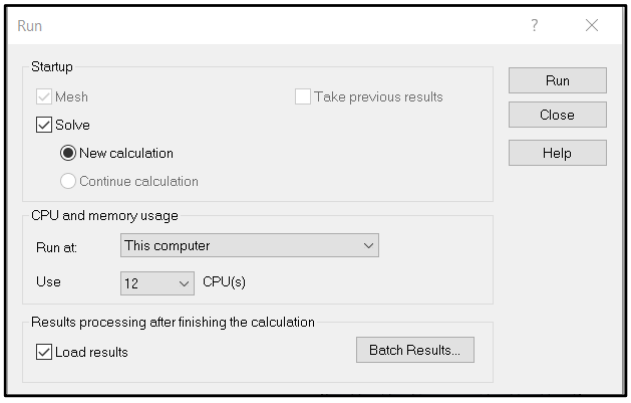

Figure (B-14) run window

6. Inserting Cut Plots

Right click on cut plots in the flow simulation analysis tree and select insert. Select temperature, pressure and velocity from the parameter drown menu.

Appendix(C): Experimental data and the results of the experimental analysis.

Table (C-1) experimental data of mass flow rate, pressure drop and temperature distribution for case 1

No. Pipe	$\dot{m}_{in}$ (l/min)	Δp (kpa)	T_{in} (°C)	T_{out} (°C)	$T_{0.2\,m}$ (° C)	$T_{0.4m}$ (° C)	$T_{0.8\mathrm{m}}$ (° C)	$T_{1\,m}$ (° C)	$T_{1.2\,m}$ (° C)	$T_{1.6\,m}$ (° C)	$T_b - T_w$ (° C)
Pipe 1	40	3	40.8	38.5				39.7			0.75
Pipe 2	60	1.2	28	31.8				29.4			0.6
Pipe 3	40	1.3	38.5	34.7	38.1	38	37.7	36.1	35.8	34.9	0.9
Pipe 4	70	0.3	28	32.3	29.2	29.3	29.9	30.2	30.6	31.4	0.2

Table (C-2) experimental data of mass flow rate, pressure drop and temperature distribution for case 2

No. pipe	$\dot{m}_{in}$ (l/min)	Δp (kpa)	T_{in} (°C)	T_{out} (° C)	$T_{0.2\,m}$ (° C)	$T_{0.4m}$ (° C)	$T_{0.8\,m}$ (° C)	$T_{1\,m}$ (° C)	$T_{1.2\,m}$ (° C)	$T_{1.6\,m}$ (° C)	$T_b - T_w$ (° C)
Pipe 1	40	3	40.8	39.3				40.2			0.7
Pipe 2	50	0.8	28	31.5				29.3			1
Pipe 3	40	1.3	39.3	35.3	38.9	38.6	38	37.5	36.5	35.9	1
Pipe 4	70	0.3	28	31.8	29.1	29.3	29.7	30	30.5	30.9	0.2

Table (C-3) experimental data of mass flow rate, pressure drop and temperature distribution for case 3

No. pipe	$\dot{m}_{in}$ (l/min)	Δp (kpa)	T_{in} (°C)	T_{out} (° C)	$T_{0.2\,m}$ (° C)	$T_{0.4m}$ (° C)	$T_{0.8\,m}$ (° C)	$T_{1\,m}$ (° C)	$T_{1.2\,m}$ (° C)	$T_{1.6\,m}$ (° C)	$T_b - T_w$ (° C)
Pipe 1	40	3	40.8	39.4				40.3			0.7
Pipe 2	40	0.13	28	31.1				29.4			0.8
Pipe 3	40	1.3	39.4	35.9	38.2	37.9	37.3	36.9	36.7	36.1	0.9
Pipe 4	70	0.3	28	30.1	28.6	28.8	29	29.1	29.2	29.3	0.2

Table (C-4) experimental data of mass flow rate, pressure drop and temperature distribution for case 4

No. pipe	$\dot{m}_{in}$ (l/min)	Δp (kpa)	T_{in} (°C)	T_{out} (° C)	$T_{0.2\,m}$ (° C)	$T_{0.4m}$ (° C)	$T_{0.8\,m}$ (° C)	$T_{1\,m}$ (° C)	$T_{1.2\,m}$ (° C)	$T_{1.6\,m}$ (° C)	$T_b - T_w$ (° C)
Pipe 1	40	3	40.8	39.5				40.2			0.7
Pipe 2	40	0.13	28	30				29.2			1.3
Pipe 3	40	1.3	39.5	36.3	39.1	38.8	38.3	37.5	36.9	36.5	1
Pipe 4	60	0.25	28	29.5	28.3	28.5	28.7	28.9	29	29.2	0.2

Table (C-5) experimental data of mass flow rate, pressure drop and temperature distribution for case 5

No. pipe	$\dot{m}_{in}$ (l/min)	Δp (kpa)	T_{in} (°C)	T_{out} (° C)	$T_{0.2\,m}$ (° C)	$T_{0.4m}$ (° C)	$T_{0.8\,m}$ (° C)	$T_{1\,m}$ (° C)	$T_{1.2\,m}$ (° C)	$T_{1.6\,m}$ (° C)	$T_b - T_w$ (° C)
Pipe 1	40	3	40.8	39.8				40.3			0.8
Pipe 2	40	0.13	28	30.3				29.5			1.5
Pipe 3	40	1.3	39.8	36.9	39.2	38.8	38.4	38.2	37.9	37.4	1.1
Pipe 4	50	0.21	28	28.9	28.2	28.3	28.4	28.5	28.6	28.7	0.2

Table (C-6) experimental data of mass flow rate, pressure drop and temperature distribution for case 6

No. pipe	$\dot{m}_{in}$ (l/min)	Δp (kpa)	T_{in} (°C)	T_{out} (° C)	$T_{0.2\,m}$ (° C)	$T_{0.4m}$ (° C)	$T_{0.8\,m}$ (° C)	$T_{1\,m}$ (° C)	$T_{1.2\,m}$ (° C)	$T_{1.6\,m}$ (° C)	$T_b - T_w$ (° C)
Pipe 1	40	3	40.8	39.3				40.2			0.8
Pipe 2	50	0.8	28	30.5				29.4			0.8
Pipe 3	40	1.3	39.3	35.6	38.3	37.7	37.2	36.9	36.2	35.7	0.9
Pipe 4	60	0.25	28	32	29.2	29.6	30	30.5	30.8	31.5	0.2

Table (C-7) experimental calculation for first pipe and third pipe of FCPHE (hot water)

	d_h mm	$\dot{m}$ (l/min)	v m/sec	Re	R*	Pr	f_t	Nu	h W/m^2. °C
Pipe 1	25.4	40	1.25	46711.77	-	4.67	0.005322	260.0155	6226.005
Pipe3	25.4	40	0.25	9125.25	6098.5	4.67	0.03542	84.8118	2083.56

Table (C-8) experimental calculation for second pipe of $d_h =$ 25.4 mm and different mass flow rate of FCPHE (raw water)

m° (l/min)	v m/sec	Re	Pr	Nu	R*	f_t	h W/m^2. °C
60	0.609556	19621	5.33	192.7	13168	0.0286	4673.4
50	0.50776	16345	5.33	166.49	10969	0.03	4037.8
40	0.406574	13087	5.33	139.37	8782.8	0.0319	3380.1

Table (C-9) experimental calculation for fourth pipe of $d_h = 27.8$ mm and different mass flow rate of FCPHE (raw water)

m° (l/min)	v m/sec	Re	Pr	Nu	R*	f_t	h W/m^2. °C
70	0.297919	10496	5.33	93.133	7008.6	0.034	2063.7
60	0.255286	8994	5.33	82.309	6005.6	0.0356	1823.8
50	0.212654	7492	5.33	71.115	5002.7	0.0376	1575.8

Table (C-10) overall heat transfer coefficient

$\dot{m}_2$ (l/min)	U_{o1} (W/m^2. C)	U_{i2} (W/m^2. C)	U_{o2} (W/m^2. C)	$\dot{m}_4$ (l/min)	U_{i3} (W/m^2. C)	U_{total} (W/m^2. C)
60	2343.37	1365.39	1401.3	70	889.27	333.64
50	2171.92	1305.36	1333.9	60	838.83	315.63
40	1966.13	1228.11	1248.02	50	778.98	293.44

Table (C-11) logarithmic mean temperature difference

Number of case	$LMTD_1$(°C)	$LMTD_2$(°C)	$LMTD_3$(°C)	$LMTD_{av.}$(°C)
case1	9.7	5.9	7.9	7.8
case2	10.3	6.9	9.7	9.0
case3	10.5	7.6	15.5	11.2
case4	11.1	8.6	14.1	11.3
case5	11.1	8.9	22.1	14.1
case6	10.8	7.8	8.6	9.1

Table (C-12) heat transfer and effectiveness at $(\dot{m}_h = 40, \dot{m}_4 = 70)$ L/min *and different values of mass flow rate for water flow in second pipe*

$\dot{m}_2$ (l/min)	$\dot{Q}_h$ watt	$\dot{Q}_{n2}$ watt	$\dot{Q}_{n4}$ watt	ε
60	16992.06	15880.68	20965.28	0.755
50	15320.71	12189.11	18527.45	0.646
40	13788.64	8636.858	10238.86	0.458

Table (C-13) heat transfer and effectiveness at $(\dot{m}_h = 40, \dot{m}_2 = 40)$ L/min ***and different values of mass flow rate for water flow in fourth pipe***

$\dot{m}_2$ l/min	$\dot{Q}_h$ watt	$\dot{Q}_{n2}$ watt	$\dot{Q}_{n4}$ watt	ε
70	13788.6	10587.1	20965.28	0.49
60	12535.1	5572.2	14626.94	0.34
50	10863.8	6408.0	7313.469	0.29

Appendix (D): Uncertainties calculated of Nusselt Number and Heat Transfer Coefficient.

The experimental error for the Nusselt Number can be calculated but in the first we should calculate the experimental error for Reynolds number, friction coefficient and Prandtl number.

$$Nu_1 = \frac{(f_t/2)(Re_1 - 1000)Pr}{1+12.7(f_t/2)^{0.5}(Pr^{0.67}-1)} \quad \text{..... (D.1)}$$

$$Re = \frac{4\rho\, m}{\pi\, d\, \mu} \quad \text{..... (D.2)}$$

$$\frac{\partial Re}{\partial \rho} = C_1 \left[\frac{m}{d\,\mu}\right] \quad \text{..... (D.3)}$$

$$\frac{\partial Re}{\partial m} = C_1 \left[\frac{\rho}{d\,\mu}\right] \quad \text{..... (D.4)}$$

$$\frac{\partial Re}{\partial d} = -C_1 \left[\frac{m}{d^2\mu}\right] \quad \text{..... (D.5)}$$

$$\frac{\partial Re}{\partial \mu} = C_1 \left[\frac{\rho m}{d\mu^2}\right] \quad \text{..... (D.6)}$$

$$U_{Re} = \left[\left(\left(\frac{\partial Re}{\partial \rho}\right) * U_\rho\right)^2 + \left(\left(\frac{\partial Re}{\partial m}\right) * U_m\right)^2 + \left(\left(\frac{\partial Re}{\partial d}\right) * U_d\right)^2 + \left(\left(\frac{\partial Re}{\partial \mu}\right) * U_\mu\right)^2\right]^{0.5} \quad \text{.....(D.7)}$$

$$f_t = (1.58\ln(Re) - 3.28)^{-2} \quad \text{..... (D.8)}$$

$$\frac{\partial\ f_t}{\partial Re} = -2[1.58\ln Re - 3.28]^{-3} * \frac{1.58}{Re} \quad \text{..... (D.9)}$$

$$U_{Re} = \left[\left(\left(\frac{\partial\ f_t}{\partial Re}\right) * U_{Re}\right)^2\right]^{0.5} \quad \text{..... (D.10)}$$

$$Pr = \frac{\mu\, c_p}{k} \quad \text{..... (D.11)}$$

$$\frac{\partial Pr}{\partial \mu} = \frac{c_p}{k} \quad \text{..... (D.12)}$$

$$\frac{\partial Pr}{\partial c_p} = \frac{\mu}{k} \quad \text{..... (D.13)}$$

$$\frac{\partial Pr}{\partial k} = -k^{-2}\mu c_p \quad \text{..... (D.14)}$$

$$U_{Pr} = \left[\left(\left(\frac{\partial Pr}{\partial \mu}\right) * U_\mu\right)^2 + \left(\left(\frac{\partial Pr}{\partial c_p}\right) * U_{c_p}\right)^2 + \left(\left(\frac{\partial Pr}{\partial k}\right) * U_k\right)^2\right]^{0.5} \quad \text{..... (D.15)}$$

$$\frac{\partial Nu}{\partial Re} = \frac{(f_t/2)Pr}{1+12.7(f_t/2)^{0.5}(Pr^{0.67}-1)} \quad \text{..... (D.16)}$$

$$\frac{\partial Nu}{\partial Pr} = \frac{1+12.7(f_t/2)^{0.5}(Pr^{0.67}-1)\left[\frac{f_t}{2}Re-1000\right]-(f_t/2)(Re_1-1000)Pr*6.02f_t^{0.5}*Pr^{-0.33}}{[1+12.7(f_t/2)^{0.5}(Pr^{0.67}-1)]^2}$$

..... (D.17)

$$\frac{\partial Nu}{\partial f_t} = \frac{1+12.7(f_t/2)^{0.5}\left(Pr^{0.67}-1\right)(0.5Re\,Pr-500Pr)-(f_t/2)(Re_1-1000)Pr*3.175\left(\frac{2}{f_t}\right)^{0.5}[Pr^{0.67}-1]}{[1+12.7(f_t/2)^{0.5}(Pr^{0.67}-1)]^2}$$

..... (D.18)

$$U_{Nu} = \left[\left(\left(\frac{\partial Nu}{\partial Re}\right) * U_{Re}\right)^2 + \left(\left(\frac{\partial Nu}{\partial Pr}\right) * U_{Pr}\right)^2 + \left(\left(\frac{\partial Nu}{\partial f_t}\right) * U_{f_t}\right)^2\right]^{0.5}$$

.....(D.19)

The heat transfer coefficient is given in the form:

$$h = \frac{Nu.k}{d} \quad \text{..... (D.20)}$$

$$\frac{\partial h}{\partial Nu} = \frac{k}{d} \quad \text{..... (D.21)}$$

$$\frac{\partial h}{\partial k} = \frac{Nu}{d} \quad \text{..... (D.22)}$$

$$\frac{\partial h}{\partial d} = -d^{-2}\, Nu\, k \qquad \text{..... (D.23)}$$

$$U_h = \left[\left(\left(\frac{\partial h}{\partial Nu}\right) * U_{Nu}\right)^2 + \left(\left(\frac{\partial h}{\partial k}\right) * U_k\right)^2 + \left(\left(\frac{\partial h}{\partial d}\right) * U_d\right)^2\right]^{0.5} \qquad \text{..... (D.24)}$$

Appendix (E): Numerical procedure

1. Finite volume method

The finite volume method (FVM) is a method for representing and evaluating partial differential equations in the form of algebraic equations. In the finite volume method, volume integrals in a partial differential equation that contain a divergence term are converted to surface integrals, using the divergence theorem, that is presented by **LeVeque [79]**. These terms are then evaluated as fluxes at the surfaces of each finite volume. Because the flux entering a given volume is identical to that leaving the adjacent volume, these methods are conservative. Another advantage of the finite volume method is that it is easily formulated to allow for unstructured meshes. The method is used in many computational fluid dynamics packages. "Finite volume" refers to the small volume surrounding each node point on a mesh.

2. Finite volume basic methodology

The main steps of this method can be summarized as follows:

1- Divide the domain into control volumes

2- Integrate the differential equation over the control volume and apply the divergence theorem.

3-To evaluate derivative terms, values at the control volume faces are needed: have to make an assumption about how the value varies.

4-Result is a set of linear algebraic equations: one for each control volume.

5-Solve iteratively or simultaneously.

3. Typical control volume

The net flux through the control volume boundary is the sum of integrals over the four control volume faces (six in 3D). The control volumes do not overlap. The value of the integrand is not available at the control volume faces and is determined by interpolation. Figure (E-1) explains the computational node.

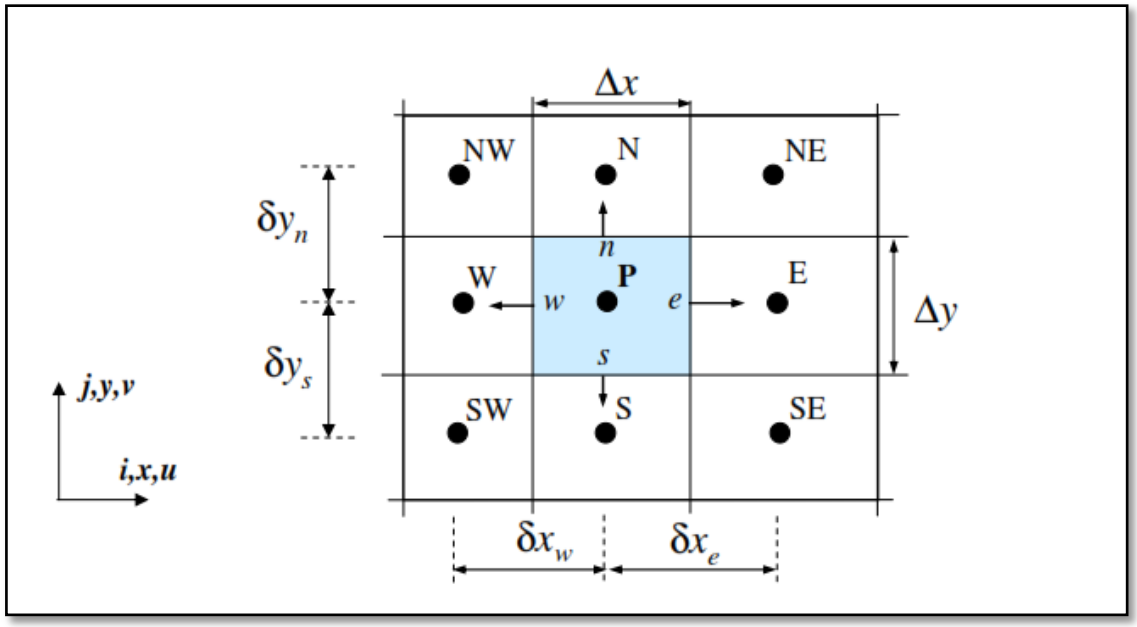

Figure (E-1) scheme for control volume

4. General approach

For the conservation equation for variable φ the following steps are taken:

1- Integration of conservation equation in each cell.

2- Calculation of face values in terms of cell-centered value

3- Collection of like terms.

The result is represented the following discretization equation by **Marshall and Bakker [80]** as :

$$a_P \phi_P = \sum_{nb} a_{nb} \phi_{nb} + b \quad \ldots (E.1)$$

Where nb refers to the neighboring cells. The coefficients a_{nb} and b will be different for every cell in the domain at every iteration.

5. Relaxation

At each iteration, at each cell, a new value for variable φ in cell P can then be calculated from that equation. It is common to apply relaxation that showed by **Marshall and Bakker[80]** as:

$$\phi_P^{\text{new,used}} = \phi_P^{\text{old}} + U\left(\phi_P^{\text{new, predicted}} - \phi_P^{\text{old}}\right) \quad \ldots (E.2)$$

where U is the relaxation factor:

U < 1 is under relaxation. This may slow down speed of convergence but increases the stability of the calculation, i.e. it decreases the possibility of divergence or oscillations in the solutions.

U = 1 corresponds to no relaxation. One uses the predicted value of the variable.

U > 1 is over relaxation. It can sometimes be used to accelerate convergence but will decrease the stability of the calculation.

6. Convergence

The iterative process is repeated until the change in the variable from one iteration to the next becomes so small that the solution can be considered converged. At convergence all discrete conservation equations (momentum, energy, etc.) are obeyed in all cells to a specified tolerance, the solution no longer changes with additional iterations, and mass, momentum, energy and scalar balances are obtained.

Residuals measure imbalance (or error) in conservation equations. The absolute residual at point P is defined by **Marshall and Bakker[80]**as :

$$R_P = |a_P\phi_P - \sum_{nb}\ a_{nb}\phi_{nb} - b| \qquad \ldots (E.3)$$

Residuals are usually scaled relative to the local value of the property φ in order to obtain a relative error:

$$R_{P,\text{ scaled}} = \frac{|a_P\phi_P - \sum_{nb} a_{nb}\phi_{nb} - b|}{|a_P\phi_P|} \qquad \ldots (E.4)$$

They can also be normalized, by dividing them by the maximum residual that was found at any time during the iterative process. An overall measure of the residual in the domain is:

$$R^{\phi} = \frac{\sum_{\text{all cells}} |a_P\phi_P - \sum_{nb} a_{nb}\phi_{nb} - b|}{\sum_{\text{all cells}} |a_P\phi_P|} \qquad \ldots (E.5)$$

It is common to require the scaled residuals to be on the order of 10^{-3} to10^{-4} or less for convergence.

7. Numerical scheme (QUICK scheme)

A QUICK stand for Quadratic Upwind Interpolation for Convective Kinetics is presented by **Nishikawa[63]**. A quadratic curve is fitted through two upstream nodes and one downstream node. This is a very accurate scheme, but in regions with strong gradients, overshoots and undershoots can occur. This can lead to stability problems in the calculation. Figure (E-2) show the interpolated value.

The previously discussed numerical scheme assumes some shape of the function φ. These functions can be approximated by Taylor series polynomials as follows:

$$\phi(x_e) = \phi(x_P) + \frac{\phi'(x_P)}{1!}(x_e - x_P) + \frac{\phi''(x_P)}{2!}(x_e - x_P)^2 + \cdots + \frac{\phi^n(x_P)}{n!}(x_e - x_P)^n + \cdots \quad \ldots (E.6)$$

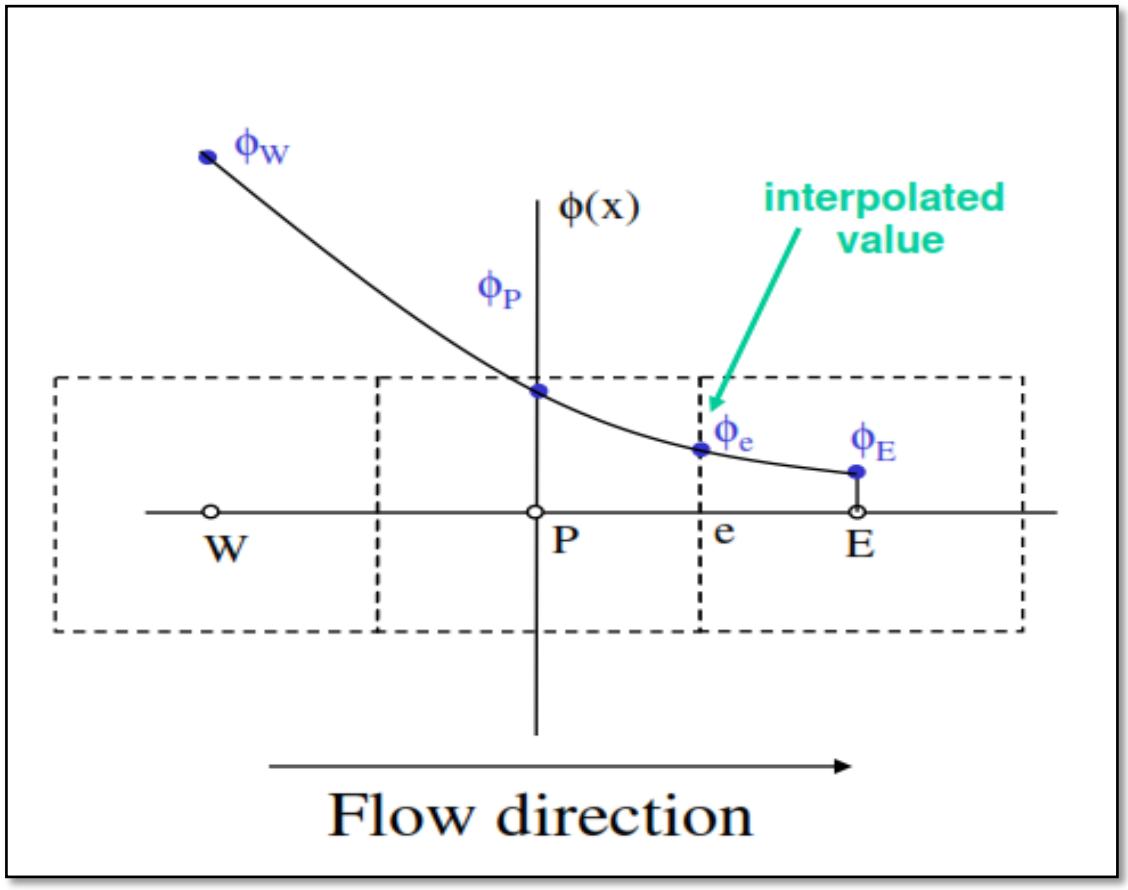

Figure (E-2) quadratic upwind interpolation

Higher order schemes will be more accurate. They will also be less stable and will increase computational time. QUICK does take the second order derivative into account, but ignores the third order derivative. This is then considered third order accurate.

Appendix (F): Published researches

Advances in Mechanics
Volume 9, Issue 3, 2021
Page 408-424

Design A Prototype Module for Al-Mussaib Thermal Power Plant

Rana Ali Husseini[1], Adil Abbas Alwan[2], Isam Mejbel Abed[3]
[1]Power Mechanics Engineering Department, Al-Musaib Technical College, Al-Furat Al-Awsat Technical
[2,3]Mechanical Engineering Department, College of Engineering, University of Babylon, Hilla, Babylon, 5001, Iraq
Email: ranaa.h.78@atu.edu.iq

Article history:
Received 02 April 2021
Revised 08 May 2021
Accepted 15 June 2021

Abstract
The most widely utilized utilization of heat transfer takes place in planning practical equipment which serves to give and receive heat out of one fluid toward another. This equipment of effective transfer is normally entitled as heat exchanger. The most commonly utilized heat exchange equipment could be shell and tube exchangers. In this work, the emphasis is directed toward designing a prototype shell and tube heat exchanger for Al-Mussaib thermal power plant. In order to do this design, there is a need to calculate all thermal physical properties and data of these properties for the working fluid which was following through this design. Kern method depends on this design and it is generally accepted when compared with others methods. Then, it uses solidwork to calculate these parameters and limitations of working fluid by designing theoretically a prototype module in order to simulate and analyze these values with actual data for Al-Mussaib thermal power plant.
Keywords: Kern Method, Solidwork, Heat Exchanger Design.

Journal of Engineering Science and Technology
Vol. 16, No. 2 (2021) 1761 – 1781

EXPERIMENTAL INVESTIGATION AND ANALYSIS OF HEAT TRANSFER RATE IN CONICAL TUBE HEAT EXCHANGER: A NOVEL ENHANCEMENT APPROACH

RANA A. HUSSEIN[1,*], ADIL A. ALWAN[2], ISAM M. ABED[2]

[1]Power Mechanics Engineering Department, Al-Musaib Technical College, Al-Furat Al-Awsat Technical, Iraq
[2]Mechanical Engineering Department, College of Engineering, University of Babylon, Hilla, Babylon, 5001, Iraq
*Corresponding Author: ranaa.h.78@atu.edu.iq

Abstract

Heat exchangers are devices employed in transferring thermal energy from one fluid to another at varying temperature rates within thermal contact. Recent uses of such devices are found in oil refineries and (petro-) chemistry, as well as power generating projects, as all of these accommodate shell and tube type heat exchangers (STHEs). The present paper describes the major component of STHE and the modification of heat exchangers that are used in thermal power plants. The STHE is used as a heat exchanger based on its simple design and performance aspects. Even though these shell and tube heat exchangers operate at their designed point, they can be even effectively designed to achieve a better heat transfer rate by using different changes in parameters. In terms of engineering, an optimal design would involve maximal heat transferring and minimal costs. This paper also reviewed different types of STHE enhancements, including modifications in the arrangement and number of tubes, as well as their diameters, length, pitches, and types. Other aspects considered are the height of fins, and baffle types, and their spacing ratios. The outer cylindrical tube of an ordinary heat exchanger-type concentrate tube was replaced by a conical tube during the present experimental analysis. The use of epoxy resin and fibre has been developed to create new conic tubes with different diameter values. Conical tubes had a diameter of 0.882, 0.741, and 0.612. For a conical tube heat exchanger with a length of 1 meter, experiments were performed. For the inner tube, 1 LPM and the outside conical tube 1 LPM to 7 LPM were considered. The conical tube thermal transmission results were analysed and compared with cylindrical tube results. Results show that the heat transfer rate is inversely proportionate to the ratio of diameter. For HTR water flowing through conical external tubes, a correlation was developed. There were results that showed up to 22 present higher heat transfer rates.

Keywords: Baffle type, Conical tube, Heat transfer, Regression analysis, Tube arrangement.

الخلاصة

تُستخدم المبادلات الحرارية بشكل شائع كمكونات مهمة في أنظمة الاستخلاص والاستعادة الحرارية لمحطة توليد الطاقة. في العديد من التطبيقات ، تعتبر وظيفة نقل الحرارة عالية الأداء أمرًا بالغ الأهمية.يتم إنجاز تصميم جديد للمبادل الحراري لحل المشكلة في محطة كهرباء المسيب الحرارية. يتكون هذا التصميم من أربعة أنابيب نحاسية بقطر 1 بوصة (25.4 مم) و 2 بوصة (50.8 مم) و 3 بوصات (76.2 مم) و 4 بوصات (101.6 مم) ويبلغ طول الأنابيب 2 م. يتم تبريد الماء الساخن على مرحلتين.

المرحلة الأولى ، يتم انتقال الحرارة بين الماء الساخن في الأنبوب الأول والماء البارد في الأنبوب الثاني. بينما في المرحلة الثانية ، يحدث انتقال الحرارة بين الماء الساخن في الأنبوب الثالث والماء البارد في الأنبوب الثاني والأنبوب الرابع.يكون ترتيب التدفق في المرحلة الأولى هو التدفق المعاكس بينما يكون ترتيب التدفق في المرحلة الثانية متوازيًا.

يتم استخدام Solidworks في تصميم المبادلات الحرارية للأنابيب الأربعة متحدة المركز. تبلغ درجة حرارة مدخل الماء الساخن 40.8 درجة مئوية ومعدل تدفق كتلة الماء الساخن 40 لتر / دقيقة. تبلغ درجة حرارة مدخل الماء البارد للأنبوبين الثاني والرابع 28 درجة مئوية ومعدل تدفق كتلة الماء العادي في الأنبوبين الثاني والرابع 60 لترًا / دقيقة و 70 لترًا / دقيقة على التوالي. الغرض من التصميم هو خفض درجة حرارة الماء الساخن إلى 35 درجة مئوية وهي درجة الحرارة المطلوبة في محطة كهرباء المسيب الحرارية.

في هذه الدراسة تم عمل نموذج يعتمد على التحليل العددي CFD للتنبؤ بدرجة الحرارة والضغط والسرعة للماء خلال المبادل الحراري . يتم تحقيق ذلك عدديًا عن طريق حل معادالات الاستمرارية، الزخم، والطاقة من خلال المحاكاة تم الحصول على توزيع درجات الحرارة والسرع المكانية داخل المبادل الحراري.تم استخدام برنامج solidwork لحل المعادلات بالاعتماد على k-Ɛمودل.

وقد تم تنفيذ الاختبارات العملية اللازمة لاختبار اداء المبادل الحراري الجديد وتم قياس درجات الحرارة عند مدخل ومخرج كل أنبوب وتوزيع درجة الحرارة عبر الأنابيب. يتم قياس انخفاض الضغط وقيمة الضغط عند المدخل والمخرج لكل أنبوب . يتم إجراء الاختبارات التجريبية بقيم مختلفة لمعدل تدفق كتلة الماء العادي. وجد أن درجة حرارة الماء الساخن تنخفض إلى 34.7 درجة مئوية عند معدل تدفق الكتلة للماء العادي (60 و 70) لتر / دقيقة عند الأنبوب الثاني والرابع

على التوالي. هذه هي درجة حرارة الخروج المطلوبة من آلية عمل المبادل الحراري. تم الحصول على تطابق وتقارب جيد في النتائج بين الجانبين العملي والنظري حيث كانت النسبة المئوية لأخطاء قيم درجة الحرارة هو (0.38 ، 2.2 ، 3.4 و 4.3)٪ عند الأنبوب الأول ، الأنبوب الثاني ، الأنبوب الثالث ، الأنبوب الرابع على التوالي.تمت مقارنة النتائج التجريبية مع عمل أداء shell and tube والمبادل الحراري ثلاثي الأنبوب. وتبين أن هذه المبادلات الحرارية لا تستطيع حل مشاكل محطة كهرباء المسيب الحرارية.

جمهورية العراق
وزارة التعليم العالي والبحث العلمي
جامعة بابل / كلية الهندسة
قسم الهندسة الميكانيكية

دراسة الخصائص الحرارية الهيدروليكية لمبادل حراري ذو أربعة أنابيب متحدة المركز في محطة المسيب الحرارية

رسالة
مقدمة إلى كلية الهندسة – جامعة بابل وهي جزء من متطلبات نيل درجة الدكتوراه فلسفة في الهندسة / الهندسة الميكانيكية/ قدرة

أعدت من قبل
رنا علي حسين علوان

بأشراف

أ. د. عادل عباس الموسوي

أ.د. عصام مجبل عبيد

2022